Hyperglycemia-induced activation of the Hexosamine Biosynthetic Pathway causes Myocardial Cell Death

Uthra Rajamani

Dissertation presented for the Degree of

DOCTOR OF PHILOSOPHY

in the Department of Physiological Sciences at the Stellenbosch University.

Supervisor: Prof. M. Faadiel Essop

December 2009

Declaration

By submitting this dissertation electronically, I declare that the entirety of the work contained therein is my own, original work, that I am the owner of the copyright thereof (unless to the extent explicitly otherwise stated) and that I have not previously in its entirety or in part submitted it for obtaining any qualification.

December 2009

ABSTRACT

OBJECTIVE – Oxidative stress increases flux through the hexosamine biosynthetic pathway (HBP) resulting in greater *O*-GlcNAcylation of target proteins. Since increased oxidative stress and HBP flux are associated with insulin resistance, we hypothesized that its activation leads to greater *O*-GlcNAcylation of BAD (pro-apoptotic) and increased myocardial apoptosis.

RESEARCH DESIGN AND METHODS – To investigate our hypothesis, we employed two experimental models: 1) H9c2 cardiomyoblasts exposed to high glucose (33 mM glucose) ± HBP modulators ± antioxidant treatment vs. matched controls (5.5 mM glucose); and 2) a rat model of high fat diet-induced insulin resistance and hyperglycemia. We evaluated apoptosis *in vitro* by Hoechst nuclear staining, Annexin-V staining, caspase activity measurements and immunoblotting while *in vivo* apoptosis was assessed by immunoblotting. *In vitro* reactive oxygen species (ROS) levels were quantified by H2DCFDA staining (fluorescence microscopy, flow cytometry). We determined overall and BAD *O*-GlcNAcylation, both by immunoblotting and immunofluorescence microscopy. As BAD-Bcl-2 dimer formation enhances apoptosis, we performed immunoprecipitation analysis and immunofluorescence microscopy (co-localization) to determine BAD-cl-2 dimerization. *In vivo* overall *O*-GlcNAcylation, BAD *O*-GlcNAcylation and BAD-Bcl-2 dimerization was determined by immunoprecipitation and immunoblotting.

RESULTS – High glucose treatment of cells significantly increased the degree of apoptosis as revealed by Hoechst nuclear staining (54 ± 9%, $p<0.01$ vs. 5.5 mM), Annexin-V staining (43 ± 5%), caspase activity assay (26 ± 2%) and immunoblotting. In parallel, overall *O*-GlcNAcylation ($p<0.001$ vs. 5.5 mM), BAD *O*-GlcNAcylation ($p<0.05$ vs. 5.5 mM) and ROS levels were increased (fluorescence microscopy – $p<0.05$ vs. 5.5 mM; flow cytometry – $p<0.001$ vs. 5.5 mM). HBP inhibition using DON and antioxidant treatment (α-OHCA) attenuated these effects while HBP activation by PUGNAc exacerbated it. Likewise, insulin resistant rat hearts exhibited significantly higher caspase-3 ($p<0.05$ vs. controls), overall *O*-GlcNAcylation ($p<0.05$ vs. controls) and BAD *O*-GlcNAcylation levels ($p<0.05$ vs. 5.5 mM). BAD-Bcl-2 dimer formation was increased in cells exposed to hyperglycemia [immunoprecipitation analysis and co-localization] and in insulin resistant hearts.

CONCLUSIONS - Our study identified a novel pathway whereby hyperglycemia results in greater oxidative stress, resulting in increased HBP activation and increased BAD *O*-GlcNAcylation. We also found greater BAD-Bcl-2 dimerization increasing myocardial apoptosis, suggesting that this pathway may play a crucial role in the onset of the diabetic cardiomyopathy.

UITTREKSEL

DOELWIT – Oksidatiewe stres verhoog fluks deur die heksosamien biosintetiese weg (HBW) wat in ‘n groter O-GlcNAsetilering van teiken proteïene resulteer. Weens die feit dat verhoogde oksidatiewe stres en HBW fluks verband hou met insulienweerstandigheid, hipotetiseer ons dat die aktivering hiervan tot groter O-GlcNAsetilering van BAD (pro-aptoptoties) en verhoogde miokardiale apoptose lei.

NAVORSINGS ONTWERP EN METODES – Om die hipotese te ondersoek het ons twee modelle ontplooi: 1) H9c2 kardiomioblaste is blootgestel aan hoë glukose konsentrasie (33mM glucose) ± HBW moduleerders ± antioksidant behandeling vs. gepaarde kontrole (5.5mM glucose); en 2) ‘n hoë vet dieetgeïnduseerde insulienweerstandige rotmodel en hiperglukemie. Ons het apoptose *in vitro* deur middel van Hoescht nukleuskleuring geëvalueer, kasapase aktiwiteit bepalings en immunoblotting terwyl apoptose *in vivo* getoets is deur immunoblotting. Reaktiewe suurstofspesie (RSS) vlakke is deur middel van H2DCFDA verkleuring (fluoresensie mikroskopie, vloeisitometrie) bepaal. Algehele en BAD O-GlcNAsetilering is beide deur immunoblotting en immunofluoresensie mikroskopie bepaal. BAD-Bcl-2 dimeervorming bevorder apoptose, om BAD-cl-2 dimerisasie te bepaal is daar van immunopresipitering analise en immunofluoresensie mikroskopie (ko-lokalisasie) gebruik gemaak. *In vivo* is algehele *O*-GlcNAsetiliering, BAD *O*-GlcNAsetiliering en BAD-Bcl-2 dimerisasie deur immunopresipitasie en immunoblotting bepaal.

RESULTE – Hoë glukose behandeling van selle het die graad van apotpose betekenisvol verhoog soos blootgelê deur Hoechst nukleuskleuring (54 ± 9%, $p<0.01$ vs. 5.5 mM), Annexin-V kleuring (43 ± 5%), kaspase aktiviteit assay (26 ± 2%) en immunoblotting. In parallel, algehele *O*-GlcNAsetilering ($p<0.001$ vs. 5.5 mM), BAD *O*-GlcNAsetilering ($p<0.05$ vs. 5.5 mM) en RSS vlakke is verhoog (fluoresensie mikroskopie– $p<0.05$ vs. 5.5 mM; vloeisitometrie– $p<0.001$ vs. 5.5 mM). HBW inhibering deur van DON en van antioksidant behandeling gebruik te maak (α-OHCA) het hierdie effekte verlaag terwyl HBW aktivering deur PUGNAc dit verhoog het. Netso, het insulienweerstandige rotharte betekenisvolle hoë kaspase -3 ($p<0.05$ vs. kontrole), algeheel *O*-GlcNAsetilering ($p<0.05$ vs. kontrole) en BAD *O*-GlcNAsetiliering vlakke ($p<0.05$ vs. 5.5 mM) getoon. BAD-Bcl-2 dimeervorming is verhoog in hiperglukemies blootgestelde selle [immunopresipitering analise en ko-lokalisering] en in insulienweerstandige harte.

GEVOLGTREKKINGS – Ons studie het ‘n nuwe weg geïdenifiseer waar hiperglukemie in groter oksidatiewe stres resulteer wat weer HBW aktivering verhoog en BAD *O*-GlcNAsetilering verhoog het. Ons het verder bevind dat groter BAD-Bcl-2 dimerisasie miokardiale apoptose verhoog wat voorstel dat hierdie weg ‘n belangrike rol in diabetiese kardiomiopatie speel.

Heart is the seat of spirituality

(Laghu nyaasam, 500 BCE.)

Acknowledgements

Firstly, I would like to thank my supervisor, Prof. M. Faadiel Essop, for not only being a supervisor, but also a friend, philosopher and guide. For spending his precious time with me, uplifting my mood during the not-so-pleasant times. For showing me the definition of an ideal supervisor a student could wish for. For imparting at least a fraction of his writing and "story-telling" skills. For helping me grow not only as a scientist, but also more importantly as a human being. This thesis simply would not have been possible but for you, Prof.

I have no words to express my gratitude to my parents, my mom and dad, who despite being overseas, extended their fullest support in every possible way, be it encouraging me to complete my work on time, giving me moral support, or even putting up with my varying moods (over international calls) during my write up. I am forever grateful to them for their unconditional love. Mom and Dad, I doubt if I would have gotten anywhere without you both.

My thanks to all my colleagues at the Department of Physiological Sciences. I especially wish to thank Gordon Williams (Gordy) and Mark (The Shark) Thomas, for their intellectual prowess and thought-provoking inputs. I am also grateful to everyone else in the department for making my work environment pleasant and for being such great friends.

I would like to express my sincere gratitude to:

- Mr. Benjamin Loos for his technical support with fluorescence microscopy and flow cytometer, and for being a special friend

- Mr. Jamie Imbriolo for initially familiarizing me with cell culture techniques
- Dr. Theo Nell for the Afrikaans translation of my abstract, for proof-reading my thesis and for his virtually round-the-clock help with possibly any issue
- Dr. Rob Smith for being available to help anytime and for his technical inputs
- Dr. James Meiring, Dr. Nihar Singh, Danzil Joseph and Kathleen Reyskens for being wonderful group mates and for all their inputs.

A special thanks to my loving husband, Mr. Koushik Chatterjee, for all his support and help with the household chores when I was still at work.

Finally, I thank God Almighty for being with me in every step of my life and for giving me the strength and courage to deal with testing situations.

TABLE OF CONTENTS

ABBREVIATIONS

α-OHCA	- α – cyano 4 – hydroxyl cinnamic acid
ACC	- Acetyl-CoA carboxylase
ADP	- Adenosine di phosphate
AGE	- Advanced glycation end products
AMP	- Adenosine monophosphate
AMPK	- AMP-activated protein kinase
ATP	- Adenosine triphosphate
BAD	- Bcl-2-associated death promoter
Ca^{2+}	- Calcium ion
cAMP	- Cyclic AMP
CO_2	- Carbon dioxide
CPT	- Carnitine palmitoyl transferase
CVD	- Cardiovascular disease
DAG	- Diacyl glycerol
DAPI	- 4´-6´ diamidino-2-phenylindole
DCFDA	- Dichloro fluorescein diacetate
DISC	- Death-inducing signal complex
DMEM	- Dulbecco's Modified Eagle's medium
DMSO	-Dimethyl sulphoxide
DNA	- Deoxy ribonucleic acid
dnGFAT	- dominant negative GFAT
DON	- 6-diazo 5-oxo-L-norleucine
eNOS	- endothelial nitric oxide synthase

FABP - Fatty acid binding protein

FACS - Fatty Acyl-CoA synthase

FAD - Flavin adenine dinucloetide

FasL - Fas ligand

FAT - Fatty acid translocase

FFA - Free fatty acids

FITC - Fluorescein isothiocyanate

FLIP - FLICE-inhibitory protein

FLICE - FADD-like IL-1β-converting enzyme

GAPDH - Glyceraldehyde-3-phosphate dehydrogenase

GFAT - Glutamine:fructose-6-phosphate amidotranferase

GLUT - Glucose Transporter

HBP - Hexosamine biosynthetic pathway

HF - Heart Failure

IR - Insulin Resistance

JNK - c-Jun NH_2-reminal kinase

KAT - Ketoacyl CoA thiolase

MCD - Malonyl CoA decarboxylase

mRNA - messenger ribo nucleicacid

NAD^+ - Nicotinamide Adenine dinucleotide

NEFA - Non-esterified fatty acids

NFκB - Nuclear factor κ B

O-GlcNAc - *O*-linked N-acetyl glucosamine

OGT - *O*-GlcNAc transferase

PAGE - Polyacrylamide gel electrophoresis

PARP	- Poly ADP ribose polymerase
PBS	- Phosphate buffer solution
PDH	- Pyruvate dehydrogenase
PDK	- PDH kinase
PFK	- Phosphofructokinase
PGC	- PPAR coactivator
Pi	- Phosphate ion
PKC	- Protein Kinase C
PPAR	- Peroxisome proliferator activated receptor
PPRE	- Peroxisome proliferator response elements
PPP	- Pentose phosphate pathway
PTP	- Protein tyrosine phosphatise
PUGNAc	- O-(2-acetamido-2-deoxy-D-glucopyranosylidene)amino N-phenyl carbamate
RACK	- Membrane-bound receptor for protein kinase-c proteins
RAGE	- AGE receptors
RBC	- Red blood corpuscles
RIPA	- Radioimmunoprecipitation assay
ROS	- Reactive oxygen species
SDS	- Sodium dodecyl sulphate
SOD	- Superoxide dismutase
T2DM	- Type 2 Diabetes Mellitus
TNF	- Tumor necrosis factor
UCP	- Uncoupling proteins
UDP	- Uridine di-phosphate

VLDL - Very low density lipoproteins

List of tables

List of figures

1. INTRODUCTION

Type 2 diabetes mellitus (T2DM) is one of the most rapidly emerging global health challenges of the 21st century and a major cause of premature death. For example, ~ every 10 seconds a person dies from diabetes-related causes, and death rates are predicted to rise by ~ 25% during the next decade [1]. Recent data released by the International Diabetes Federation (IDF) show that more than 230 million people, almost 6% of the world's adult population, now live with diabetes. Moreover, it is estimated that the number of individuals affected by diabetes will increase from 135 million in 1995 to 300 million by 2025 [1, 2], while the World Health Organization (WHO) extends this estimate to ~366 million by 2030 [3, 4].

Compounding the problem is statistics showing that the metabolic syndrome (a pre-diabetic condition) is also very common, with an approximate 65 million individuals in the United States affected [5]. Metabolic syndrome is a cluster of metabolic abnormalities which is strongly associated with the risk of development of both T2DM and cardiovascular diseases (CVD). It is characterized by impaired glucose metabolism, dyslipidaemia, hypertension and obesity [6]. Hence the metabolic syndrome equals a pre-diabetic condition that could manifest as T2DM at a later stage, therefore meaning that future projections of T2DM may even be higher than present estimates [7]. Moreover, this is likely to increase further as obesity and sedentary lifestyles become more endemic in younger populations. Similarly, developing nations are also at increased risk for higher T2DM incidences and associated burdens of disease, e.g. CVD. It is currently estimated that ~19 million individuals in India are affected by T2DM, which is likely to triple by 2025 [7]. Such increases will place a significant burden on developing countries such as India and South Africa. The reasons for this escalation may include a rapidly changing lifestyle and/or greater aging of these populations. Moreover, low birth weight due to poor nutritional

intake in developing countries is also proposed to increase the likelihood of developing T2DM during adulthood [7].

1.1 CARDIOVASCULAR COMPLICATIONS ASSOCIATED WITH T2DM

Diabetes causes several cardiovascular complications that are the major cause of mortality associated with this condition [8-10]. For example, diabetes may be responsible for a range of complications such as increased atherosclerosis in large arteries (carotids, aorta, and femoral arteries) and also lesser ones e.g. coronary arteries [11] -these are classed as macrovascular and microvascular. This increases the risk for myocardial infarction, stroke, and limb loss [12]. Micro-angiopathy may also contribute to retinopathy and renal failure, and cardiac pathology [2, 13, 14]. In addition to angiopathy, T2DM can affect cardiac structure and function in the absence of changes in blood pressure and coronary artery disease, a condition referred to as the diabetic cardiomyopathy. Here altered fuel substrate metabolism is strongly implicated in this process [15].

Mortality from heart disease is ~ 2 to 4-fold higher in diabetic patients when compared to non-diabetics with the same magnitude of vascular diseases [16]. Moreover, diabetic cardiomyopathy can occur without any vascular pathogenesis [16, 17]. The epidemiological link between diabetes mellitus and the development of heart failure (HF) [18], independent of atherosclerotic cardiovascular disease is well established. These studies show a higher risk of HF in diabetic patients after considering age, blood pressure, weight, cholesterol and the history of coronary

artery disease [19-21]. Indeed, the Framingham Heart Study showed that the frequency of HF is 2.4-fold and 5-fold higher in diabetic men and women, respectively. Age also plays a role, i.e. for elderly diabetic patients the prevalence of HF was as high as 30% [18].

The risk of developing HF is also associated with stress-induced increases in plasma glucose levels [22]. For example, the development of HF was predicted by insulin resistance (IR) in individuals prospectively assessed over a 9-year period. Moreover, one standard deviation decrease in insulin sensitivity increases the risk of HF by approximately one third [23]. This robust association is largely due to the prevalence of elevated blood pressure, high blood sugar levels and associated free radical generation [24], microvascular dysfunction, and ischemic heart disease in IR states [25]. These studies therefore point towards a strong link between T2DM and the onset of heart diseases and necessitate a thorough understanding of underlying mechanisms driving this process. However, to recognize the diabetic cardiomyopathy as a distinct entity raises the hypothesis that altered metabolism and IR may have a detrimental effect(s) on the myocardium [21, 25-31]. Since metabolic alterations may play a crucial role in this process, and the emphasis of this thesis is on hyperglycaemia, the focus will now be on the important aspects of a) glucose and b) fat metabolism of the heart.

Under conditions of perturbed glucose and fat metabolism, e.g. hyperglycaemia, there are downstream effects on oxidative phosphorylation and the activation of alternative glucose utilizing pathways such as pentose phosphate pathway, polyol pathway, and the hexosamine biosynthetic pathway Together these factors conspire and play a crucial role in mediating detrimental effects of hyperglycaemia on heart. These aspects will be further discussed in the following sections.

1.2 GLUCOSE METABOLISM – A PRIMER

Glycogen stores and exogenous glucose supply are the main sources of glycolytic substrates. The heart's glycogen pool is comparatively small, i.e. ~30 μmol/g wet weight compared to ~150 μmol/g wet weight in skeletal muscle [15, 32] and is rapidly turned over despite constant tissue concentrations [33]. Greater supply of exogenous fuel substrates and/or hyperinsulinemia can eventually lead to increased glycogen storage [34-36]. Conversely, adrenergic stimulation, decreased myocardial ATP levels and elevated inorganic phosphate levels e.g. during ischaemia or intense exercise [34, 37, 38], activates glycogenolysis thereby promoting increased glycolytic flux (Figure 1.1).

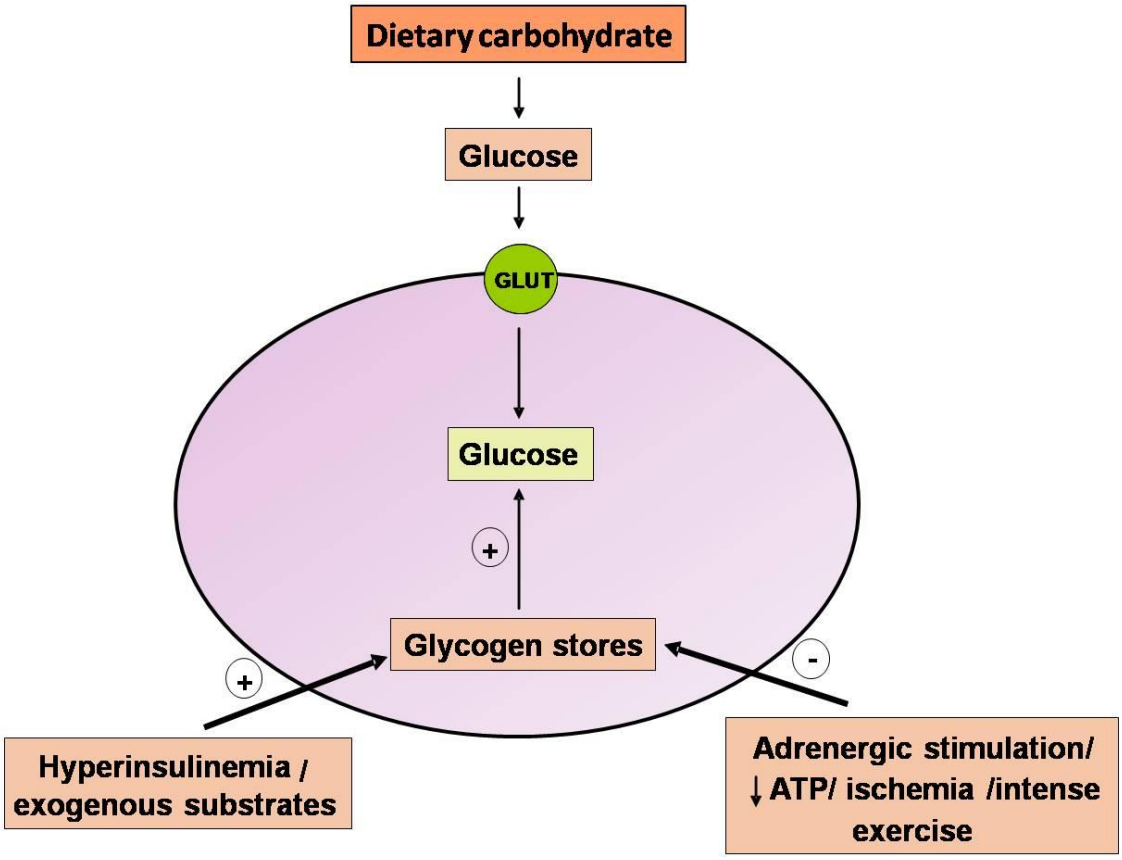

Figure 1.1: **A representation of exogenous and intracellular sources of glucose.**

Glucose transport into cells is regulated by the transmembrane glucose gradient and the number of glucose transporters (GLUTs) present on the sarcolemma. For cardiomyocytes, GLUT-4 is the major transporter, with GLUT-1 to a lesser extent. GLUT-4 resides within intracellular vesicles and is translocated to the sarcolemma in response to insulin stimulation, exercise or ischaemia [34, 39, 40] thereby enhancing glucose uptake (Figure 1.2).

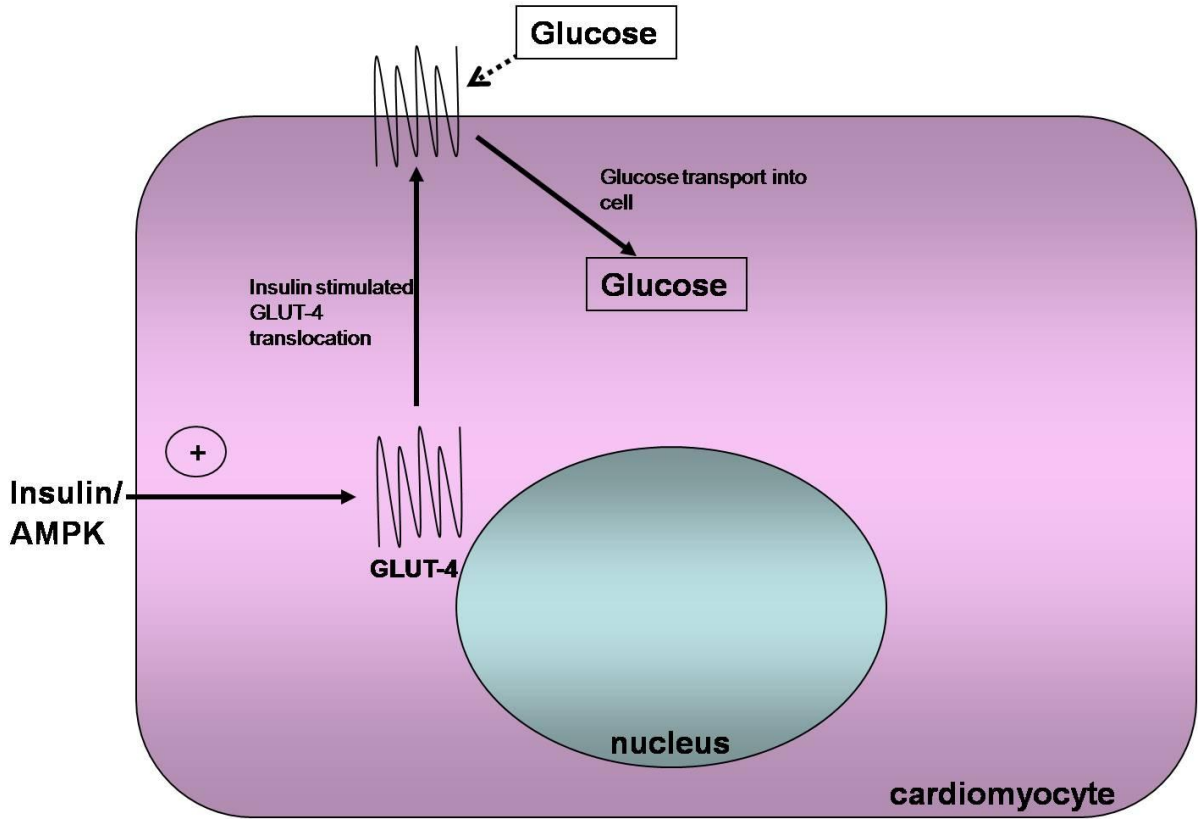

Figure 1.2: Insulin and AMPK regulate GLUT-4 translocation and myocardial glucose uptake.

GLUT-4 translocation can also be stimulated by AMP-activated protein kinase (AMPK), for e.g. response to ischaemia [41] or exercise [39, 41, 42]. Moreover, mice expressing cardiac-specific dominant negative AMPK, exhibit lower rates of glucose transport [42], further supporting a role for AMPK in myocardial glucose uptake. In agreement, Russell *et al.* [43] also found that transgenic mice expressing inactive AMPK display normal GLUT-4 expression, baseline and insulin-stimulated cardiac glucose uptake, but fail to increase glucose uptake and glycolysis during ischaemia [43]. This study demonstrates a key role for AMPK in mediating insulin-independent and also stress-induced glucose uptake. The role of AMPK in regulating glycogen content in heart has also come to the fore in recent years [42, 44, 45]. Inactive AMPK with a

mutation in its regulatory subunit showed an association with glycogen accumulation and hypertrophic cardiomyopathy [44, 46, 47]. In contrast, acute activation of AMPK activates glycogenolysis thereby increasing glycolytic substrate supply [48, 49].

Exogenous glucose uptake and glucose derived from glycogenolysis eventually feed into glycolysis. Phosphofructokinase-1 (PFK-1) is a regulatory enzyme that catalyzes the first irreversible step in glycolysis, i.e. converting fructose 6-phosphate to fructose 1,6-bisphosphate (Figure 1.3). This step requires 1x ATP and its breakdown products are important regulators of PFK-1, i.e. ATP inhibits it while it is activated by ADP, AMP and inorganic phosphate. Hence when intracellular phosphorylation potential is low, flux through glycolysis can be increased. AMPK activates PFK-2 [50, 51] by phosphorylation, and the fructose 2,6-bisphosphate formed can also activate PFK-1 [38, 52]. The enzyme aldolase then converts fructose-1,6-bisphosphate to glyceraldehyde-3-phosphate. Glyceraldehyde-3-phosphate dehydrogenase (GAPDH) converts glyceraldehyde-3-phosphate to 1,3-diphosphoglycerate, producing NADH. GAPDH is an important regulatory step in the glycolytic pathway. Here NADH accumulation within the cytoplasm inhibits GAPDH while NAD^+ increases its activity [53]. The regeneration of NAD^+ from NADH is inhibited by lactate and 1,3-diphosphoglycerate.

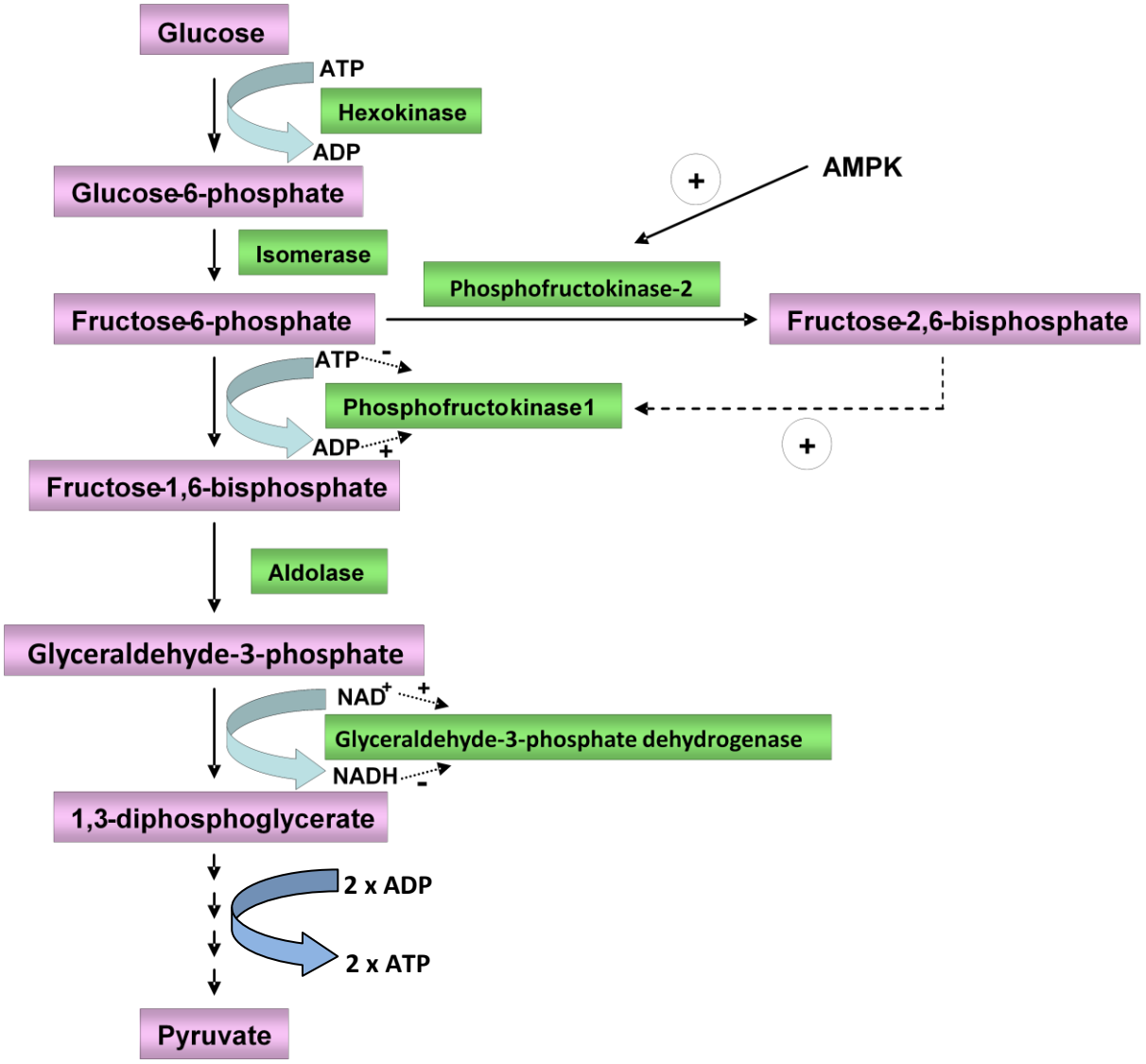

Figure 1.3: A schematic representation of the glycolytic pathway and the various regulators of the pathway. *PFK-1 is regulated by the ADP/ATP ratio and fructose-2,6-bisphosphate levels. PFK-2 is activated by AMPK. Glyceraldehyde-3-phosphate dehydrogenase is regulated by the NAD^+/NADH ratio.*

The glycolytic pathway converts glucose 6-phosphate to pyruvate reducing NAD^+ to NADH and generates 2x ATP per glucose molecule. The NADH and pyruvate formed as a result of glycolysis are either diverted to the mitochondrial matrix to generate CO_2 and NAD^+ that completes the aerobic oxidation process, or the pyruvate is converted to lactate and NAD^+ in the

cytosol (non-oxidative glycolysis). The myocardium produces net lactate only under conditions like diabetes [54-56] or ischaemia [34, 57, 58]. Pyruvate formed at the end of glycolysis has three major fates: 1) conversion to lactate, 2) carboxylation to oxaloacetate or malate and 3) decarboxylation to acetyl-CoA.

1.3 FATTY ACID METABOLISM – A PRIMER

1.3.1 Exogenous fatty acid uptake

Myocardial fatty acid uptake is largely determined by plasma free fatty acids (FFA) availability [59-61]. FFA levels can vary up to four-fold during the course of a day in humans (~0.2 to 0.8 mM), while under conditions of metabolic stress for e.g. ischaemia, diabetes or starvation it can be significantly increased (~1.0 mM) [62]. FFA are transported in non-esterified form attached to albumin, covalently bound to triglyceride contained within chylomicrons, or very low density lipoproteins (VLDL) [60] which are hydrolysed by lipoprotein lipase on the cardiomyocytes [63-66].

FA are taken in by cardiomyocytes via passive diffusion or by protein-mediated transport across the sarcolemma [67]. The latter is mediated by fatty acid translocase (FAT) or plasma membrane fatty acid binding protein ($FABP_{pm}$) [67-69] (Figure 1.4). CD36 is a specific 88 kDa FAT protein that is abundantly expressed in cardiac and skeletal muscle and is the predominant FAT form in

the heart [67, 68]. CD36 also partially regulates myocardial fatty acid uptake in humans [70]. FFA bind to FABP and are esterified to fatty acyl-CoA by fatty acyl-CoA synthase (FACS). Recent studies show that there are CD36-associated FABP and FACS proteins in the cytosol, therefore meaning that transported FA can immediately be esterified to fatty acyl-CoA [68]. Intriguingly, some studies found that there is translocation of FAT/CD36 from an intracellular location to the sarcolemma in response to contraction, increased energy demand [71-73] and also to insulin stimulation [73]. However, these responses need to be confirmed under physiologically relevant conditions.

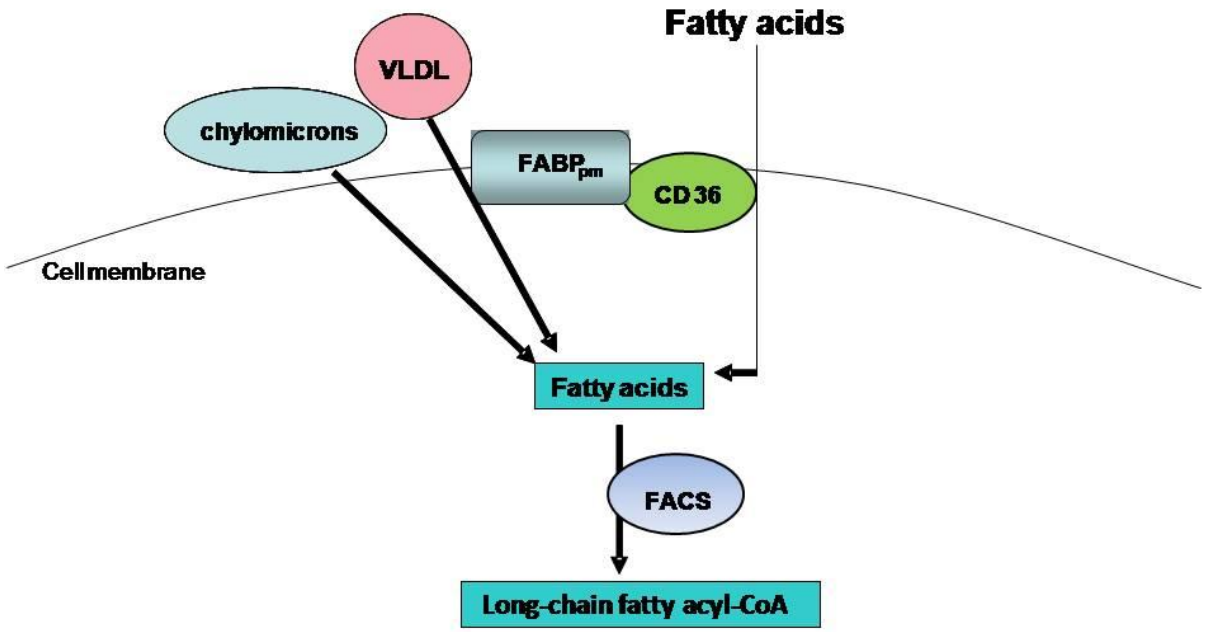

Figure 1.4: Fatty acid transport into the cell. *FA enter the cardiomyocyte by either passive diffusion or protein-mediated transport through the sarcolemma via plasma membrane fatty acid binding protein ($FABP_{pm}$) or CD36/fatty acid translocase (FAT). The FA are then esterified by the actions of fatty acyl-CoA synthase (FACS) and are now ready to enter mitochondria to undergo β-oxidation. VLDL- very low density lipoprotein.*

1.3.2 Mitochondrial fatty acid uptake

Fatty acid β-oxidation mainly occurs in mitochondria [74, 75]. Long-chain acyl-CoAs must be transported into the mitochondria by specific carriers since the inner mitochondrial membrane is relatively impermeable. This transport is carried out by a carnitine-dependent transport system [59, 76], i.e. carnitine palmitoyl transferase – 1 (CPT-1) which catalyzes formation of long-chain acylcarnitine from long-chain fatty acyl-CoA in the intermembrane space of mitochondria; the carnitine acyltranslocase that transports long-chain acylcarnitine across the inner mitochondrial membrane; and finally carnitine palmitoyltransferase- 2 (CPT-2) that regenerates long-chain acyl-CoA within the mitochondrial matrix (Figure 1.5).

CPT-1 is the key regulatory step of mitochondrial fatty acid uptake [59, 76] and has two isoforms: CPT-1α enriched in the liver and CPT-1β in the heart [77, 78]. CPT-Iβ is 30-fold more sensitive than CPT-1α and is also more strongly inhibited by malonyl-CoA than CPT-1α [77-79]. Malonyl-CoA strongly inhibits CPT-1 by binding to its cytosolic side [76, 77, 80], thus a key regulator of mitochondrial fatty acid oxidation decreased malonyl-CoA levels increase its uptake and oxidation [81-83] while increased levels result in the reverse effect [84, 85]. Malonyl-CoA has a rapid turnover in the heart [86, 87] and is formed from acetyl-CoA by acetyl-CoA carboxylase [88]. AMPK activation results in increased fatty acid oxidation by inhibiting ACC and thereby reducing malonyl-CoA levels [89, 90].

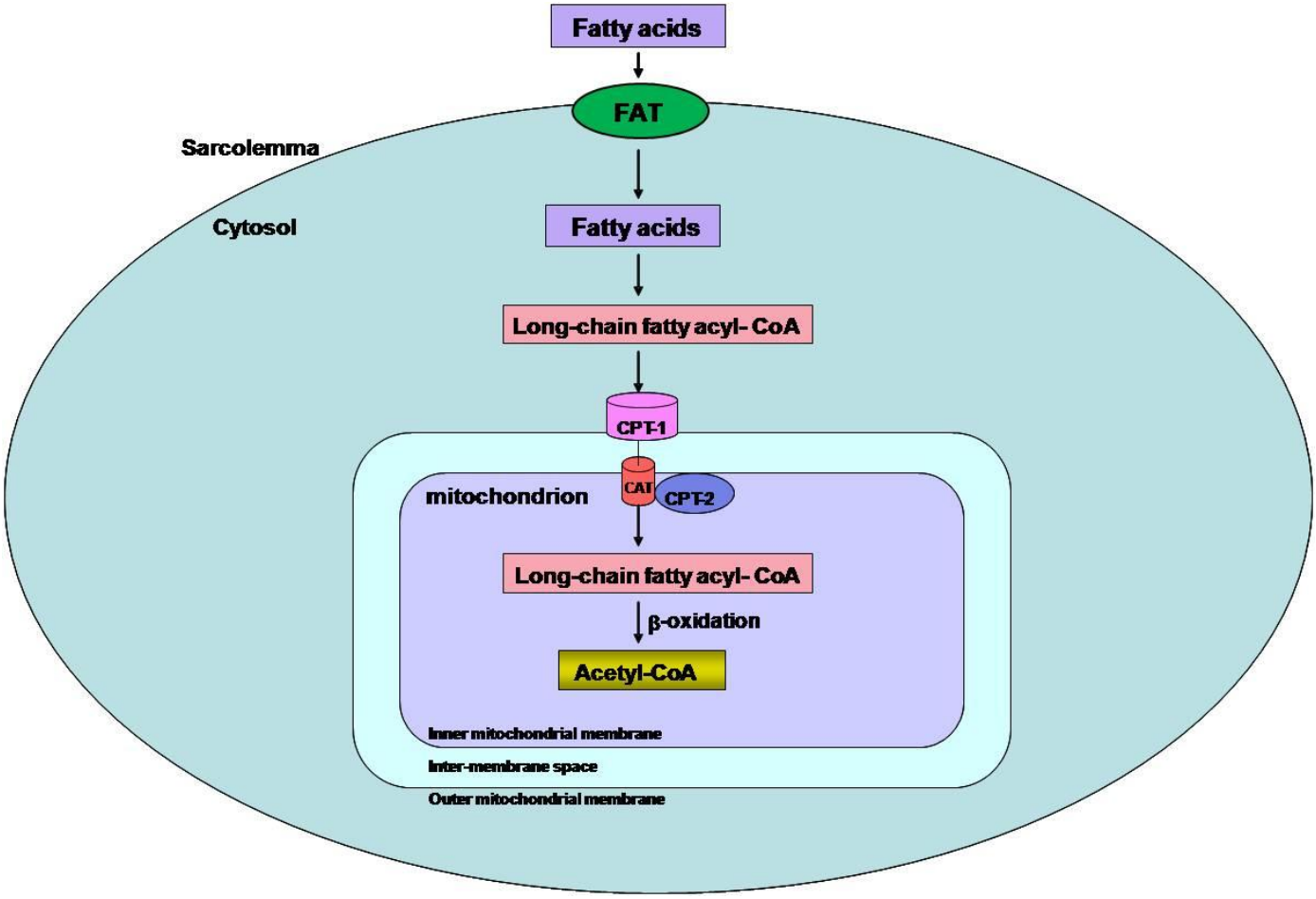

Figure 1.5: Mitochondrial fatty acid transport. *Fatty acyl-CoAs are shuttled into the mitochondria by CPT-1 (carnitine palmitoyl transferase-1) that converts it to acyl-carnitine. Carnitine acyl translocase (CAT) then transports it through the inter-mitochondrial space to CPT-2 where the long-chain fatty acyl-CoA is regenerated inside the mitochondrial matrix. (FAT= Fatty acid translocase.)*

Once taken up by mitochondria, long-chain fatty acyl-CoA undergoes β-oxidation, a process that sequentially cleaves off acetyl-CoA units and generating reducing equivalents (NADH and $FADH_2$) in the process. The β-oxidation spiral involves four reactions i.e. acyl-CoA dehydrogenase, 2-enyl CoA hydratase, 3-hydroxyacyl CoA dehydrogenase, and the last reaction catalyzed by 3-ketoacyl CoA thiolase (3-KAT). Reducing equivalents that are generated can then undergo oxidative phosphorylation to generate ATP [59].

1.4 MITOCHONDRIAL OXIDATIVE PHOSPHORYLATION

Oxidative phosphorylation involves the flow of electrons through the electron transport chain, i.e. from electron donors such as NADH and $FADH_2$ to the final electron acceptors. The electron transport chain consists of complexes I - IV located within the inner membrane of the mitochondrion [91] (Figure 1.6). NADH-coenzyme Q oxidoreductase, also known as NADH dehydrogenase or complex I, is the first protein in the electron transport chain [92]. Complex I binds to flavin mononucleotide (FMN), and is immediately re-oxidized to NAD. NAD is "recycled," acting as an energy shuttle. FMN receives a proton from NADH and also picks up a proton from the matrix. In this reduced form, it passes the electrons to iron-sulfur clusters that are part of the complex, and forces two protons into the intermembrane space [92]. This is the only enzyme that is part of both the citric acid cycle and the electron transport chain [93, 94].

Q-cytochrome c oxidoreductase is also known as cytochrome c reductase, cytochrome bc1 complex, or simply complex III [95, 96]. Protons are transferred to this complex from an intermediate Coenzyme Q. The movement of protons from Coenzyme Q to complex III is a proton translocation event. Cytochrome c oxidase, also known as complex IV, is the final protein complex in the electron transport chain [97]. More protons are translocated by Complex IV, and it is at this site that oxygen binds along with protons. Using the electron pair and remaining free energy, oxygen is reduced to water. Since molecular oxygen is diatomic, it actually takes two electron pairs and two cytochrome oxidase complexes to complete the reaction sequence for the

reduction of oxygen. This last step in electron transport serves the critical function of removing electrons from the system so that electron transport can operate continuously [98]. The enzymes in the electron transport system use the energy released from the oxidation of NADH to pump protons across the inner membrane of the mitochondrion thereby generating an electrochemical gradient. The potential energy stored is then used by ATP synthase to produce mitochondrial ATP. Succinate-Q oxidoreductase, also known as complex II or succinate dehydrogenase, is a second entry point to the electron transport chain [99].

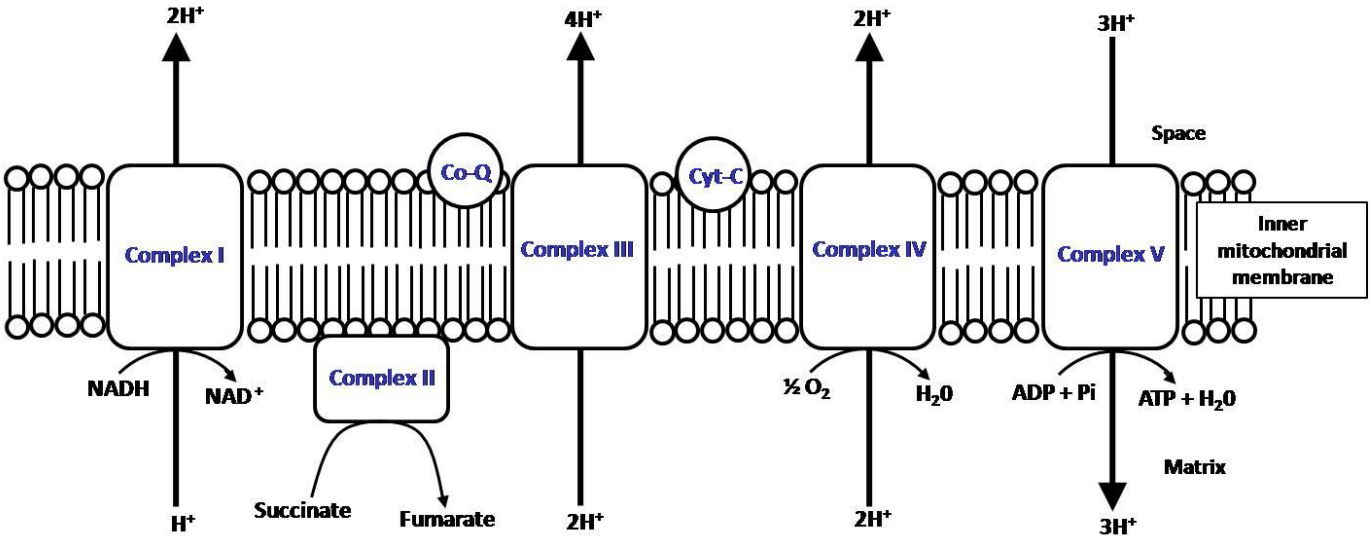

Figure 1.6: A schematic representation of the electron transport chain and complexes.

After discussing the essential features of glucose and fatty acid metabolism, it is important to note that these two major catabolic pathways are inter-related in terms of its utilization. This phenomenon was first described by Philip Randle during the 1960s [100].

1.5 RANDLE CYCLE

The basic premise is that elevated glucose concentrations stimulate pancreatic insulin secretion that subsequently attenuates FFA release from adipose tissue. Thus, glucose utilization is stimulated by insulin, unaffected by high fatty acid concentrations [100]. However, when glucose and insulin concentrations are low, FA become the major fuel substrate for skeletal and cardiac muscle [100]. Under conditions of high FA oxidation, there is an increased yield of acetyl-CoA, citrate and NADH levels. Increased levels of citrate inhibit PFK, thus attenuating glycolysis. Furthermore, increased acetyl-CoA and NADH levels inhibit PDH thereby decreasing glucose oxidation [101]. The inhibition of PDH and PFK results in accumulation of upstream glycolytic metabolites, e.g. glucose 6-phosphate that inhibits hexokinase thereby also lowering glycolytic flux. Hence at higher fatty acid oxidation rates, there is reduced glucose oxidation and *vice versa* [100] (Figure 1.7). However, Shulman's laboratory [102] challenged this hypothesis since they observe decreased intramuscular glucose 6-phosphate levels under conditions of fat-induced insulin resistance. Moreover, fat accumulation interferes with the GLUT4 transporter activity and/or hexokinase II activity.

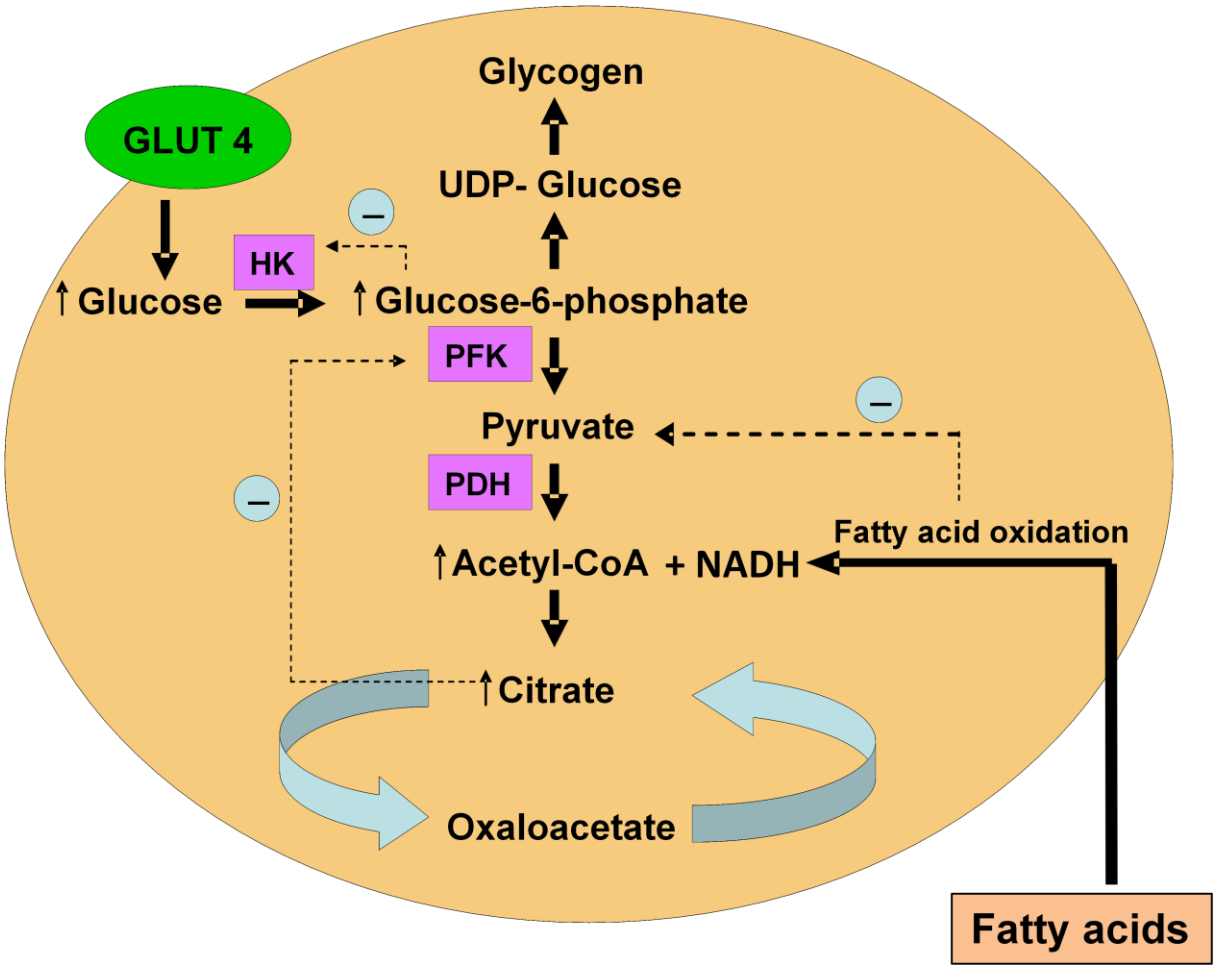

Figure 1.7: The glucose-fatty acid cycle (Randle cycle) in muscle. *Fatty acid oxidation attenuates pyruvate dehydrogenase (PDH) and glucose oxidation, while citrate diminishes phosphofructokinase (PFK) and glycolysis.*

1.6 THE HEART AND PERTURBED METABOLISM

1.6.1 Myocardial ischaemia

Mitochondrial oxidative metabolism is critically dependent on oxygen supply to the heart, and its curtailment results in attenuated mitochondrial ATP production and decreased function [16]. An initial adaptive response is to increase glycolysis, allowing for glycolytic ATP production that is useful to maintain intracellular ionic homeostasis [20]. However, due to ischemic shock the heart is also exposed to high concentrations of FFA [16, 102]. In addition, AMPK is activated to enhance glucose uptake. However, AMPK activation also increases fatty acid oxidation. Thus, counter-intuitively, fatty acid oxidation becomes the main residual source of mitochondrial oxidative metabolism during ischaemia-reperfusion [62]. As a result of the Randle cycle higher FA oxidation diminishes glucose oxidation causing a "de-linking" between higher glycolysis rates and lower glucose oxidation [14]. Interestingly, clinical therapy that improves the coupling of glycolysis to glucose oxidation can reduce myocardial tissue acidosis and lactate build-up, thereby blunting functional recovery in response to ischaemia-reperfusion[103].

1.6.2 Diabetic heart

Altered myocardial substrate and energy metabolism is an important contributing factor to the development of the diabetic cardiomyopathy [104, 105]. With T2DM, carbohydrate metabolism is usually reduced and FA metabolism enhanced [54, 106]. Despite increased FA utilization by the diabetic heart, its FA uptake exceeds FA oxidation rates thereby resulting in intracellular myocardial lipid accumulation [107-109] (Figure 1.8). Lipid intermediates like ceramides may

promote apoptosis in cardiomyocytes thus leading to cardiac dysfunction, a phenomenon known as "lipotoxicity" [110].

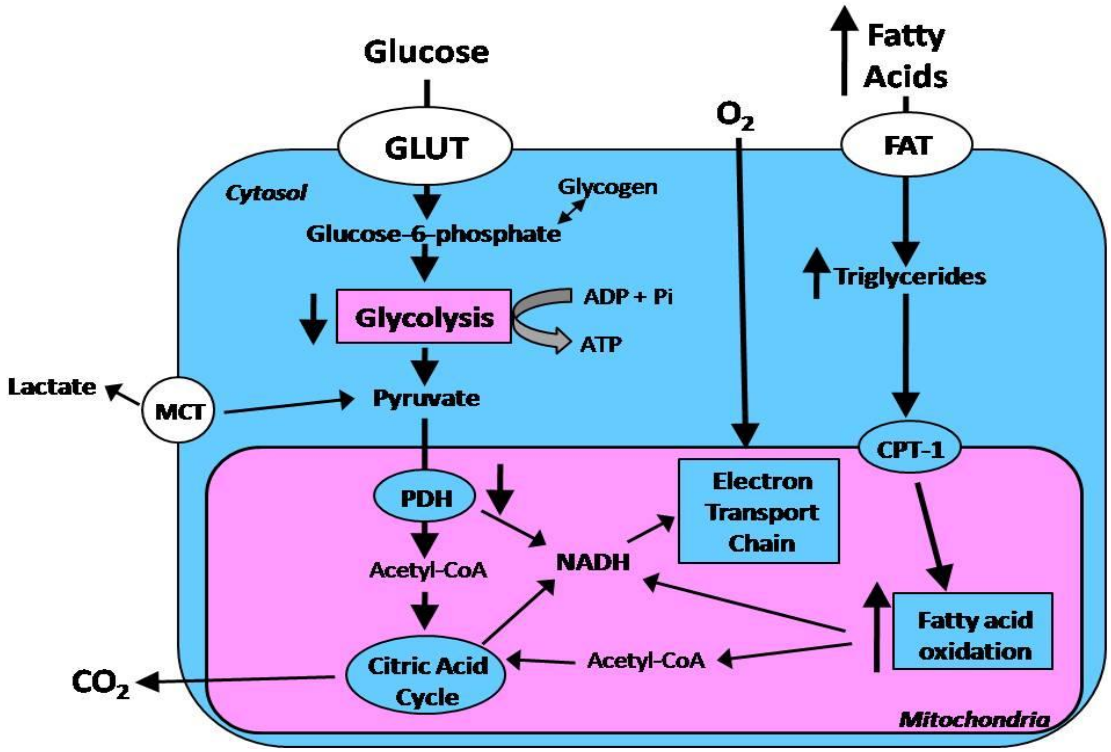

Figure 1.8: Alterations in cardiac energy metabolism in the obese heart. *FA and carbohydrates are the key sources of energy supply for the heart. With obesity, a switch in energy metabolism occurs such that FA becomes the more prominent source of acetyl-CoA for the tricarboxylic acid cycle. FAT indicates fatty acid transporter; PDH, pyruvate dehydrogenase; MCT, monocarboxylate carrier; GLUT, glucose transporter.*

Mitochondrial substrate oxidation results in production of reducing equivalents like NADH and $FADH_2$ which enter the electron transport chain that generates an electrochemical proton gradient across the mitochondrial membrane to drive ATP synthesis. In perfectly coupled mitochondria, there is no proton "leak" across the mitochondrial membrane, i.e. the entire gradient is utilized for ATP synthesis. However, under baseline conditions some proton leak

occurs with uncoupling proteins (UCPs) providing a mechanism whereby protons re-enter the mitochondrial matrix [111].

There is evidence that fatty acid-mediated uncoupling reduces cardiac efficiency in the diabetic heart [112]. Studies have shown that with obesity, there is elevated UCP2 expression and with high circulating fatty acids there is increased UCP 3 mRNA synthesis [113]. Thus higher UCP levels may promote uncoupling of mitochondrial oxidative phosphorylation meaning that ATP production and cardiac efficiency may be compromised [113]. Increased superoxide production is another potential activator of UCPs in the diabetic heart. Here UCPs are activated to limit the production of ROS by reducing the mitochondrial membrane potential [114]. However, higher FA utilization increases delivery of reducing equivalents to the electron transport chain, elevating superoxide production and resulting in greater mitochondrial uncoupling. The higher uncoupling results in attenuated mitochondrial ATP production and reduced contractile function with diabetes [115].

To sum up, high FFA and glucose supply in the bloodstream is purposed to result in detrimental consequences for the diabetic heart (Figure 1.9) [104]. Increased FFA supply enhances FA oxidation that may lead to mitochondrial uncoupling [115]. Moreover, FA supply exceeds FA oxidation rates leading to intracellular lipid accumulation, higher ceramide levels and increased apoptosis or "lipotoxicity" [2]. High FA supply also has gene effects, i.e. FAs are ligands for peroxisome proliferator-activated receptor-α (PPARα), a key transcription factor regulating several FA metabolic genes, thus further elevating FA oxidation rates [116]. PPARα also induces expression of PDK4, a negative regulator of PDH [116], thereby leading to reduced glucose uptake and oxidation. High glucose levels also have several deleterious effects mediated via elevated ROS production (this will be discussed later in the thesis - Section 1.7).

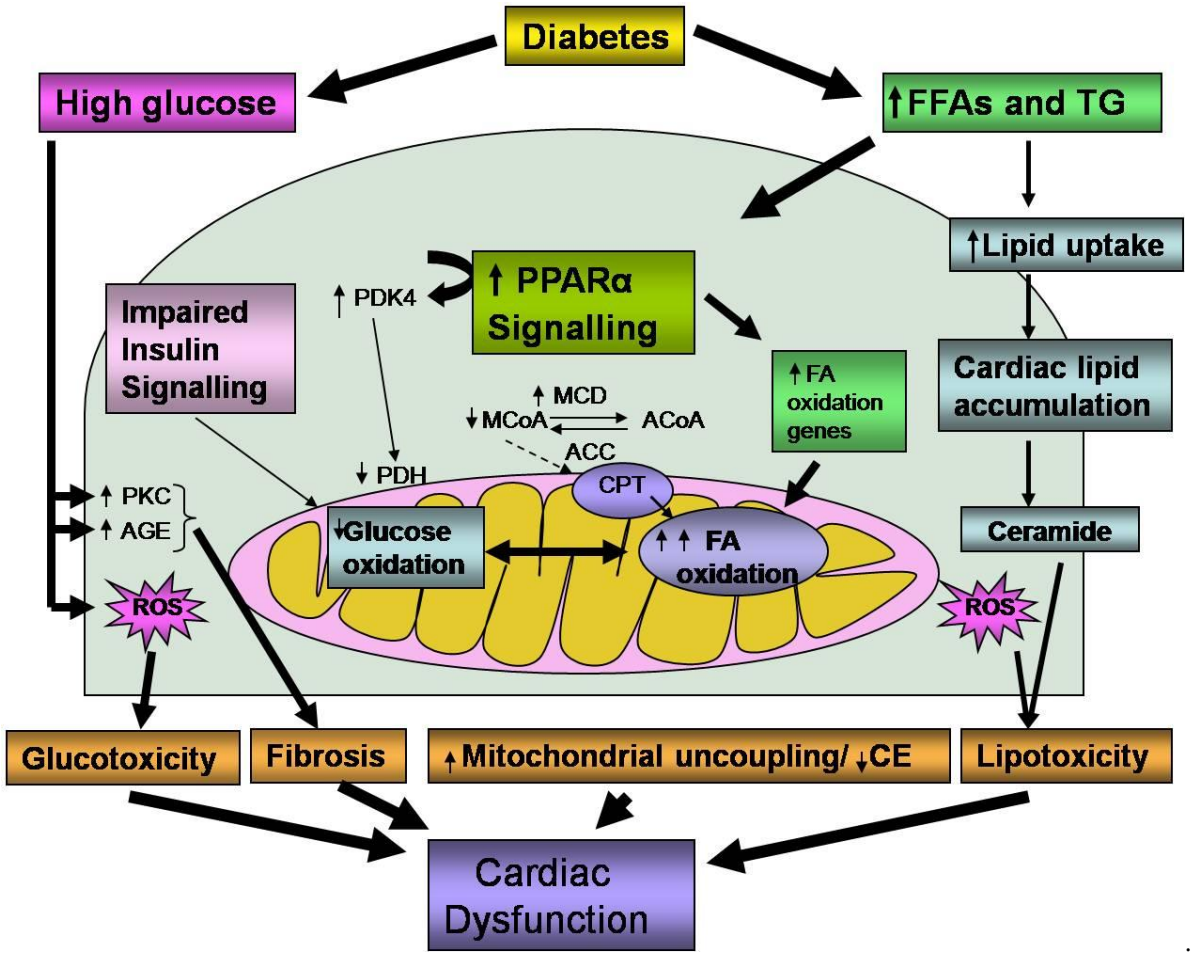

Figure 1.9: Potential contributors to the development of diabetic cardiomyopathy. *Increased FFA activates PPARα signaling, leading to increased transcription of genes involved in FA oxidation. Increased delivery of FA decreases insulin sensitivity and activates transcriptional pathways like PPARα. PPARα activation reduces glucose oxidation by increasing pyruvate dehydrogenase kinase 4 (PDK4) expression increasing CD36 expression. Another PPARα target malonyl-CoA decarboxylase (MCD), degrades malonyl-CoA. This stimulates CPT-1 thereby increasing FA uptake by the mitochondrion. Other PPARα target genes include medium- and long-chain acyl CoA dehydrogenase and hydroxyl acyl CoA dehydrogenase. Eventually this leads to increased ROS, ceramide and AGEs, lipotoxicity, glucotoxicity, apoptosis and reduced cardiac efficiency. TG indicates triglycerides; GLUTs- glucose transporters; PDK4- pyruvate dehydrogenase kinase 4; MCD- malonyl-coenzyme A decarboxylase; MCoA- malonyl-coenzyme A; ACoA- acetyl-coenzyme A; ACC- acetyl coenzyme A carboxylase; CPT1- carnitine palmitoyl-transferase 1; PDH- pyruvate dehydrogenase; CE- cardiac efficiency; PKC- protein kinase C; and AGE- glycation end products. Modified from [2].*

1.7 OXIDATIVE STRESS AND DIAETIC COMPLICATIONS

Production of increased amounts of reactive oxygen species is known to have detrimental effects on cellular function [117]. Oxidative stress is caused by an imbalance between the production of reactive oxygen and the organism's innate ability to deactivate reactive intermediates and/or easily repair the resulting damage. This may occur under conditions of higher substrate influx, e.g. hyperglycaemia and/or hyperlipidaemia [118]. While high glucose conditions increase superoxide production, high fat levels elevate peroxynitrite and superoxide production.

It is known that increased oxidative stress participates in the development and progression of diabetes and its complications [118-120]. The proposed mechanisms of oxidative stress-mediated diabetic complications include activation of transcription factors, advanced glycation end products (AGE) and protein kinase C (PKC).

Excess free radicals damage cellular proteins, membrane lipids and nucleic acids and eventually cause cell death. Glucose oxidation is a major source of free radical production [121]. Glucose (enediol form) is oxidized in a transition metal-dependant reaction to an enediol radical anion which is then converted to reactive ketoaldehydes and superoxide anion radicals [121]. The latter then undergoes dismutation to form hydrogen peroxide degraded by catalase or glutathione peroxidase (Figure 1.10).

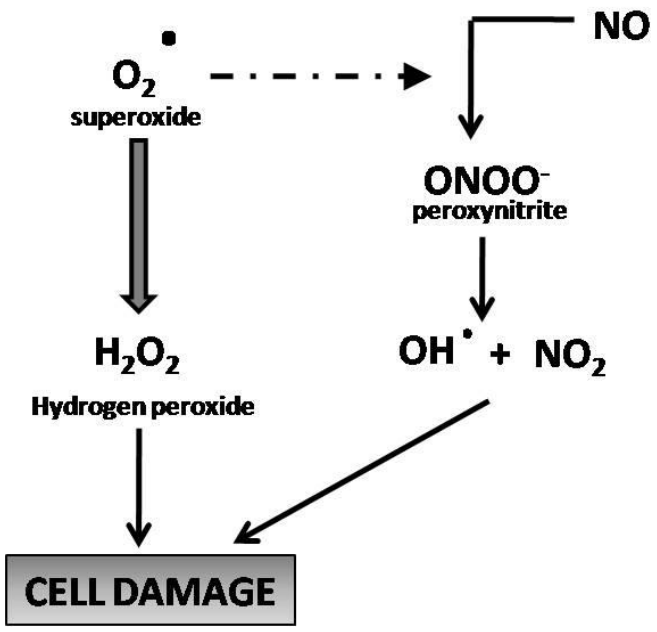

Figure 1.10: Production of free radicals.

However, if hydrogen peroxide is not degraded it can form extremely reactive hydroxyl radicals in the presence of transition metals [121, 122]. In addition, superoxide anion radicals can also react with nitric oxide forming reactive peroxynitrite radicals [121-126]. Under hyperglycaemic conditions, lipid peroxidation of low density lipoproteins (LDL) is also promoted by a superoxide-dependent pathway that generates free radicals [127, 128].

ROS may damage cells by the inhibition of GAPDH, a key glycolytic enzyme. Here increased ROS levels result in apoptosis by causing DNA strands to break, leading to poly (ADP-ribose) polymerase (PARP) activation. PARP then ADP-ribosylates GAPDH, thereby attenuating glycolysis [129]. Subsequently, glucose is routed through other glucose-utilizing pathways like

the polyol pathway, pentose phosphate pathway and the hexosamine biosynthetic pathway which will now be discussed in more detail.

1.8 HYPERGLYCAEMIA ACTIVATES ALTERNATE METABOLIC PATHWAYS

1.8.1 Polyol pathway

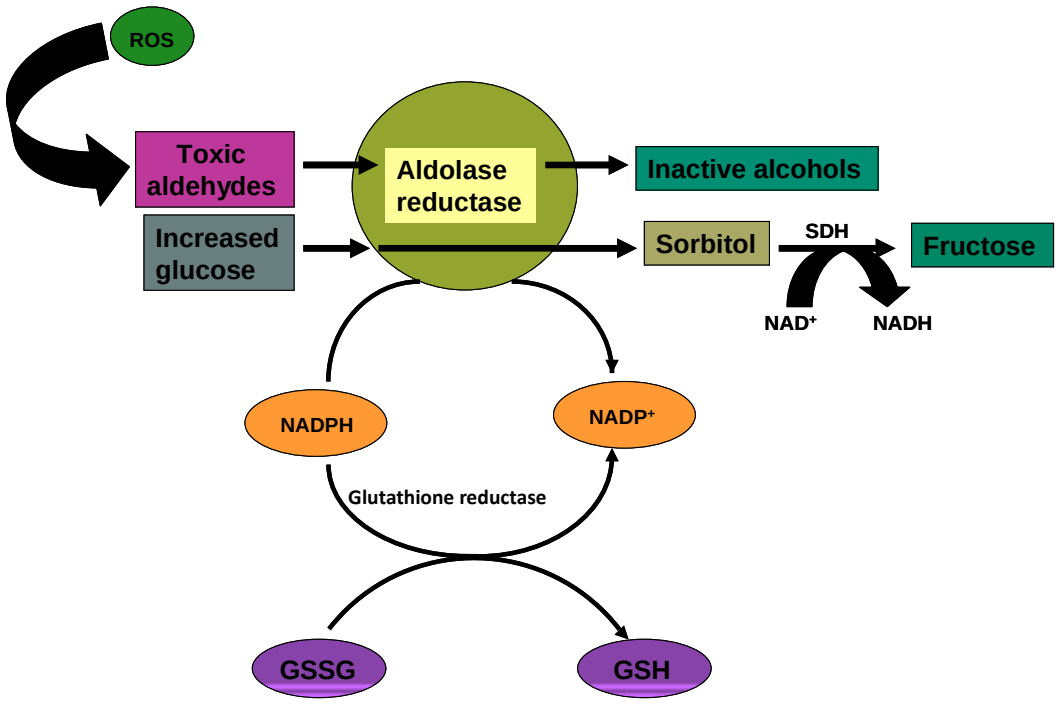

Figure 1.11: Hyperglycaemia increases flux through the polyol pathway. *Reproduced and modified from [130]. GSSG: Glutathione; GSH: Reduced gluthathione; SDH: Sorbitol dehydrogenase.*

Aldose reductase is a key enzyme in the polyol pathway that reduces toxic aldehyde into inactive alcohols (Figure 1.11) [131]. However, with diabetes-induced hyperglycaemia, aldolase reductase reduces glucose to sorbitol that is later oxidized to fructose. As a result, aldolase reductase uses up reducing equivalents (NADPH) [132]. Since NADPH is also needed for regenerating reduced glutathione (a critical intracellular antioxidant), a decrease in reduced glutathione levels due to lesser availability of NADPH, increases susceptibility to intracellular oxidative stress [131] and subsequent ROS-mediated effects. Activation of the polyol pathway also results in decreased $NADP^+$ and NAD^+, necessary cofactors in redox reactions throughout the body. Decreased levels of these cofactors lead to lesser synthesis of reduced glutathione, nitric oxide, myo-inositol, and taurine. Sorbitol may also glycate nitrogen residues of proteins like collagen, and the products of these glycations are referred to as AGE [130].

1.8.2 Intracellular production of AGE precursors

The intracellular production of AGE precursors is another important mechanism that stresses cells. AGE are molecules formed during a non-enzymatic reaction between proteins and sugar residues, known as the Maillard reaction [133]. AGE accumulates in the body with aging and its accumulation may increase with conditions like diabetes mellitus, renal failure and oxidative stress. At the chemical level, a sugar residue reacts with the amino group of a protein to form a Schiff-base (Figure 1.12) [133]. This is a rapid and reversible reaction. The Schiff-base then forms a more stable Amadori product. Further steps result in the formation of irreversible and

stable AGE compounds. The final step of the Maillard reaction is ROS-driven. AGE accelerate oxidation and thus favour their own production [134].

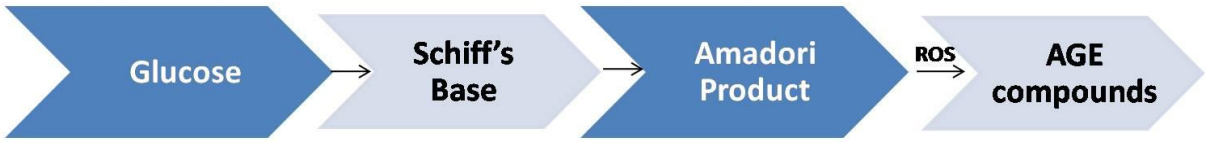

Figure 1.12: A schematic representation of the mechanism involved in the formation of AGE compounds.

AGEs are also involved in the development of heart failure in both diabetic and non-diabetic patients, i.e. they increase rigidity of heart tissue leading to diastolic and systolic dysfunction through coronary artery disease and vascular dysfunction [133]. AGE precursors may damage cells in three different ways. Firstly, they modify intracellular proteins including gene transcriptional alteration [135, 136]. Secondly, AGE precursors can diffuse out of the cell and modify nearby extracellular matrix molecules [137], thus changing signaling between the extracellular matrix and the cell thereby causing cellular dysfunction [138]. Lastly, AGE precursors are able to diffuse out of the cell and modify circulating proteins such as albumin [139]. Modified circulating proteins can bind to and activate AGE receptors, hence causing an inflammatory response in the vasculature through the production of cytokines and growth factors [139-148]. Through their receptors (RAGEs), AGEs inactivate enzymes by altering their structures and functions [149], promoting free radical formation [118, 120], and impair the anti-proliferative effects of nitric oxide [150, 151]. Moreover, AGEs increase intracellular oxidative

stress thereby activating the transcription factor NF-κB and promoting up-regulation of its target genes [152] including Bax, Bcl-xL, Bcl-2, caspase-11 and Fas-Ligand [153]. NF-κB also enhances production of nitric oxide, thought to contribute to pancreatic islet β-cell damage [153]. Such apoptotic gene induction together with increased free radical (superoxide) production results in c-Jun NH_2-reminal kinase (JNK) and caspase-dependent apoptosis [154].

1.8.3 PKC activation

Another mechanism known to stress hyperglycaemic cells is the PKC pathway. PKC is a family of enzymes that control the function of target proteins by phosphorylation of hydroxyl groups of serine and threonine amino acid residues. PKC enzymes are activated by upstream signals, e.g. diacylglycerol (DAG) [155]. Hyperglycaemia increases the production of DAG that is an important co-activator of the classic isoforms of PKC, i.e. β, δ, and α [155-158]. When PKC is activated by intracellular hyperglycaemia a variety of effects occur like decreased eNOS (endothelial nitric oxide synthase), reduced fibrinolysis, increased NADPH oxidases and increased ROS. Thus protective mechanisms are attenuated and detrimental effects increased [158]. Upon activation, PKC enzymes are translocated to the sarcolemma by membrane-bound receptor for activated protein kinase C proteins (RACK). PKC enzyme activation may remain long after the original trigger signal(s). This is achieved by DAG production from phosphatidylinositol by a phospholipase. Moreover, FA may also play a role in long-term activation of PKC enzymes [155].

1.8.4 Pentose phosphate pathway

Under conditions of oxidative stress, e.g. with hyperglycaemia, there is an increased flux through the pentose phosphate pathway (PPP) (Figure 1.13). Glucose 6-phosphate is the entry point of the PPP which is converted to ribulose-5-phosphate, a pentose sugar. The pathway has an oxidative phase and a non-oxidative phase. Here the conversion of glucose 6-phosphate to ribulose-5-phosphate comprises the oxidative phase, while the rest of the pathway is non-oxidative and involves synthesis of pentose sugars. Though the PPP has not directly been implicated in pathogenesis [159], higher lipid biosynthesis due to activation of the pathway may play a role in pathogenesis. Under hyperglycaemic conditions, higher NADPH utilization by the polyol pathway would increase the activity of PPP for the maintenance of the NADPH:$NADP^+$ ratio. As a result of PPP activation there is increased production of triose phosphate intermediates that facilitate the *de novo* synthesis of DAG. Here the *de novo* DAG synthesis pathway is favoured by a high NADH:NAD^+ ratio and results in increased DAG levels. Subsequently, this leads to increased dihydroxyacetone and glycolytic metabolite accumulation thereby causing further damage [160].

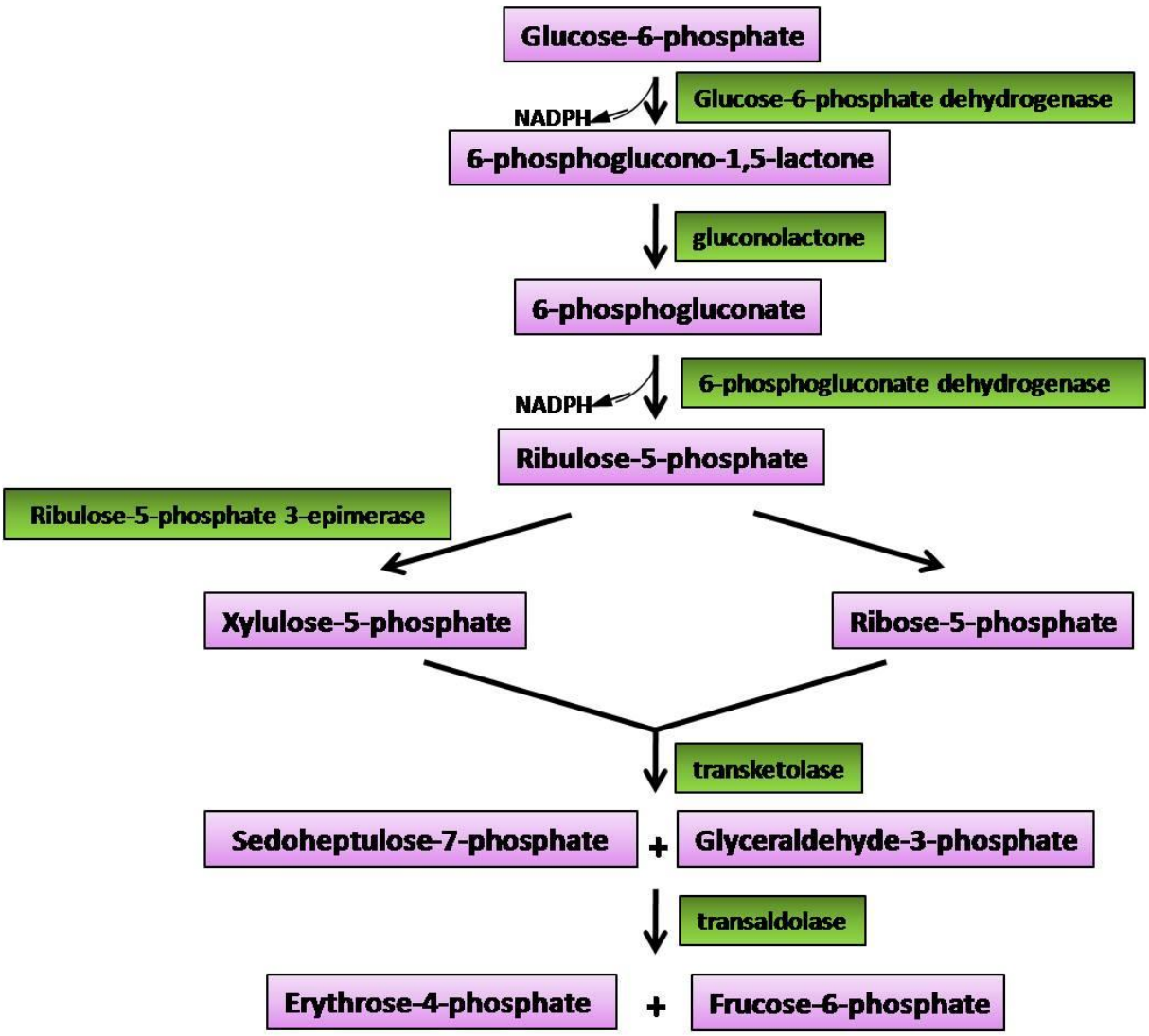

Figure 1.13: A schematic representation of the pentose phosphate pathway.

1.9 HEXOSAMINE BIOSYNTHETIC PATHWAY

Under normal conditions approximately 3% of the total glucose is diverted into the HBP [161]. In T2DM there is increased FFA availability and a decreased rate of pyruvate oxidation by PDH inhibition, i.e. the Randle effect [116]. Additionally, there is decreased entry of fructose 6-phosphate into the glycolytic pathway due to citrate-mediated inhibition of PFK. This in turn increases fructose 6-phosphate availability to enter the HBP [161].

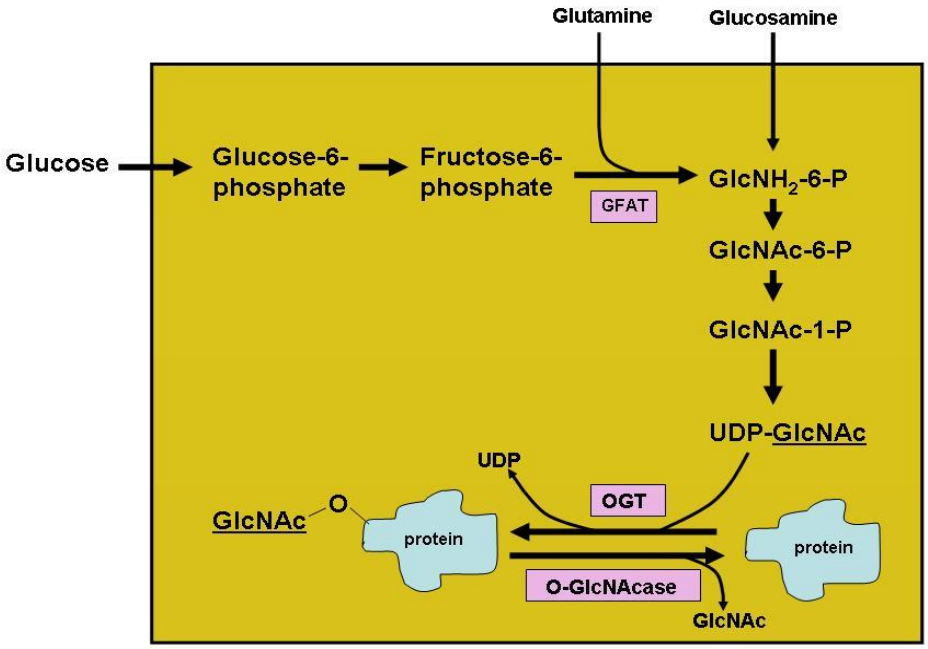

Figure 1.14: The hexosamine biosynthetic pathway. *GlcNAc: N-acetylglucosamine, GFAT: glutamine: fructose 6-phosphate amidotransferase, OGT: uridine diphospho-N-acetylglucosamine: polypeptide β-N-acetylglucosaminyltransferase.*

When fructose 6-phosphate enters the HBP the enzyme glutamine:fructose 6-phosphate amidotransferase (GFAT) converts it to glucosamine-6 phosphate (Figure 1.14). Through a series of subsequent reactions, glucosamine 6-phosphate is converted into uridine diphosphate *N*-acetyl glucosamine (UDP-GlcNAc), the end-product of the HBP. Subsequently, *N*-acetyl glucosamine is transferred in an O-linkage to specific serine and threonine residues of proteins and transcription factors, similar to the more familiar phosphorylation process [162]. In fact, the *O*-GlcNAcylation sites are identical or adjacent to known phosphorylation sites suggesting a regulatory function. The O-linkage to target proteins is carried out by *O*-GlcNAc transferase (OGT) [162]. Thus the HBP is an important regulatory pathway that functions by post-translationally modifying target proteins and altering their functions (Table 1.1) [162].

Protein	Metabolic Relevance	Species	Tissue	Residues *O*-GlcNAcylated	Effect of *O*-GlcNAc	Ref. No.
Sp1	Transcription factor. Regulates expression of multiple genes and proteins including SERCA2a, PAI-1, etc.	Rat	Neonatal rat ventricular myocytes	612-702 (Ser^{612}, Thr^{640}, Ser^{641}, Ser^{698} and $Ser^{702)}$	Decreased transcriptional activity	[163, 164]
p53	Regulates stress responses during glucose starvation	Rat, Human	Adult rat ventricular myocytes, HEK-293 cells	141-156 (Ser^{149})	Increased activity	[165, 166]
NF-κβ	Regulates promoter activation	Rat	Mesangial cells	322-352 (Thr^{322}, Thr^{352})	Increased activity	[167, 168]
IRS-1	Regulates insulin signaling	Rat, Human	Skeletal muscles, HEK-293 cells	1027-1073 (Ser^{1036})	Decreased activity	[169, 170]
PI3K	Mediates various signaling pathways	Human	Human coronary artery endothelial cells		Decreased activity and less phosphorylation	[171]
GLUT-4	Mediates glucose transport	Rat	Primary adipocytes	486-498, 469-472	Decreased translocation	[172, 173]
Akt2	Role in insulin signaling	Rat	Primary adipocytes		Decreased insulin response	[172]
Glycogen synthase	Mediates glycogen synthesis	Rat	3T3-L1 adipocytes	(Ser^{7}, Ser^{640})	Decreased activation	[174]
eNOS	Regulates vascular function	Bovine heart	Bovine aortic endothelial cells	($Ser^{1177)}$	Decreased activity	[175]
c-Myc	Transcription factor, oncogene	Human	Sf9 insect cells	53-65 (Thr^{58})	Affects transcription	[176]

Table 1.1: Some targets of *O*-GlcNAcylation and its effect on the protein.

1.9.1 HBP as a "fuel sensor"

The HBP acts as a "fuel sensor" that senses/regulates the rates of glucose and FFA flux into the cell [177]. Studies also show that HBP not only "senses" nutrients at the cellular level but also at whole body level by regulating leptin expression [177]. Nutrient availability e.g. glucose, FA, amino acids and nucleotides, modulate intracellular UDP-GlcNAc levels. For example, glucose levels regulate *O*-glycosylation on various proteins including OGT [178]. OGT is known to have altered specificity at different levels of *O*-GlcNAc, thereby suggesting a role as nutrient sensor [179]. The HBP also acts as a sensor of lipids e.g. hexosamines act as sensors to divert excess calories to be stored as fat [180].

Under a highly fed state when *O*-GlcNAc levels are high, it may have a negative feedback effect, resulting in decreased glucose uptake via the PI3/Akt/PKB or AMPK pathways [181, 182]. *O*-GlcNAc can mediate such effects by direct protein modification or indirectly by modification of transcription factors and expression levels, or by protein degradation [178]. There is considerable data showing that GFAT over expression in liver results in increased fat export to adipocytes even under lower plasma glucose levels [183]. Moreover, it also leads to increased fat accretion and hyperlipidemia in fat tissues and autoregulatory decrease in insulin-stimulated glucose uptake in muscle cells [180]. These data obtained from transgenic animal models correlate with human studies [184]. OGT homologs also exist in plants and yeast. When the OGT homolog in plants (SPINDLY) is deleted this results in tall and skinny plants which do not store starch in their roots [185]. Together these data show that the HBP is able to sense nutrient levels and direct excess nutrient intake into storage depots for later use [186].

However, with the onset of T2DM there is increased HBP flux [187]. Skeletal muscle GFAT activity is markedly increased in T2DM patients [188]. Similar studies also show that obese mice with elevated blood glucose and insulin levels exhibit higher GFAT activity [189]. In agreement, increased UDP-GlcNAc levels were found in diabetic rats [163]. *In vivo* insulin resistance was associated with impaired translocation of GLUT4 to the sarcolemma [190] proposed to occur as a result of HBP activation. Moreover, with hyperglycaemia there is also oxidative and endoplasmic reticulum stress that could also lead to insulin resistance [191]. Although this is a fairly recent mechanism recognized to play a role in pathogenesis of diabetic complications, it plays a role both in hyperglycaemia-induced abnormalities [192] and in hyperglycaemia-induced cardiomyocyte dysfunction [163].

1.10 DIABETES AND APOPTOSIS

Several studies have shown that high glucose levels cause apoptosis [193, 194] and hyperglycaemia-mediated ROS production and subsequent mitochondrial cytochrome-c release and caspase activation are strongly implicated in this process [195]. Before discussing details of the link between diabetes and apoptosis, the focus will now shift on some of the basics of apoptosis.

1.10.1 Apoptosis

Apoptosis (programmed cell death) is a highly regulated process to eliminate dysfunctional cells in the body. During this process the genome breaks, the cell shrinks and disintegrates into smaller apoptotic bodies that are then phagocytosed by macrophages before the cell contents leak into the environment [196]. This is unlike necrosis where the cell swells and bursts, releasing its contents into the environment and causing an inflammatory response (Table 1.2).

Apoptosis	Necrosis
Morphology	
➢ Membrane blebbing but no loss of integrity ➢ Aggregation of chromatin at the nuclear membrane ➢ Begins with shrinking of cytoplasm and condensation of nucleus ➢ Ends with fragmentation of cell into smaller bodies ➢ Formation of membrane-bound vesicles (apoptotic bodies) ➢ Mitochondria become leaky due to pore formation involving proteins of the Bcl-2 family	➢ Loss of membrane integrity ➢ Begins with swelling of cytoplasm and mitochondria ➢ No vesicle formation, complete lysis ➢ Disintegration (swelling) of organelles
Biochemical Features	
➢ Well regulated enzymatic steps ➢ Energy (ATP)-dependent (active process, does not occur at lower temperatures) ➢ Non-random length fragmentation of DNA (Ladder pattern in agarose gel) ➢ Pre-lytic DNA fragmentation ➢ Cytochrome-c/AIF release by mitochondria into cytoplasm ➢ Activation of caspase cascade ➢ Alterations in membrane symmetry (phosphatidyl serine from cytoplasmic to extracellular side of membrane)	➢ Loss of regulation of ion homeostasis ➢ No energy required (passive process, can occur at 4°C) ➢ Random digestion of DNA (smear of DNA in agarose gel) ➢ Post-lytic DNA fragmentation (late event death)
Physiological Significance	
➢ Affects individual cells ➢ Induced by physiological stimuli (lack of growth hormone) ➢ Phagocytosis by adjacent cells or macrophages ➢ No inflammatory response	➢ Affects groups of cells ➢ Induced by non-physiological stimuli (lytic virus, hypothermia, hypoxia, ischemia) ➢ Phagocytosis by macrophages ➢ Significant inflammatory response

Table 1.2: Differences between apoptosis and necrosis

Apoptosis can be triggered in 2 ways i.e. (1) extrinsic and (2) intrinsic pathways [196]. Extrinsic apoptosis is initiated by transmembrane death receptors such as Fas, while the intrinsic pathway is triggered by signals released from organelles, e.g. mitochondria [196].

The extrinsic pathway is triggered by signal molecules (ligands) that are released by other cells. For example, Fas ligand (FasL) binds to transmembrane death receptors of the target cell and induce apoptosis [197]. When ligands bind to death receptors on target cells, it triggers various receptors to aggregate on the cell surface. These aggregated receptors recruit an adaptor protein known as the death domain (DD) protein which in turn recruits caspase-8 to the complex making it a death-inducing signal complex (DISC) (Figure 1.15). Caspase-8 (an initiator protein) subsequently activates caspase-3, an effector protein, thereby initiating cell death [197].

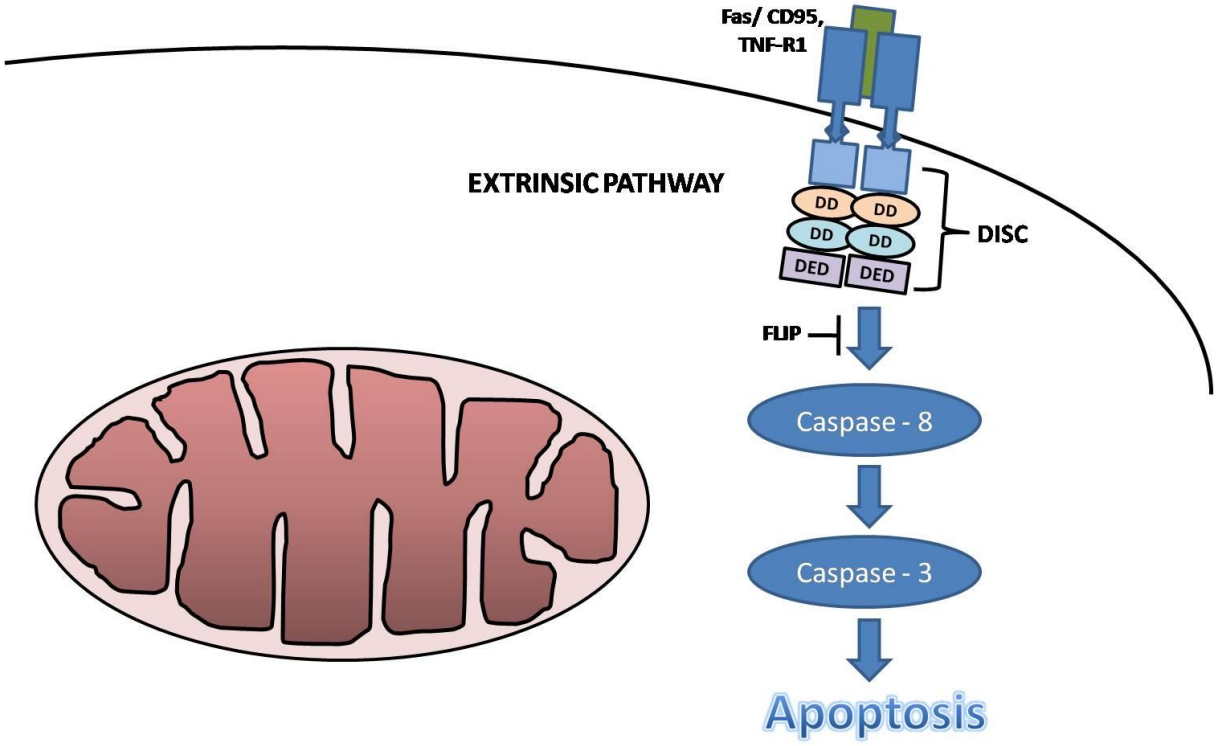

Figure 1.15: A schematic representation of extrinsic apoptotic pathway. *DD: Death domain; DISC: Death-inducing signal complex; DED: Death effector domain; FLIP: FADD-like IL-1β-converting enzyme (FLICE)-inhibitory protein.*

As the name suggests, the intrinsic pathway is triggered by intracellular stress, specifically mitochondrial stress [198]. In response to a stress signal, pro-apoptotic proteins in the cytoplasm e.g. Bax bind to the outer membrane of mitochondria and trigger the release of mitochondrial

contents and cytochrome-c (Figure 1.16) [198]. Following this, cytochrome-c forms a complex with ATP and Apaf-1 in the cytoplasm. This activates caspase-9 that joins the complex and forms an apoptosome that activates caspase-3 to initiate cellular degradation [198].

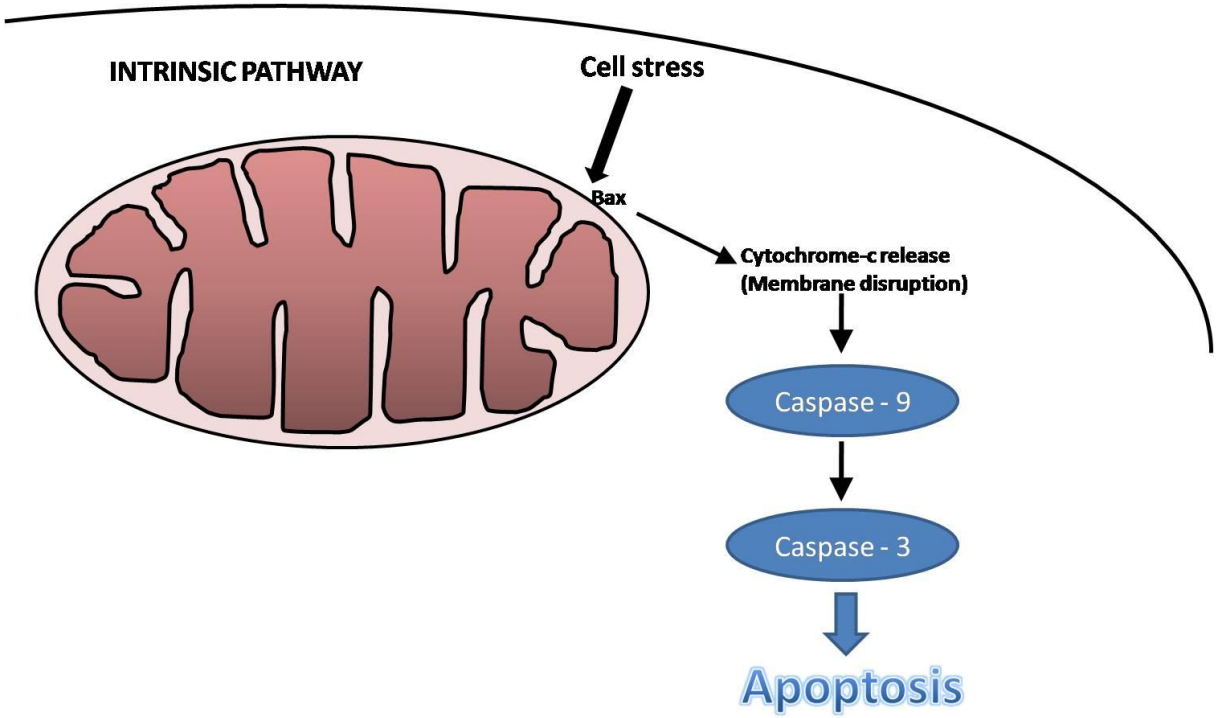

Figure 1.16: A schematic representation of intrinsic apoptotic pathway.

In the context of this thesis, disruption of the mitochondrial membrane plays a key role in mediating the intrinsic apoptotic pathway. Activation of pro-apoptotic proteins BAD and Bax and inactivation of anti-apoptotic protein Bcl-2 are involved in this process [199]. Here phosphorylated BAD can dimerize with the 14.3.3 protein and prevent the usual apoptotic cascade. When BAD is dephosphorylated it carries out its pro-apoptotic function by dimerizing with Bcl-2 (Figure 1.17) [199]. Bcl-2 is inactivated upon dimerization and is unable to perform its anti-apoptotic function, i.e. binding Bax to prevent it from disrupting the mitochondrial membrane. Hence Bax is now able form homodimers, insert into the mitochondrial membrane

and subsequently cause membrane disruption and release of mitochondrial contents and cytochrome-c, thereby leading to intrinsic cell death [200].

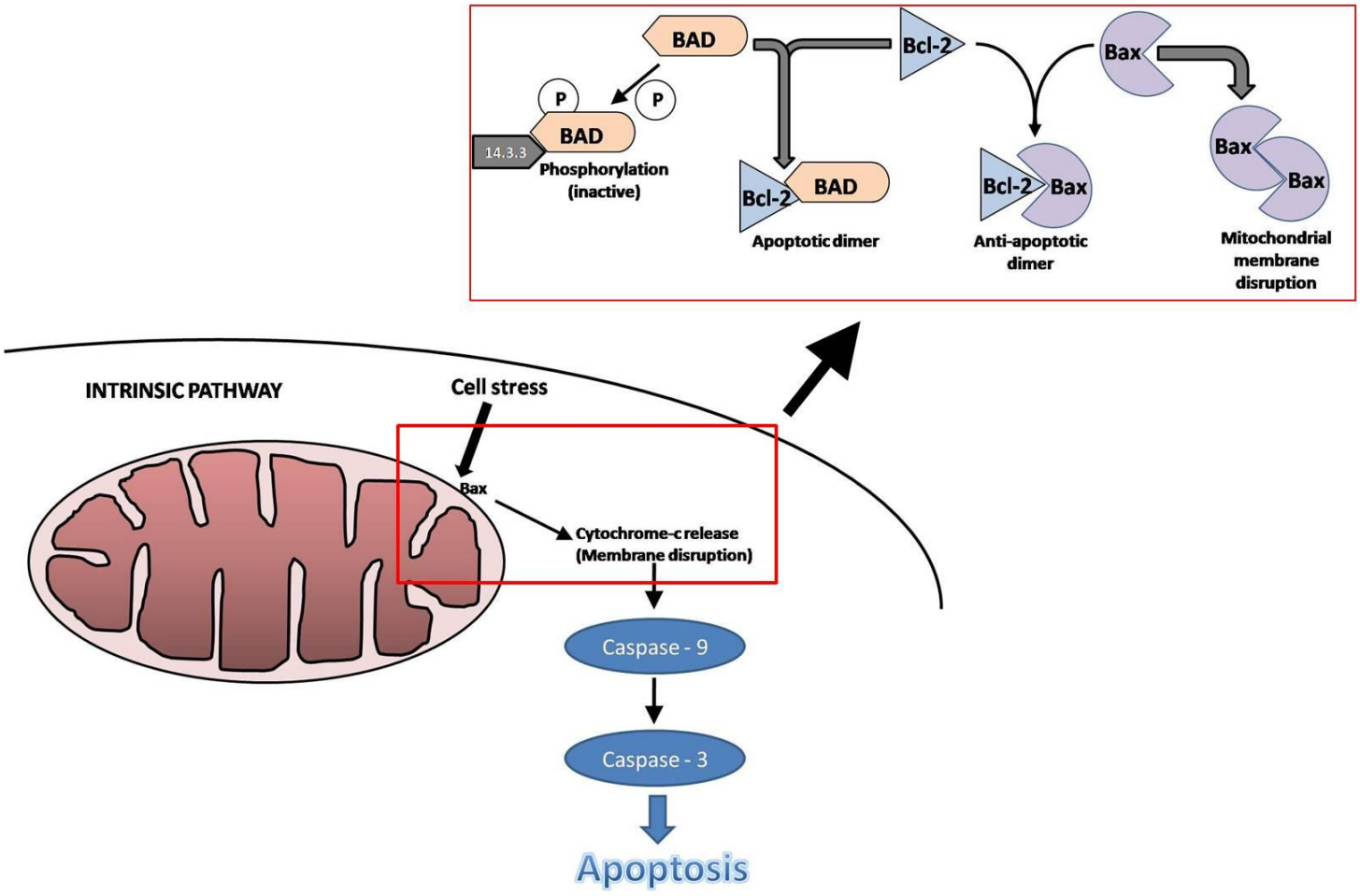

Figure 1.17: Diagram representing the mechanism behind mitochondrial membrane disruption.

For this thesis, we focused on ways to measure the intrinsic mode of apoptosis triggered by hyperglycaemia, as diabetes-mediated apoptosis largely occurs due to intracellular signals deriving from organelles like the mitochondria.

1.10.2 Hyperglycaemia-mediated apoptosis

With diabetes there is increased cellular stress which leads to altered fuel intake and increased ROS production and glucotoxicity as explained earlier. Apoptosis is an important contributor to heart failure in patients with diabetes [201]. An early response of myocardial cells to hyperglycaemia includes metabolic remodeling, sub cellular defects and abnormal expression of genes, all of which may eventually contribute to cardiac cell death [193]. In agreement, previous studies show that hyperglycaemia mediates apoptosis [193, 194]. For example, human umbilical vein endothelial cells exposed to 30 mM glucose for 72 hours exhibited increased apoptosis [202]. Moreover, aortic endothelial cells exposed to 30 mM glucose culturing conditions displayed greater glucose oxidation, increased superoxide production [24] and DNA damage. PARP is subsequently activated [129] resulting in apoptosis [203]. hyperglycaemia may also act as a stress signal, resulting in cytochrome-c release, the activation of caspase-3 [193] and apoptosis. Moreover, apoptotic cell death in response to hyperglycaemia may be dose-dependent indicating a greater degree of apoptosis with higher glucose levels [193]. As mentioned in Section 1.8, hyperglycaemia-induced apoptosis may be mediated by various pathways including the pentose phosphate pathway, polyol pathway, PKC activation and AGEs. Furthermore, studies show that the HBP also plays a role in apoptosis [204] - this forms the basis of my research project.

Although the HBP is a contributor to cell death during diabetes [204], the exact mechanisms underlying this process in the heart are unclear. Interestingly, studies have shown that *O*-

GlcNAcylation of certain proteins can lead to increased apoptosis. For example, hyperglycaemia-induced HBP flux leads to greater *O*-GlcNAcylation of p53 resulting in increased angiotensin synthesis and apoptosis [165]. Others have also reported that decreased levels of BAD, a pro-apoptotic Bcl-2 homolog, may be implicated in HBP-mediated pancreatic β–cell death [205]. However, despite these advances the underlying mechanisms mediating hyperglycaemia-mediated myocardial cell death are still poorly defined.

1.11 HYPOTHESIS

Within the diabetic setting there is increased onset of CVD [8-10] associated with elevated intracellular oxidative stress [118-120]. This leads to increased HBP flux and "glucose toxicity" [188] proposed to occur via increased *O*-GlcNAc modification of target proteins [129]. Since elevated intracellular oxidative stress and greater HBP flux are robustly associated with the diabetic phenotype, **we hypothesized that higher oxidative stress under hyperglycaemic conditions causes greater *O*-GlcNAcylation of BAD, thereby increasing myocardial apoptosis.**

1.12 AIMS

1. Establish an *in vitro* model of hyperglycaemia-induced apoptosis
2. Evaluate oxidative stress in response to hyperglycaemia
3. Assess the role of the HBP in hyperglycaemia-mediated apoptosis
4. Determine the degree of BAD *O*-GlcNAcylation with hyperglycaemia
5. Test our hypothesis in hearts of a rat model of hyperglycaemia/insulin resistance

References for Introduction

1. King, H., R.E. Aubert, and W.H. Herman, *Global burden of diabetes, 1995-2025: prevalence, numerical estimates, and projections.* Diabetes Care, 1998. 21(9): p. 1414-31.

2. Boudina, S. and E.D. Abel, *Diabetic cardiomyopathy revisited.* Circulation, 2007. 115(25): p. 3213-23.

3. Wild, S., et al., *Global prevalence of diabetes: estimates for the year 2000 and projections for 2030.* Diabetes Care, 2004. 27(5): p. 1047-53.

4. Morino, K., K.F. Petersen, and G.I. Shulman, *Molecular mechanisms of insulin resistance in humans and their potential links with mitochondrial dysfunction.* Diabetes, 2006. 55 Suppl 2: p. S9-S15.

5. Ford, E.S., W.H. Giles, and A.H. Mokdad, *Increasing prevalence of the metabolic syndrome among u.s. Adults.* Diabetes Care, 2004. 27(10): p. 2444-9.

6. Smith, C. and M.F. Essop, *Gender differences in metabolic risk factor prevalence in a South African student population.* Cardiovasc J Afr, 2009. 20(3): p. 178-82.

7. Pradeepa, R., R. Deepa, and V. Mohan, *Epidemiology of diabetes in India--current perspective and future projections.* J Indian Med Assoc, 2002. 100(3): p. 144-8.

8. Garcia, M.J., et al., *Morbidity and mortality in diabetics in the Framingham population. Sixteen year follow-up study.* Diabetes, 1974. 23(2): p. 105-11.

9. Saydah, S.H., et al., *Age and the burden of death attributable to diabetes in the United States.* Am J Epidemiol, 2002. 156(8): p. 714-9.

10. Morgan, C.L., C.J. Currie, and J.R. Peters, *Relationship between diabetes and mortality: a population study using record linkage.* Diabetes Care, 2000. 23(8): p. 1103-7.

11. Blann, A.D., et al., *Vascular endothelial growth factor and its receptor, Flt-1, in the plasma of patients with coronary or peripheral atherosclerosis, or Type II diabetes.* Clin Sci (Lond), 2002. 102(2): p. 187-94.

12. Pecoraro, R.E., G.E. Reiber, and E.M. Burgess, *Pathways to diabetic limb amputation. Basis for prevention.* Diabetes Care, 1990. 13(5): p. 513-21.

13. Iltis, I., et al., *Noninvasive characterization of myocardial blood flow in diabetic, hypertensive, and diabetic-hypertensive rats using spin-labeling MRI.* Microcirculation, 2005. 12(8): p. 607-14.

14. Fein, F.S., *Diabetic cardiomyopathy.* Diabetes Care, 1990. 13(11): p. 1169-79.

15. Botker, H.E., et al., *Determination of high energy phosphates and glycogen in cardiac and skeletal muscle biopsies, with special reference to influence of biopsy technique and delayed freezing.* Cardiovasc Res, 1994. 28(4): p. 524-7.

16. Rubler, S., et al., *New type of cardiomyopathy associated with diabetic glomerulosclerosis.* Am J Cardiol, 1972. 30(6): p. 595-602.

17. Devereux, R.B., et al., *Impact of diabetes on cardiac structure and function: the strong heart study.* Circulation, 2000. 101(19): p. 2271-6.

18. Bell, D.S., *Heart failure: the frequent, forgotten, and often fatal complication of diabetes.* Diabetes Care, 2003. 26(8): p. 2433-41.

19. Ho, K.K., et al., *The epidemiology of heart failure: the Framingham Study.* J Am Coll Cardiol, 1993. 22(4 Suppl A): p. 6A-13A.

20. Kannel, W.B., M. Hjortland, and W.P. Castelli, *Role of diabetes in congestive heart failure: the Framingham study.* Am J Cardiol, 1974. 34(1): p. 29-34.

21. Poornima, I.G., P. Parikh, and R.P. Shannon, *Diabetic cardiomyopathy: the search for a unifying hypothesis.* Circ Res, 2006. 98(5): p. 596-605.

22. Capes, S.E., et al., *Stress hyperglycaemia and increased risk of death after myocardial infarction in patients with and without diabetes: a systematic overview.* Lancet, 2000. 355(9206): p. 773-8.

23. Ingelsson, E., et al., *Insulin resistance and risk of congestive heart failure.* JAMA, 2005. 294(3): p. 334-41.

24. Nishikawa, T., et al., *Normalizing mitochondrial superoxide production blocks three pathways of hyperglycaemic damage.* Nature, 2000. 404(6779): p. 787-90.

25. Masoudi, F.A. and S.E. Inzucchi, *Diabetes mellitus and heart failure: epidemiology, mechanisms, and pharmacotherapy.* Am J Cardiol, 2007. 99(4A): p. 113B-132B.

26. Fang, Z.Y., J.B. Prins, and T.H. Marwick, *Diabetic cardiomyopathy: evidence, mechanisms, and therapeutic implications.* Endocr Rev, 2004. 25(4): p. 543-67.

27. Marwick, T.H., *Diabetic heart disease.* Heart, 2006. 92(3): p. 296-300.

28. Banerjee, S. and L.R. Peterson, *Myocardial metabolism and cardiac performance in obesity and insulin resistance.* Curr Cardiol Rep, 2007. 9(2): p. 143-9.

29. **Diamant, M., et al.,** ***Diastolic dysfunction is associated with altered myocardial metabolism in asymptomatic normotensive patients with well-controlled type 2 diabetes mellitus.*** **J Am Coll Cardiol, 2003. 42(2): p. 328-35.**

30. **Picano, E.,** ***Diabetic cardiomyopathy. the importance of being earliest.*** **J Am Coll Cardiol, 2003. 42(3): p. 454-7.**

31. **Galderisi, M.,** ***Diastolic dysfunction and diabetic cardiomyopathy: evaluation by Doppler echocardiography.*** **J Am Coll Cardiol, 2006. 48(8): p. 1548-51.**

32. **Stanley, W.C., et al.,** ***Acute myocardial ischemia causes a transmural gradient in glucose extraction but not glucose uptake.*** **Am J Physiol, 1992. 262(1 Pt 2): p. H91-6.**

33. **Henning, S.L., et al.,** ***Contribution of glycogen to aerobic myocardial glucose utilization.*** **Circulation, 1996. 93(8): p. 1549-55.**

34. **Stanley, W.C., et al.,** ***Regulation of myocardial carbohydrate metabolism under normal and ischaemic conditions. Potential for pharmacological interventions.*** **Cardiovasc Res, 1997. 33(2): p. 243-57.**

35. **Kruszynska, Y.T., J.G. McCormack, and N. McIntyre,** ***Effects of glycogen stores and non-esterified fatty acid availability on insulin-stimulated glucose metabolism and tissue pyruvate dehydrogenase activity in the rat.*** **Diabetologia, 1991. 34(4): p. 205-11.**

36. **Laughlin, M.R., et al.,** ***Nonglucose substrates increase glycogen synthesis in vivo in dog heart.*** **Am J Physiol, 1994. 267(1 Pt 2): p. H219-23.**

37. **Goldfarb, A.H., J.F. Bruno, and P.J. Buckenmeyer,** ***Intensity and duration effects of exercise on heart cAMP, phosphorylase, and glycogen.*** **J Appl Physiol, 1986. 60(4): p. 1268-73.**

38. **Hue, L., et al.,** ***Regulation of glucose metabolism in cardiac muscle.*** **Biochem Soc Trans, 1995. 23(2): p. 311-4.**

39. **Young, L.H., D.L. Coven, and R.R. Russell, 3rd,** ***Cellular and molecular regulation of cardiac glucose transport.*** **J Nucl Cardiol, 2000. 7(3): p. 267-76.**

40. **Young, L.H., et al.,** ***Low-flow ischemia leads to translocation of canine heart GLUT-4 and GLUT-1 glucose transporters to the sarcolemma in vivo.*** **Circulation, 1997. 95(2): p. 415-22.**

41. **Russell, R.R., 3rd, et al.,** ***Translocation of myocardial GLUT-4 and increased glucose uptake through activation of AMPK by AICAR.*** **Am J Physiol, 1999. 277(2 Pt 2): p. H643-9.**

42. **Coven, D.L., et al.,** ***Physiological role of AMP-activated protein kinase in the heart: graded activation during exercise.*** **Am J Physiol Endocrinol Metab, 2003. 285(3): p. E629-36.**

43. **Russell, R.R., 3rd, et al., *AMP-activated protein kinase mediates ischemic glucose uptake and prevents postischemic cardiac dysfunction, apoptosis, and injury.* J Clin Invest, 2004. 114(4): p. 495-503.**

44. **Arad, M., et al., *Transgenic mice overexpressing mutant PRKAG2 define the cause of Wolff-Parkinson-White syndrome in glycogen storage cardiomyopathy.* Circulation, 2003. 107(22): p. 2850-6.**

45. **Xing, Y., et al., *Glucose metabolism and energy homeostasis in mouse hearts overexpressing dominant negative alpha2 subunit of AMP-activated protein kinase.* J Biol Chem, 2003. 278(31): p. 28372-7.**

46. **Arad, M., et al., *Constitutively active AMP kinase mutations cause glycogen storage disease mimicking hypertrophic cardiomyopathy.* J Clin Invest, 2002. 109(3): p. 357-62.**

47. **Gollob, M.H., *Glycogen storage disease as a unifying mechanism of disease in the PRKAG2 cardiac syndrome.* Biochem Soc Trans, 2003. 31(Pt 1): p. 228-31.**

48. **Polekhina, G., et al., *AMPK beta subunit targets metabolic stress sensing to glycogen.* Curr Biol, 2003. 13(10): p. 867-71.**

49. **Longnus, S.L., et al., *5-Aminoimidazole-4-carboxamide 1-beta -D-ribofuranoside (AICAR) stimulates myocardial glycogenolysis by allosteric mechanisms.* Am J Physiol Regul Integr Comp Physiol, 2003. 284(4): p. R936-44.**

50. **Hue, L., et al., *New targets of AMP-activated protein kinase.* Biochem Soc Trans, 2003. 31(Pt 1): p. 213-5.**

51. **Marsin, A.S., et al., *Phosphorylation and activation of heart PFK-2 by AMPK has a role in the stimulation of glycolysis during ischaemia.* Curr Biol, 2000. 10(20): p. 1247-55.**

52. **Hue, L. and M.H. Rider, *Role of fructose 2,6-bisphosphate in the control of glycolysis in mammalian tissues.* Biochem J, 1987. 245(2): p. 313-24.**

53. **Stanley, W.C., F.A. Recchia, and G.D. Lopaschuk, *Myocardial substrate metabolism in the normal and failing heart.* Physiol Rev, 2005. 85(3): p. 1093-129.**

54. **Stanley, W.C., G.D. Lopaschuk, and J.G. McCormack, *Regulation of energy substrate metabolism in the diabetic heart.* Cardiovasc Res, 1997. 34(1): p. 25-33.**

55. **Hall, J.L., et al., *Impaired pyruvate oxidation but normal glucose uptake in diabetic pig heart during dobutamine-induced work.* Am J Physiol, 1996. 271(6 Pt 2): p. H2320-9.**

56. **Avogaro, A., et al., *Myocardial metabolism in insulin-deficient diabetic humans without coronary artery disease.* Am J Physiol, 1990. 258(4 Pt 1): p. E606-18.**

57. **Depre, C., M.H. Rider, and L. Hue, *Mechanisms of control of heart glycolysis.* Eur J Biochem, 1998. 258(2): p. 277-90.**

58. **Swanton, E.M. and E.D. Saggerson, *Effects of adrenaline on triacylglycerol synthesis and turnover in ventricular myocytes from adult rats.* Biochem J, 1997. 328 (Pt 3): p. 913-22.**

59. **Lopaschuk, G.D., et al., *Regulation of fatty acid oxidation in the mammalian heart in health and disease.* Biochim Biophys Acta, 1994. 1213(3): p. 263-76.**

60. **Bing, R.J., et al., *Metabolism of the human heart. II. Studies on fat, ketone and amino acid metabolism.* Am J Med, 1954. 16(4): p. 504-15.**

61. **Wisneski, J.A., et al., *Myocardial metabolism of free fatty acids. Studies with 14C-labeled substrates in humans.* J Clin Invest, 1987. 79(2): p. 359-66.**

62. **Lopaschuk, G.D., et al., *Plasma fatty acid levels in infants and adults after myocardial ischemia.* Am Heart J, 1994. 128(1): p. 61-7.**

63. **Merkel, M., R.H. Eckel, and I.J. Goldberg, *Lipoprotein lipase: genetics, lipid uptake, and regulation.* J Lipid Res, 2002. 43(12): p. 1997-2006.**

64. **Augustus, A.S., et al., *Routes of FA delivery to cardiac muscle: modulation of lipoprotein lipolysis alters uptake of TG-derived FA.* Am J Physiol Endocrinol Metab, 2003. 284(2): p. E331-9.**

65. **Yagyu, H., et al., *Lipoprotein lipase (LpL) on the surface of cardiomyocytes increases lipid uptake and produces a cardiomyopathy.* J Clin Invest, 2003. 111(3): p. 419-26.**

66. **Yokoyama, M., et al., *Apolipoprotein B production reduces lipotoxic cardiomyopathy: studies in heart-specific lipoprotein lipase transgenic mouse.* J Biol Chem, 2004. 279(6): p. 4204-11.**

67. **van der Vusse, G.J., M. van Bilsen, and J.F. Glatz, *Cardiac fatty acid uptake and transport in health and disease.* Cardiovasc Res, 2000. 45(2): p. 279-93.**

68. **Schaffer, J.E., *Fatty acid transport: the roads taken.* Am J Physiol Endocrinol Metab, 2002. 282(2): p. E239-46.**

69. **Glatz, J.F., J.J. Luiken, and A. Bonen, *Involvement of membrane-associated proteins in the acute regulation of cellular fatty acid uptake.* J Mol Neurosci, 2001. 16(2-3): p. 123-32; discussion 151-7.**

70. **Kintaka, T., et al., *CD36 genotype and long-chain fatty acid uptake in the heart.* Circ J, 2002. 66(9): p. 819-25.**

71. **Luiken, J.J., et al., *Regulation of cardiac long-chain fatty acid and glucose uptake by translocation of substrate transporters.* Pflugers Arch, 2004. 448(1): p. 1-15.**

72. **Luiken, J.J., et al.,** ***Contraction-induced fatty acid translocase/CD36 translocation in rat cardiac myocytes is mediated through AMP-activated protein kinase signaling.*** **Diabetes, 2003. 52(7): p. 1627-34.**

73. **Luiken, J.J., et al.,** ***Electrostimulation enhances FAT/CD36-mediated long-chain fatty acid uptake by isolated rat cardiac myocytes.*** **Am J Physiol Endocrinol Metab, 2001. 281(4): p. E704-12.**

74. **Kunau, W.H., V. Dommes, and H. Schulz,** ***beta-oxidation of fatty acids in mitochondria, peroxisomes, and bacteria: a century of continued progress.*** **Prog Lipid Res, 1995. 34(4): p. 267-342.**

75. **Schulz, H.,** ***Regulation of fatty acid oxidation in heart.*** **J Nutr, 1994. 124(2): p. 165-71.**

76. **Kerner, J. and C. Hoppel,** ***Fatty acid import into mitochondria.*** **Biochim Biophys Acta, 2000. 1486(1): p. 1-17.**

77. **McGarry, J.D., et al.,** ***Observations on the affinity for carnitine, and malonyl-CoA sensitivity, of carnitine palmitoyltransferase I in animal and human tissues. Demonstration of the presence of malonyl-CoA in non-hepatic tissues of the rat.*** **Biochem J, 1983. 214(1): p. 21-8.**

78. **McGarry, J.D. and N.F. Brown,** ***The mitochondrial carnitine palmitoyltransferase system. From concept to molecular analysis.*** **Eur J Biochem, 1997. 244(1): p. 1-14.**

79. **Weis, B.C., et al.,** ***Use of a selective inhibitor of liver carnitine palmitoyltransferase I (CPT I) allows quantification of its contribution to total CPT I activity in rat heart. Evidence that the dominant cardiac CPT I isoform is identical to the skeletal muscle enzyme.*** **J Biol Chem, 1994. 269(42): p. 26443-8.**

80. **Zammit, V.A., F. Fraser, and C.G. Orstorphine,** ***Regulation of mitochondrial outer-membrane carnitine palmitoyltransferase (CPT I): role of membrane-topology.*** **Adv Enzyme Regul, 1997. 37: p. 295-317.**

81. **Abu-Elheiga, L., et al.,** ***Continuous fatty acid oxidation and reduced fat storage in mice lacking acetyl-CoA carboxylase 2.*** **Science, 2001. 291(5513): p. 2613-6.**

82. **Hall, J.L., et al.,** ***Increased cardiac fatty acid uptake with dobutamine infusion in swine is accompanied by a decrease in malonyl CoA levels.*** **Cardiovasc Res, 1996. 32(5): p. 879-85.**

83. **Kudo, N., et al.,** ***High rates of fatty acid oxidation during reperfusion of ischemic hearts are associated with a decrease in malonyl-CoA levels due to an increase in 5'-AMP-activated protein kinase inhibition of acetyl-CoA carboxylase.*** **J Biol Chem, 1995. 270(29): p. 17513-20.**

84. **Saddik, M., et al.,** ***Acetyl-CoA carboxylase regulation of fatty acid oxidation in the heart.*** **J Biol Chem, 1993. 268(34): p. 25836-45.**

85. **Stanley, W.C., et al.,** ***Pyruvate dehydrogenase activity and malonyl CoA levels in normal and ischemic swine myocardium: effects of dichloroacetate.*** **J Mol Cell Cardiol, 1996. 28(5): p. 905-14.**

86. **Reszko, A.E., et al.,** ***Assay of the concentration and 13C-isotopic enrichment of malonyl-coenzyme A by gas chromatography-mass spectrometry.*** **Anal Biochem, 2001. 298(1): p. 69-75.**

87. **Reszko, A.E., et al.,** ***Regulation of malonyl-CoA concentration and turnover in the normal heart.*** **J Biol Chem, 2004. 279(33): p. 34298-301.**

88. **Goodwin, G.W. and H. Taegtmeyer,** ***Regulation of fatty acid oxidation of the heart by MCD and ACC during contractile stimulation.*** **Am J Physiol, 1999. 277(4 Pt 1): p. E772-7.**

89. **Dyck, J.R., et al.,** ***Phosphorylation control of cardiac acetyl-CoA carboxylase by cAMP-dependent protein kinase and 5'-AMP activated protein kinase.*** **Eur J Biochem, 1999. 262(1): p. 184-90.**

90. **Dyck, J.R. and G.D. Lopaschuk,** ***Malonyl CoA control of fatty acid oxidation in the ischemic heart.*** **J Mol Cell Cardiol, 2002. 34(9): p. 1099-109.**

91. **Boxma, B., et al.,** ***An anaerobic mitochondrion that produces hydrogen.*** **Nature, 2005. 434(7029): p. 74-9.**

92. **Hirst, J.,** ***Energy transduction by respiratory complex I--an evaluation of current knowledge.*** **Biochem Soc Trans, 2005. 33(Pt 3): p. 525-9.**

93. **Yankovskaya, V., et al.,** ***Architecture of succinate dehydrogenase and reactive oxygen species generation.*** **Science, 2003. 299(5607): p. 700-4.**

94. **Horsefield, R., S. Iwata, and B. Byrne,** ***Complex II from a structural perspective.*** **Curr Protein Pept Sci, 2004. 5(2): p. 107-18.**

95. **Berry, E.A., et al.,** ***Structure and function of cytochrome bc complexes.*** **Annu Rev Biochem, 2000. 69: p. 1005-75.**

96. **Crofts, A.R.,** ***The cytochrome bc1 complex: function in the context of structure.*** **Annu Rev Physiol, 2004. 66: p. 689-733.**

97. **Calhoun, M.W., J.W. Thomas, and R.B. Gennis,** ***The cytochrome oxidase superfamily of redox-driven proton pumps.*** **Trends Biochem Sci, 1994. 19(8): p. 325-30.**

98. **Koopman, W.J., et al.,** ***Inhibition of complex I of the electron transport chain causes O2-. -mediated mitochondrial outgrowth.*** **Am J Physiol Cell Physiol, 2005. 288(6): p. C1440-50.**

99. **Cecchini, G.,** ***Function and structure of complex II of the respiratory chain.*** **Annu Rev Biochem, 2003. 72: p. 77-109.**

100. Randle, P.J., et al., *The glucose fatty-acid cycle. Its role in insulin sensitivity and the metabolic disturbances of diabetes mellitus.* Lancet, 1963. 1(7285): p. 785-9.

101. Randle, P.J., E.A. Newsholme, and P.B. Garland, *Regulation of glucose uptake by muscle. 8. Effects of fatty acids, ketone bodies and pyruvate, and of alloxan-diabetes and starvation, on the uptake and metabolic fate of glucose in rat heart and diaphragm muscles.* Biochem J, 1964. 93(3): p. 652-65.

102. Shulman, G.I., *Cellular mechanisms of insulin resistance.* J Clin Invest, 2000. 106(2): p. 171-6.

103. Liu, B., et al., *Cardiac efficiency is improved after ischemia by altering both the source and fate of protons.* Circ Res, 1996. 79(5): p. 940-8.

104. Lopaschuk, G.D., *Metabolic abnormalities in the diabetic heart.* Heart Fail Rev, 2002. 7(2): p. 149-59.

105. Taegtmeyer, H., P. McNulty, and M.E. Young, *Adaptation and maladaptation of the heart in diabetes: Part I: general concepts.* Circulation, 2002. 105(14): p. 1727-33.

106. Carley, A.N. and D.L. Severson, *Fatty acid metabolism is enhanced in type 2 diabetic hearts.* Biochim Biophys Acta, 2005. 1734(2): p. 112-26.

107. McGavock, J.M., et al., *Adiposity of the heart, revisited.* Ann Intern Med, 2006. 144(7): p. 517-24.

108. Sharma, S., et al., *Intramyocardial lipid accumulation in the failing human heart resembles the lipotoxic rat heart.* FASEB J, 2004. 18(14): p. 1692-700.

109. Szczepaniak, L.S., et al., *Myocardial triglycerides and systolic function in humans: in vivo evaluation by localized proton spectroscopy and cardiac imaging.* Magn Reson Med, 2003. 49(3): p. 417-23.

110. Zhou, Y.T., et al., *Lipotoxic heart disease in obese rats: implications for human obesity.* Proc Natl Acad Sci U S A, 2000. 97(4): p. 1784-9.

111. Cannon, B. and J. Nedergaard, *The biochemistry of an inefficient tissue: brown adipose tissue.* Essays Biochem, 1985. 20: p. 110-64.

112. Cadenas, S., et al., *The basal proton conductance of skeletal muscle mitochondria from transgenic mice overexpressing or lacking uncoupling protein-3.* J Biol Chem, 2002. 277(4): p. 2773-8.

113. Skulachev, V.P., *Anion carriers in fatty acid-mediated physiological uncoupling.* J Bioenerg Biomembr, 1999. 31(5): p. 431-45.

114. Echtay, K.S., et al., *A signalling role for 4-hydroxy-2-nonenal in regulation of mitochondrial uncoupling.* EMBO J, 2003. 22(16): p. 4103-10.

115. **Boudina, S., et al., *Reduced mitochondrial oxidative capacity and increased mitochondrial uncoupling impair myocardial energetics in obesity.* Circulation, 2005. 112(17): p. 2686-95.**

116. **Randle, P.J., A.L. Kerbey, and J. Espinal, *Mechanisms decreasing glucose oxidation in diabetes and starvation: role of lipid fuels and hormones.* Diabetes Metab Rev, 1988. 4(7): p. 623-38.**

117. **Finkel, T. and N.J. Holbrook, *Oxidants, oxidative stress and the biology of ageing.* Nature, 2000. 408(6809): p. 239-47.**

118. **Baynes, J.W. and S.R. Thorpe, *Role of oxidative stress in diabetic complications: a new perspective on an old paradigm.* Diabetes, 1999. 48(1): p. 1-9.**

119. **Ceriello, A., *Oxidative stress and glycemic regulation.* Metabolism, 2000. 49(2 Suppl 1): p. 27-9.**

120. **Baynes, J.W., *Role of oxidative stress in development of complications in diabetes.* Diabetes, 1991. 40(4): p. 405-12.**

121. **Jiang, Z.Y., A.C. Woollard, and S.P. Wolff, *Hydrogen peroxide production during experimental protein glycation.* FEBS Lett, 1990. 268(1): p. 69-71.**

122. **Wolff, S.P. and R.T. Dean, *Glucose autoxidation and protein modification. The potential role of 'autoxidative glycosylation' in diabetes.* Biochem J, 1987. 245(1): p. 243-50.**

123. **Halliwell, B. and J.M. Gutteridge, *Role of free radicals and catalytic metal ions in human disease: an overview.* Methods Enzymol, 1990. 186: p. 1-85.**

124. **Saxena, A.K., et al., *Impaired antioxidant status in diabetic rat liver. Effect of vanadate.* Biochem Pharmacol, 1993. 45(3): p. 539-42.**

125. **McLennan, S.V., et al., *Changes in hepatic glutathione metabolism in diabetes.* Diabetes, 1991. 40(3): p. 344-8.**

126. **Hogg, N., et al., *Inhibition of low-density lipoprotein oxidation by nitric oxide. Potential role in atherogenesis.* FEBS Lett, 1993. 334(2): p. 170-4.**

127. **Tsai, E.C., et al., *Reduced plasma peroxyl radical trapping capacity and increased susceptibility of LDL to oxidation in poorly controlled IDDM.* Diabetes, 1994. 43(8): p. 1010-4.**

128. **Kawamura, M., J.W. Heinecke, and A. Chait, *Pathophysiological concentrations of glucose promote oxidative modification of low density lipoprotein by a superoxide-dependent pathway.* J Clin Invest, 1994. 94(2): p. 771-8.**

129. **Du, X., et al., *Inhibition of GAPDH activity by poly(ADP-ribose) polymerase activates three major pathways of hyperglycemic damage in endothelial cells.* J Clin Invest, 2003. 112(7): p. 1049-57.**

130. **Brownlee, M., *Biochemistry and molecular cell biology of diabetic complications.* Nature, 2001. 414(6865): p. 813-20.**

131. **Brownlee, M., *The pathobiology of diabetic complications: a unifying mechanism.* Diabetes, 2005. 54(6): p. 1615-25.**

132. **Lee, A.Y. and S.S. Chung, *Contributions of polyol pathway to oxidative stress in diabetic cataract.* FASEB J, 1999. 13(1): p. 23-30.**

133. **Hartog, J.W., et al., *Advanced glycation end-products (AGEs) and heart failure: pathophysiology and clinical implications.* Eur J Heart Fail, 2007. 9(12): p. 1146-55.**

134. **Miyata, T., et al., *Reactive carbonyl compounds related uremic toxicity ("carbonyl stress").* Kidney Int Suppl, 2001. 78: p. S25-31.**

135. **Giardino, I., D. Edelstein, and M. Brownlee, *Nonenzymatic glycosylation in vitro and in bovine endothelial cells alters basic fibroblast growth factor activity. A model for intracellular glycosylation in diabetes.* J Clin Invest, 1994. 94(1): p. 110-7.**

136. **Shinohara, M., et al., *Overexpression of glyoxalase-I in bovine endothelial cells inhibits intracellular advanced glycation endproduct formation and prevents hyperglycemia-induced increases in macromolecular endocytosis.* J Clin Invest, 1998. 101(5): p. 1142-7.**

137. **McLellan, A.C., et al., *Glyoxalase system in clinical diabetes mellitus and correlation with diabetic complications.* Clin Sci (Lond), 1994. 87(1): p. 21-9.**

138. **Charonis, A.S., et al., *Laminin alterations after in vitro nonenzymatic glycosylation.* Diabetes, 1990. 39(7): p. 807-14.**

139. **Doi, T., et al., *Receptor-specific increase in extracellular matrix production in mouse mesangial cells by advanced glycosylation end products is mediated via platelet-derived growth factor.* Proc Natl Acad Sci U S A, 1992. 89(7): p. 2873-7.**

140. **Li, Y.M., et al., *Molecular identity and cellular distribution of advanced glycation endproduct receptors: relationship of p60 to OST-48 and p90 to 80K-H membrane proteins.* Proc Natl Acad Sci U S A, 1996. 93(20): p. 11047-52.**

141. **Neeper, M., et al., *Cloning and expression of a cell surface receptor for advanced glycosylation end products of proteins.* J Biol Chem, 1992. 267(21): p. 14998-5004.**

142. **Smedsrod, B., et al., *Advanced glycation end products are eliminated by scavenger-receptor-mediated endocytosis in hepatic sinusoidal Kupffer and endothelial cells.* Biochem J, 1997. 322 (Pt 2): p. 567-73.**

143. **Vlassara, H., et al., *Identification of galectin-3 as a high-affinity binding protein for advanced glycation end products (AGE): a new member of the AGE-receptor complex.* Mol Med, 1995. 1(6): p. 634-46.**

144. **Abordo, E.A. and P.J. Thornalley, *Synthesis and secretion of tumour necrosis factor-alpha by human monocytic THP-1 cells and chemotaxis induced by human serum albumin derivatives modified with methylglyoxal and glucose-derived advanced glycation endproducts.* Immunol Lett, 1997. 58(3): p. 139-47.**

145. **Kirstein, M., et al., *Receptor-specific induction of insulin-like growth factor I in human monocytes by advanced glycosylation end product-modified proteins.* J Clin Invest, 1992. 90(2): p. 439-46.**

146. **Schmidt, A.M., et al., *Advanced glycation endproducts interacting with their endothelial receptor induce expression of vascular cell adhesion molecule-1 (VCAM-1) in cultured human endothelial cells and in mice. A potential mechanism for the accelerated vasculopathy of diabetes.* J Clin Invest, 1995. 96(3): p. 1395-403.**

147. **Skolnik, E.Y., et al., *Human and rat mesangial cell receptors for glucose-modified proteins: potential role in kidney tissue remodelling and diabetic nephropathy.* J Exp Med, 1991. 174(4): p. 931-9.**

148. **Vlassara, H., et al., *Cachectin/TNF and IL-1 induced by glucose-modified proteins: role in normal tissue remodeling.* Science, 1988. 240(4858): p. 1546-8.**

149. **McCarthy, A.D., S.B. Etcheverry, and A.M. Cortizo, *Effect of advanced glycation endproducts on the secretion of insulin-like growth factor-I and its binding proteins: role in osteoblast development.* Acta Diabetol, 2001. 38(3): p. 113-22.**

150. **Vlassara, H., *Recent progress in advanced glycation end products and diabetic complications.* Diabetes, 1997. 46 Suppl 2: p. S19-25.**

151. **Wautier, J.L., et al., *Advanced glycation end products (AGEs) on the surface of diabetic erythrocytes bind to the vessel wall via a specific receptor inducing oxidant stress in the vasculature: a link between surface-associated AGEs and diabetic complications.* Proc Natl Acad Sci U S A, 1994. 91(16): p. 7742-6.**

152. **Mohamed, A.K., et al., *The role of oxidative stress and NF-kappaB activation in late diabetic complications.* Biofactors, 1999. 10(2-3): p. 157-67.**

153. **Greene, D.A., et al., *Complications: neuropathy, pathogenetic considerations.* Diabetes Care, 1992. 15(12): p. 1902-25.**

154. **Hong, J.Y., et al., *Oxidant stress-induced liver injury in vivo: role of apoptosis, oncotic necrosis, and c-Jun NH2-terminal kinase activation.* Am J Physiol Gastrointest Liver Physiol, 2009. 296(3): p. G572-81.**

155. **Koya, D., et al., *Characterization of protein kinase C beta isoform activation on the gene expression of transforming growth factor-beta, extracellular matrix components, and prostanoids in the glomeruli of diabetic rats.* J Clin Invest, 1997. 100(1): p. 115-26.**

156. **Koya, D. and G.L. King, *Protein kinase C activation and the development of diabetic complications.* Diabetes, 1998. 47(6): p. 859-66.**

157. **Derubertis, F.R. and P.A. Craven, *Activation of protein kinase C in glomerular cells in diabetes. Mechanisms and potential links to the pathogenesis of diabetic glomerulopathy.* Diabetes, 1994. 43(1): p. 1-8.**

158. **Xia, P., et al., *Characterization of the mechanism for the chronic activation of diacylglycerol-protein kinase C pathway in diabetes and hypergalactosemia.* Diabetes, 1994. 43(9): p. 1122-9.**

159. **Bouche, C., et al., *The cellular fate of glucose and its relevance in type 2 diabetes.* Endocr Rev, 2004. 25(5): p. 807-30.**

160. **Larkins, R.G. and M.E. Dunlop, *The link between hyperglycaemia and diabetic nephropathy.* Diabetologia, 1992. 35(6): p. 499-504.**

161. **Hawkins, M., et al., *Role of the glucosamine pathway in fat-induced insulin resistance.* J Clin Invest, 1997. 99(9): p. 2173-82.**

162. **Buse, M.G., *Hexosamines, insulin resistance, and the complications of diabetes: current status.* Am J Physiol Endocrinol Metab, 2006. 290(1): p. E1-E8.**

163. **Clark, R.J., et al., *Diabetes and the accompanying hyperglycemia impairs cardiomyocyte calcium cycling through increased nuclear O-GlcNAcylation.* J Biol Chem, 2003. 278(45): p. 44230-7.**

164. **Chung, S.S., et al., *Activation of PPARgamma negatively regulates O-GlcNAcylation of Sp1.* Biochem Biophys Res Commun, 2008. 372(4): p. 713-8.**

165. **Fiordaliso, F., et al., *Hyperglycemia activates p53 and p53-regulated genes leading to myocyte cell death.* Diabetes, 2001. 50(10): p. 2363-75.**

166. **Yang, W.H., et al., *Modification of p53 with O-linked N-acetylglucosamine regulates p53 activity and stability.* Nat Cell Biol, 2006. 8(10): p. 1074-83.**

167. **James, L.R., et al., *Flux through the hexosamine pathway is a determinant of nuclear factor kappaB- dependent promoter activation.* Diabetes, 2002. 51(4): p. 1146-56.**

168. Yang, W.H., et al., *NFkappaB activation is associated with its O-GlcNAcylation state under hyperglycemic conditions.* Proc Natl Acad Sci U S A, 2008. 105(45): p. 17345-50.

169. Patti, M.E., et al., *Activation of the hexosamine pathway by glucosamine in vivo induces insulin resistance of early postreceptor insulin signaling events in skeletal muscle.* Diabetes, 1999. 48(8): p. 1562-71.

170. Ball, L.E., M.N. Berkaw, and M.G. Buse, *Identification of the major site of O-linked beta-N-acetylglucosamine modification in the C terminus of insulin receptor substrate-1.* Mol Cell Proteomics, 2006. 5(2): p. 313-23.

171. Federici, M., et al., *Insulin-dependent activation of endothelial nitric oxide synthase is impaired by O-linked glycosylation modification of signaling proteins in human coronary endothelial cells.* Circulation, 2002. 106(4): p. 466-72.

172. Park, S.Y., J. Ryu, and W. Lee, *O-GlcNAc modification on IRS-1 and Akt2 by PUGNAc inhibits their phosphorylation and induces insulin resistance in rat primary adipocytes.* Exp Mol Med, 2005. 37(3): p. 220-9.

173. Buse, M.G., et al., *Enhanced O-GlcNAc protein modification is associated with insulin resistance in GLUT1-overexpressing muscles.* Am J Physiol Endocrinol Metab, 2002. 283(2): p. E241-50.

174. Parker, G., et al., *Hyperglycemia and inhibition of glycogen synthase in streptozotocin-treated mice: role of O-linked N-acetylglucosamine.* J Biol Chem, 2004. 279(20): p. 20636-42.

175. Du, X.L., et al., *Hyperglycemia inhibits endothelial nitric oxide synthase activity by posttranslational modification at the Akt site.* J Clin Invest, 2001. 108(9): p. 1341-8.

176. Chou, T.Y., G.W. Hart, and C.V. Dang, *c-Myc is glycosylated at threonine 58, a known phosphorylation site and a mutational hot spot in lymphomas.* J Biol Chem, 1995. 270(32): p. 18961-5.

177. Rossetti, L., *Perspective: Hexosamines and nutrient sensing.* Endocrinology, 2000. 141(6): p. 1922-5.

178. Zachara, N.E. and G.W. Hart, *O-GlcNAc a sensor of cellular state: the role of nucleocytoplasmic glycosylation in modulating cellular function in response to nutrition and stress.* Biochim Biophys Acta, 2004. 1673(1-2): p. 13-28.

179. Wells, L., K. Vosseller, and G.W. Hart, *A role for N-acetylglucosamine as a nutrient sensor and mediator of insulin resistance.* Cell Mol Life Sci, 2003. 60(2): p. 222-8.

180. McClain, D.A., *Hexosamines as mediators of nutrient sensing and regulation in diabetes.* J Diabetes Complications, 2002. 16(1): p. 72-80.

181. **Whiteman, E.L., H. Cho, and M.J. Birnbaum, *Role of Akt/protein kinase B in metabolism.* Trends Endocrinol Metab, 2002. 13(10): p. 444-51.**

182. **Hardie, D.G., et al., *Management of cellular energy by the AMP-activated protein kinase system.* FEBS Lett, 2003. 546(1): p. 113-20.**

183. **Tang, J., et al., *Transgenic mice with increased hexosamine flux specifically targeted to beta-cells exhibit hyperinsulinemia and peripheral insulin resistance.* Diabetes, 2000. 49(9): p. 1492-9.**

184. **Daniels, M.C., et al., *Glutamine:fructose-6-phosphate amidotransferase activity in cultured human skeletal muscle cells: relationship to glucose disposal rate in control and non-insulin-dependent diabetes mellitus subjects and regulation by glucose and insulin.* J Clin Invest, 1996. 97(5): p. 1235-41.**

185. **Jacobsen, S.E., K.A. Binkowski, and N.E. Olszewski, *SPINDLY, a tetratricopeptide repeat protein involved in gibberellin signal transduction in Arabidopsis.* Proc Natl Acad Sci U S A, 1996. 93(17): p. 9292-6.**

186. **McDaniel, M.L., et al., *Metabolic and autocrine regulation of the mammalian target of rapamycin by pancreatic beta-cells.* Diabetes, 2002. 51(10): p. 2877-85.**

187. **Marshall, S., V. Bacote, and R.R. Traxinger, *Discovery of a metabolic pathway mediating glucose-induced desensitization of the glucose transport system. Role of hexosamine biosynthesis in the induction of insulin resistance.* J Biol Chem, 1991. 266(8): p. 4706-12.**

188. **Yki-Jarvinen, H., et al., *Increased glutamine:fructose-6-phosphate amidotransferase activity in skeletal muscle of patients with NIDDM.* Diabetes, 1996. 45(3): p. 302-7.**

189. **Buse, M.G., et al., *Increased activity of the hexosamine synthesis pathway in muscles of insulin-resistant ob/ob mice.* Am J Physiol, 1997. 272(6 Pt 1): p. E1080-8.**

190. **Cooksey, R.C., et al., *Mechanism of hexosamine-induced insulin resistance in transgenic mice overexpressing glutamine:fructose-6-phosphate amidotransferase: decreased glucose transporter GLUT4 translocation and reversal by treatment with thiazolidinedione.* Endocrinology, 1999. 140(3): p. 1151-7.**

191. **Gregor, M.F. and G.S. Hotamisligil, *Thematic review series: Adipocyte Biology. Adipocyte stress: the endoplasmic reticulum and metabolic disease.* J Lipid Res, 2007. 48(9): p. 1905-14.**

192. **Kolm-Litty, V., et al., *High glucose-induced transforming growth factor beta1 production is mediated by the hexosamine pathway in porcine glomerular mesangial cells.* J Clin Invest, 1998. 101(1): p. 160-9.**

193. **Cai, L., et al., *Hyperglycemia-induced apoptosis in mouse myocardium: mitochondrial cytochrome C-mediated caspase-3 activation pathway.* Diabetes, 2002. 51(6): p. 1938-48.**

194. **Moley, K.H., et al.,** ***Hyperglycemia induces apoptosis in pre-implantation embryos through cell death effector pathways.*** **Nat Med, 1998. 4(12): p. 1421-4.**

195. **Li, P., et al.,** ***Early release of cytochrome C and activation of caspase-3 in hyperglycemic rats subjected to transient forebrain ischemia.*** **Brain Res, 2001. 896(1-2): p. 69-76.**

196. **Raff, M.,** ***Cell suicide for beginners.*** **Nature, 1998. 396(6707): p. 119-22.**

197. **Csipo, I., et al.,** ***Effect of Fas+ and Fas- target cells on the ability of NK cells to repeatedly fragment DNA and trigger lysis via the Fas lytic pathway.*** **Apoptosis, 1998. 3(2): p. 105-14.**

198. **Hague, A. and C. Paraskeva,** ***Apoptosis and disease: a matter of cell fate.*** **Cell Death Differ, 2004. 11(12): p. 1366-72.**

199. **Hsu, S.Y., et al.,** ***Interference of BAD (Bcl-xL/Bcl-2-associated death promoter)-induced apoptosis in mammalian cells by 14-3-3 isoforms and P11.*** **Mol Endocrinol, 1997. 11(12): p. 1858-67.**

200. **Tilly, J.L.,** ***Commuting the death sentence: how oocytes strive to survive.*** **Nat Rev Mol Cell Biol, 2001. 2(11): p. 838-48.**

201. **Frustaci, A., et al.,** ***Myocardial cell death in human diabetes.*** **Circ Res, 2000. 87(12): p. 1123-32.**

202. **Ido, Y., D. Carling, and N. Ruderman,** ***Hyperglycemia-induced apoptosis in human umbilical vein endothelial cells: inhibition by the AMP-activated protein kinase activation.*** **Diabetes, 2002. 51(1): p. 159-67.**

203. **Zhang, D.X., et al.,** ***Production and metabolism of ceramide in normal and ischemic-reperfused myocardium of rats.*** **Basic Res Cardiol, 2001. 96(3): p. 267-74.**

204. **Fulop, N., R.B. Marchase, and J.C. Chatham,** ***Role of protein O-linked N-acetyl-glucosamine in mediating cell function and survival in the cardiovascular system.*** **Cardiovasc Res, 2007. 73(2): p. 288-97.**

205. **Park, J., et al.,** ***Proteomic analysis of O-GlcNAc modifications derived from streptozotocin and glucosamine induced beta-cell apoptosis.*** **J Biochem Mol Biol, 2007. 40(6): p. 1058-68.**

2. MATERIALS AND METHODS

Our initial approach was to establish a hyperglycemic cell model. Subsequently, we evaluated the role of the HBP in mediating cell death under these conditions .Finally, we tested our hypothesis by employing an in vivo rat model of insulin resistance.

2.1 CELL CULTURE: *In vitro* model

H9c2 rat cardiomyoblasts were used for experiments as they are a precursor cell line to cardiomyocytes (Sigma-Aldrich, Steinheim, Germany) [1]. Cells were cultured at 37˚C (5% CO_2, 95% air) in T75 culture flasks using Dulbecco Modified Eagle's Medium (DMEM) (Sigma-Aldrich, Steinheim, Germany) containing 10% fetal bovine serum (Invitrogen, Carlsbad, CA). The final glucose concentration in DMEM was 5.5 mmol/L. Cells were sub cultured when the flasks were ~ 80% confluent. This usually took between three and four days.

2.1.1 Pharmacologic treatment to modulate flux through the HBP

After seeding, cells were allowed to plate where after various treatments were employed to test our hypothesis. On the first day, cells were split into three groups. One group was given a low glucose DMEM (5.5 mM), and the second and third groups treated with high glucose DMEM containing 22 and 33 mM glucose, respectively [2-4]. *[Note: The choice of 22 and 33 mM glucose is based on previous studies which employed the same high glucose concentrations [2-*

4]. The rationale is that since H9c2s are usually maintained in a 25 mM glucose-DMEM when not used in glucose-dependent experiments, we chose 33 mM glucose as a ''hyperglycaemic'' dose.] To simulate chronic hyperglycaemia, the high glucose treatment was given for 5 days with treatment initiated on Day 1. On the second day, various pharmacological agents were introduced that either activate or inhibit the HBP. Here we used 40 µM DON (6-diazo 5-oxo-L-norleucine) (Sigma-Aldrich, St.Louis, MO) [5] an inhibitor of GFAT, the rate limiting enzyme of the HBP; 50 µM PUGNAc (O-(2-acetamido-2-deoxy-D-glucopyranosylidene)amino N-phenyl carbamate) (Sigma-Aldrich, St.Louis, MO) [6] an inhibitor of *O*-GlcNAcase; and 250 µM α-OHCA (α hydroxyl cinnamic acid) (Sigma-Aldrich, St.Louis, MO) [7] an anti-oxidant. A combination of PUGNAc and α-OHCA was also given to assess whether an antioxidant would blunt PUGNAc-mediated effects. No pharmacological agents were added to low and high glucose controls. We routinely administered pharmacological agents for three days (Day two to Day four) with fresh media where after cells were analysed to assess the degree of apoptosis on Day 5 (Figure 2.1). We employed various methods to evaluate apoptosis, i.e. Hoechst nuclear staining, caspase activity assay and Annexin-V staining (R&D Systems, Germany). We also assessed ROS levels by H2DCFDA staining.

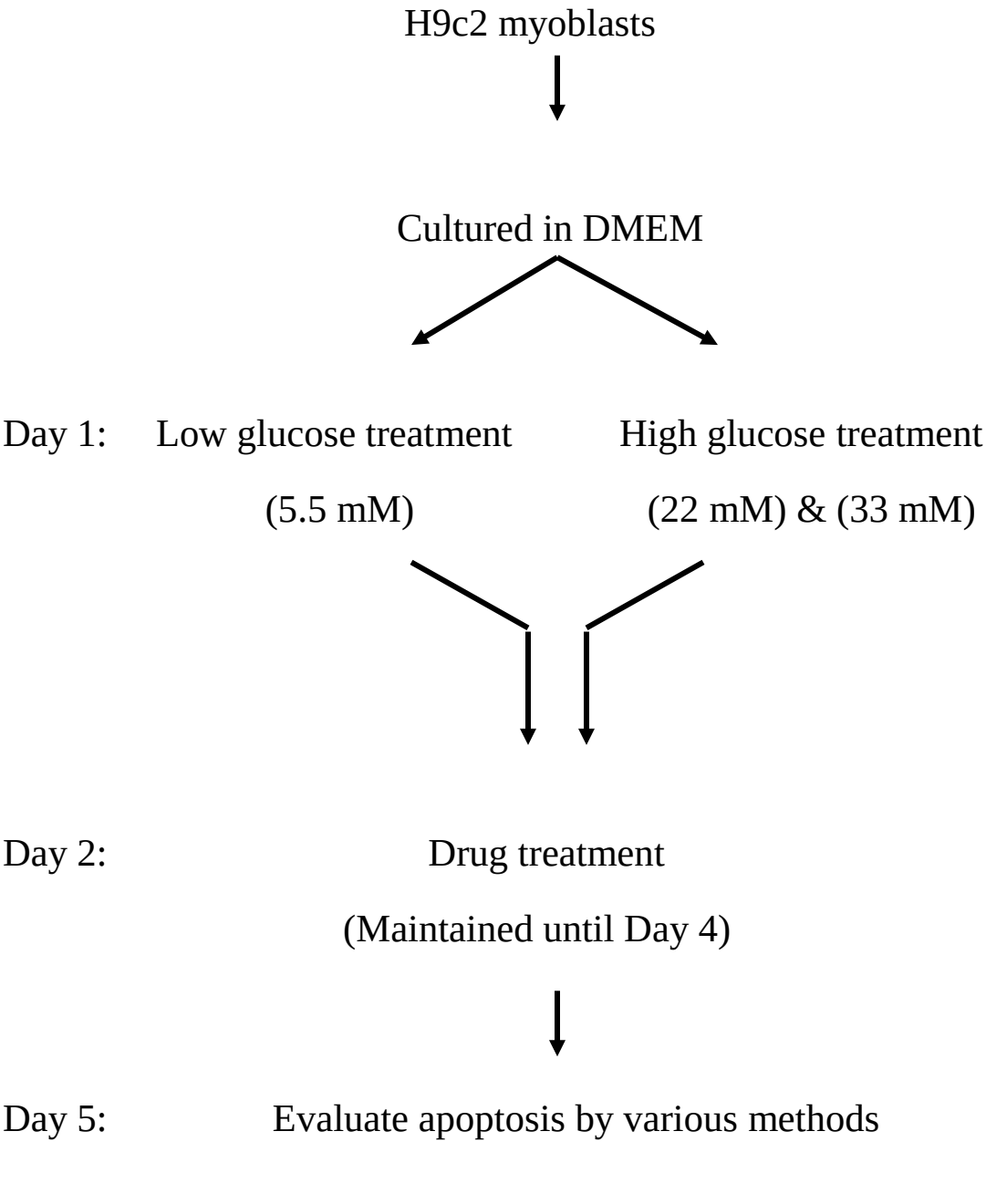

Figure 2.1: **A schematic representation of experimental plan.**

2.1.2 Transfections to enhance flux through the HBP

Transfection is a procedure where exogenous DNA (encoding candidate protein) is transferred into cells. This is useful to investigate effects of brought about by overexpression of the candidate protein in a cell-based system. Here the transfected plasmid DNA incorporates into the host DNA and the candidate protein is expressed.

For our experiments, we increased HBP flux by employing a pcDNA3-GFAT plasmid [8] construct to over express GFAT, the rate-limiting enzyme of this pathway. We also employed a dominant negative GFAT construct, pcDNA3-GFAT/676 [9] (in which 676 lysine is mutated to alanine) that should inhibit HBP flux. Both these constructs were kindly donated to us by Dr. Cora Weigert based at the University of Tübingen in Germany.

H9c2 myoblasts were trypsinized on Day 1 and counted in a haemocytometer (LASEC, South Africa). Approximately 35,000 cells were then seeded in each well of a 12-well plate with 1 ml DMEM and allowed to plate for 24 hrs. The transfection was performed on Day two (Figure 2.2). Here, we first made up 0.25 µg of pcDNA3-GFAT in DMEM without serum. We next made up a solution of the transfection reagent - Fugene 6 (Roche, Penzberg, Germany) - in DMEM without serum. We employed a 2:1 ratio for Fugene 6: plasmid DNA as is routinely done in our laboratory for similar type of experiments. The two solutions were mixed and incubated at room temperature for 15 minutes. Just before the transfection was performed, we

added 0.9 ml fresh media and 100 µL of the Fugene-DNA cocktail to the cells. The plates were gently rocked to evenly spread the cocktail and thereafter incubated at 37°C for 24 hrs. On Day three, the media was removed and fresh medium was given to the cells. On Day four, cell lysates were harvested using RIPA buffer and stored at -80°C until further use. The protein lysate was used for immunoprecipitation and Western blotting analysis. Two independent experiments were performed with each condition in triplicates.

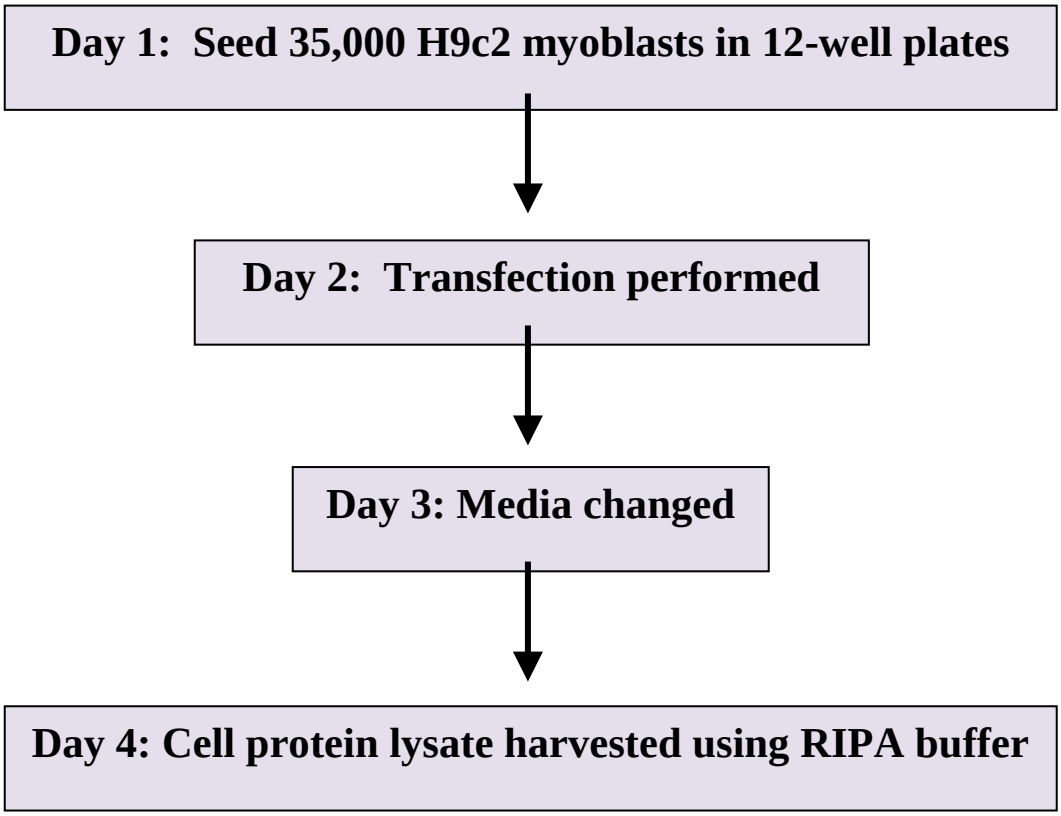

Figure 2.2: A schematic representation of the transfection procedure

2.2 *IN VIVO* RAT MODEL OF INSULIN RESISTANCE

Previously collected heart tissues provided by Dr. Saartjie Roux (Department of Biochemistry and Microbiology at the Nelson Mandela Metropolitan University, South Africa). Here, three-week-old male Wistar rats were fed high fat diet (Harlan Teklad, TD.95217, Wisconsin, USA) for 86 days and compared to matched controls (Harlan Teklad, TD.06683, Wisconsin, USA). Rats fed high fat diet displayed a moderate but significant increase in body weight (7.3 ± 1.3%, $p<0.05$ *vs.* controls). These rats became insulin resistant since muscle glucose uptake was significantly lower in high fat versus the control group (Insulin resistance was measured by calculating HOMA-IR using the formula HOMA-IR = fasting plasma immunoreactive insulin (IRI; µU/l) × fasting plasma glucose (FPG; mmol/l)/22·5. The high fat diet group showed a 3-5 fold increase in HOMA-IR values compared to the control diet group). Moreover, fasting plasma glucose levels were increased by 23.5 ± 7% in these animals ($p<0.05$ *vs.* matched controls) suggesting that they were hyperglycaemic.

2.3 EVALUATION OF APOPTOSIS

2.3.1 Hoechst nuclear staining

During apoptosis nuclei condense and fragment. With Hoechst staining, the nuclei of cells are stained and this can be used as an indicator of condensed/fragmented nuclei undergoing apoptosis [2].

H9c2 myoblasts were trypsinized and counted in a haemocytometer (LASEC, South Africa). Approximately 200,000 cells were then seeded in a 35 mm petridish with a cover slip and 2 ml of DMEM where after various treatments were administered as explained in Section 2.1.1. To exclude the possibility of cell death due to osmotic effects, we performed similar experiments as described but using 22 mM and 33 mM mannitol *vs* 5.5 mM glucose controls.

Cover slips were removed after the completion of experiments and placed over glass slides. Cover slips were then washed with 500 µL of ice cold PBS (phosphate buffer solution), treated with 1 ml of fixative (1:1 acetone : methanol) and thereafter incubated at 4°C for 10 minutes. The fixative was then removed and cover slips again washed with 500 µL ice cold PBS. 100 µL of Hoechst stain (4´-6´ diamidino-2-phenylindole - DAPI) (Sigma-Aldrich, Steinheim, Germany) (1:200 dilution of stock in PBS) was added onto cover slips an incubated in the dark for 20

minutes. Since Hoechst is a fluorescence stain, any external light might affect the signal and hence incubations were performed in the dark. The stain was then washed off twice with 500 µL PBS and the cover slips thereafter mounted on permanent slides that were then viewed under a Nikon E-400 fluorescence microscope (Nikon microscopes, Kobe, Japan). Images were acquired using a Nikon DM X 1200 colour digital camera (Nikon microscopes, Kobe, Japan) using ACT-I software (Nikon microscopes, Kobe, Japan) to process the images. Three independent experiments were conducted and four images of each condition were acquired resulting in 12 images being captured per experiment. For each image the number of condensed/fragmented nuclei was counted and expressed as a percentage of total number of nuclei counted. In this manner the percentage apoptosis was determined for each experimental condition.

2.3.2 Caspase activity assay

The caspase activity assay was used to measure the active caspase activity in cells under hyperglycaemic conditions ± various HBP drug treatments. The degree of caspase activation was taken as a marker of apoptosis. The Caspase-Glo® 3/7 assay kit (Promega, Madison, WI) contains a lysate which lyses cells. A luminogenic caspase 3/7 substrate is added to the lysed cells. Activated caspases cleave the luminogenic substrate, releasing amino-luciferin (Figure 2.3). The latter is a substrate for luciferase resulting in the production of light that is measured using a Glomax luminometer (Sigma-Aldrich, St.Louis, MO). The degree of luminescence is therefore a measure of caspase activity and apoptosis.

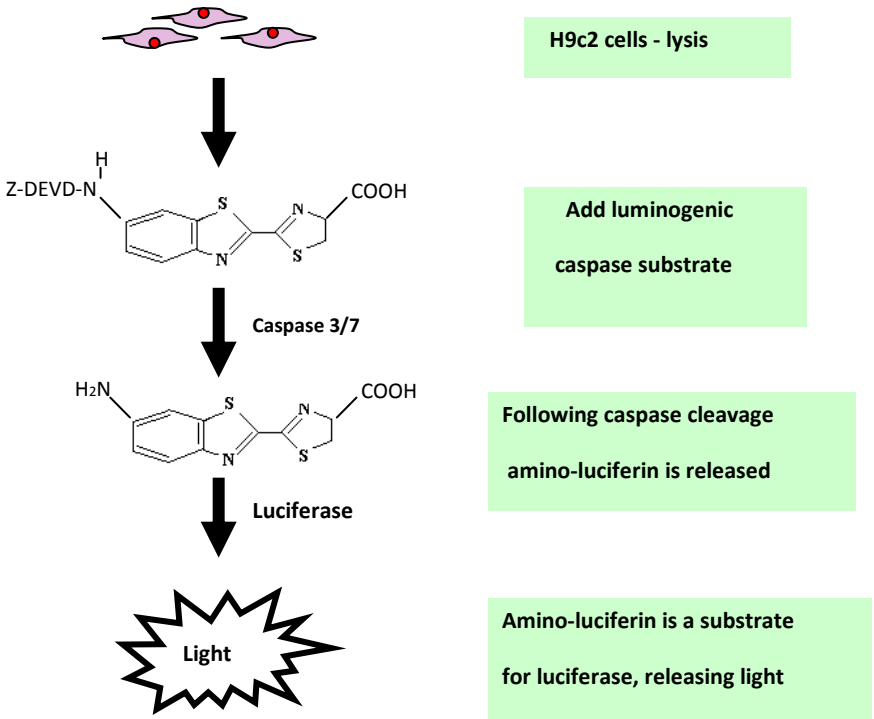

Figure 2.3: A schematic representation of the Caspase-Glo® 3/7 assay

H9c2 myoblasts were trypinized, counted in a haemocytometer (LASEC, South Africa) and ~ 10,000 cells seeded per well of a 96-well plate (Greiner, Kremsmünster, Austria). Cells were seeded with 500 µL DMEM. Negative controls were also included in these experiments and here the cells were treated with the vehicle (90% saline) only. We used 90% saline to dissolve the drugs and hence saline acted as a vehicle. We also included a blank reaction, i.e. vehicle and DMEM with no cells. The experiments were performed 6 times (n=6).

The caspase assay kit was reconstituted as detailed in the manufacturer's instruction booklet. Here the DMEM from cells was removed and 100 µL of the reconstituted assay reagent was added onto each well and mixed gently. Cells were thereafter incubated at room temperature for ~ two hours. Care is taken to incubate the cells with the reagent in dark so that the natural light does not interfere with the luminescence of the experiment. The luminescence of the samples was measured in a luminometer. For this purpose, special white walled 96-well luminometer plates (Amersham, Buckinghamshire, UK) were used. The reagent-treated experiments from the normal 96-well plate were transferred into the white-walled luminometer plate that was then placed in a luminometer and readings taken for each well. The luminescence of each well corresponds to the caspase activity in that well.

2.3.3 Annexin-V staining

During the early stage of apoptosis, the phospholipid asymmetry of the cell membrane is disrupted exposing phosphatidyl serine residues on its outer leaflet. This is an important event for macrophage recognition of cells undergoing apoptosis. Annexin-V binds to the exposed phosphatidyl serine residues, thereby tagging apoptotic cells. Annexin-V is an anti-coagulant protein that preferentially binds negatively charged phospholipids. We employed Annexin-V conjugated with FITC (R&D Systems, Germany)[10] allowing us to measure fluorescence when viewed using a fluorescence microscope.

For the purpose of fluorescence microscopy, Nunc™ chambered cover glass (Nalge Nunc, Rochester, NY) were used. As before, H9c2 myoblasts were trypsinized, counted and ~ 15,000 cells seeded per well in an 8-well Nunc™ chambered cover glass. We seeded the cells with 500 µL of DMEM. Subsequently, various pharmacologic treatments were administered as described in Section 2.1.1. of the thesis.

DMEM in the wells were removed and the cells were washed with 300 µL of warm 1 X PBS. The Annexin-V incubation buffer was prepared as detailed in the manufacturer's instruction booklet, i.e. using 10 µL of 10 X binding buffer, 10 µL propidium iodide, 0.5 µL Annexin V-FITC and 79.5 µL distilled water. Thus a total of 100 µL of incubation buffer was prepared per sample. Propidium iodide was included in the incubation buffer to differentiate between apoptotic and necrotic cell death as propidium iodide can stain the nuclei of necrotic cells with non-intact cell membranes. 100 µL of the incubation buffer was added to each well. This was incubated in the dark at room temperature for 15 minutes. As Annexin V-FITC is a fluorescence staining procedure, any external light affects the signal causing background and hence the staining needs to be performed in the dark.

After incubation, cells were washed twice with 300 µL of 1 X binding buffer provided with the kit. Thereafter, 100 µL of warm PBS was added and cells viewed under an Olympus CellˆR fluorescence 1 X 81 inverted microscope (Olympus Biosystems, Germany) using an F-view II camera (Olympus Biosystems, Germany) for image acquisition and CellˆR software, Olympus Biosystems, Germany) for processing images. Warm PBS was used since the cells being viewed

are still alive and therefore this procedure should minimize stress on these cells. The temperature of the microscope system was maintained at 37°C for live cell imaging using a Solent Scientific microscope incubator chamber (Solent Scientific, UK). The green intensity of all cells expressing Annexin-V signal were measured, providing a numerical value for the degree of apoptosis. Four independent experiments were conducted and three images acquired per well. Cells displaying propidium iodide staining were considered necrotic and were excluded from our analysis.

2.3.4 Western blot analysis

Western blotting analysis was used to quantify peptide levels of O-GlcNAcylated and apoptotic proteins. Protein extracts from the in vitro and in vivo experiments are resolved using SDS-polyacrylamide gel electrophoresis (PAGE), probed for candidate proteins and quantified to estimate protein expression.

2.3.4.1 Isolation of cellular protein extracts

H9c2 myoblasts were trypsinized, counted and ~ 300,000 cells seeded in 5 ml DMEM in T-25 flasks (Greiner, Kremsmünster, Austria). Subsequently, various pharmacologic treatments were administered (described in Section 2.1.1). Following treatment protein was harvested by scrapping cells off the flask using freshly prepared modified RIPA buffer (refer Appendix 1.1).

The collected lysate was then sonicated and centrifuged (ALC PK121R Multispeed refrigerated centrifuge) for 10 minutes at 4300 x g at 4°C and subsequently the supernatants were stored at -80°C. Total protein was quantified by the Bradford method (refer Appendix 2).

2.3.4.2 Isolation of heart tissue protein extracts

To extract proteins from the heart tissues, small pieces of the heart tissues were placed inside homogenizing tubes containing freshly prepared modified RIPA (Appendix 1.1) and homogenized for about a minute, and thereafter left on ice for an hour until foam subsided. This was subsequently centrifuged at 4300 x g set for 10 minutes at 4°C. The supernatant was collected and re-centrifuged as before. The supernatant was collected and stored at -80°C until further use. Total protein in the samples was quantified using Bradford method (Appendix 2).

2.3.4.3 SDS-PAGE

Western Blot protein samples (cellular and tissue extracts) were prepared by adding 50 µg of protein to an equal amount of sample buffer (3x sample buffer: 33.3 ml stacking buffer, 8.8 g SDS, 20 g glycerol and bromophenol blue in 75 ml distilled water; 850 µL 3x sample buffer + 150 µL mercaptoethanol was used as the working sample buffer solution). Samples were subsequently boiled for 5 minutes before being loaded for PAGE. The samples were electrophoresed on a 10% SDS-PAGE gel (with a 4% stacking gel) at 200 V for one hour. 10 µL

of protein marker (Bio-RAD Plus Protein™ Dual Colour Standards, CA) was included (Lane 1), with experimental samples loaded in the remaining lanes. After one hour, proteins from the gel were transferred to a PVDF membrane (Immobilon-P, Millipore Corporation, MA) by semi-dry electrotransfer (refer Appendix 3). This membrane was used to probe for caspase-3, BAD and cytochrome-c (Cell Signaling, MA) in order to assess the degree of apoptosis (refer Appendix 4 for protein detection methodology).

Protein expression was determined by densitometry. Here the developed film was scanned using an HP Scanjet 3500c scanner (Hewlett packard, Palo Alto, CA) and densitometry was performed using Un-Scan-It Gel version 5.1 (Silk software, Orem, UT). The densitometry value of the investigated proteins was normalised to the densitometry value of the corresponding β-actin. The normalized densitometric value was used for statistical analysis when evaluating relative differences in protein expression.

2.4 ASSESSMENT OF OXIDATIVE STRESS

2.4.1 DCF-DA staining

Derivatives of reduced fluorescein and calcein act as cell-permeable indicators for ROS. Chemically reduced and acetylated forms of 2',7'-dichlorofluorescein (DCF) are non-fluorescent until the acetate groups are removed by intracellular esterases. Esterase cleavage of the lipophilic blocking groups yields a charged form of the dye that is much better retained by cells than its parent compound. This can fluoresce when excited and hence higher fluorescence indicates greater ROS levels. Oxidation of probes can be detected by monitoring increased fluorescence. The latter may be assessed by a variety of methods, e.g. flow cytometry or fluorescence microscopy [2, 11]. With hyperglycaemia there is increased ROS production [12-15] that may result in detrimental effects. We employed this ROS staining procedure to measure ROS levels in response to hyperglycaemia ± HBP pharmacologic modulators.

For the purpose of fluorescence microscopy, Nunc™ chambered cover glass (Nalge Nunc, Rochester, NY) were employed. As before, H9c2 myoblasts were trypsinized, counted and ~ 15,000 cells seeded per well in an 8-well Nunc™ chambered cover glass. We seeded the cells with 500 µL DMEM. Subsequently, various pharmacologic treatments were administered as described in Section 2.1.1.

DMEM in wells were removed and H9c2 myoblasts were washed with 300 µL of warm 1 X PBS. We originally prepared a 1 M H2DCFDA stock by dissolving it in 210 µL distilled water. Several aliquots of 10 mM stocks were thereafter made by diluting 10 µL of 1 M stock into 990 µL of DMSO. The working solution was prepared by a 1:200 dilution of the 10 mM dye stocks in PBS. 100 µL of the working H2DCFDA solution was added per well and incubated in the dark for 10 minutes at 37°C. Since the cleaved DCF is a fluorescent substrate, any external light affects the signal causing background and hence this procedure needs to be performed in the dark. The dye was then removed and 100 µL PBS added to cells. Cells were thereafter viewed using a Olympus Cellˆ R fluorescence 1 X 81 inverted microscope (Olympus Biosystems, Germany) using an F-view II camera (Olympus Biosystems, Germany) for image acquisition and Cellˆ R software (Olympus Biosystems, Germany) for processing images. The temperature of the microscope system was maintained at 37°C for live cell imaging using a Solent Scientific microscope incubator chamber (Solent Scientific, UK). The green intensity of all cells expressing DCF signal was measured, generating a numerical value corresponding to ROS levels and oxidative stress. Four independent experiments were conducted and 3 images per experiment acquired. Thus an n=12 was generated for each experiment.

2.4.2 ROS measurement by flow cytometry

We also assessed ROS levels by flow cytometry in order to obtain population data (versus single cell data) [16]. Flow cytometry simultaneously measures and analyzes multiple physical characteristics of single particles, usually cells, as they flow in a fluid stream through a beam of

light. The properties measured include a particle's relative size, granularity or internal complexity, and fluorescence intensity. These characteristics are determined using an optical-to-electronic coupling system that records how the cell or particle scatters incident laser light and emits fluorescence.

H9c2 myoblasts were trypsinized, counted and ~ 300,000 cells seeded in 5 ml DMEM in T-25 flasks (Greiner, Kremsmünster, Austria). Subsequently, various pharmacologic treatments were administered to test our hypothesis (described in Section 2.1.1).

DMEM from flasks was removed and H9c2 myoblasts were washed with 2 ml of warm PBS. Warm PBS was used since the cells being viewed are still alive and the slightest stress may affect ROS levels. Cells were then trypsinized with 2 ml of Trypsin-EDTA solution (Sigma-Aldrich, St.Louis, MO) and pelleted by centrifuging in a Digicen 20-R Ortoalresa centrifuge (United Scientific, South Africa) for 2 minutes at 1358 x g at 37˚C. The cell pellet was then treated with 1 ml of working solution of the dye. We originally prepared a 1 M H2DCFDA stock by dissolving it in 210 µL distilled water. Several aliquots of 10 mM stocks were thereafter made by diluting 10 µL of 1 M stock into 990 µL of DMSO. The working solution was prepared by a 1:200 dilution of the 10 mM dye stocks in PBS. The dye-treated cell pellet was suspended without clumps and incubated in the dark for 20 minutes at 37°C. As the cleaved DCF is a fluorescent substrate, any external light affects the signal causing background and hence the staining needs to be performed in darkness. The cells were then run through FACS Aria flow cytometer (Becton-Dickinson, CA) and population data obtained.

Cells not treated with ROS dye served as negative controls, and stained cells treated with 100 µL hydrogen peroxide (30% w/v hydrogen peroxide) incubated for 10 minutes served as positive controls. Three independent experiments were conducted for each condition investigated. The geometric mean of the fluorescence of a cell population represented the numerical value of the experiment which was used for analysis.

2.5 ASSESSMENT OF HBP FLUX

2.5.1 Measurement of *O*-GlcNAc by fluorescence staining

Fluorescence microscopy can be used to visualize and measure proteins or similar groups on proteins by tagging them with a specific primary antibody which can then be picked up by its specific secondary antibody which is fluorescent. This process is known as immunohistochemistry. When O-GlcNAc is bound to its antibody and in turn to a fluorescent secondary antibody, it can fluoresce and this fluorescence intensity can be used as a measure of the amount of O-GlcNAc present within the system. The greater the fluorescence intensity, the more protein present.

For the purpose of fluorescence microscopy, Nunc™ chambered cover glass (Nalge Nunc, Rochester, NY) were employed. As before, H9c2 myoblasts were trypsinized, counted and ~

15,000 cells seeded per well in an 8-well Nunc™ chambered cover glass. We seeded the cells with 500 µL of DMEM. Subsequently, various pharmacologic treatments were administered as described in Section 2.1.1.

DMEM in wells were removed and H9c2 myoblasts were washed with 300 µL of cold PBS. Cells were then fixed in acetone:methanol (1:1) fixative for 10 minutes. Thereafter they were incubated in 5% donkey serum for 20 minutes to block non-specific binding sites. The cells were then incubated in 1:50 *O*-GlcNAc primary antibody overnight at 4˚C. They were then thoroughly washed with cold PBS four to five times and thereafter treated with the secondary Texas Red antibody (1:200 dilution) for 30 minutes in the dark. Since the secondary Texas Red antibody is fluorescent, any external light affects the signal causing background and hence this procedure needs to be performed in the dark. Subsequently, cells were thoroughly washed using cold PBS 4 to 5 times and henceforth maintain under a thin film of cold PBS for imaging. Cells were thereafter viewed using a Olympus CellˆR fluorescence 1 X 81 inverted microscope (Olympus Biosystems, Germany) using an F-view II camera (Olympus Biosystems, Germany) for image acquisition and CellˆR software (Olympus Biosystems, Germany) for processing images. The red intensity of all cells expressing *O*-GlcNAc signal were measured, generating a numerical value corresponding to *O*-GlcNAc levels and HBP flux. Three independent experiments were conducted and 4 images per experiment acquired.

2.5.2 Assessment of *O*-GlcNAcylation by Western blot analysis

O-GlcNAc modification of proteins via the HBP pathway is a relatively common phenomenon. When protein extracts are probed for O-GlcNAc, differences in the degree of O-GlcNAcylation may be observed which would help us determine the effects of various treatments on O-GlcNAc modifications.

2.5.2.1 Isolation of cellular protein extracts

H9c2 myoblasts were trypsinized, counted and ~ 300,000 cells seeded in 5 ml DMEM in T-25 flasks (Greiner, Kremsmünster, Austria). Subsequently, various pharmacologic treatments were administered (described in Section 2.1.1). Following treatment, protein was harvested by scrapping cells off the flask using freshly prepared modified RIPA buffer (refer Appendix 1.1). The collected lysate was then sonicated and centrifuged (ALC PK121R Multispeed refrigerated centrifuge) for 10 minutes at 4300 x g at 4°C and subsequently the supernatants were stored at -80°C. Total protein was quantified by the Bradford method (refer Appendix 2).

2.5.2.2 Isolation of heart tissue protein extracts

To extract proteins from the heart tissues, small pieces were placed inside homogenizing tubes containing freshly prepared modified RIPA (Appendix 1.1) and homogenized for about a minute, allowed to stand on ice for an hour until foam subsided. This was subsequently centrifuged at 4300 x g for 10 minutes at 4°C. The supernatant was collected and re-centrifuged as before. The supernatant was thereafter stored at -80°C. Total protein in the samples was quantified using Bradford method (Appendix 2).

2.5.2.3 SDS-PAGE

Western Blot protein samples were prepared by adding 50 µg of protein to an equal amount of sample buffer (3x sample buffer: 33.3 ml stacking buffer, 8.8 g SDS, 20 g glycerol and bromophenolblue in 75 ml distilled water; 850 µL 3x sample buffer + 150 µL mercaptoethanol was used as the working sample buffer solution). Samples were subsequently boiled for 5 minutes before being loaded for PAGE. The samples were electrophoresed on a 10% SDS-PAGE (with a 4% stacking gel) at 200 V for one hour. 10 µL of protein marker (Bio-RAD Plus Protein™ Dual Colour Standards, CA) was included (Lane 1), with experimental samples loaded in the remaining lanes. After one hour, the proteins from the gel were transferred onto a PVDF membrane (Immobilon-P, Millipore Corporation, MA) by semi-dry electrotransfer (refer

Appendix 3). This membrane was used to probe for *O*-GlcNAc (Pierce, Rockford, IL) to assess degree of *O*-GlcNAcylation (refer Appendix 5). The amount of protein detected was analysed using densitometry as explained in section 2.3.4.

2.6 ASSESSMENT OF HBP MODIFICATION OF PROTEINS

2.6.1 Measurement of *O*-GlcNAcylation of BAD by fluorescence staining

Immunohistochemistry can also be used to detect multiple proteins or groups simultaneously by tagging them with different secondary antibodies fluorescing in different wavelengths. For instance Bad tagged to FITC green and O-GlcNAc tagged to Texas Red can be visualised simultaneously and the co-localisation studies of these two tags also helps us determine if Bad and O-GlcNAc are present in the same proteins vicinity which gives us a measure of Bad O-GlcNAcylation.

For the purpose of fluorescence microscopy, Nunc™ chambered cover glass (Nalge Nunc, Rochester, NY) were employed. As before, H9c2 myoblasts were trypsinized, counted and ~ 15,000 cells seeded per well in an 8-well Nunc™ chambered cover glass. We seeded the cells with 500 µL of DMEM. Subsequently, various pharmacologic treatments were administered as described in Section 2.1.1.

DMEM in wells were removed and H9c2 myoblasts were washed with 300 µL of cold PBS. Cells were then fixed in acetone:methanol (1:1) fixative for 10 minutes. Thereafter they were incubated in 5% donkey serum for 20 minutes to block non-specific binding sites. The cells were then incubated overnight at 4°C with a 1:50 Bad (Cell Signaling, MA) and 1:50 *O*-GlcNAc primary antibody (Piercenet, Woburn, MA) cocktail. They were then thoroughly washed with cold PBS and thereafter treated with a secondary antibody cocktail containing anti-rabbit FITC-green (1:200) (Invitrogen, Carlsbad, CA) against Bad and anti-mouse Texas Red (1:200) (Invitrogen, Carlsbad, CA) against *O*-GlcNAc in the dark for 30 minutes. Since the secondary antibodies are fluorescent, any external light affects the signal causing background and hence this procedure needs to be performed in the dark. Subsequently, cells were thoroughly washed using cold PBS four to five times and henceforth maintained under a thin film of cold PBS for imaging. Cells were thereafter viewed using a Olympus CellˆR fluorescence 1 X 81 inverted microscope (Olympus Biosystems, Germany) using an F-view II camera (Olympus Biosystems, Germany) for image acquisition and CellˆR software (Olympus Biosystems, Germany) for processing images. The degree of Bad *O*-GlcNAcylation was determined using FITC and Texas Red filters. Bad *O*-GlcNAcylation was determined by measuring the area of co-localization of red and green stains from the images obtained, i.e. producing a yellow color. Three independent experiments were conducted and 4 images per experiment acquired.

2.6.2 Measurement of BAD *O*-GlcNAcylation by immunoprecipitation analysis

Immunoprecipitation is a technique that employs protein-specific antibodies to isolate target proteins from the total protein fraction. The antibody-protein complexes are precipitated out of solution using an insoluble form of antibody-binding proteins obtained by coupling them to agarose or sepharose beads.

H9c2 myoblasts were trypsinized, counted and ~ 300,000 cells seeded in 5 ml DMEM in T-25 flasks (Greiner, Kremsmünster, Austria). Subsequently, various pharmacologic treatments were administered (described in Section 2.1.1). Following the treatment, the cells were treated with 100 µL of freshly prepared lysis buffer (refer Appendix 1.2 for denaturing lysis buffer for immunoprecipitation). For rat heart tissues, the tissue pieces were homogenized and collected over denaturing lysis buffer.

Lysates (both cellular and heart tissue) were thereafter vigorously vortexed for ~two to three seconds and then transferred to a microfuge tube. Due to the release of DNA the suspension remained viscous. The samples were then denatured by boiling for five minutes, diluted using 900 µL non-denaturing lysis buffer (refer Appendix 1.3) and gently mixed. Triton X-100 in the non-denaturing buffer quenches the SDS present in the denaturing buffer. DNA contributing to viscosity was fragmented by pipetting the lysed suspension several times through a micropipette

tip until the suspension became less viscous and manageable. The suspension was thereafter incubated for 5 minutes at 4ºC and then immunoprecipitated.

The immunoprecipitation procedure consists of two steps, i.e. a preclearing step followed by the actual immunoprecipitation. A quick preclearing step was performed to prevent non-specific binding of proteins to the beads. Here 50 µL of serum was added to the cell lysate and incubated for an hour on ice. This is done to allow formation of complex between serum and non-specific proteins. 100 µL of A-G bead slurry (Protein A/G Plus Agarose, Santa Cruz Biotechnology Inc., CA) was then added followed by 30 minutes incubation at 4ºC (with agitation). This allows the beads to bind to the complex formed between serum and non-specific proteins. The mixture was centrifuged (ALC PK121R Multispeed refrigerated centrifuge) at ~ 14,000 x g (4ºC) for ~10 minutes. The pellet was thereafter discarded and the supernatant used for immunoprecipitation.

About 100 µL of the protein lysate was treated with 100 µL of the *O*-GlcNAc antibody (1:200 dilution) and incubated for 1 hour at 4ºC (with agitation). Thereafter, a 100 µL of bead slurry was added to the samples.[*Note: for pipetting of the beads, pipette tips were cut off 5 mm from the tip to prevent breaking of the beads during pipetting and blockage of the tips.]* This mixture was further incubated for four hours at 4ºC. The samples were then centrifuged at 14,000 x g and the supernatant discarded. The pellet containing the beads was then washed two to three times and centrifuged to obtain the maximum yield of the beads. 50 µL of sample buffer was then added to the beads and boiled for 5 minutes to denature proteins and to separate beads from precipitated proteins. This was then centrifuged at 14,000 x g for 10 minutes and the supernatant

was used for Western blot analysis, i.e. probed for BAD (Cell Signaling, MA). Alternatively, the supernatant was frozen at -80°C until later use. Likewise, an additional immunoprecipitation experiment was performed using the BAD antibody (same protocol followed as described for the *O*-GlcNAc antibody). Immunoprecipitated BAD was then probed for O-GlcNAc to confirm our findings.

2.7 ASSESSMENT OF DIMERIZATION

2.7.1 Co-Immunoprecipitation

Co-immunoprecipitation is a useful technique to investigate protein-protein associations and to identify interacting partners of a target protein. It works under the same principle as immunoprecipitation. However, the difference being that when proteins are co-immunoprecipitated they are isolated together with their interacting proteins. This helps us identify the specific interacting protein.

The preparation of samples, preclearing and the preparation of the bead-sample slurry is similar as described in Section 2.6.2.

100 µL of the protein lysate was treated with 100 µL of BAD antibody (Cell Signaling, MA) (1:500 dilution) and incubated for 1 hour at 4ºC (with agitation). Thereafter, 100 µL of the bead slurry (Protein A/G Plus Agarose, Santa Cruz Biotechnology Inc., CA) was added to the samples. [*Note: for pipetting of beads, the pipette tips were cut off 5 mm from the tip to prevent breaking of the beads during pipetting.]* This mixture was further incubated for 4 hours at 4ºC. The samples were then centrifuged at 14,000 x g in an ALC PK121R Multispeed refrigerated centrifuge and the supernatant discarded. The pellet containing the beads were washed two to three times and centrifuged to obtain the maximum yield of beads. 50 µL of sample buffer was then added to the beads and boiled for 5 minutes to denature proteins and to separate beads from precipitated proteins. This was then centrifuged at 14,000 x g for 10 minutes and the supernatant used for Western blot analysis and probed for interacting proteins like Bcl-2 (Cell Signaling, MA). Alternatively, samples were frozen at -80°C until later use. When the blot is probed with various antibodies, the actual protein interacting with Bad can be known.

2.7.2 Immunofluorescence microscopy – co-localization

Immunohistochemistry was used to detect dimerization by tagging multiple proteins simultaneously with different secondary antibodies fluorescing in different wavelengths. For instance Bad tagged to FITC green and Bcl-2 tagged to Texas Red can be visualised simultaneously and the co-localisation studies of these two tags also helps us determine if Bad and Bcl-2 are present in close vicinity which gives us a measure of Bad-Bcl-2 dimerization.

The seeding and staining was done just as explained in section 2.6.1. Here, we used a rabbit-source 1:50 Bad (Cell Signaling, MA) and a goat-source 1:50 Bcl-2 (Imgenex, San diego, CA), primary antibody cocktail. As for the secondary antibody, we employed an anti-rabbit FITC-green (1:200) (Invitrogen, Carlsbad, CA) against Bad and anti-goat Texas Red (1:200) (Invitrogen, Carlsbad, CA) against Bcl-2. Again the viewing and co-localization was done as explained in section 2.6.1.

2.8 A SECOND CELL-BASED MODEL OF APOPTOSIS

To confirm that the changes we observed are indeed specific for our model of hyperglycaemia-mediated apoptosis, we also employed a positive control, i.e. an alternate cell model of apoptosis. For this we employed a well-established model that results in a significant degree of apoptosis, i.e. we treated 5.5 mM glucose cells with 50 ng/ml TNF-α [17]for 48 hours. We performed our experiments ± 40 μM DON and 50 μM PUGNAc, respectively. Subsequently, cells were assessed for the degree of apoptosis by Hoechst nuclear staining.

2.9 STATISTICAL ANALYSIS

Statistical analysis was performed using Graph Pad Prism (version 4). Results were expressed as mean ± standard error of the mean (SEM) of experiments. One-way analysis of variance (ANOVA) and Students-Newman-Keuls tests were performed on the data. Values were considered significant when $p<0.05$.

REFERENCES FOR MATERIALS AND METHODS

1. **Kimes, B.W. and B.L. Brandt, *Properties of a clonal muscle cell line from rat heart.* Exp Cell Res, 1976. 98(2): p. 367-81.**

2. **Cai, L., et al., *Hyperglycemia-induced apoptosis in mouse myocardium: mitochondrial cytochrome C-mediated caspase-3 activation pathway.* Diabetes, 2002. 51(6): p. 1938-48.**

3. **Baumgartner-Parzer, S.M., et al., *High-glucose--triggered apoptosis in cultured endothelial cells.* Diabetes, 1995. 44(11): p. 1323-7.**

4. **Du, X.L., et al., *Introduction of apoptosis by high proinsulin and glucose in cultured human umbilical vein endothelial cells is mediated by reactive oxygen species.* Diabetologia, 1998. 41(3): p. 249-56.**

5. **Lagranha, C.J., et al., *Glutamine enhances glucose-induced mesangial cell proliferation.* Amino Acids, 2008. 34(4): p. 683-5.**

6. **Clark, R.J., et al., *Diabetes and the accompanying hyperglycemia impairs cardiomyocyte calcium cycling through increased nuclear O-GlcNAcylation.* J Biol Chem, 2003. 278(45): p. 44230-7.**

7. **Gombau, L., et al., *Polypodium leucotomos extract: antioxidant activity and disposition.* Toxicol In Vitro, 2006. 20(4): p. 464-71.**

8. **Burt, D.J., et al., *P38 mitogen-activated protein kinase mediates hexosamine-induced TGFbeta1 mRNA expression in human mesangial cells.* Diabetologia, 2003. 46(4): p. 531-7.**

9. **Weigert, C., et al., *Glutamine:fructose-6-phosphate aminotransferase enzyme activity is necessary for the induction of TGF-beta1 and fibronectin expression in mesangial cells.* Diabetologia, 2003. 46(6): p. 852-5.**

10. **Hamilton, C. and E.D. Saggerson, *Malonyl-CoA metabolism in cardiac myocytes.* Biochem J, 2000. 350 Pt 1: p. 61-7.**

11. **Wang, G.W., J.B. Klein, and Y.J. Kang, *Metallothionein inhibits doxorubicin-induced mitochondrial cytochrome c release and caspase-3 activation in cardiomyocytes.* J Pharmacol Exp Ther, 2001. 298(2): p. 461-8.**

12. **Baynes, J.W. and S.R. Thorpe, *Role of oxidative stress in diabetic complications: a new perspective on an old paradigm.* Diabetes, 1999. 48(1): p. 1-9.**

13. **Baynes, J.W., *Role of oxidative stress in development of complications in diabetes.* Diabetes, 1991. 40(4): p. 405-12.**

14. **Chang, K.C., et al., *Possible superoxide radical-induced alteration of vascular reactivity in aortas from streptozotocin-treated rats.* J Pharmacol Exp Ther, 1993. 266(2): p. 992-1000.**

15. **Young, I.S., et al., *The effects of desferrioxamine and ascorbate on oxidative stress in the streptozotocin diabetic rat.* Free Radic Biol Med, 1995. 18(5): p. 833-40.**

16. **Ricci, J.E., R.A. Gottlieb, and D.R. Green, *Caspase-mediated loss of mitochondrial function and generation of reactive oxygen species during apoptosis.* J Cell Biol, 2003. 160(1): p. 65-75.**

17. **Rossig, L., et al., *Congestive heart failure induces endothelial cell apoptosis: protective role of carvedilol.* J Am Coll Cardiol, 2000. 36(7): p. 2081-9.**

3. RESULTS

3.1 MODEL OF HYPERGLYCAEMIA-MEDIATED APOPTOSIS

H9c2 myoblasts cultured under hyperglycaemic conditions (22 mM and 33 mM) for five days were assessed for apoptosis. Here hyperglycaemic conditions caused an increase of 53.1 ± 6.3% ($n=3$, $p<0.01$) and 54.1 ± 9.7% ($n=3$, $p<0.01$) in apoptotic nuclei in response to 22 mM and 33 mM glucose, respectively (Figure 3.1).

A.

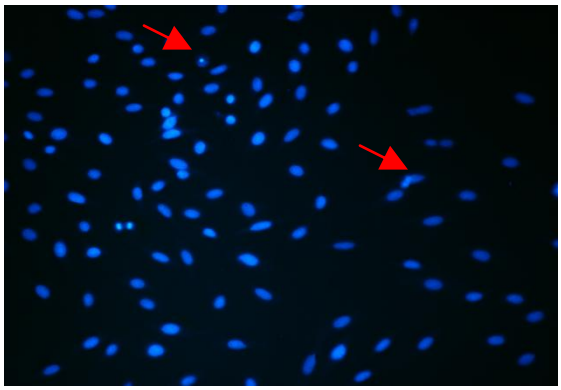

5.5 mM Glucose

B.

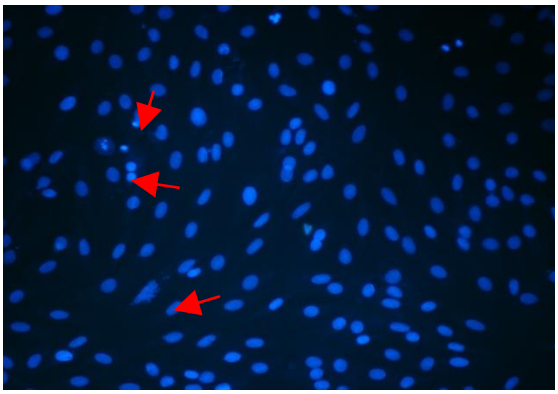

22 mM Glucose

C.

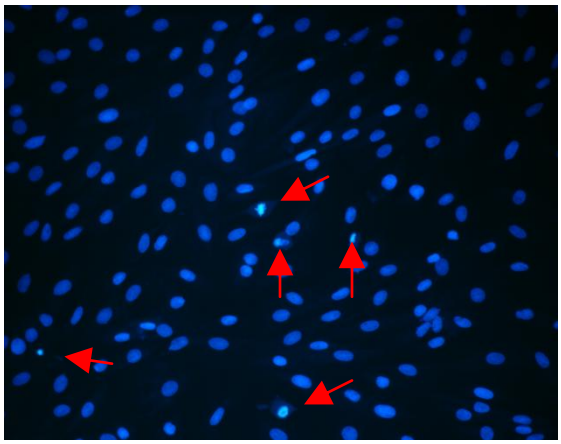

33 mM Glucose

D.

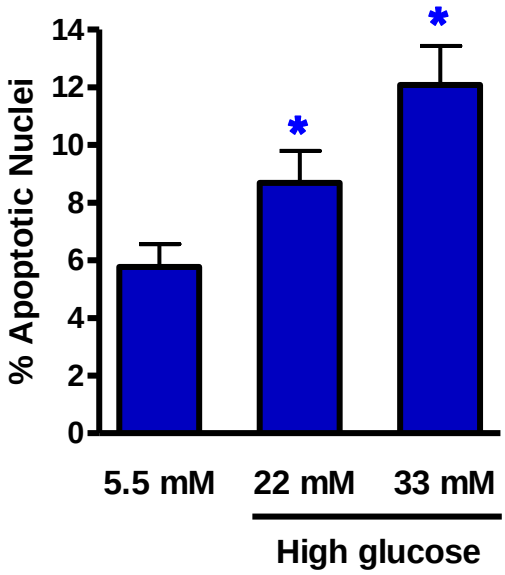

<u>Figure 3.1:</u> Hoechst nuclear staining demonstrating hyperglycaemia-mediated apoptosis.

*A) 5.5 mM glucose, B) 22 mM glucose, C) 33 mM glucose (red arrows indicate apoptotic nuclei) and D) bar graphs represent the number of apoptotic nuclei counted using criteria stipulated in the Materials and Methods section of this thesis (Section 2.4.1). Values are expressed as mean ± SEM (n=3). * p<0.01 vs. control.*

We also carried out Hoechst staining experiments with mannitol (22 mM and 33 mM mannitol) treated for 5 days, in order to exclude cell death due to osmotic effects (Figure 3.2).

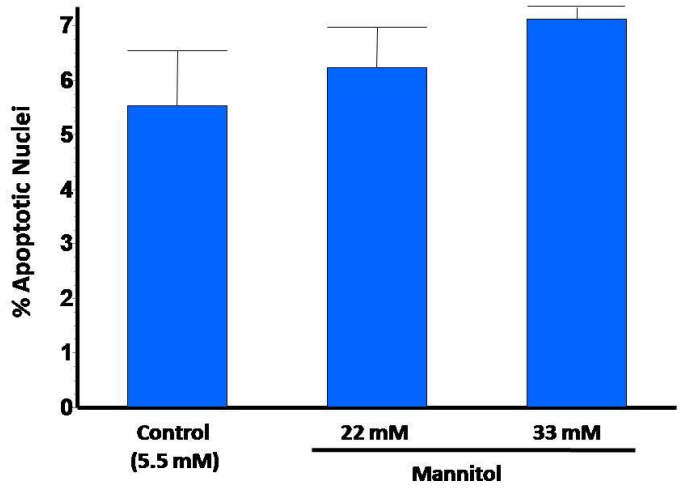

Figure 3.2: Unaltered incidence of apoptosis (Hoechst staining) in response to increasing mannitol concentrations.

Bar graphs represent the number of apoptotic nuclei counted using criteria stipulated in the Materials and Methods section of this thesis (Section 2.4.1) n=3.

To further strengthen our findings, we next assessed the degree of hyperglycaemia-induced apoptosis using a caspase activity assay. Here we found that hyperglycaemic conditions increased caspase activity by 26.4 ± 2.1% in response to 33 mM glucose ($n=6$, $p<0.05$) (Figure 3.3).

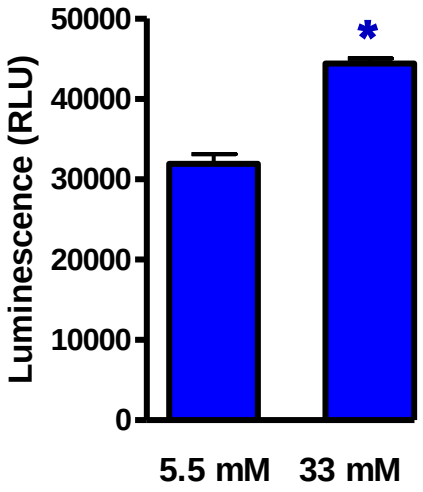

Figure 3.3: Increased caspase activity in response to high glucose.

*Caspase activity was assessed using the Caspase-Glo® 3/7 assay method as described in the Materials and Methods section of the thesis (Section 2.3.2). Bar graphs represent caspase activity as measured by luminescence. RLU: Relative Light Units. Values are expressed as mean ± SEM (n=6). * p<0.05 vs. control.*

Encouraged by these findings we next set out to determine the stage of apoptosis and used Annexin-V staining to measure membrane integrity. Our data show increased staining under hyperglycaemic conditions (43.1 ± 4.5% *vs.* 5.5 mm controls). Moreover, nuclei are clearly condensed compared to control culturing conditions (Figure 3.4).

A. **B.**

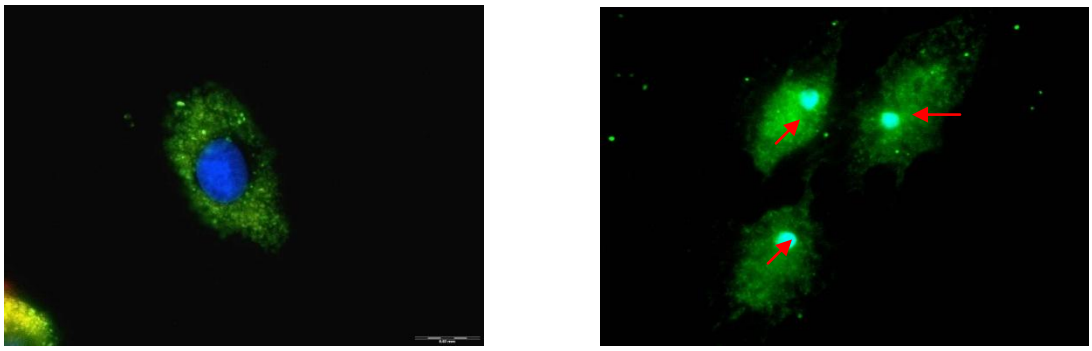

5.5 mM Glucose 33 mM Glucose

C.

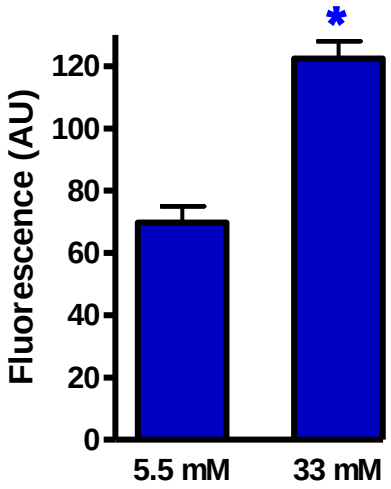

<u>Figure 3.4:</u> Annexin-V staining demonstrating increased apoptosis under hyperglycaemic conditions.

*A) 5.5 mM glucose and B) 33 mM glucose (red arrows indicate condensed nuclei) and C) bar graphs represent the fluorescence intensity of staining as described in the Materials and Methods section of this thesis (Section 2.3.3). AU: Arbitrary Units. Values are expressed as mean ± SEM (n=3). * p<0.001 vs. control.*

To further confirm these data we also performed Western blotting analysis for caspase-3, a well-described apoptotic marker. In agreement with our previous findings, hyperglycaemic conditions caused a significant increase in caspase-3 levels (Figure 3.5).

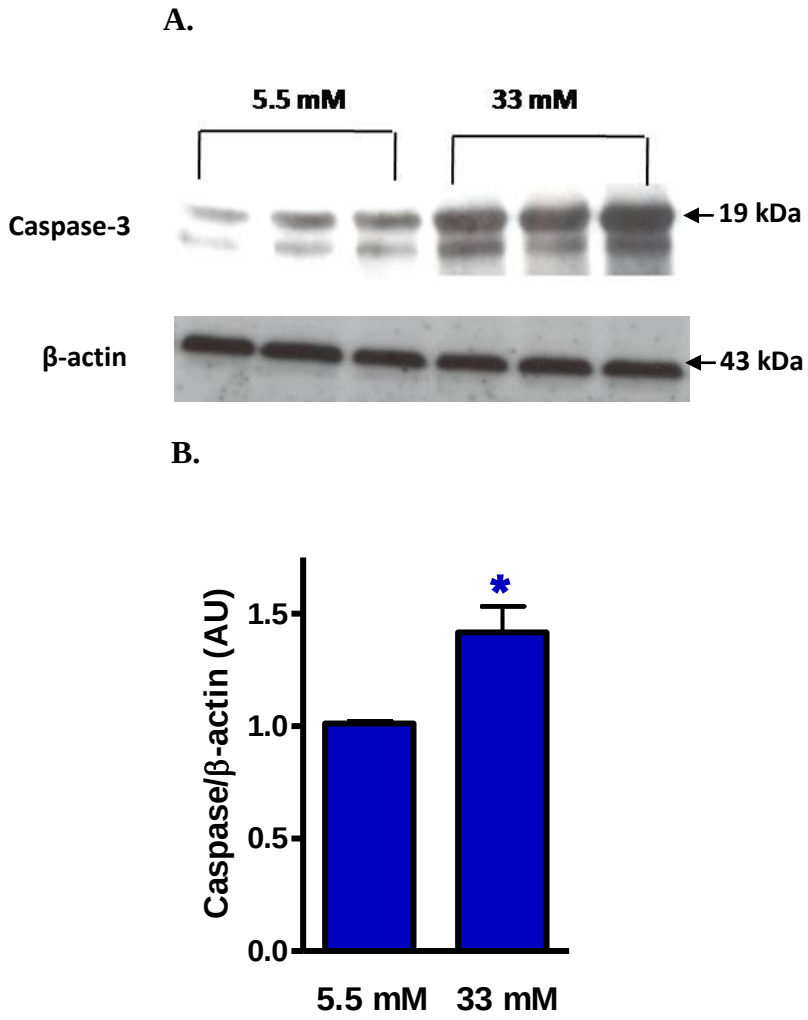

Figure 3.5: Caspase-3 Western blot analysis demonstrating hyperglycaemia-mediated apoptosis.

A) Representative blot showing increased caspase-3 expression under hyperglycaemic conditions compared to matched controls (5.5 mM glucose). B) Bar graphs show densitometric representation of caspase-3 levels (normalized to β-actin) (p<0.05 vs. control; n=4). AU: Arbitrary units. Values are expressed as mean ± SEM.*

3.2 ROLE OF THE HEXOSAMINE BIOSYNTHETIC PATHWAY IN HYPERGLYCAEMIA-MEDIATED APOPTOSIS

3.2.1 Inhibition of GFAT, the HBP rate-limiting step

Having established an *in-vitro*-based method for hyperglycaemia-induced apoptosis, we next proceeded to test our hypothesis, i.e. the role of the HBP in this process. We began by inhibiting GFAT, the rate-limiting step of the HBP, by using 40 μM DON. The degree of apoptosis was thereafter assessed as before. We found that GFAT inhibition markedly attenuated hyperglycaemia-induced apoptosis, i.e. by 24.5 ± 7.9% in response to 22 mM ($n=3$, $p<0.05$ *vs.* controls) and 53.3 ± 6.2% in response to 33 mM glucose ($n=3$, $p<0.001$ *vs.* controls) (Figure 3.6).

A.

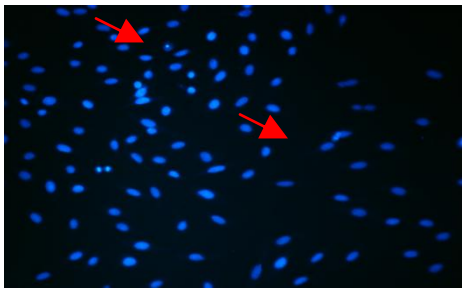

5.5 mM Glucose

D.

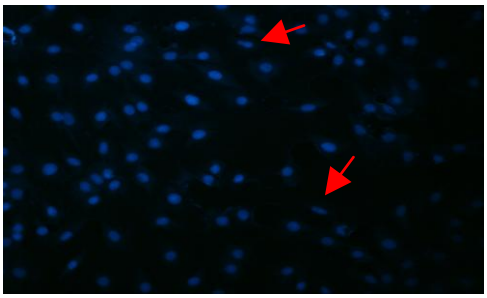

5.5 mM Glucose + DON

B.

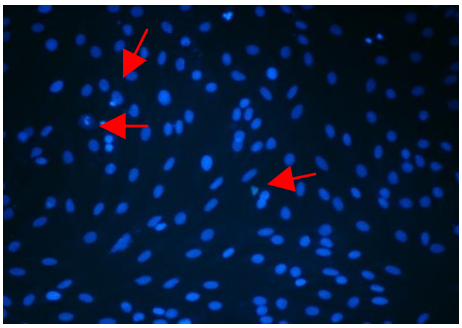

22 mM Glucose

E.

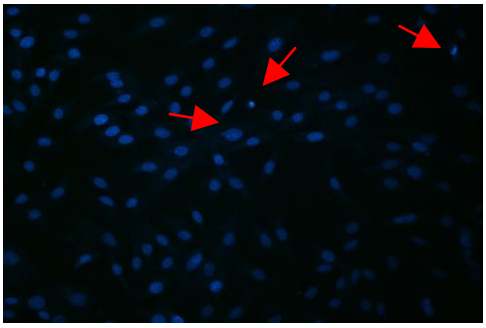

22 mM Glucose + DON

C.

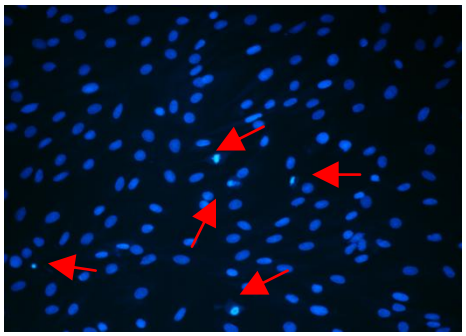

33 mM Glucose

F.

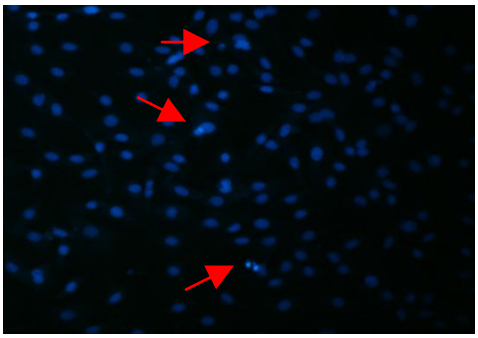

33 mM Glucose + DON

G.

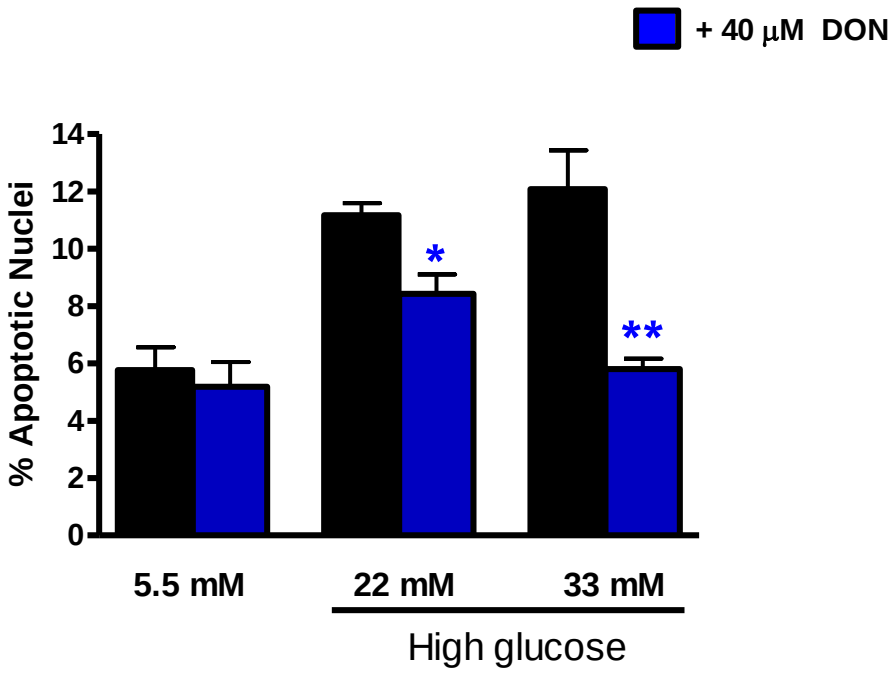

Figure 3.6: Inhibition of the HBP rate-limiting step (with 40 μM DON) attenuates hyperglycaemia-mediated apoptosis.

*A) 5.5 mM glucose, B) 22 mM glucose, C) 33 mM glucose, D) 5.5 mM glucose + DON, E) 22 mM glucose + DON and F) 33 mM glucose + DON (red arrows indicate apoptotic nuclei), G) bar graphs represent the number of apoptotic nuclei counted using criteria stipulated in the Materials and Methods section of this thesis (Section 2.4.1). Values are expressed as mean ± SEM (n=3). * p<0.01 vs. 22 mM glucose, ** p<0.001 vs. 33 mM glucose.*

Caspase activity assays performed in the presence of DON further supported these results. DON administration decreased hyperglycaemia-mediated caspase activity by 13.2 ± 3% compared to untreated controls (n=6, $p<0.05$ *vs.* 33 mM glucose) (Figure 3.7).

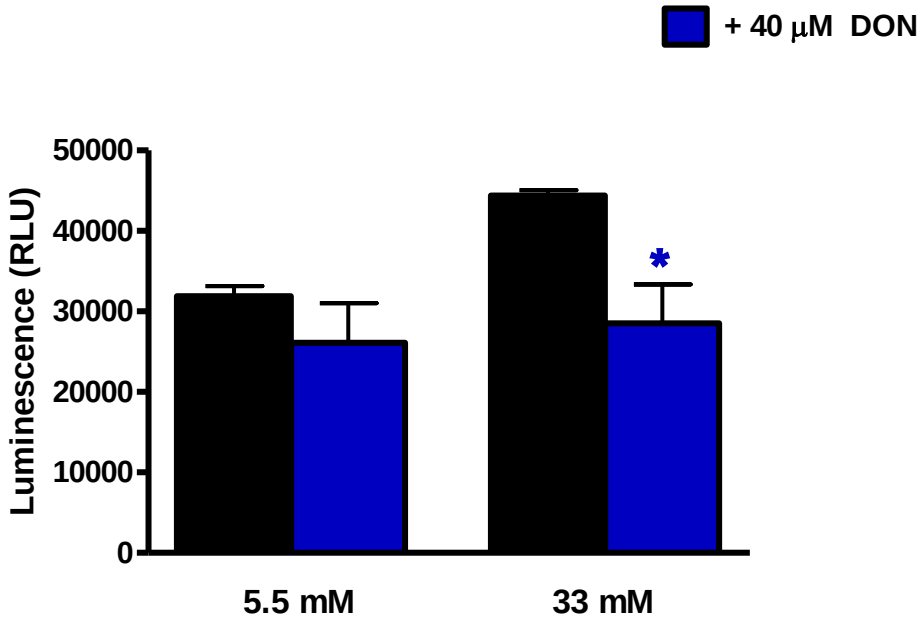

Figure 3.7: Inhibition of HBP rate-limiting step attenuates hyperglycaemia-induced caspase activity.

*Caspase activity was assessed using the Caspase-Glo® 3/7 assay method as described in the Materials and Methods section of the thesis (Section 2.3.2). Bar graphs represent caspase activity as measured by luminescence. RLU: Relative Light Units. Values are expressed as mean ± SEM (n=6). * p<0.05 vs. 33 mM glucose*.

We also evaluated the effects of DON on hyperglycaemia-mediated apoptosis by measuring Annexin-V staining. In agreement with our previous findings, DON administration showed a decreasing apoptotic trend though it did not show statistical significance (p=0.08 *vs.* 33 mM glucose) in response to high glucose exposure (Figure 3.8).

A.

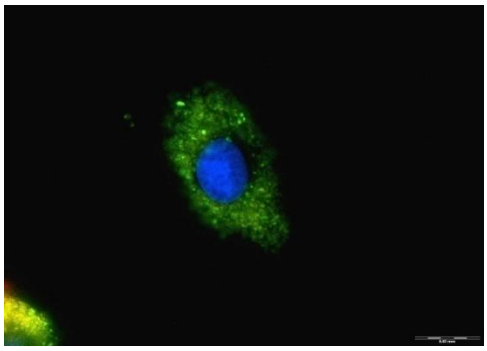

5.5 mM Glucose

C.

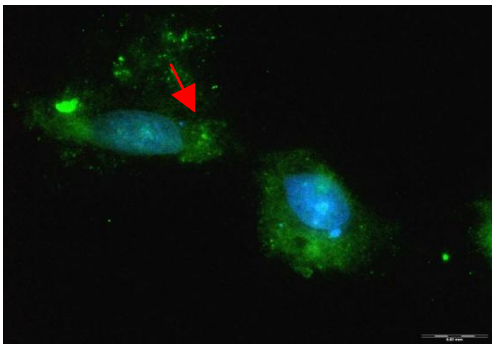

5.5 mM Glucose + DON

B.

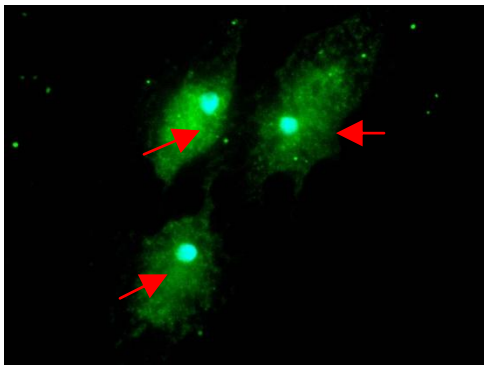

33 mM Glucose

D.

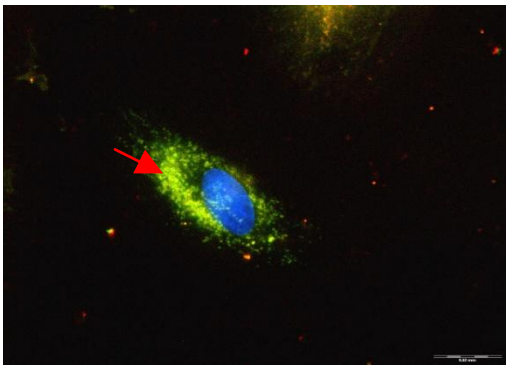

33 mM Glucose + DON

E.

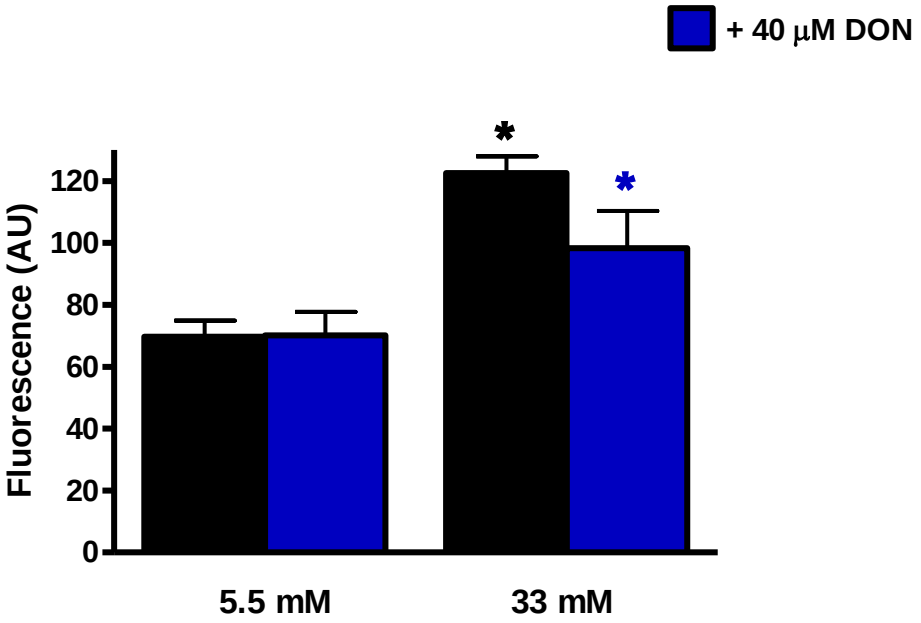

Figure 3.8: Inhibition of HBP rate-limiting enzyme attenuates Hyperglycaemia-mediated apoptosis.

*A) 5.5 mM glucose, B) 33 mM glucose, C) 5.5 mM glucose + DON, D) 33 mM glucose + DON (red arrows indicate Annexin stain fluorescence) and E) bar graphs represent the fluorescence intensity of staining as described in the Materials and Methods section of this thesis (section 2.3.3). AU: Arbitrary Units. Values are expressed as mean ± SEM (n=3). * p<0.001 vs. 5.5 mM control.*

3.2.2 Inhibition of *O*-GlcNAcase, enzyme cleaving off *O*-GlcNAc residues

Assessing the effects of inhibition of *O*-GlcNAcase, an enzyme that removes *O*-GlcNAc residues from target proteins, by using PUGNAc, the inhibition of *O*-GlcNAcase should therefore result in higher *O*-GlcNAcylation of target proteins and increased apoptosis. We found increased apoptosis in response to PUGNAc treatment. PUGNAc administration increased apoptosis, although this did not reach statistical significance, i.e. p=0.07 in response to both 22 mM and 33 mM glucose exposure. However, there was a significant increase in apoptotic nuclei for 5.5 mM glucose experiments treated with PUGNAc (p=0.01 *vs.* 5.5 mM glucose) (Figure 3.9).

A.

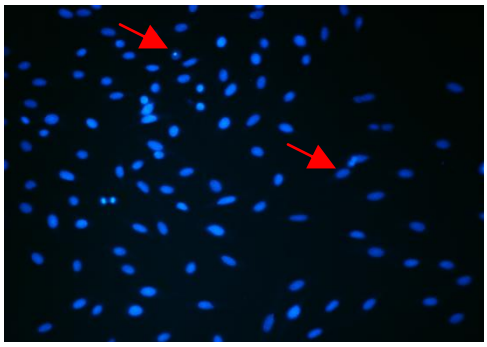

5.5 mM Glucose

D.

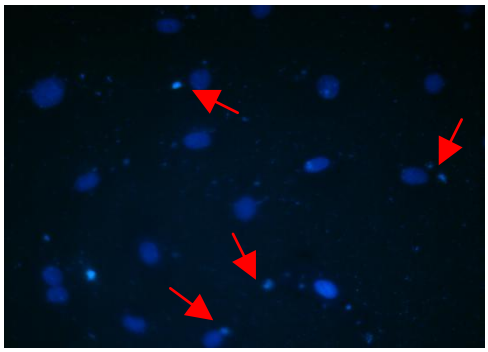

5.5 mM Glucose + PUGNAc

B.

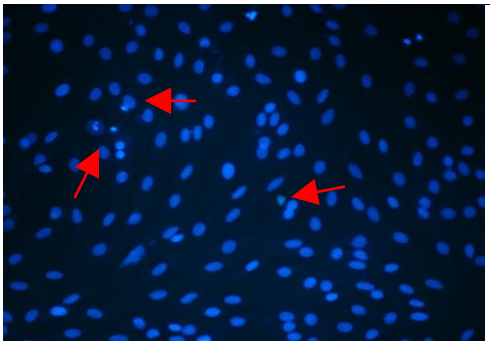

22 mM Glucose

E.

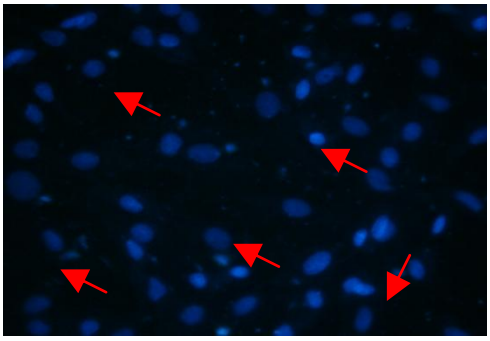

22 mM Glucose + PUGNAc

C.

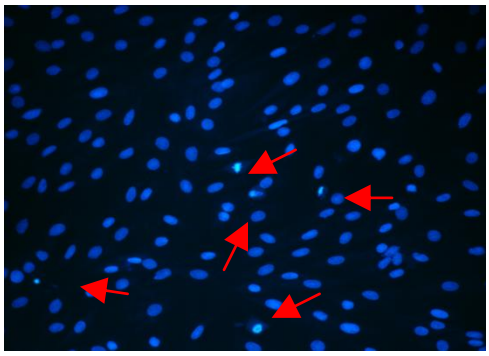

33 mM Glucose

F.

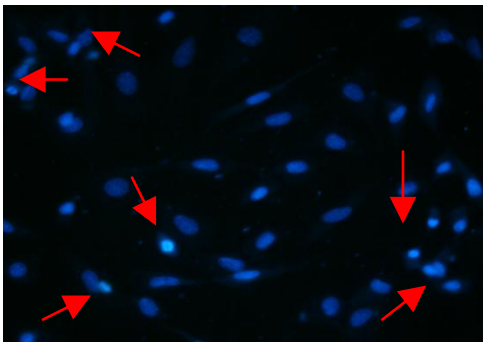

33 mM Glucose + PUGNAc

G.

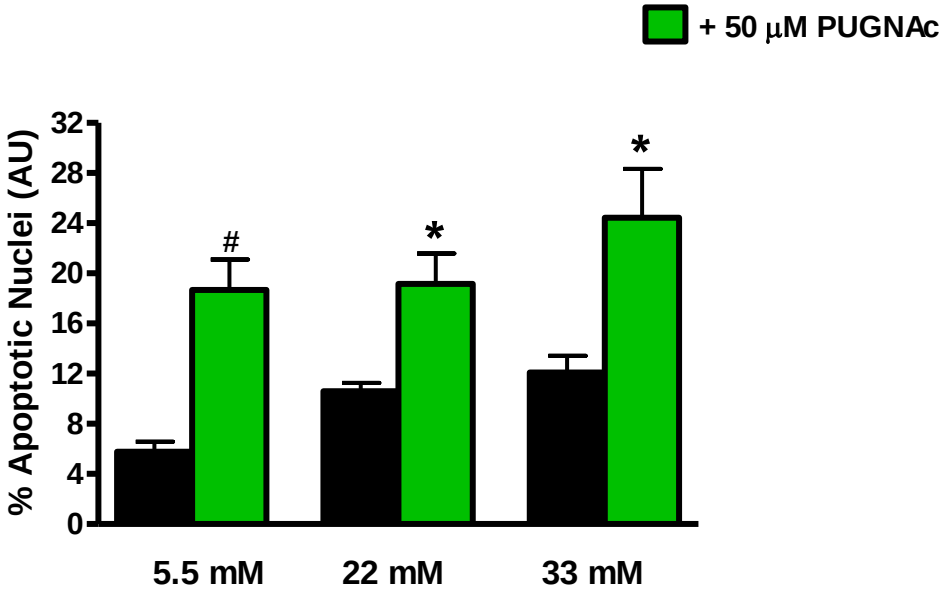

Figure 3.9: PUGNAc treatment (50 μM) increases apoptosis under high glucose conditions.

*A) 5.5 mM glucose, B) 22 mM glucose, C) 33 mM glucose, D) 5.5 mM glucose + PUGNAc, E) 22 mM glucose + PUGNAc, F) 33 mM glucose + PUGNAc (red arrows indicate apoptotic nuclei) and images were obtained using a 10x magnification; G) bar graphs represent the number of apoptotic nuclei counted using criteria stipulated in the Materials and Methods section of this thesis (Section 2.4.1). Values are expressed as mean ± SEM (n=3). # p<0.01 vs. 5.5 mM glucose, * p=0.07 vs. 22 mM and 33 mm glucose, respectively.*

To further strengthen the Hoechst staining data, we next performed caspase activity assays in the presence or absence of 50 μM PUGNAc administration. PUGNAc treatment with high glucose increased caspase activity by 81.6 ± 5%. (n=6, p<0.001 *vs.* untreated 33 mM glucose) (Figure 3.10). Moreover, PUGNAc treatment also increased caspase activity under low glucose culturing conditions.

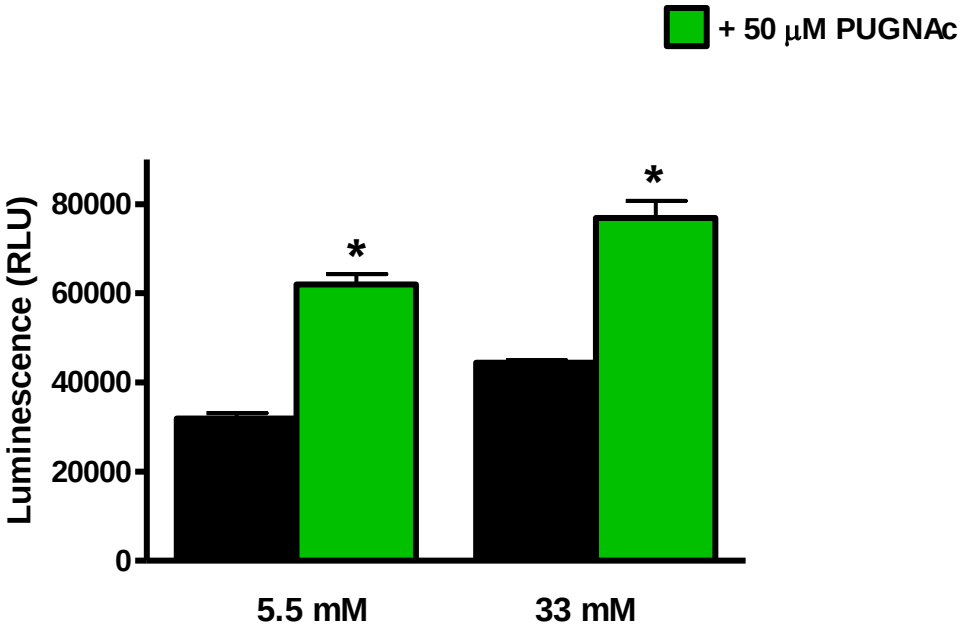

<u>Figure 3.10:</u> PUGNAc treatment (50 μM) increases caspase activity under hyperglycaemic conditions.

*Caspase activity was assessed using the Caspase-Glo® 3/7 assay method as described in the Materials and Methods section of this thesis (Section 2.3.2). Bar graphs represent caspase activity as measured by luminescence. RLU: Relative Light Units. Values are expressed as mean ± SEM (n=6). * p<0.001 vs. matching control.*

We also performed Annexin-V staining to confirm our earlier findings with PUGNAc treatment. Here PUGNAc administration under high glucose culturing conditions resulted in greater Annexin-V staining (50 ± 2.9% *vs.* untreated controls, n=3, p<0.001) thus demonstrating increased apoptosis (Figure 3.11).

A.

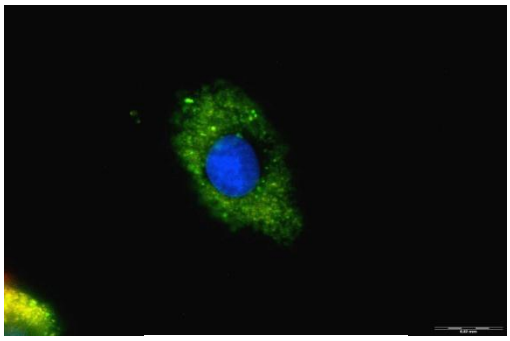

5.5 mM Glucose

C.

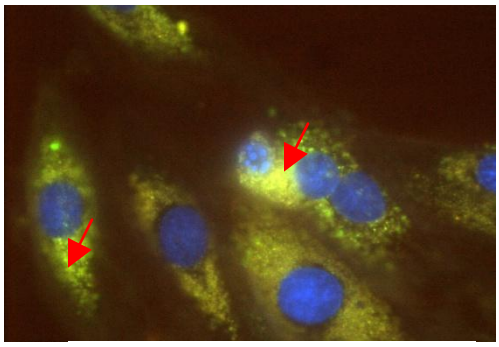

5.5 mM Glucose + PUGNAc

B.

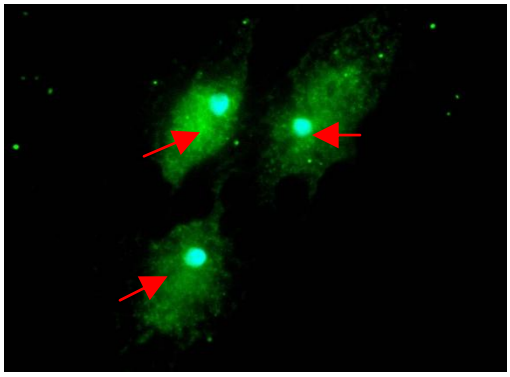

33 mM Glucose

D.

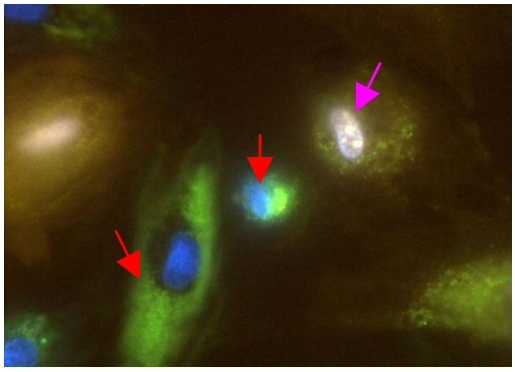

33 mM Glucose + PUGNAc

E.

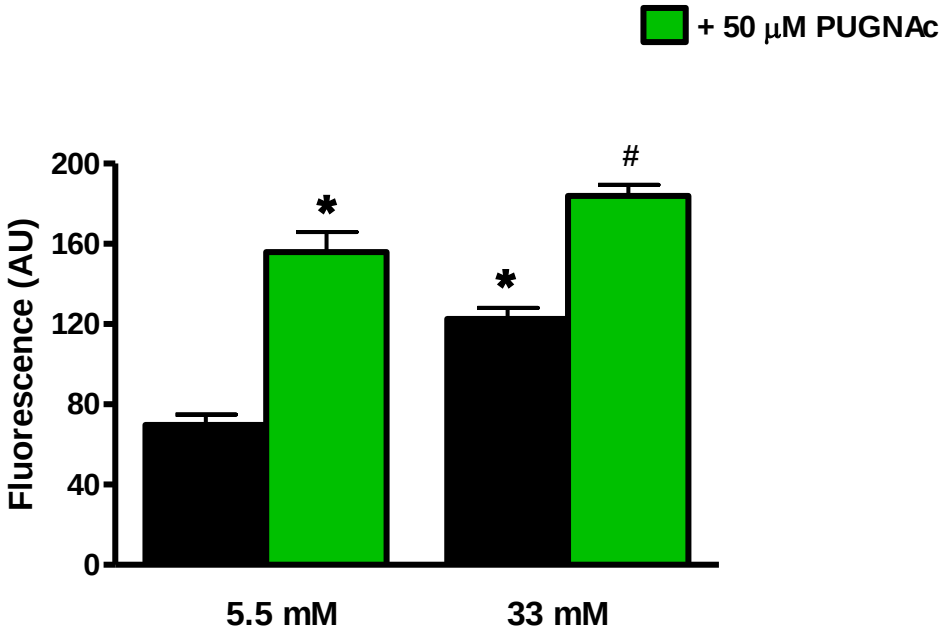

<u>Figure 3.11:</u> Annexin-V staining showing that PUGNAc treatment increases apoptosis under high glucose conditions.

*A) 5.5 mM glucose, B) 33 mM glucose, C) 5.5 mM glucose + PUGNAc, D) 33 mM glucose + PUGNAc (red arrows indicate Annexin stain fluorescence; pink arrow indicates nuclear condensation and PI staining due to advanced apoptosis) and E) bar graph represents the fluorescence intensity of staining as described in the Materials and Methods section of this thesis (Section 2.3.3). Values are expressed as mean ± SEM (n=3). * p<0.001 vs. 5.5 mM glucose, # p<0.001 vs. 33 mM glucose.*

3.3 EVALUATING THE ROLE OF OXIDATIVE STRESS IN HBP-MEDIATED APOPTOSIS

3.3.1 H2DCFDA staining

We began by measuring ROS levels by H2DCFDA staining. Our data show that there is an increase of ROS production in response to hyperglycaemia (n=3, $p<0.01$ *vs.* 5.5 mM controls) (Figure 3.12).

A.

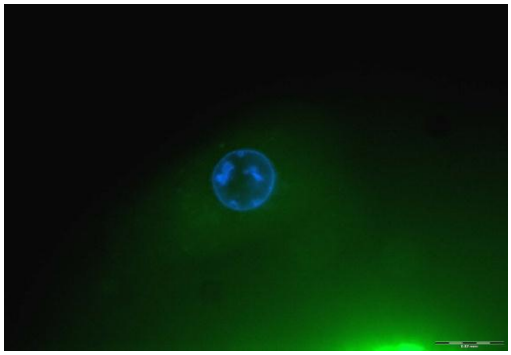

5.5 mM Glucose

B.

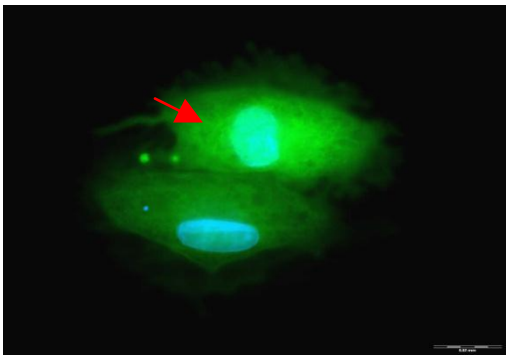

33 mM Glucose

C.

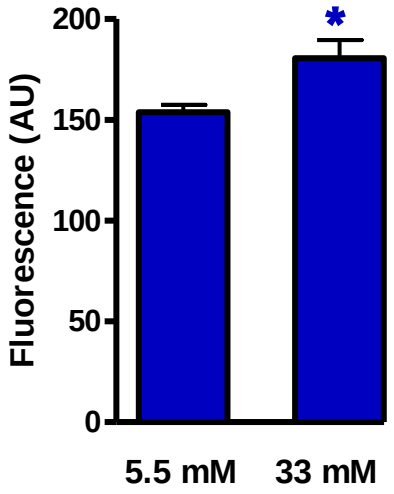

Figure 3.12: Increased ROS production in response to high glucose exposure.

*A) 5.5 mM glucose, B) 33 mM glucose (red arrow indicates ROS stain fluorescence) and C) bar graphs represent the fluorescence intensity of staining as described in the Materials and Methods section of this thesis (Section 2.4.1). AU: Arbitrary Units. Values are expressed as mean ± SEM (n=3). * p<0.01 vs. 5.5 mM control.*

When the cells were treated with 50 µM PUGNAc, ROS levels were increased by 22.1 ± 5.1% (n=3, $p<0.05$ *vs.* matching control) and 21.9 ± 3.5% (n=3, $p<0.01$ *vs.* matching controls) for both low and high glucose conditions, respectively (Figure 3.13).

A.

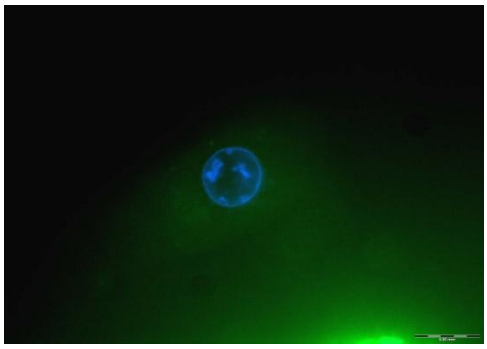

5.5 mM Glucose

C.

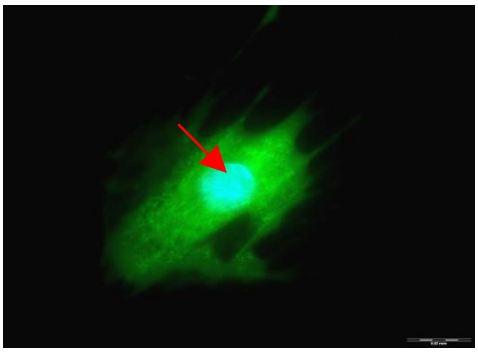

5.5 mM Glucose + PUGNAc

B.

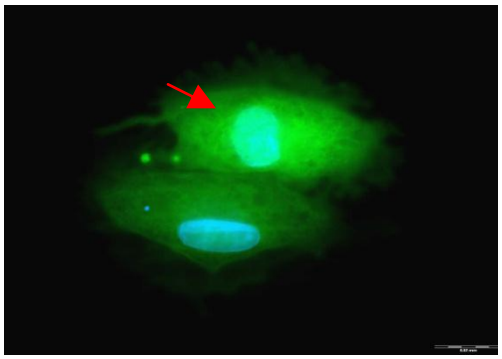

33 mM Glucose

D.

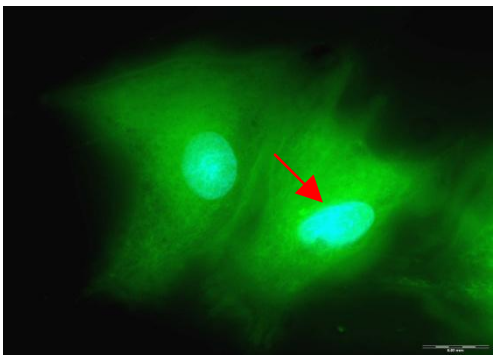

33 mM Glucose + PUGNAc

E.

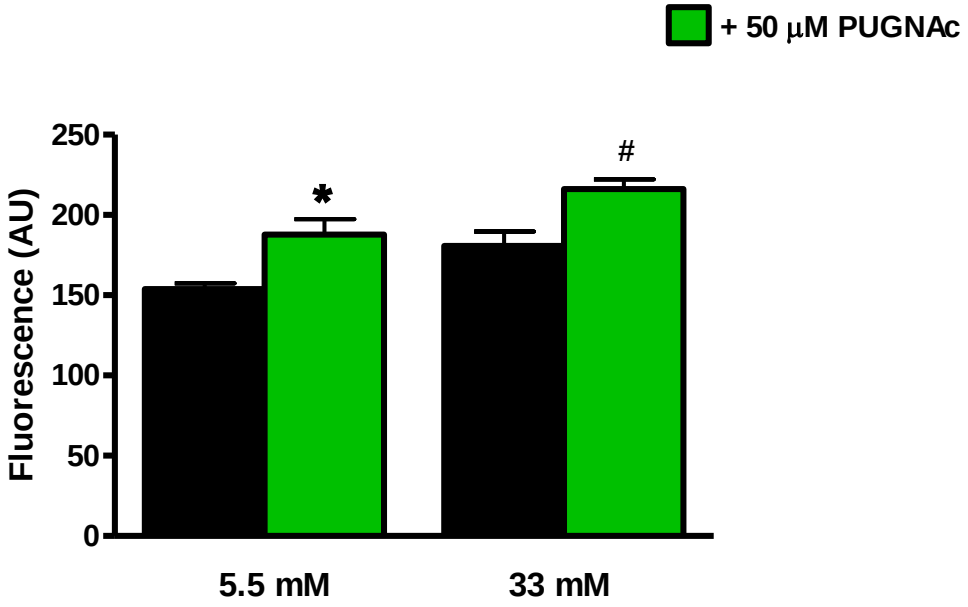

Figure 3.13: Administration of PUGNAc (50 μM) increases ROS production.

*A) 5.5 mM glucose, B) 33 mM glucose, C) 5.5 mM glucose + PUGNAc, D) 33 mM glucose + PUGNAc (red arrow indicates ROS stain fluorescence) E) bar graph represents the fluorescence intensity of staining as described in the Materials and Methods section of this thesis (Section 2.4.1). AU: Arbitrary Units. Values are expressed as mean ± SEM (n=3). * p<0.05 vs. 5.5 mM glucose, # p<0.01 vs. 33 mM glucose.*

Having established that ROS production is increased under hyperglycaemic conditions, we next tested whether administration of an anti-oxidant, α-hydroxy cinnamic acid (α-OHCA), diminishes ROS production. We found that α-OHCA administration blunted ROS production by 18.8 ± 4.2% under high glucose conditions (n=3, $p<0.05$ *vs.* 33 mM glucose) (Figure 3.14).

A.

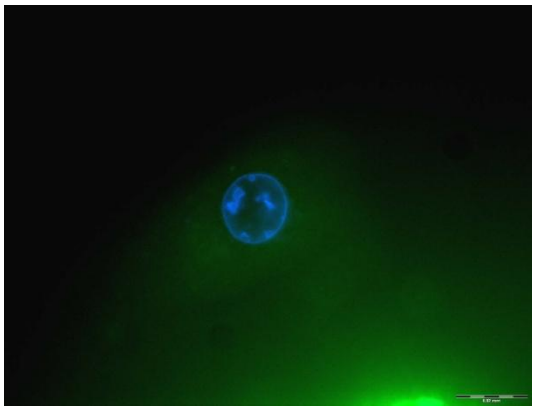

5.5 mM Glucose

C.

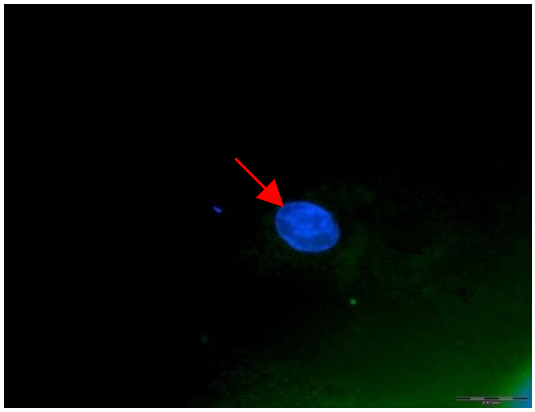

5.5 mM Glucose + α-OHCA

B.

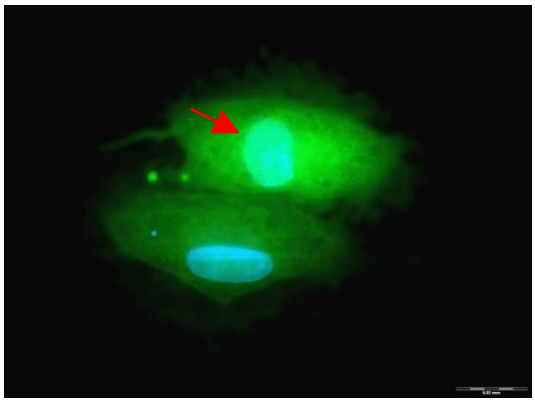

33 mM Glucose

D.

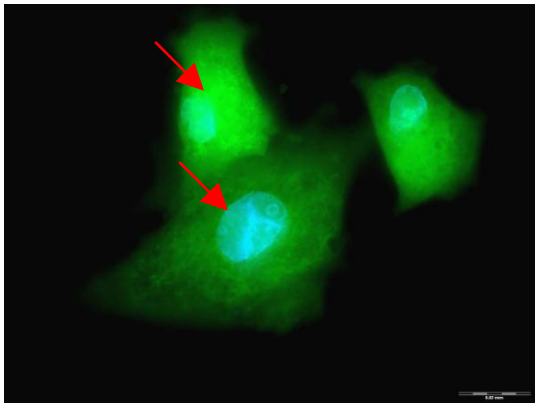

33 mM Glucose + α-OHCA

E.

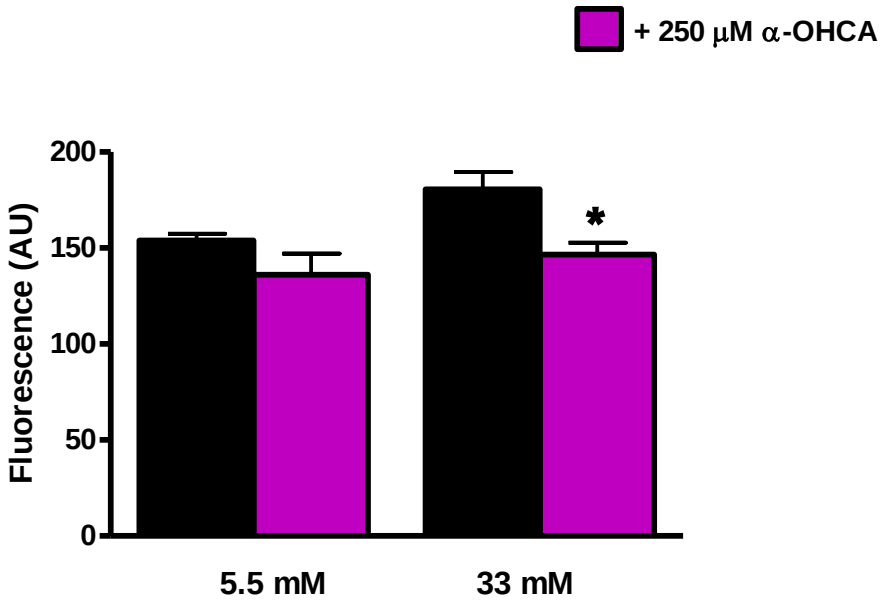

Figure 3.14: Antioxidant treatment (250 μM α-OHCA) diminishes hyperglycaemia-mediated ROS production.

*A) 5.5 mM glucose, B) 33 mM glucose, C) 5.5 mM glucose + α-OHCA, D) 33 mM glucose + α-OHCA (red arrows indicate ROS stain fluorescence) and E) bar graphs represent the fluorescence intensity of staining as described in the Materials and Methods section of this thesis (Section 2.4.1). Values are expressed as mean ± SEM (n=3). * p<0.05 vs. 33 mM control.*

Since PUGNAc treatment increased ROS levels and α-OHCA administration had the opposite effect, we next set out to determine whether α-OHCA would be able to attenuate PUGNAc-mediated apoptosis. In light of this, these agents were co-administered and ROS levels and the degree of apoptosis assessed.

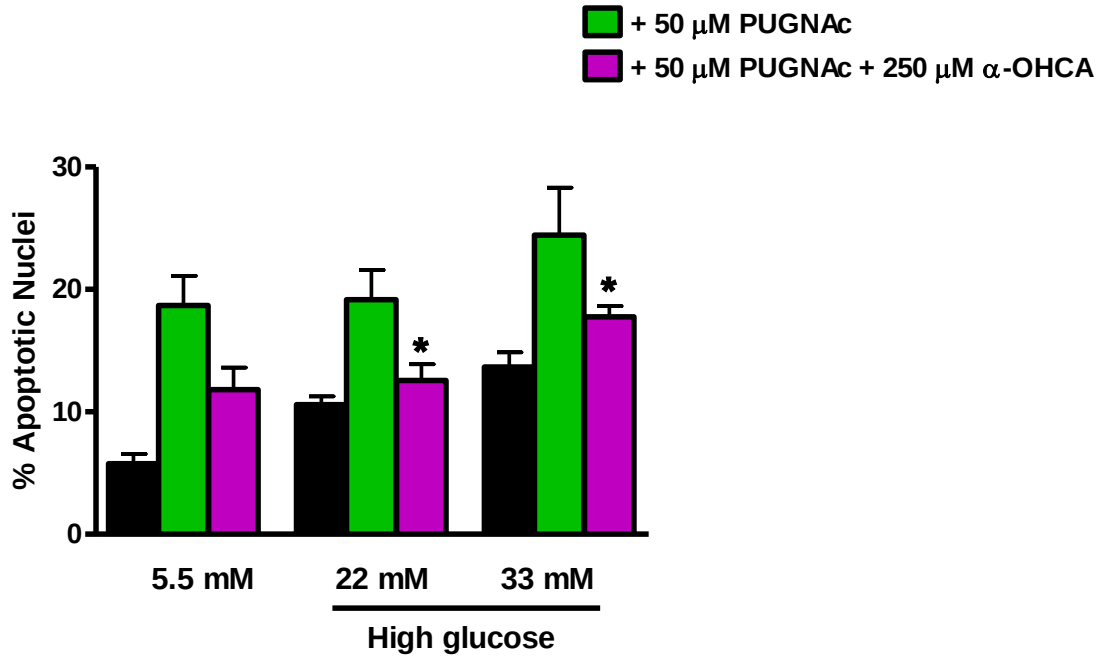

Figure 3.15: Antioxidant administration (250 μM α-OHCA) attenuates PUGNAc-mediated apoptosis.

*Bar graphs represent the number of apoptotic nuclei counted from Hoechst staining using criteria stipulated in the Materials and Methods section of this thesis (Section 2.4.1). Values are expressed as mean ± SEM (n=3). * p<0.05 vs. matched PUGNAc treatment.*

In agreement, we found that the PUGNAc-mediated increase in Hoechst staining and caspase activity was reduced when α-OHCA was co-administered (Figure 3.15 and 3.16). This observation was made for both low and high glucose culturing conditions.

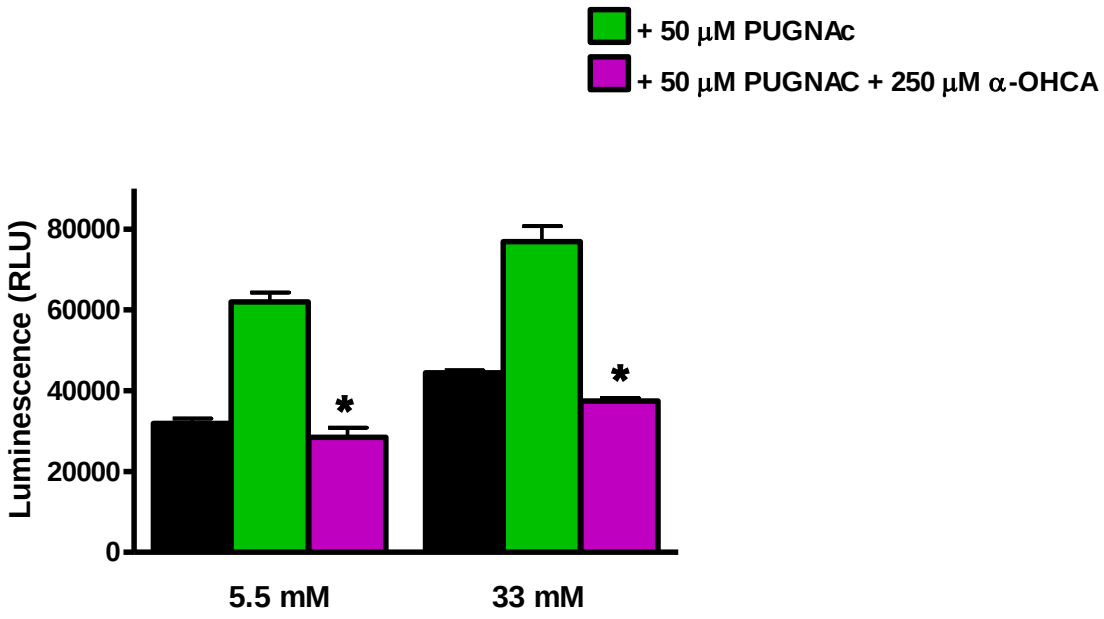

Figure 3.16: Antioxidant (250 μM α-OHCA) treatment diminishes PUGNAc-mediated increase in caspase activity.

*Caspase activity was assessed using the Caspase-Glo® 3/7 assay method as described in the Materials and Methods section of this thesis (Section 2.3.2). Bar graphs represent caspase activity as measured by luminescence. RLU: Relative Light Units. Values are expressed as mean ± SEM (n=6). * p<0.001 vs. matched PUGNAc experiments.*

Annexin-V staining data further support these findings and indicate that this occurs during the early stages of the apoptotic cascade (Figure 3.17).

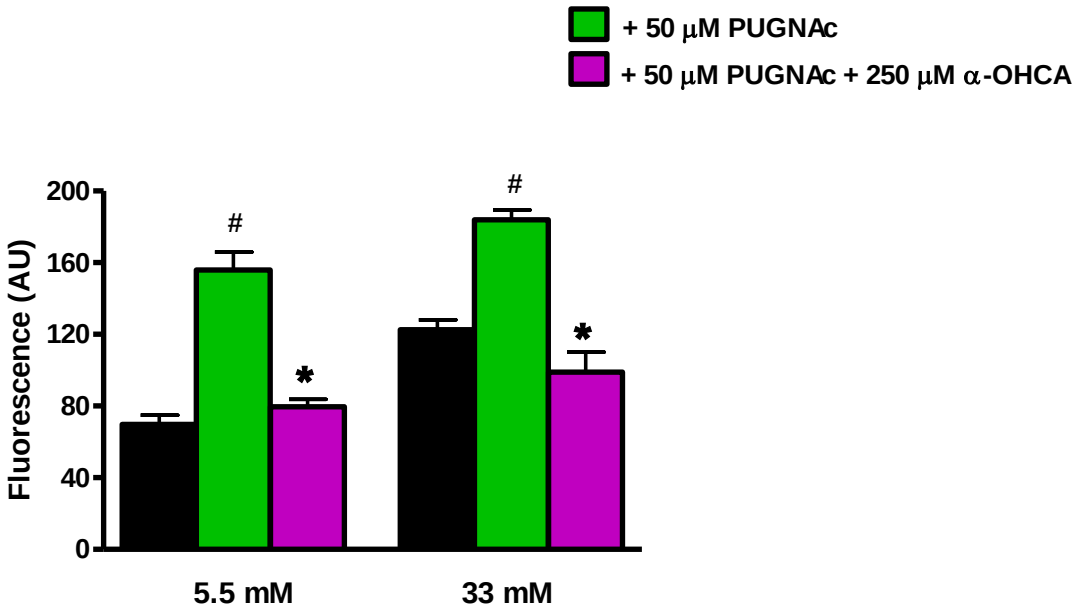

Figure 3.17: Antioxidant (250 μM α-OHCA) treatment reduces PUGNAc-mediated apoptosis.

Bar graphs represent the fluorescence intensity of Annexin staining as described in the Materials and Methods section of this thesis (Section 2.3.3). Values are expressed as mean ± SEM.

** p<0.001 vs. matched PUGNAc experiments, # p<0.001 vs. untreated 5.5 mM and 33 mM glucose.*

We next tested whether α-OHCA co-administration with PUGNAc attenuates ROS production as previously discussed. As before, antioxidant administration diminished PUGNAc-mediated ROS production (Figure 3.18).

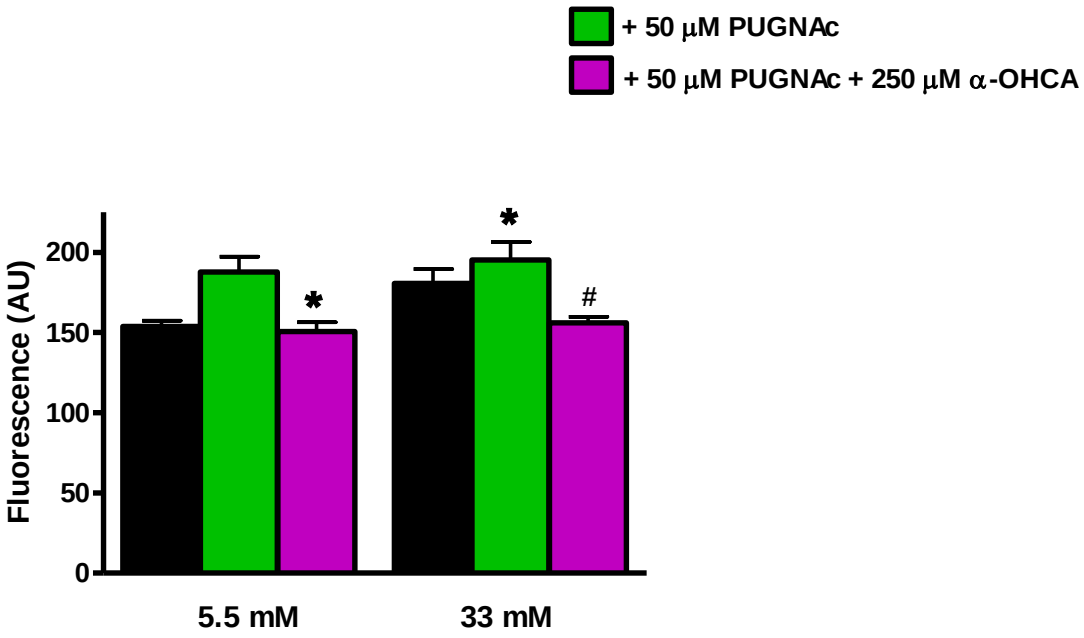

Figure 3.18: Antioxidant (250 μM α-OHCA) treatment reduces PUGNAc-mediated ROS production.

*Bar graphs represent the fluorescence intensity of H2DCFDA staining as described in the Materials and Methods section of this thesis (Section 2.4.1). Values are expressed as mean ± SEM. * p<0.05 vs. matched PUGNAc experiment, # p<0.01 vs. matched PUGNAc experiment.*

The reduction in ROS by α-OHCA when co-administered with PUGNAc was also confirmed using flow cytometry (Figure 3.19). Here PUGNAc-mediated ROS production under low glucose culturing conditions (blue curve, Figure 3.19A) was markedly reduced when α-OHCA was co-administered (brown curve Figure 3.19A). Likewise, this observation was also made under high glucose conditions (Figure 3.19B). These findings are also reflected when viewed as side scatter plots (Figure 3.19C-F). Here α-OHCA administration under high glucose conditions shifted the fluorescence scatter to the left (Figure 3.19D) compared to the untreated control (Figure 3.19C) thus indicating lower ROS levels. When PUGNAc was administered under high glucose conditions, there is a greater fluorescence (a shift to the right) indicating increased ROS levels (Figure 3.19E) which are attenuated by α-OHCA co-administration with PUGNAc (a shift to the left) (Figure 3.19F).

A.

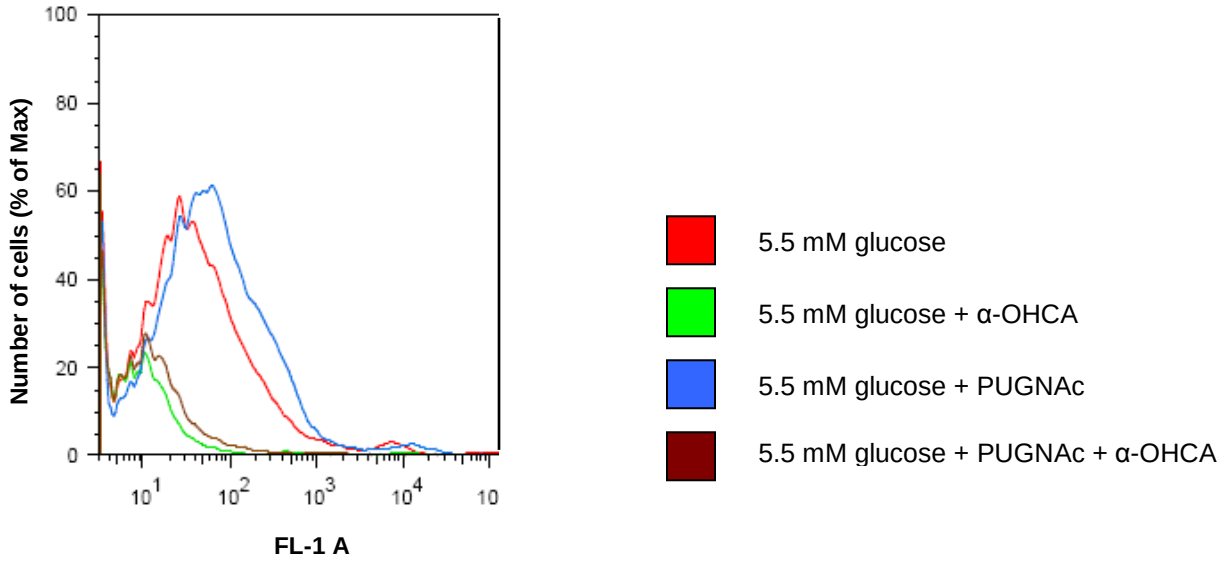
Number of cells (% of Max)
100
80
60
40
20
0
10^1
10^2
10^3
10^4
10
FL-1 A
5.5 mM glucose
5.5 mM glucose + α-OHCA
5.5 mM glucose + PUGNAc
5.5 mM glucose + PUGNAc + α-OHCA

B.

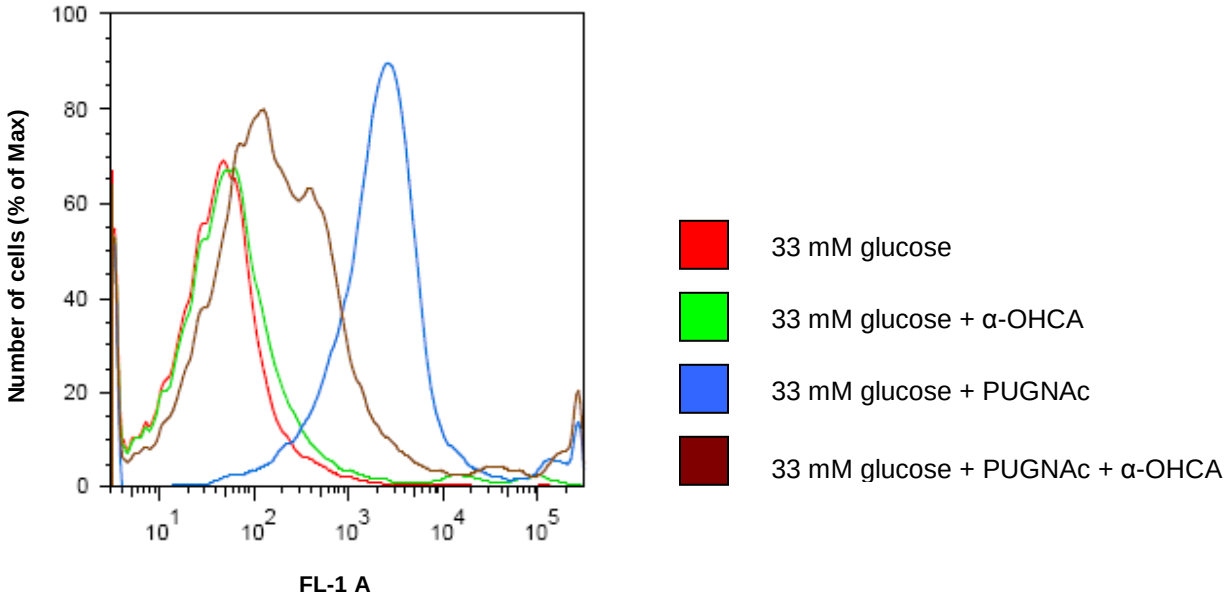
Number of cells (% of Max)
100
80
60
40
20
0
10^1
10^2
10^3
10^4
10^5
FL-1 A
33 mM glucose
33 mM glucose + α-OHCA
33 mM glucose + PUGNAc
33 mM glucose + PUGNAc + α-OHCA

C.

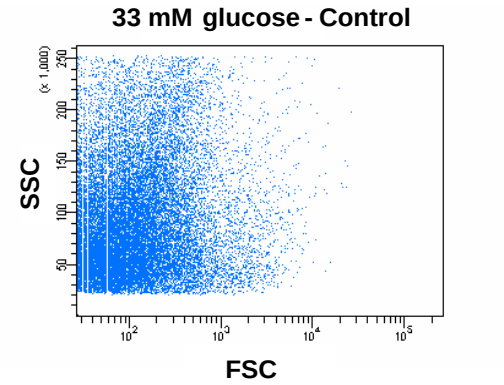
33 mM glucose - Control
SSC
FSC
(x 1,000)

D.

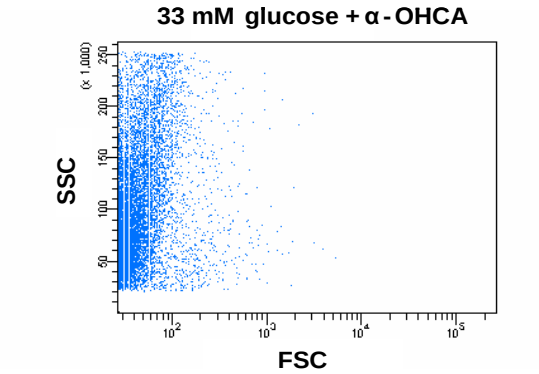
33 mM glucose + α - OHCA
SSC
FSC
(x 1,000)

E.

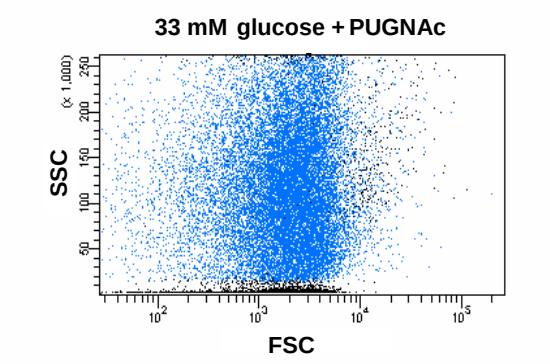
33 mM glucose + PUGNAc
SSC
FSC
(x 1,000)

F.

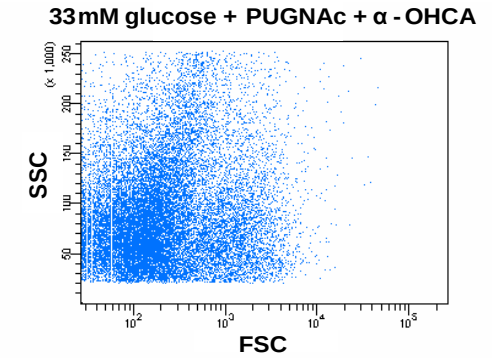
33 mM glucose + PUGNAc + α - OHCA
SSC
FSC
(x 1,000)

G.

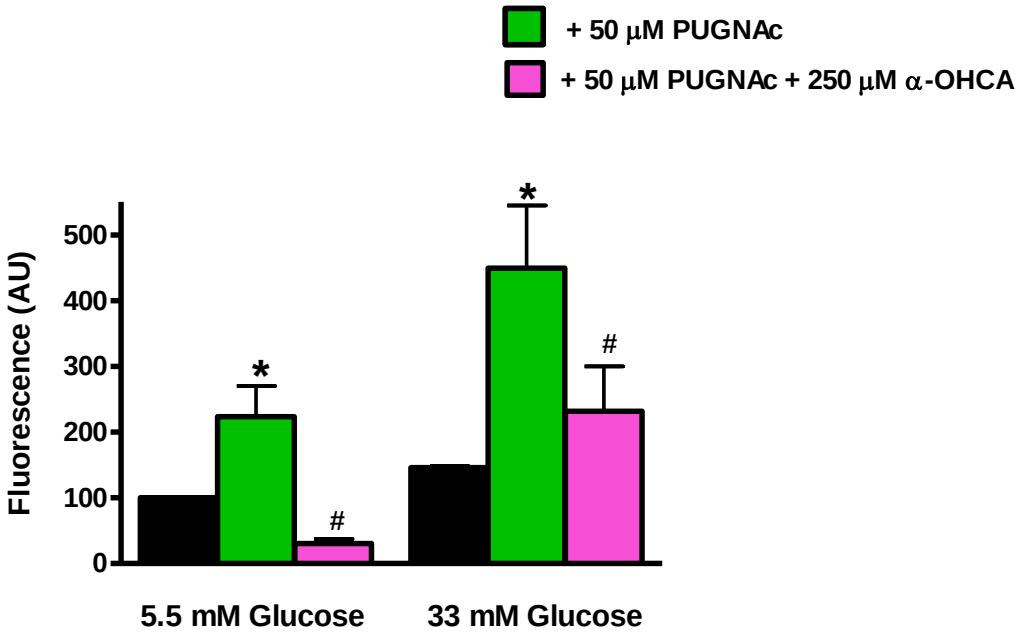

Figure 3.19: Flow cytometry demonstrating antioxidant (250 μM α-OHCA) treatment attenuating PUGNAc-mediated ROS production.

*A) Population fluorescence data of 5.5 mM glucose experiments (50,000 cells), B) population fluorescence data of 33 mM glucose (50,000 cells). FL-1 A: Alexa Fluor 488 Area. The forward scatter (FSC) and side scatter (SSC) shifts of C) 33 mM glucose, D) 33 mM glucose + α-OHCA, E) 33 mM glucose + PUGNAc, F) 33 mM glucose + α-OHCA + PUGNAc and G) bar graphs represent the fluorescence intensity of ROS staining as described in the Materials and Methods section of this thesis (Section 2.4.2). Values are expressed as mean ± SEM. * p<0.001 vs. matched PUGNAc experiment, # p<0.01 vs. matched PUGNAc experiment.*

For these set of experiments we included negative controls, i.e. cells not treated with H2DCFDA in order to check for background fluorescence. We also performed positive controls, i.e. by adding 100 μL of hydrogen peroxide (30% w/v) to samples after fluorescence measurements were completed. This was done to check if a sufficient amount of dye is still present in the sample. We found that hydrogen peroxide addition increased the fluorescence of samples,

shifting the curve to the right thus indicating that a sufficient amount of dye was still present in these samples (Figure 3.20).

A.

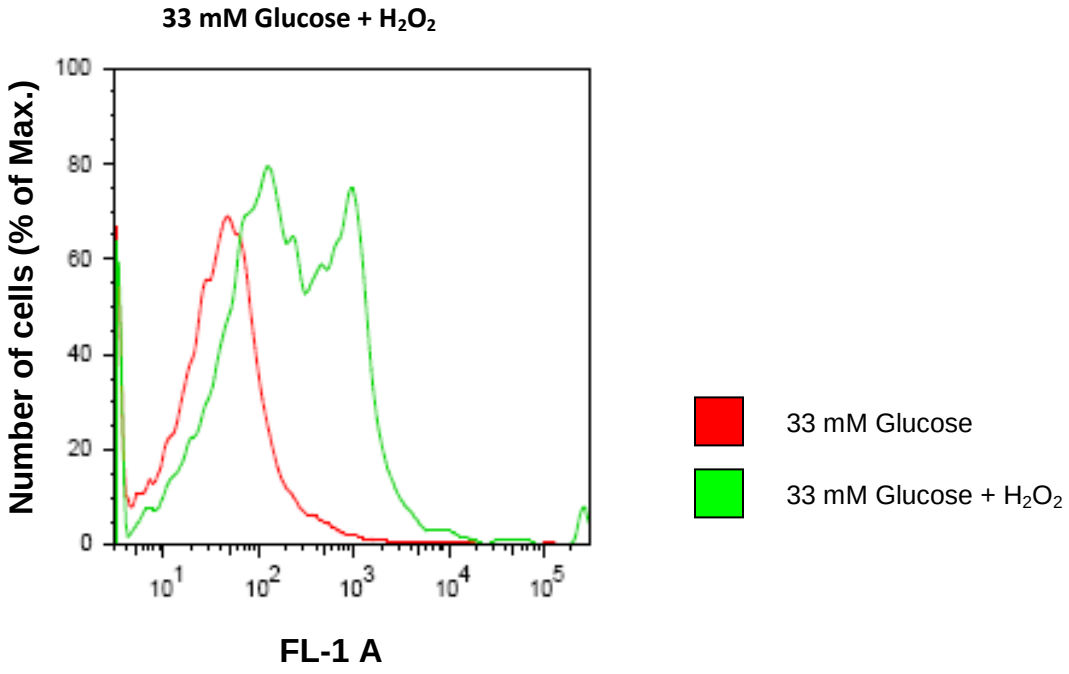

B.

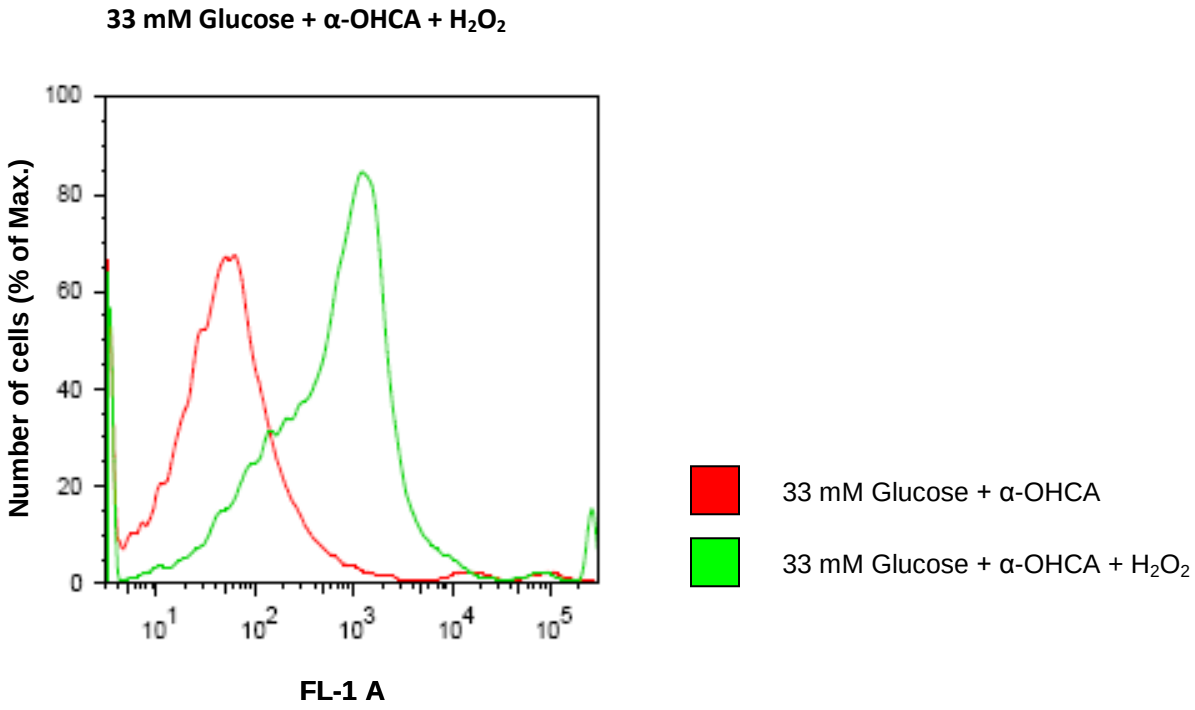
33 mM Glucose + α-OHCA + H2O2
Number of cells (% of Max.)
100
80
60
40
20
0
10^1
10^2
10^3
10^4
10^5
FL-1 A
33 mM Glucose + α-OHCA
33 mM Glucose + α-OHCA + H2O2

C.

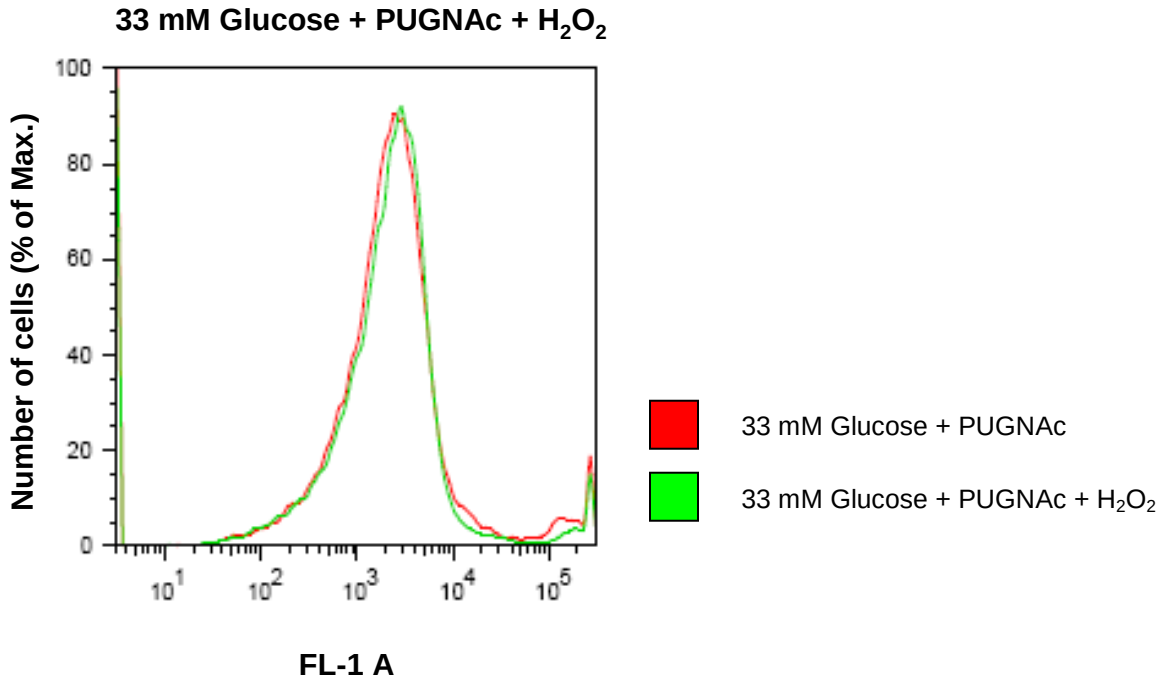
33 mM Glucose + PUGNAc + H2O2
Number of cells (% of Max.)
100
80
60
40
20
0
10^1
10^2
10^3
10^4
10^5
FL-1 A
33 mM Glucose + PUGNAc
33 mM Glucose + PUGNAc + H2O2

D.

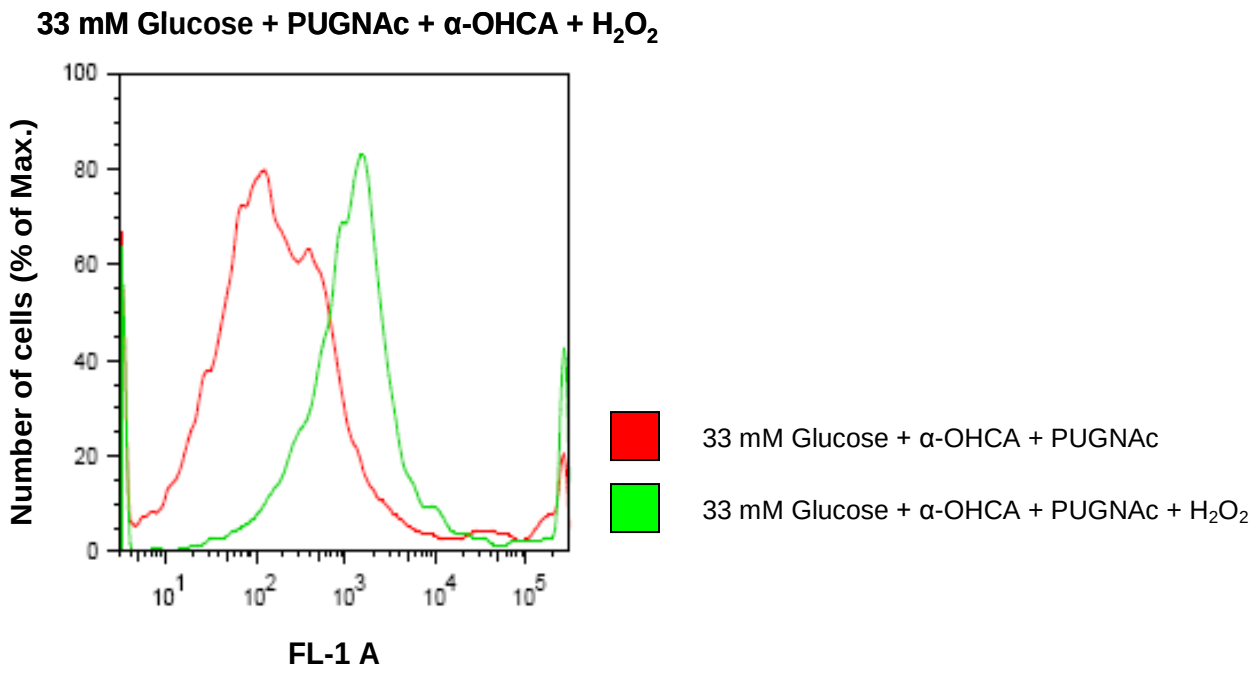

Figure 3.20: Positive controls for ROS using hydrogen peroxide.

Population fluorescence data for A) 33 mM Glucose, B) 33 mM Glucose + α-OHCA, C) 33 mM Glucose + PUGNAc, D) 33 mM Glucose + α-OHCA + PUGNAc. FL-1 A: Alexa Fluor 488 Area.

We next confirmed these interesting findings by performing Western blot analysis. Here the PUGNAc-mediated increase in apoptosis and the subsequent decrease by α-OHCA co-administration were reproduced by caspase-3, cytochrome-c and BAD peptide levels (Figure 3.21- 3.23).

A.

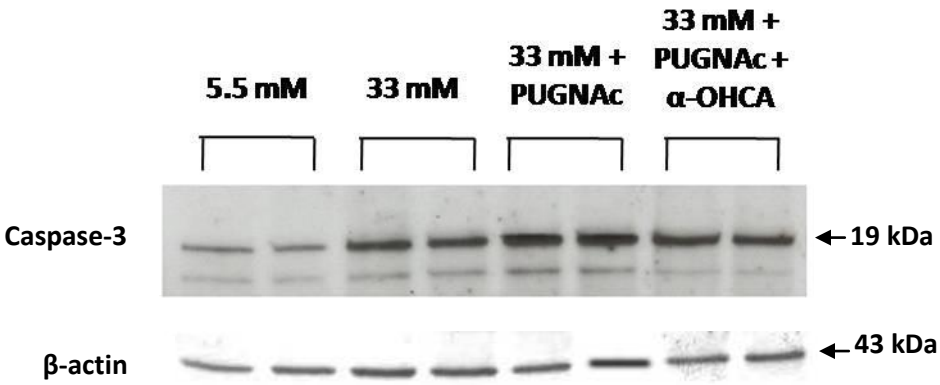

B.

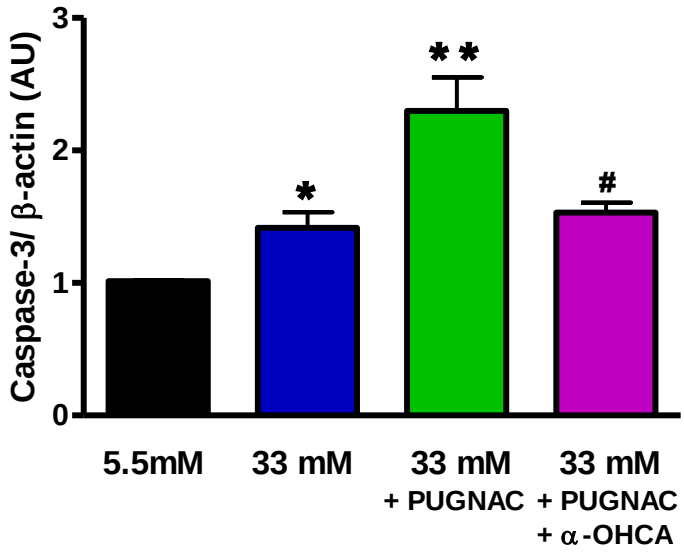

<u>Figure 3.21:</u> Increased caspase-3 peptide expression levels with HBP modulation.

A) Caspase-3 blot showing increased expression under hyperglycaemic conditions and PUGNAc administration, but decreased by antioxidant co-administration; B) Bar graphs show densitometric representation of caspase-3 normalized with β-actin. (p<0.05 vs. 5.5 mM, ** p<0.01 vs. 33 mM, # p<0.01 vs. 33 mM PUGNAc; n=4). AU: Arbitrary Units. Values are expressed as mean ± SEM.*

A.

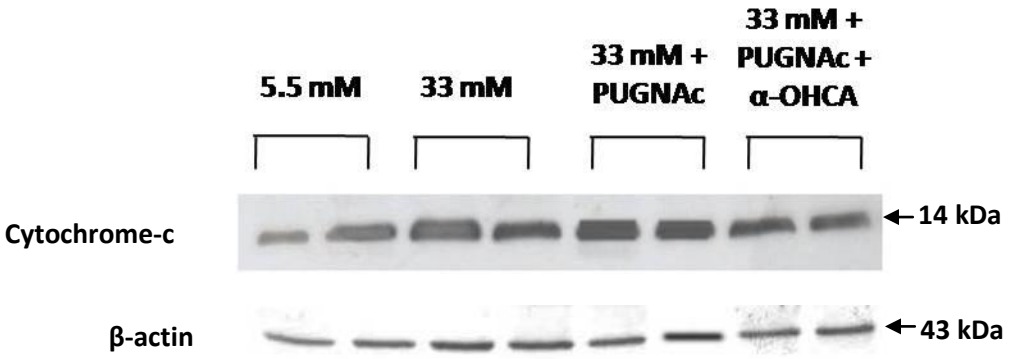

B.

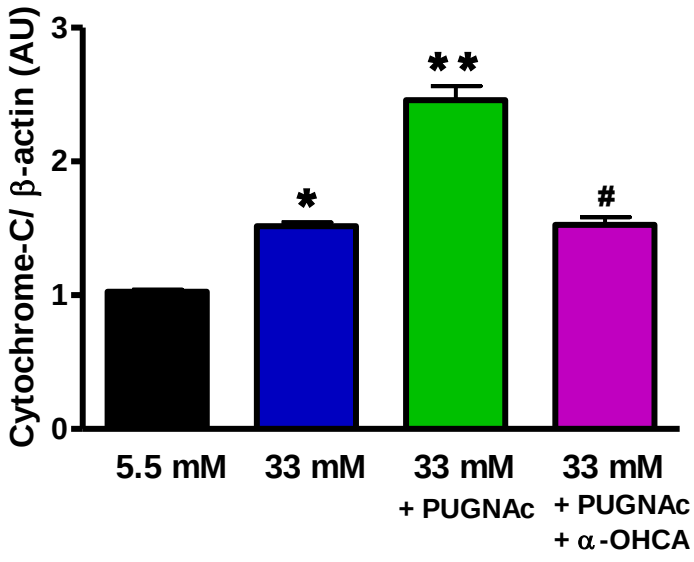

Figure 3.22: **Cytochrome-c Western blot analysis demonstrating HBP-mediated modulation of apoptosis.**

*A) Cytochrome-c blot showing increased expression under hyperglycaemic conditions and PUGNAc administration, but decreased by antioxidant co-administration; B) Bar graphs show densitometric representation of cytochrome-c levels normalized with β-actin. AU: Arbitrary Units. Values are expressed as mean ± SEM (n=4). * p<0.001 vs. 5.5 mM, ** p<0.001 vs. 33 mM, # p<0.001 vs. 33 mM PUGNAc.*

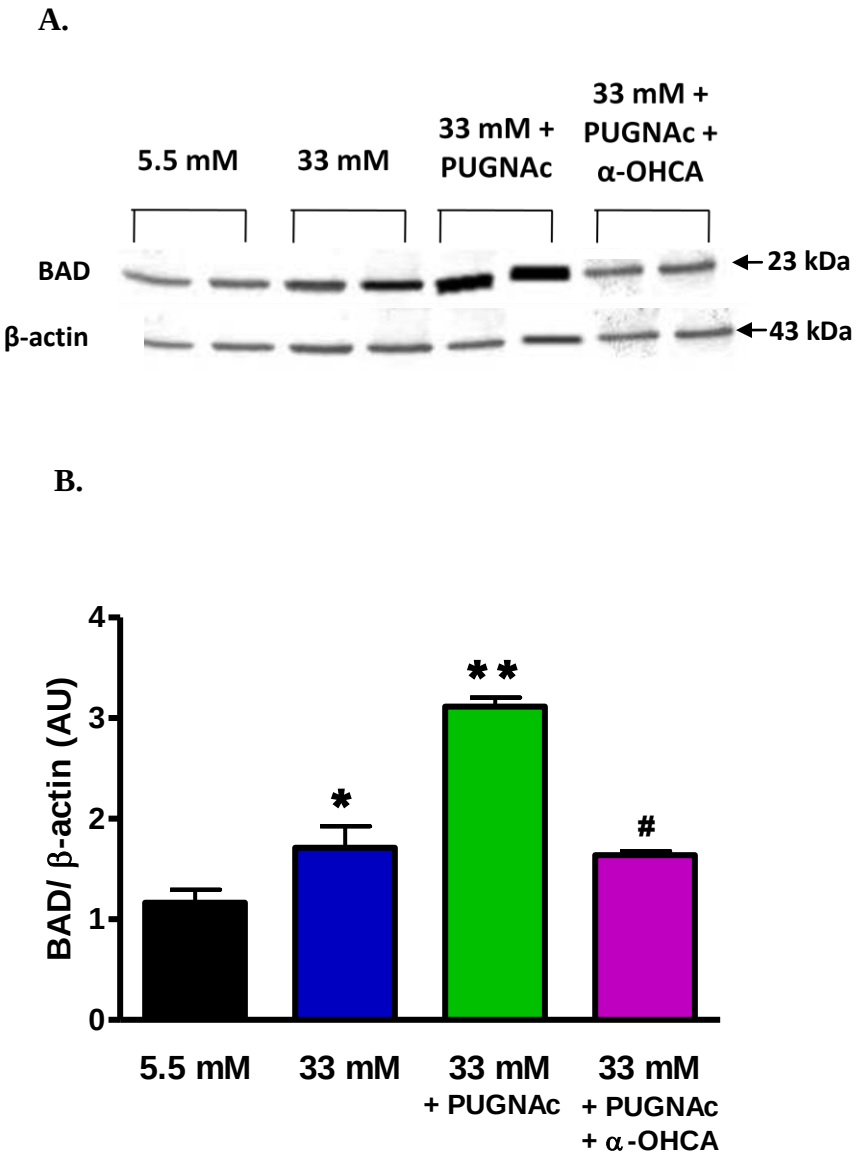

Figure 3.23: BAD Western blot analysis demonstrating HBP-mediated modulation of apoptosis.

*Representative blot showing increased BAD expression under hyperglycaemic conditions and PUGNAc administration, but decreased by antioxidant co-administration; B) Bar graphs show densitometric representation of BAD levels normalized with β-actin. AU: Arbitrary Units. Values are expressed as mean ± SEM (n=4). * p<0.01 vs. 5.5 mM, ** p<0.001 vs. 33 mM, # p<0.001 vs. 33 mM PUGNAc.*

Intrigued, we next ascertained whether these novel findings would be mirrored within an *in vivo* context. We proceeded to perform Western blot analysis on heart tissues collected from a rat model of

insulin resistance and hyperglycaemia. It was found that caspase-3, cytochrome-c and BAD peptide levels were significantly increased with the onset of insulin resistance (Figure 3.24- 3.26).

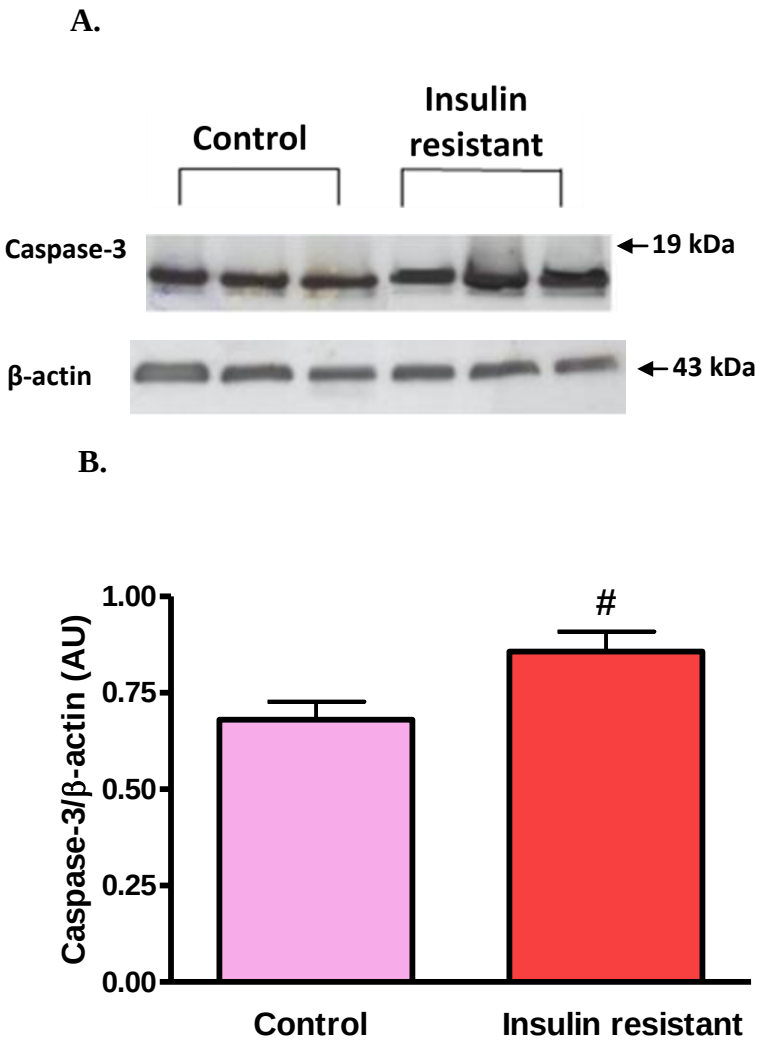

Figure 3.24: Evaluation of caspase-3 peptide levels in insulin resistant heart tissues.

Heart tissues were isolated from rats fed a high fat diet for 86 days (insulin resistant) versus matched controls. A) Representative caspase-3 blot for control and insulin resistant (hyperglycaemic) rat hearts; B) Bar graphs show densitometric analysis of caspase-3 levels normalized with β–actin. AU: Arbitrary Units. Values are expressed as mean ± SEM (n=6). # p<0.05 vs. control.

A.

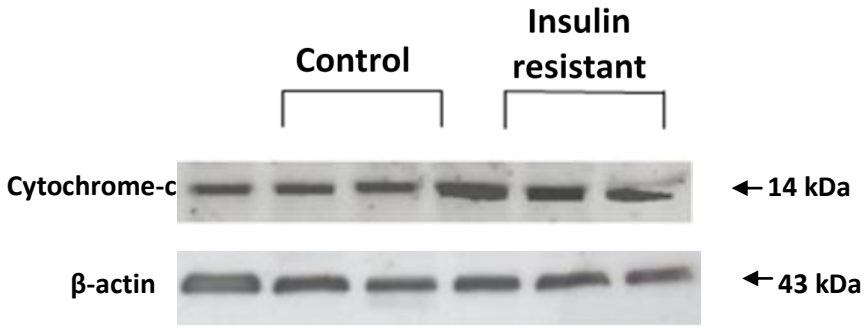

B.

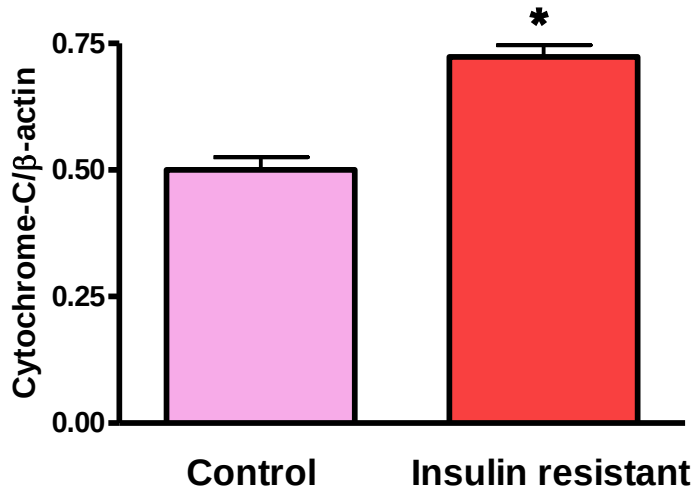

<u>Figure 3.25:</u> Determination of cytochrome-c peptide levels in insulin resistant heart tissues.

*Heart tissues were isolated from rats fed a high fat diet for 86 days (insulin resistant) versus matched controls. A) Representative cytochrome-c blot for control and insulin resistant (hyperglycaemic) rat hearts; B) Bar graphs show densitometric analysis of cytochrome-c levels normalized with β–actin. AU: Arbitrary Units. Values are expressed as mean ± SEM (n=6). * p<0.001 vs. control.*

A.

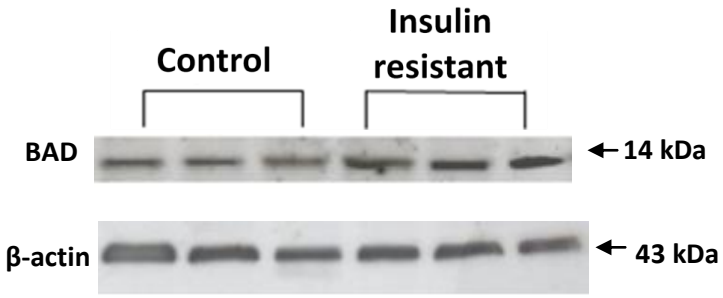

B.

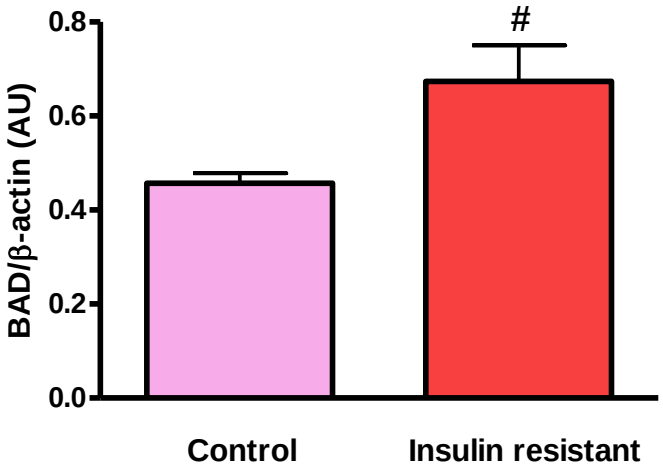

Figure 3.26: Evaluation of BAD peptide levels in insulin resistant rats.

Heart tissues were isolated from rats fed a high fat diet for 86 days (insulin resistant) versus matched controls. A) Representative BAD blot for control and insulin resistant (hyperglycaemic) rat hearts; B) Bar graphs show densitometric analysis of BAD levels normalized with β–actin. AU: Arbitrary Units. Values are expressed as mean ± SEM (n=6). # p<0.05 vs. control.

3.4 EVALUATING THE FLUX THROUGH HBP BY *O*-GlcNAc MEASUREMENT

3.4.1 *O*-GlcNAc measurement

We next set out to determine the flux through HBP under hyperglycaemic conditions by measuring *O*-GlcNAc levels within the cell by fluorescence staining of *O*-GlcNAc. It was found that under hyperglycaemic conditions there is a significant increase in *O*-GlcNAc levels compared to normal glucose controls (n=3, $p<0.001$ *vs.* 5.5 mM controls) (Figure 3.27).

A. **B.**

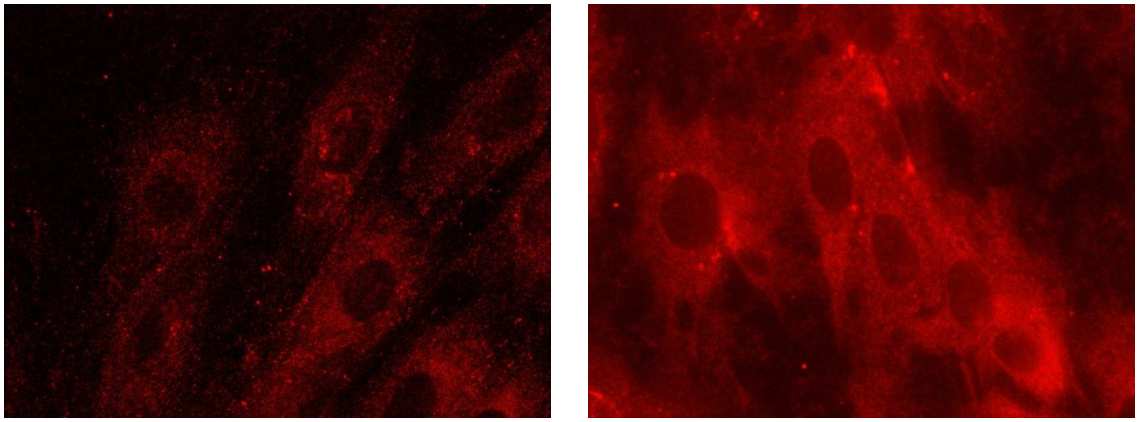

5.5 mM Glucose 33 mM Glucose

C.

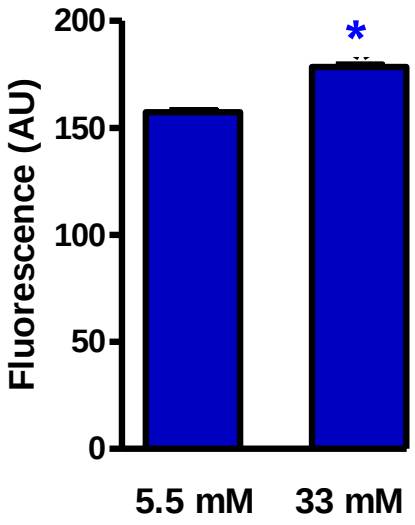

Figure 3.27: ***O*-GlcNAc staining demonstrating increased HBP activation under hyperglycaemic conditions.**

*A) 5.5 mM glucose and B) 33 mM glucose and C) bar graphs represent the fluorescence intensity of O-GlcNAc staining as described in the Materials and Methods section of this thesis (Section 2.5.1). AU: Arbitrary Units. Values are expressed as mean ± SEM (n=3). * p<0.001 vs. control.*

When the cells were treated with 40 µM DON, *O*-GlcNAc levels decreased significantly (n=3, $p<0.001$ *vs.* matching control) (Figure 3.28).

A.

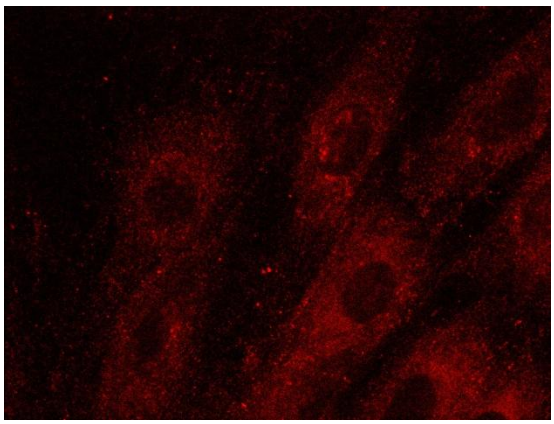

5.5 mM Glucose

B.

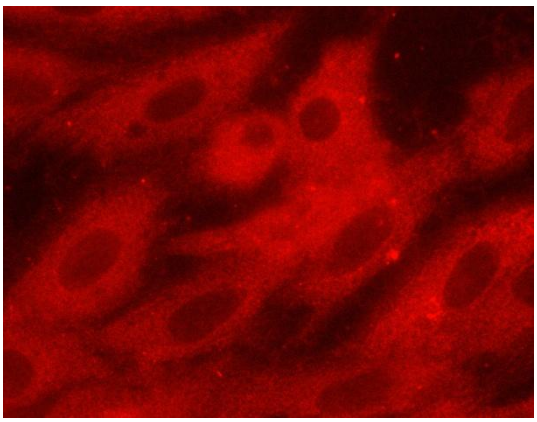

33 mM Glucose

C.

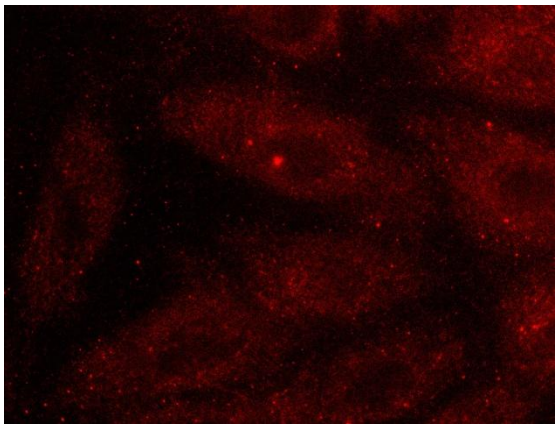

5.5 mM Glucose + DON

D.

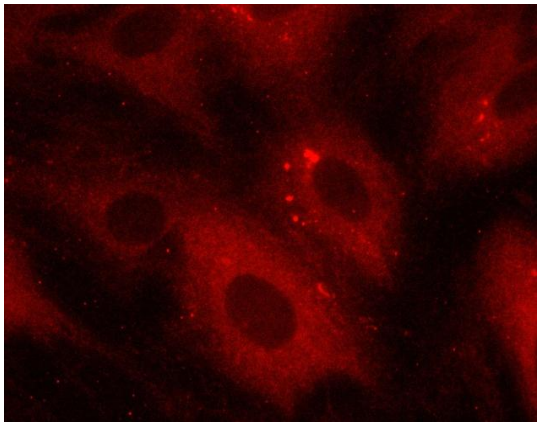

33 mM Glucose + DON

E.

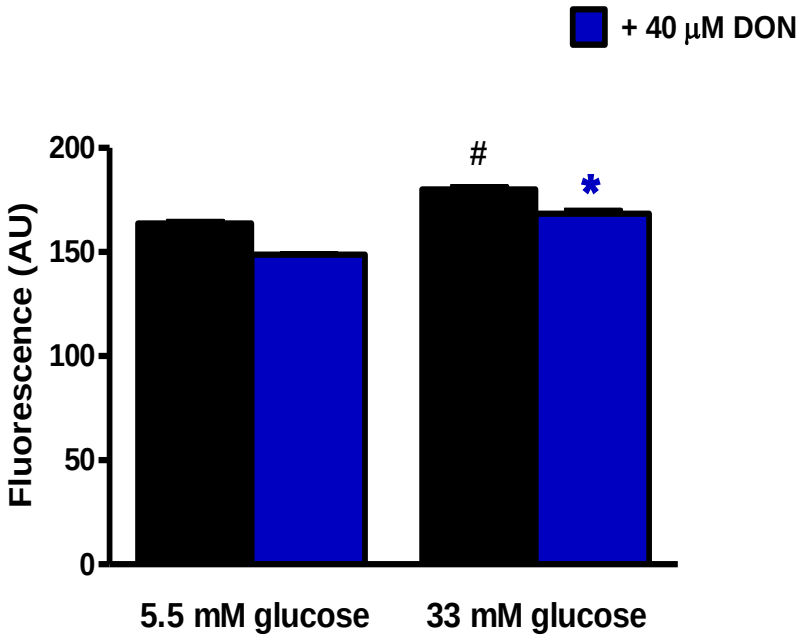

Figure 3.28: Attenuation of *O*-GlcNAc staining under HBP inhibition by DON.

*A) 5.5 mM glucose, B) 33 mM glucose, C) 5.5 mM glucose + DON and D) 33 mM glucose + DON. E) bar graphs represent the fluorescence intensity of O-GlcNAc staining as described in the Materials and Methods section of this thesis (section 2.5.1). AU: Arbitrary Units. Values are expressed as mean ± SEM (n=3). # p<0.001 vs. 5 mM control, * p<0.001 vs. 33 mM glucose.*

When the cells were administered with 50 μM PUGNAc, there was a significant increase in the *O*-GlcNAc levels under hyperglycaemic conditions (Figure 3.29).

A.

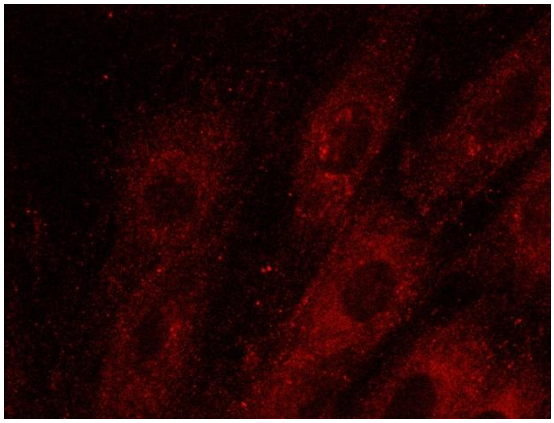

5.5 mM Glucose

B.

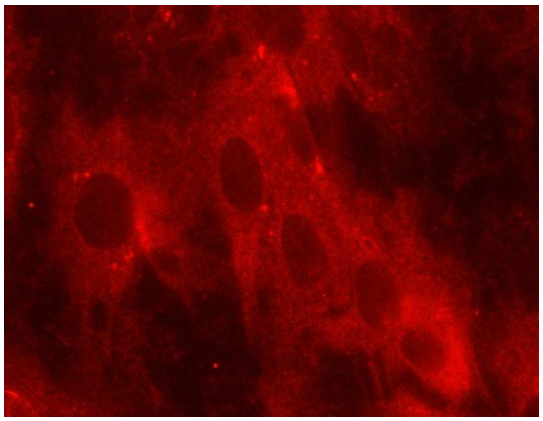

33 mM Glucose

C.

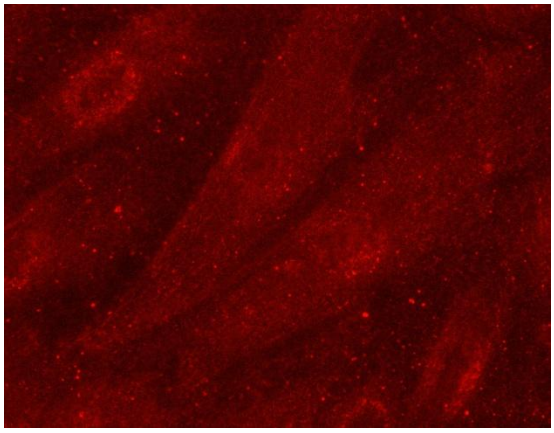

5.5 mM Glucose + PUGNAc

D.

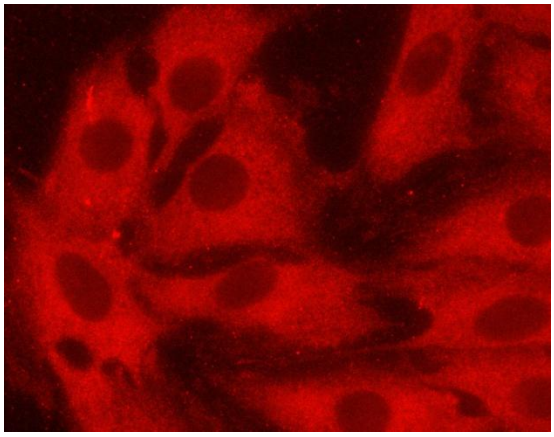

33 mM Glucose + PUGNAc

E.

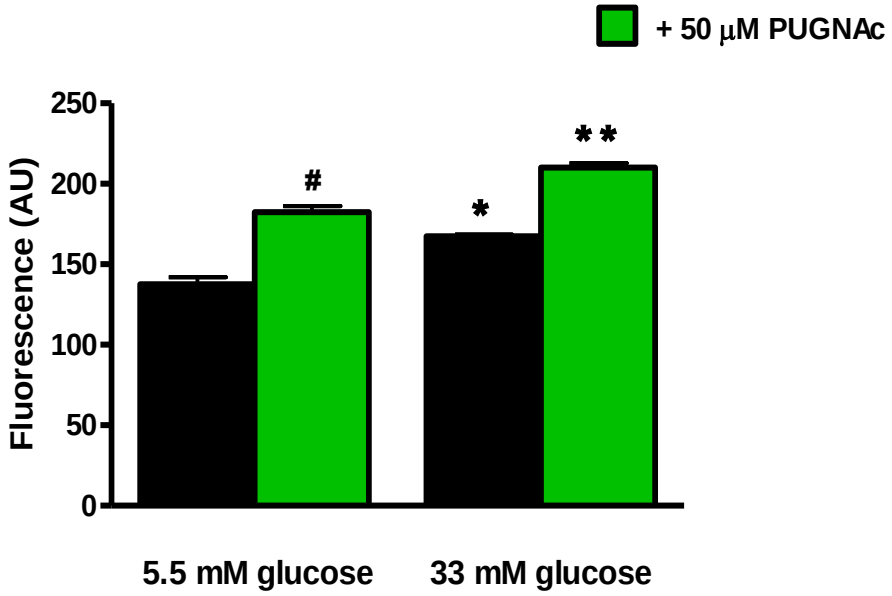

Figure 3.29: PUGNAc treatment increases *O*-GlcNAc levels under high glucose conditions.

*A) 5.5 mM glucose, B) 33 mM glucose, C) 5.5 mM glucose + PUGNAc, D) 33 mM glucose + PUGNAc and E) bar graph represents the fluorescence intensity of O-GlcNAc staining as described in the Materials and Methods section of this thesis (Section 2.5.1). Values are expressed as mean ± SEM (n=3). # p<0.001 vs. 5.5 mM glucose, * p<0.001 vs. 5.5 mM glucose, ** p<0.001 vs. 33 mM glucose.*

In agreement with the previous findings, co-administration of 250 μM α-OHCA with PUGNAc significantly decreased overall *O*-GlcNAcylation both under low and high glucose conditions (Figure 3.30 and 3.31).

A.

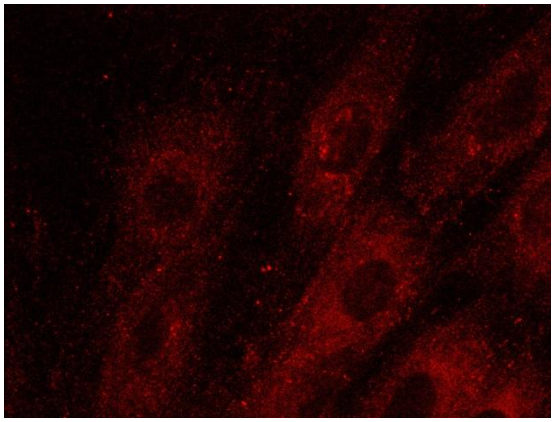

5.5 mM Glucose

B.

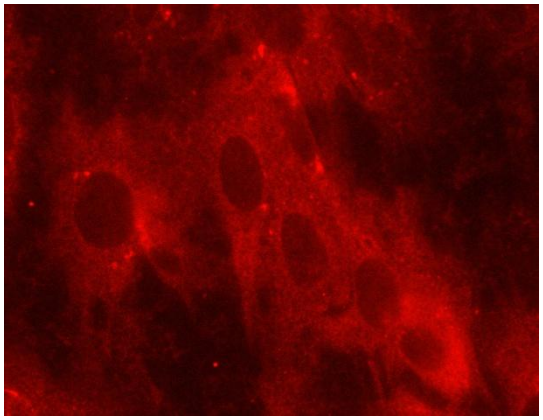

33 mM Glucose

C.

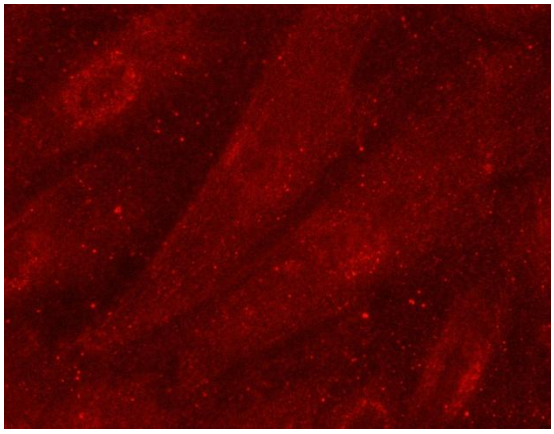

5.5 mM Glucose + PUGNAc

D.

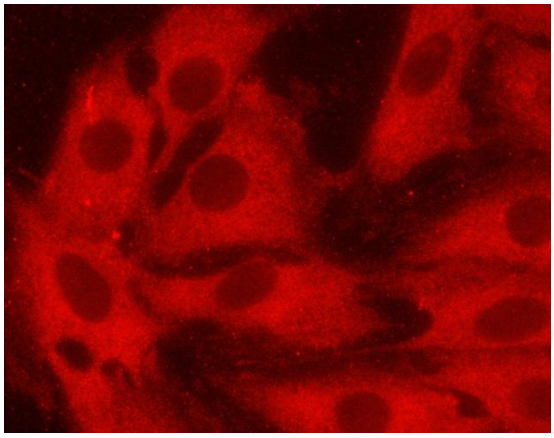

33 mM Glucose + PUGNAc

E.

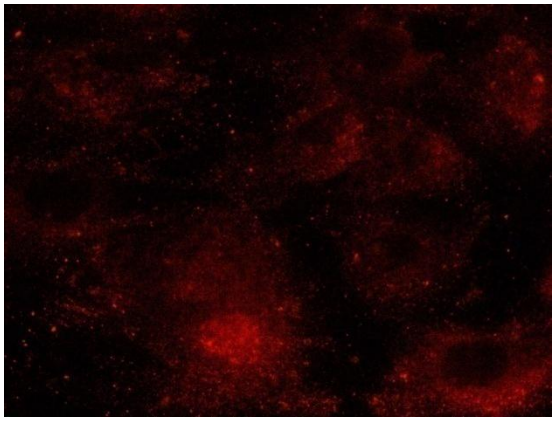

5.5 mM Glucose + PUGNAc + α-OHCA

F.

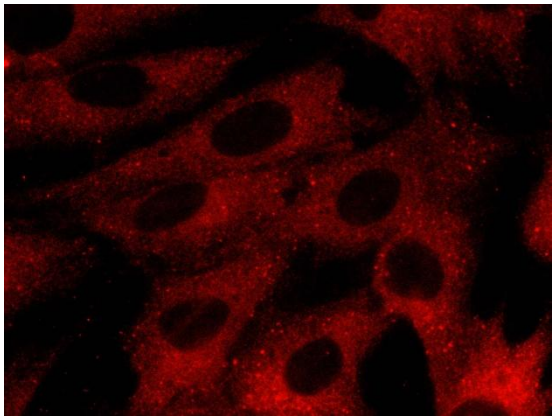

33 mM Glucose + PUGNAc + α-OHCA

G.

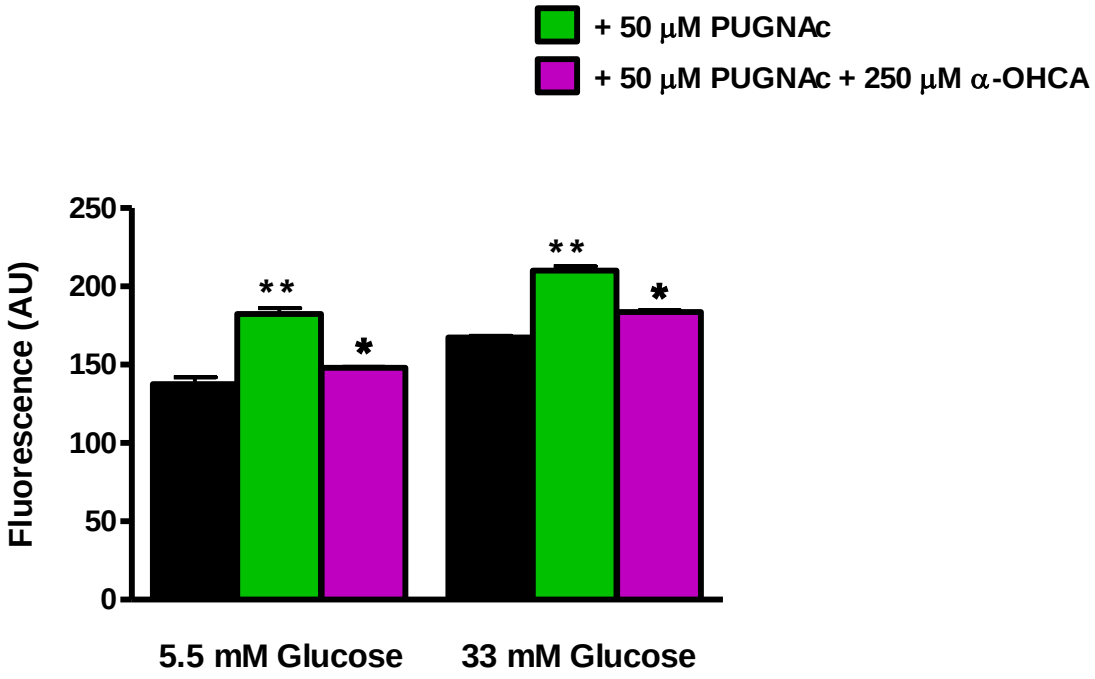

Figure 3.30: Antioxidant mediated decrease in *O*-GlcNAc levels.

*A) 5.5 mM glucose, B) 33 mM glucose, C) 5.5 mM glucose + PUGNAc, D) 33 mM glucose + PUGNAc, E) 5.5 mM glucose + PUGNAc + α-OHCA, F) 33 mM glucose + PUGNAc + α-OHCA and G) bar graph represents the fluorescence intensity of O-GlcNAc staining as described in the Materials and Methods section of this thesis (Section 2.5.1). AU: Arbitrary Units. Values are expressed as mean ± SEM (n=3). ** p<0.01 vs. matched untreated controls, * p<0.01 vs. PUGNAc treated experiments.*

A.

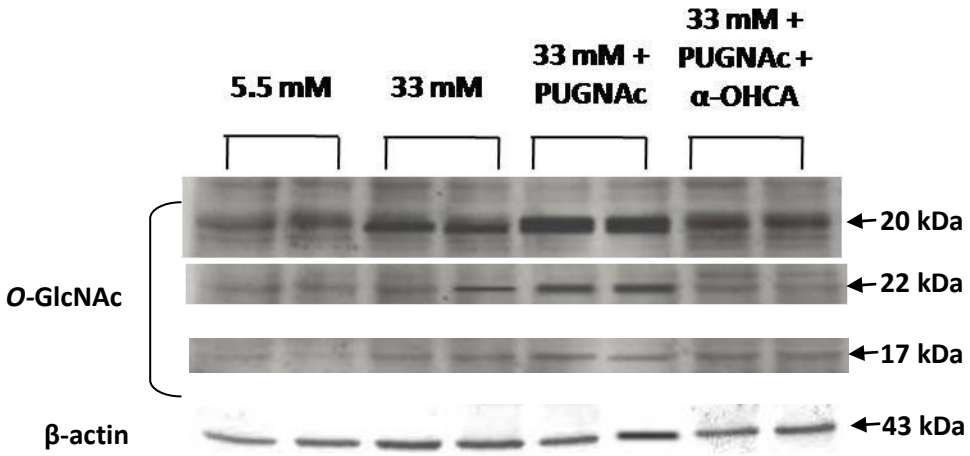

B.

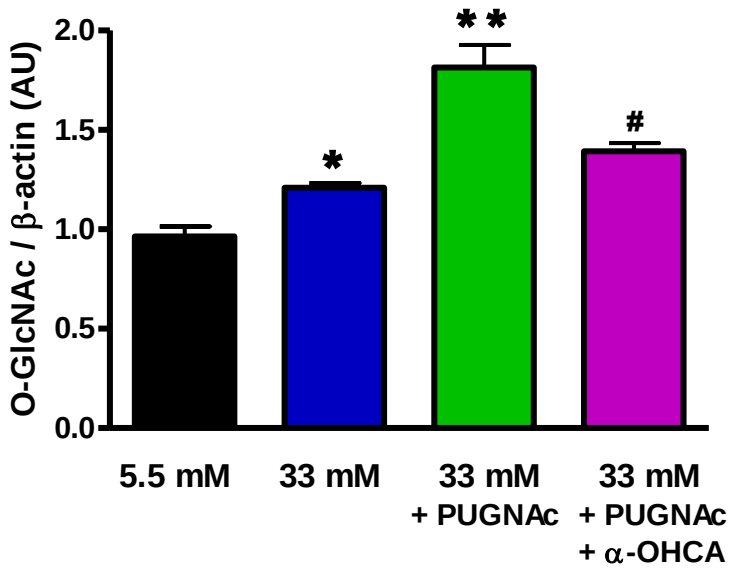

<u>Figure 3.31:</u> Western blot analysis demonstrating HBP-mediated modulation of *O*-GlcNAcylation.

*A) Representative O-GlcNAc blot showing increased O-GlcNAc levels under hyperglycaemic conditions and PUGNAc administration, but decreased by antioxidant co-administration; B) Bar graphs depict densitometric analysis of O-GlcNAc levels – data represent the average for 3 different protein bands normalized against β-actin. AU: Arbitrary Units. Values are expressed as mean ± SEM (n=4). * p<0.05 vs. 5.5 mM, ** p<0.001 vs. 33 mM, # p<0.001 vs. 33 mM PUGNAc.*

3.5 ELUCIDATION OF UNDERLYING MECHANISMS DRIVING THE ONSET OF HBP-MEDIATED CELL DEATH

3.5.1 Measurement of BAD-GlcNAcylation – fluorescence microscopy

We next set out to investigate the underlying mechanisms whereby cell death occurs when there is increased *O*-GlcNAcylation. Here we evaluated Bcl-2 Associated Death Promoter protein (BAD) as a candidate apoptotic factor and measured the *O*-GlcNAc modification of BAD under the various experimental conditions previously employed. BAD was selected because phosphorylation leads to its and activation of cell survival mechanisms. Studies suggest that phosphorylation and *O*-GlcNAcylation compete for identical or adjacent binding sites [1] thereby possibly exerting opposite effects on the protein. Hence we wanted to test if *O*-GlcNAcylation of Bad had an opposite effect on the protein compared to phosphorylation. This was initially performed using fluorescence microscopy co-localization studies as explained in Section 2.6.1 (Materials and Methods). We found a significant increase in *O*-GlcNAcylation of BAD under hyperglycaemic conditions compared to low glucose conditions (Figure 3.32) (n=3, $p<0.05$ *vs.* 5.5 mM glucose).

A.

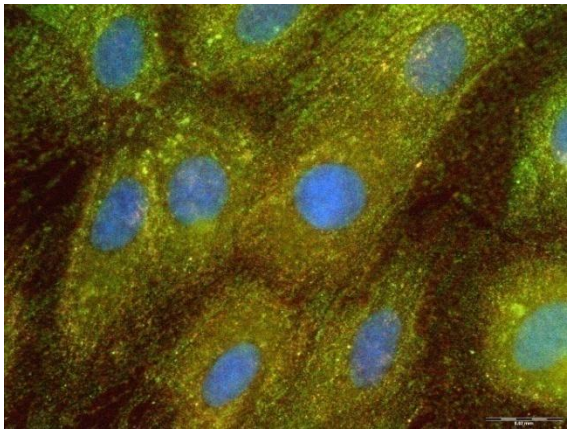

5.5 mM Glucose

B.

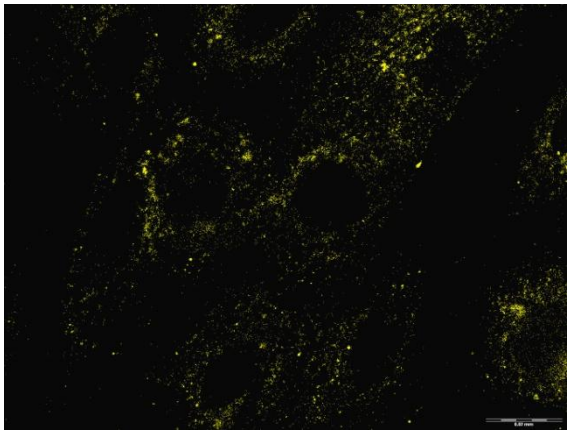

5.5 mM Glucose – co-localized

C.

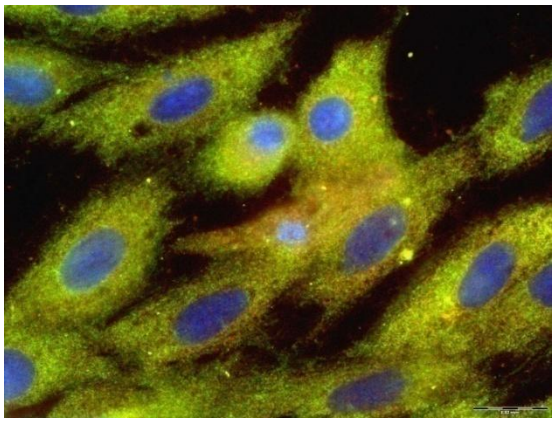

33 mM Glucose

D.

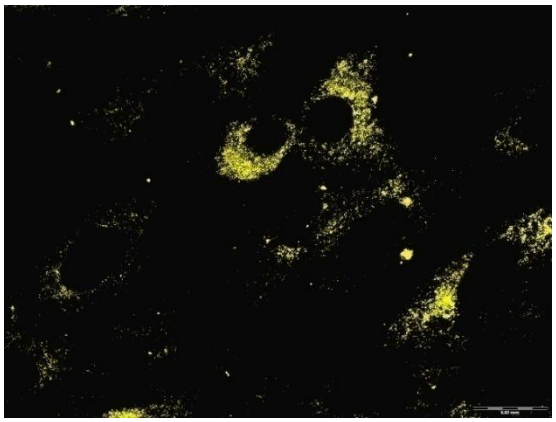

33 mM Glucose – co-localized

E.

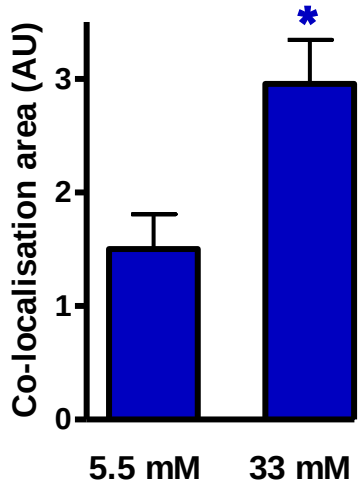

Figure 3.32: Hyperglycaemia mediated increase in BAD *O*-GlcNAcylation.

*A) 5.5 mM glucose, B) 5.5 mM glucose co-localised image, C) 33 mM glucose, D) 33 mM glucose co-localised image and E) bar graph represents the co-localisation area as described in the Materials and Methods section of this thesis (Section 2.6.1). Values are expressed as mean ± SEM (n=3). * p<0.05 vs. 5.5 mM glucose*

Conversely treatment of cells with 40 µM DON, decreased BAD *O*-GlcNAcylation levels (Figure 3.33).

A. **B.**

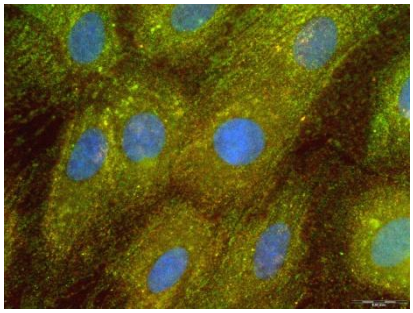

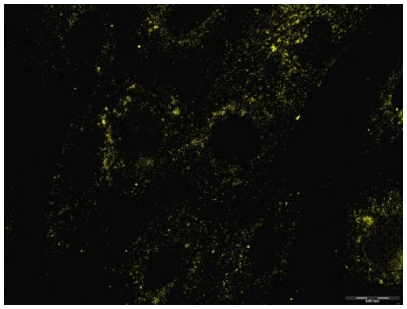

5.5 mM Glucose **5.5 mM – co-localized**

C. **D.**

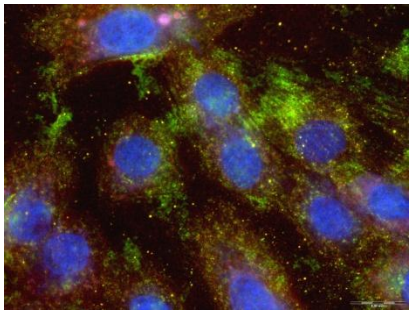

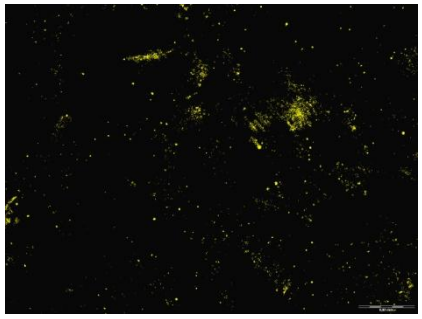

5.5 mM Glucose + DON **5.5 mM + DON – co-localized**

E. **F.**

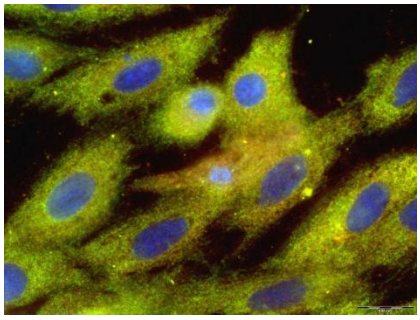

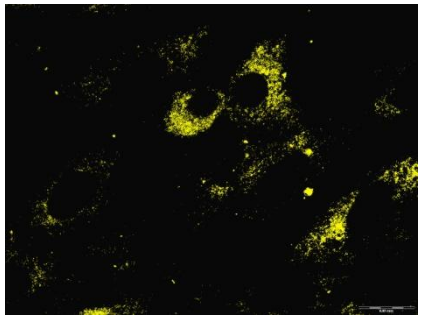

33 mM Glucose **33 mM Glucose – co-localized**

G. **H.**

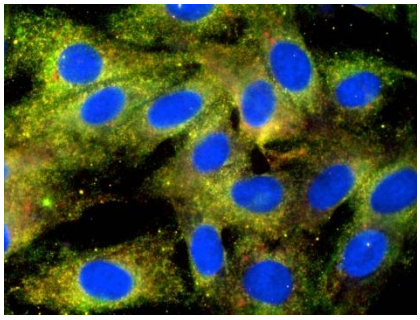

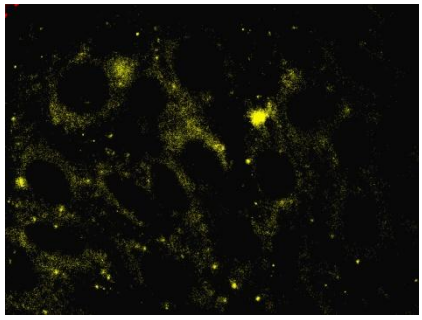

33 mM Glucose + DON **33 mM + DON – co-localized**

I.

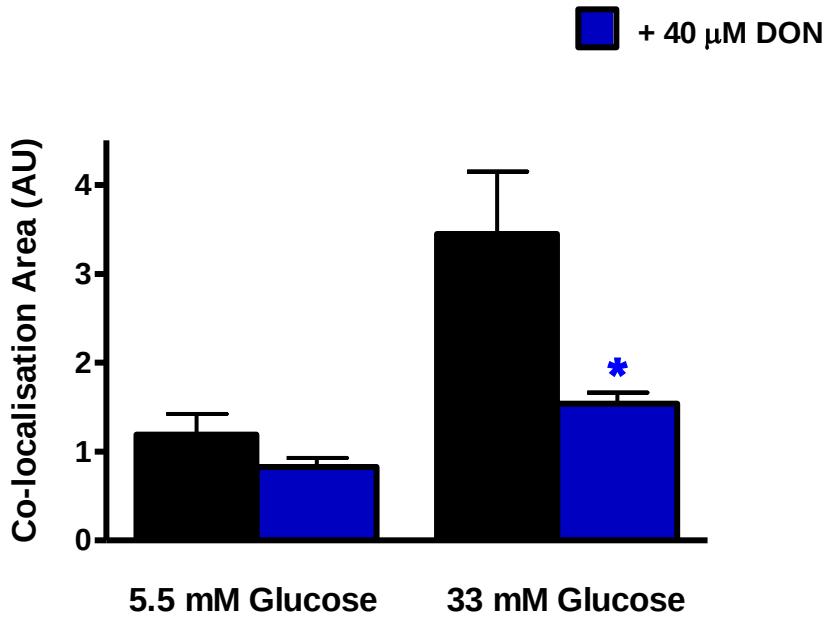

Figure 3.33: DON decreases hyperglycaemia-mediated increase in BAD *O*-GlcNAcylation.

*A) 5.5 mM glucose, B) 5.5 mM glucose co-localised image of BAD and O-GlcNAc, C) 5.5 mM + DON, D) 5.5 mM glucose + DON co-localized image, E) 33 mM glucose, F) 33 mM glucose co-localised image, G) 33 mM glucose + DON, H) 33 mM glucose + DON co-localised and I) bar graph represents the co-localisation area as described in the Materials and Methods section of this thesis (Section 2.6.1). Values are expressed as mean ± SEM (n=3). * p<0.01 vs. 5.5 mM glucose.*

Consistent with the total *O*-GlcNAc results, PUGNAc treatment significantly increased BAD-GlcNAcylation under high glucose conditions (Figure 3.34).

A. B.

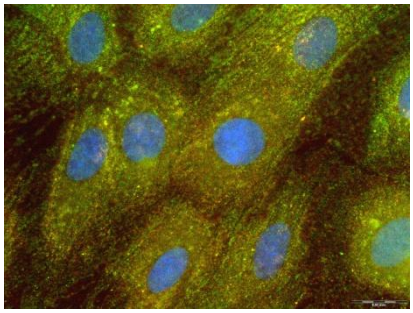

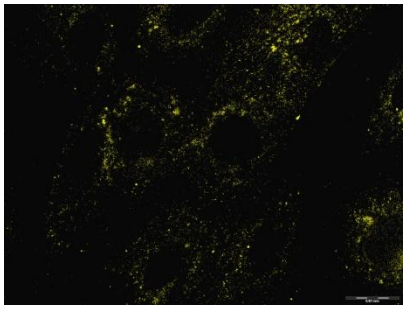

5.5 mM Glucose

5.5 mM – co-localized

C. D.

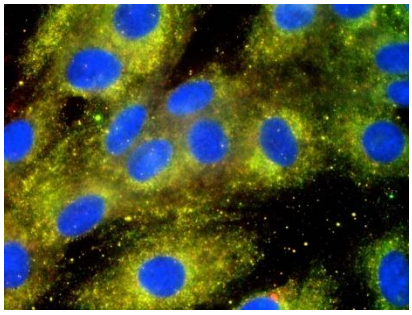

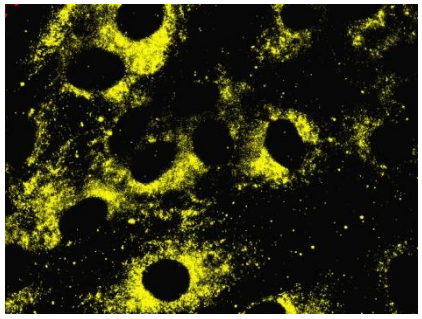

5.5 mM Glucose + PUGNAc

5.5 mM + PUGNAc – co-localized

E. F.

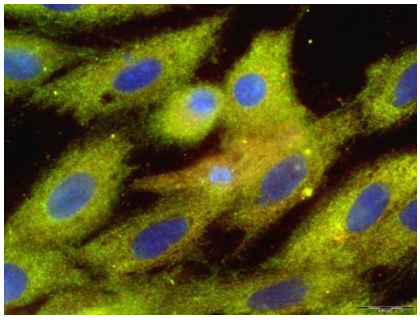

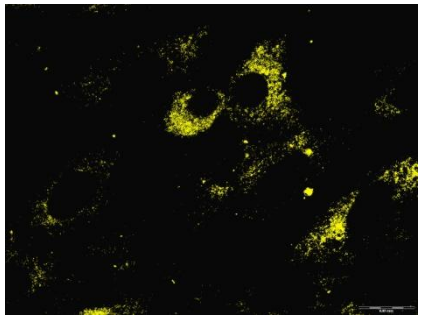

33 mM Glucose

33 mM Glucose – co-localized

G. H.

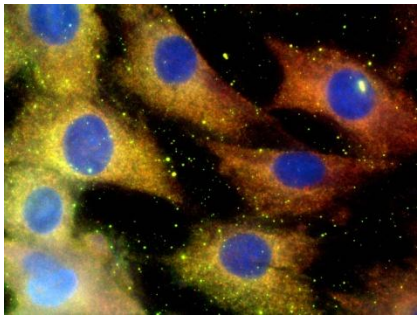

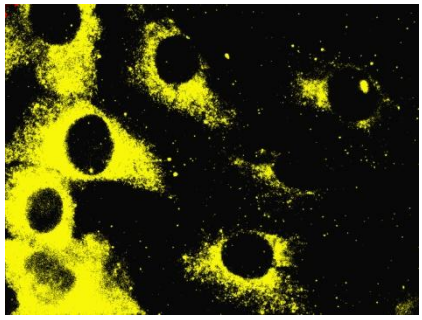

33 mM Glucose + PUGNAc

33 mM + PUGNAc – co-localized

I.

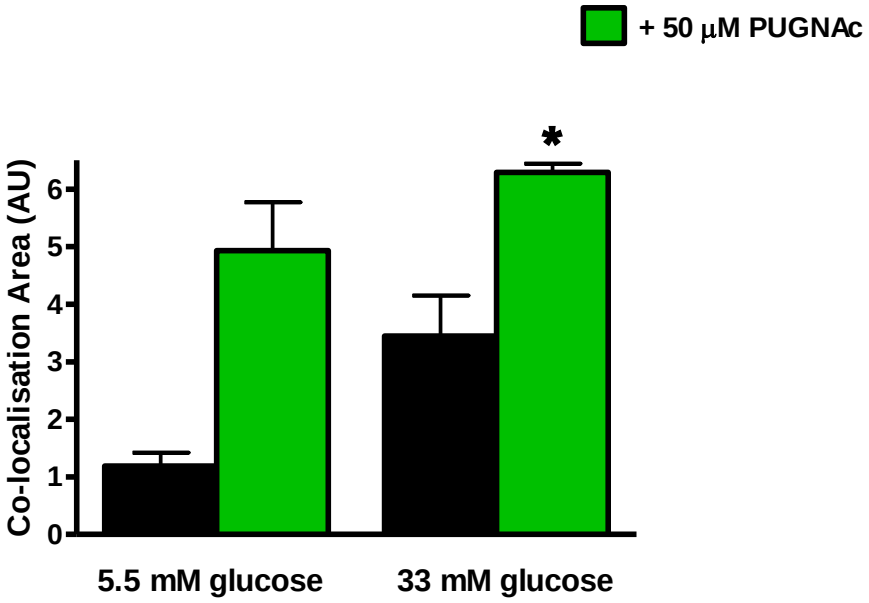

Figure 3.34: PUGNAc exacerbates BAD *O*-GlcNAcylation.

*A) 5.5 mM glucose, B) 5.5 mM glucose co-localised image, C) 5.5 mM + PUGNAc, D) 5.5 mM glucose + PUGNAc co-localised image, E) 33 mM glucose, F) 33 mM glucose co-localised image, G) 33 mM glucose + PUGNAc, H) 33 mM glucose + PUGNAc co-localised and I) bar graph represents the co-localisation area as described in the Materials and Methods section of this thesis (Section 2.6.1). Values are expressed as mean ± SEM (n=3). * p<0.05 vs. 33 mM glucose.*

In agreement with our previous data, co-administration of antioxidant (α-OHCA) along with PUGNAc significantly decreased BAD-GlcNAcylation under hyperglycaemic conditions (Figure 3.35).

A.

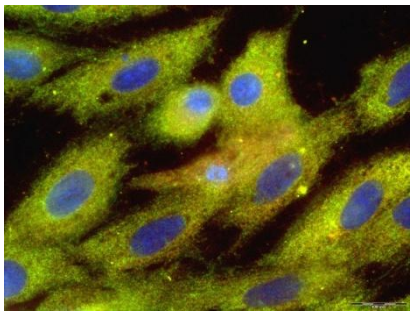

33 mM Glucose

B.

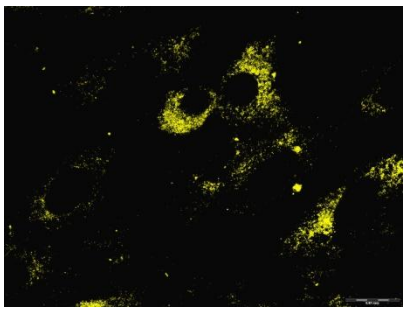

33 mM – co-localized

C.

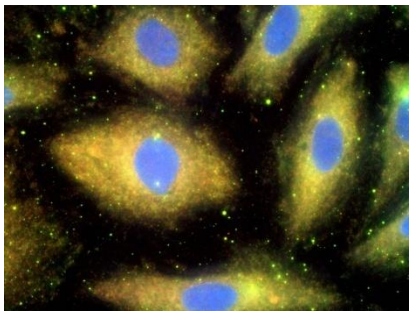

33 mM Glucose + PUGNAc

D.

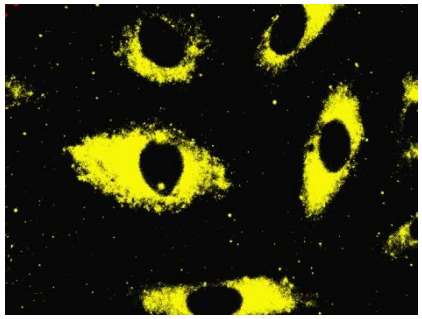

33 mM + PUGNAc – co-localized

E.

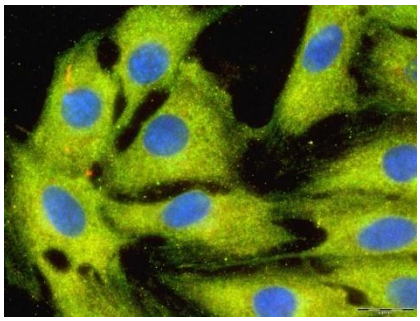

33 mM Glucose + PUGNAc + α-OHCA

F.

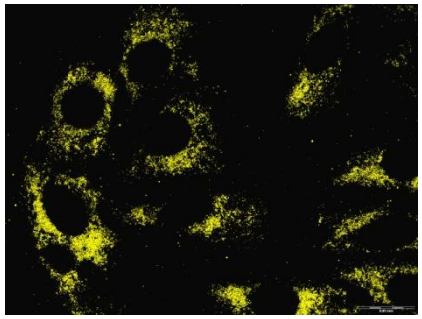

33 mM Glucose + PUGNAc + α-OHCA – co-localized

G.

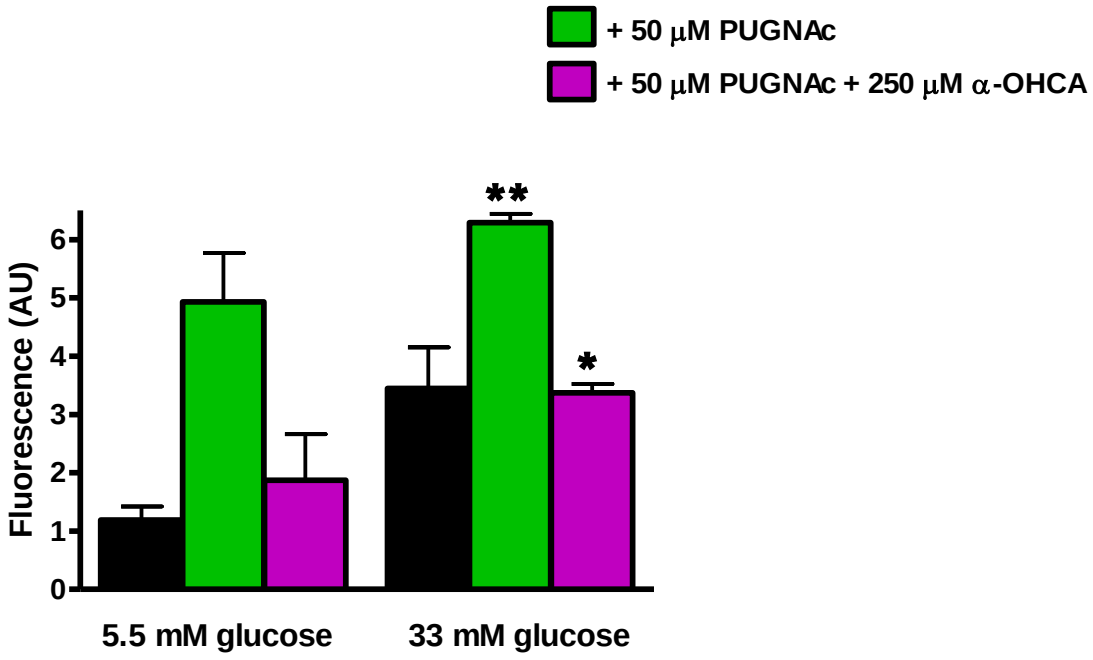

Figure 3.35: Antioxidant mediated decrease in BAD-GlcNAcylation.

*A) 33 mM glucose, B) 33 mM glucose co-localised, C) 33 mM glucose + PUGNAc, D) 33 mM glucose + PUGNAc co-localised, E) 33 mM glucose + PUGNAc + α-OHCA, F) 33 mM glucose + PUGNAc + α-OHCA co-localised and G) bar graph represents the fluorescence intensity of BAD-GlcNAcylation as described in the Materials and Methods section of this thesis (Section 2.6.1). AU: Arbitrary Units. Values are expressed as mean ± SEM (n=3). ** p<0.05 vs. matched untreated controls, * p<0.05 vs. PUGNAc treated experiments.*

3.5.2 Measurement of BAD-GlcNAcylation – Western blotting

To confirm our BAD-GlcNAcylation microscopy data we next performed immunoblotting analysis. We initially immunoprecipitated *O*-GlcNAc modified proteins, and thereafter probed the membrane with a primary antibody against BAD (Figure 3.36). Subsequently, we performed the reverse experiment, i.e. immunoprecipitated BAD and probed the membrane with a primary

antibody for *O*-GlcNAc. These experiments were performed using both our *in vitro* and *in vivo* experimental models (Figure 3.37)

A.

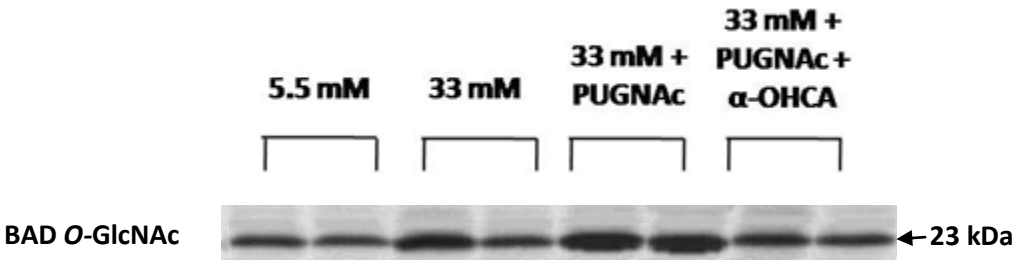

B.

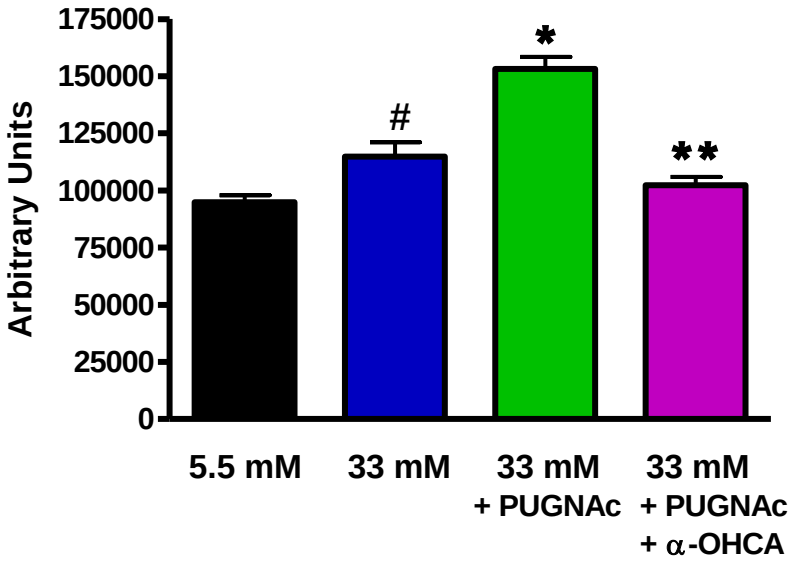

C.

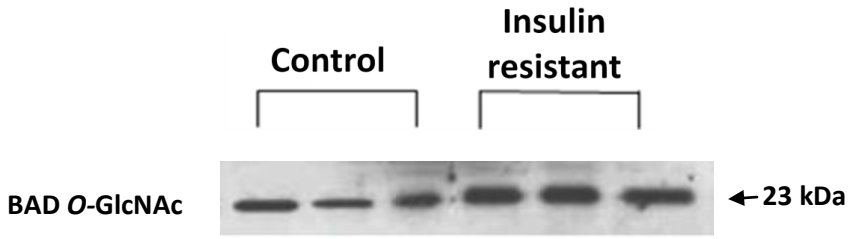

D.

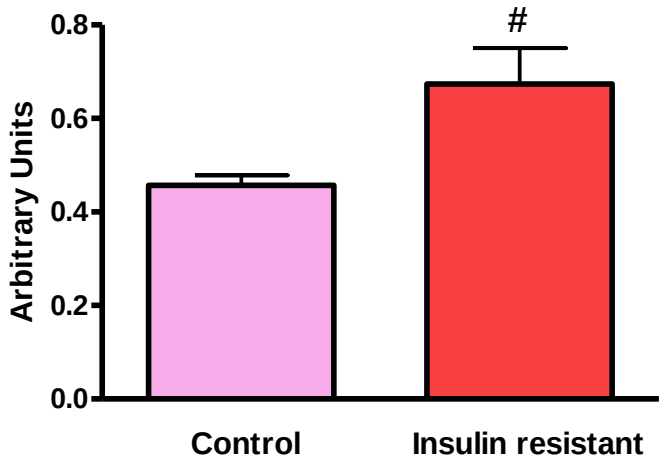

Figure 3.36: Immunoblot demonstrating HBP-mediated BAD *O*-GlcNAcylation.

*A) In vitro O-GlcNAc immunoprecipitation show increased O-GlcNAc modification of BAD under hyperglycaemic conditions and PUGNAc administration, but decreased by antioxidant co-administration; B) Bar graphs depicting densitometric analysis. (n=4). # p<0.05 vs. 5.5 mM, * p<0.001 vs. 33 mM, ** p<0.001 vs. 33 mM PUGNAc, C) In vivo BAD O-GlcNAc blots for insulin resistant rat heart tissues (fed a high fat diet for 86 days) versus matched controls, D) Bar graphs show densitometric analysis of BAD-GlcNAcylation. # p<0.05 vs. control. Values are expressed as mean ± SEM.*

A.

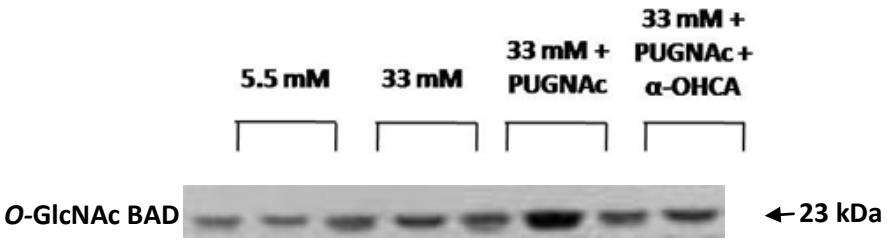
5.5 mM
33 mM
33 mM + PUGNAc
33 mM + PUGNAc + α-OHCA
O-GlcNAc BAD
23 kDa

B.

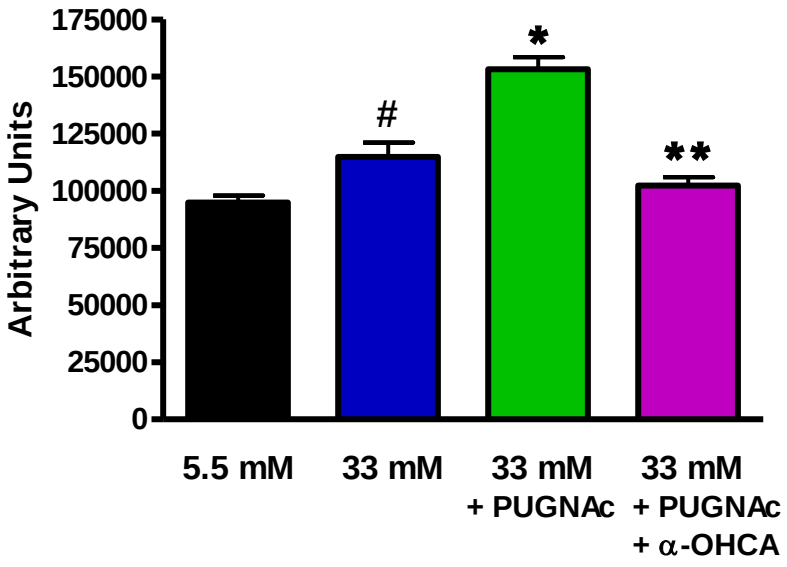
Arbitrary Units
175000
150000
125000
100000
75000
50000
25000
0
#
*
**
5.5 mM
33 mM
33 mM + PUGNAc
33 mM + PUGNAc + α-OHCA

C.

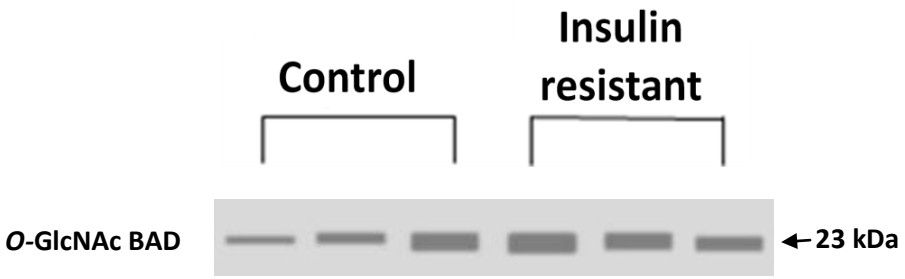

D.

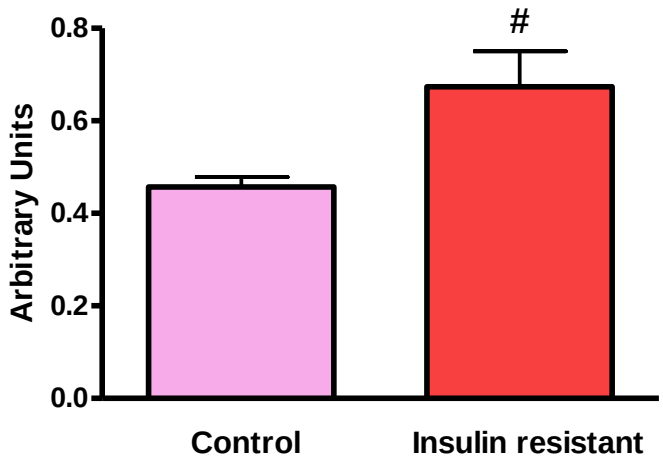

Figure 3.37: Reverse co-precipitation demonstrating HBP-mediated BAD *O*-GlcNAcylation.

*A) In vitro BAD immunoprecipitation depicting increased O-GlcNAc modification of BAD under hyperglycaemic conditions and PUGNAc administration, but decreased by antioxidant co-administration; B) Bar graphs depicting densitometric analysis (n=4). * p<0.001 vs. 33 mM, ** p<0.001 vs. 33 mM PUGNAc; C) In vivo BAD O-GlcNAc blots for insulin resistant rat heart tissues (fed a high fat diet for 86 days) versus matched controls; D) Bar graphs show densitometric analysis of BAD-GlcNAcylation (n=6). # p<0.05 vs. controls. Values are expressed as mean ± SEM.*

3.6 ELUCIDATING THE MECHANISM OF BAD-MEDIATED CELL DEATH UNDER HYPERGLYCAEMIC CONDITIONS

To understand how *O*-GlcNAcylation of BAD results in increased apoptosis, we next investigated BAD and Bcl-2 interactions. BAD is a pro-apoptotic protein that usually dimerizes with the anti-apoptotic Bcl-2, thereby preventing it from performing its anti-apoptotic function. However, BAD is inactive in its phosphorylated form. Since BAD *O*-GlcNAcylation may have a ‘’yin-yang’’ relationship with phosphorylation [2] and therefore probably resulting in an opposite functional effect, i.e. BAD activation and greater BAD-Bcl-2 dimerization, we next investigated whether BAD *O*-GlcNAcylation increased BAD-Bcl-2 dimerization under our experimental conditions.

3.6.1 Measurement of BAD-Bcl-2 dimerization by immunoprecipitation

To begin with we immunoprecipitated *O*-GlcNAc modified proteins, and probed the membrane with a primary antibody for BAD. We observed 2 protein bands on the gel, i.e. a lower one corresponding to BAD (23 kDa) and a band located higher up on the gel (50 kDa) (Figure 3. 38A). Both these bands increased in intensity under hyperglycaemic conditions and with PUGNAc administration, while attenuated by antioxidant treatment. Thus, increased BAD *O*-GlcNAcylation and greater dimerization are observed when the HBP is activated. To ascertain whether the higher protein band corresponds to BAD-Bcl-2 dimers, the same membrane was

stripped and re-probed for Bcl-2. The blot produced a higher protein band in exactly the same position (50 kDa) and a lower one corresponding to Bcl-2 (26 kDa) (Figure 3. 38B). Again, both bands increased in intensity under conditions known to induce the HBP. Collectively this data show that Bcl-2 is also GlcNAcylated and that this results in greater dimerization with BAD under these experimental conditions. The findings were supported by the reverse experiment, i.e. immunoprecipitated BAD and probed the membrane with *O*-GlcNAc and Bcl-2 (Figure 3.40). Likewise, data generated by immunoprecipitation blotting experiments with tissues isolated from insulin resistant rat heart tissues were concordant with our *in vitro* blots (Figures 3.39 - 3.41). These results parallel our *in vitro* data, further supporting greater BAD-Bcl-2 dimerization under conditions where the HBP is activated.

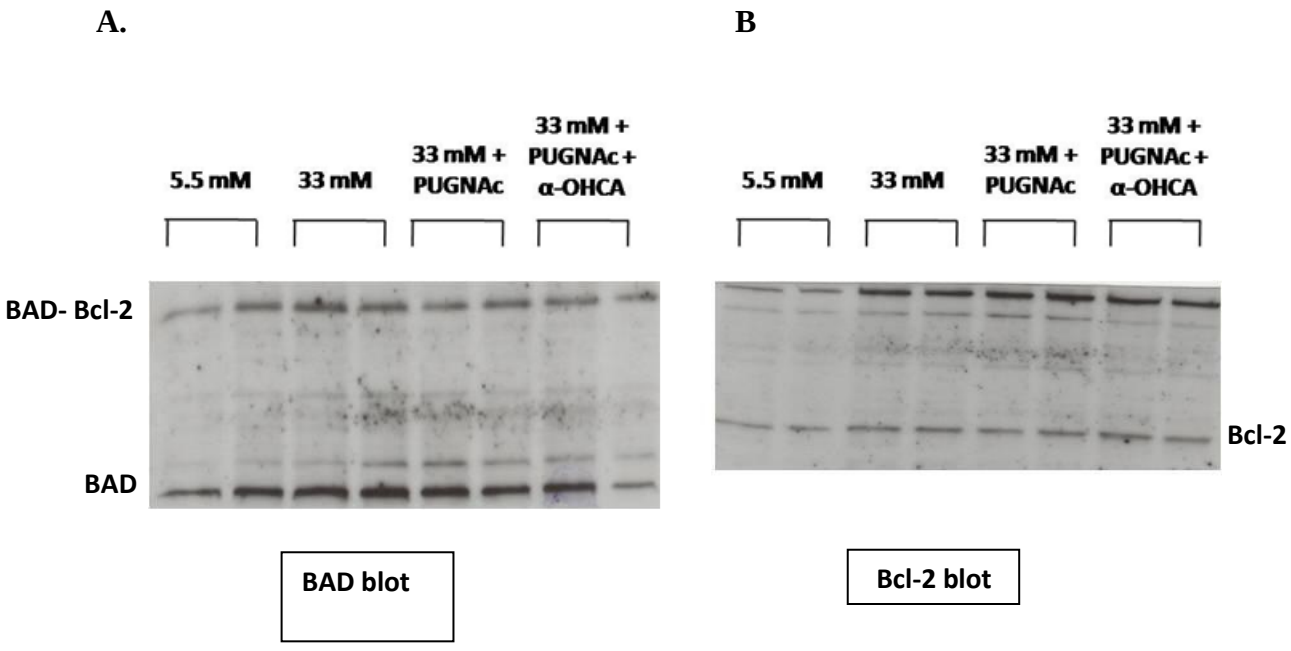

Figure 3.38: Immunoblot demonstrating greater BAD-Bcl-2 dimerization under *in vitro* hyperglycaemic conditions.

A) Immunoblot generated by O-GlcNAc immunoprecipitation and thereafter probed for BAD; 23 kDa band = BAD; ~50 kDa Band = BAD-Bcl-2 dimer; B) The same immunoblot was stripped and thereafter probed for Bcl-2; 26 kDa band = Bcl-2. (n=4).

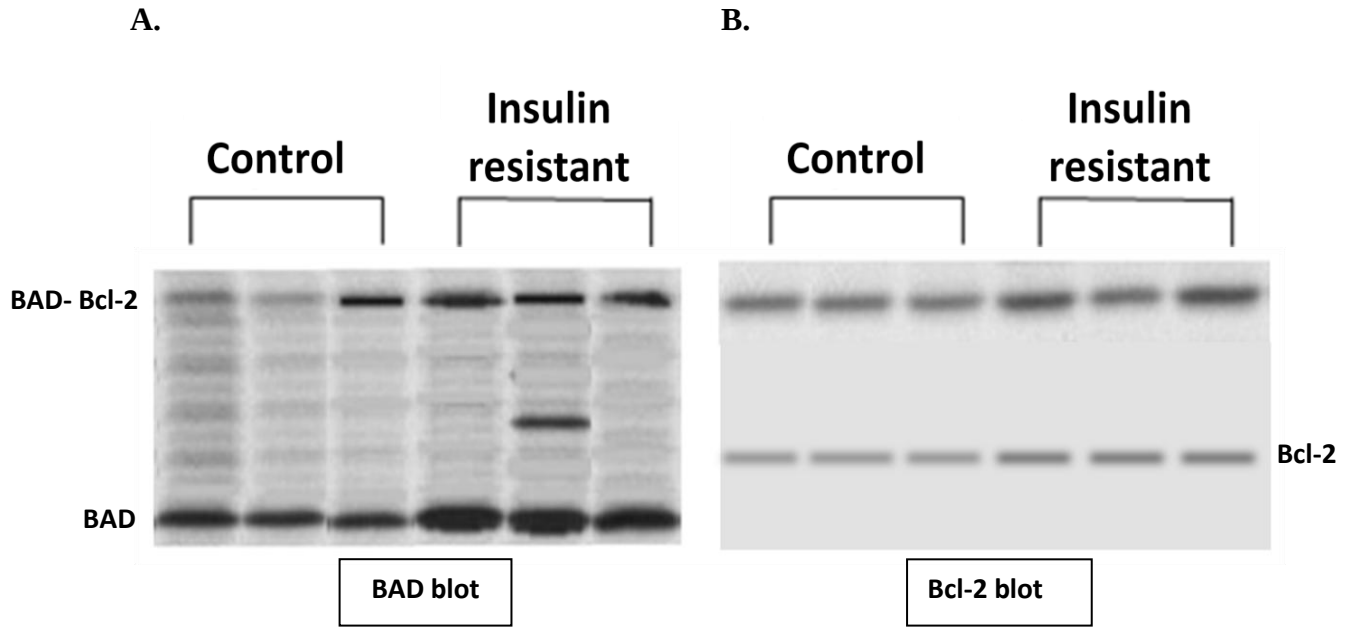

Figure 3.39: Immunoblot demonstrating greater BAD-Bcl-2 dimerization under *in vivo* hyperglycaemic conditions.

A) Immunoblot generated by O-GlcNAc immunoprecipitation and thereafter probed for BAD; 23 kDa band = BAD; ~50 kDa band = BAD-Bcl-2 dimer, B) The same immunoblot was stripped and thereafter probed for Bcl-2; 26 kDa band = Bcl-2. (n=6).

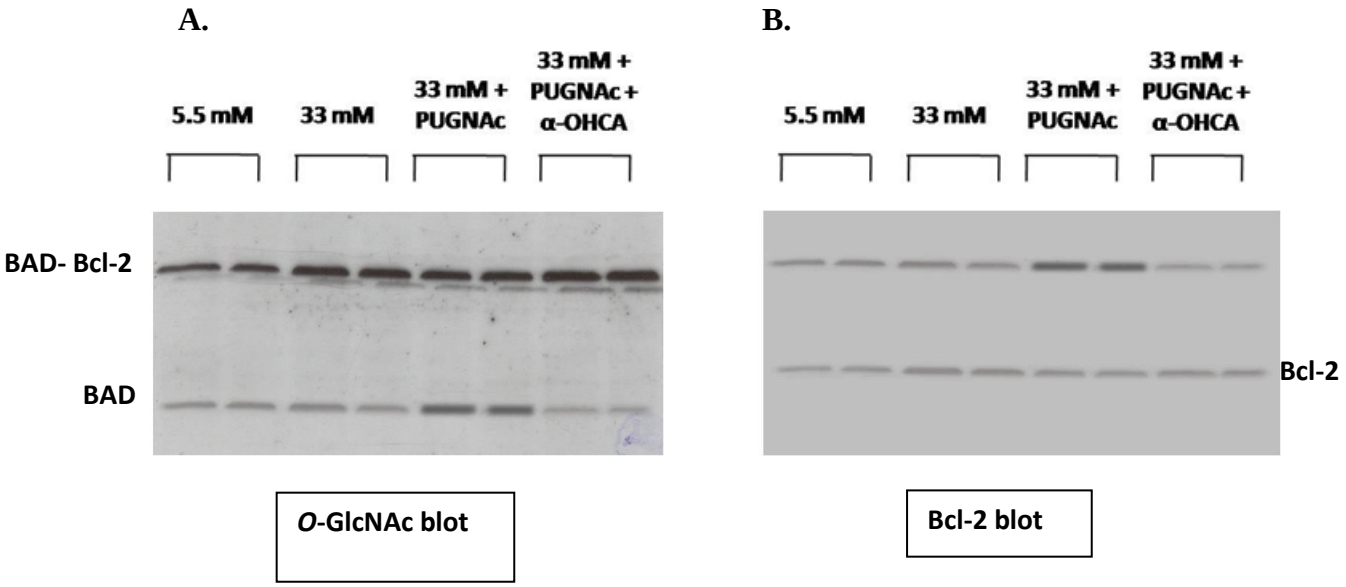

Figure 3.40: Reverse co-precipitation demonstrating greater BAD-Bcl-2 dimerization under *in vitro* hyperglycaemic conditions.

A) Immunoblot generated by BAD immunoprecipitation and thereafter probed for O-GlcNAc; 23 kDa band = BAD; ~50 kDa Band = BAD-Bcl-2 dimer; B) The same immunoblot was stripped and thereafter probed for Bcl-2; 26 kDa band = Bcl-2. (n=4).

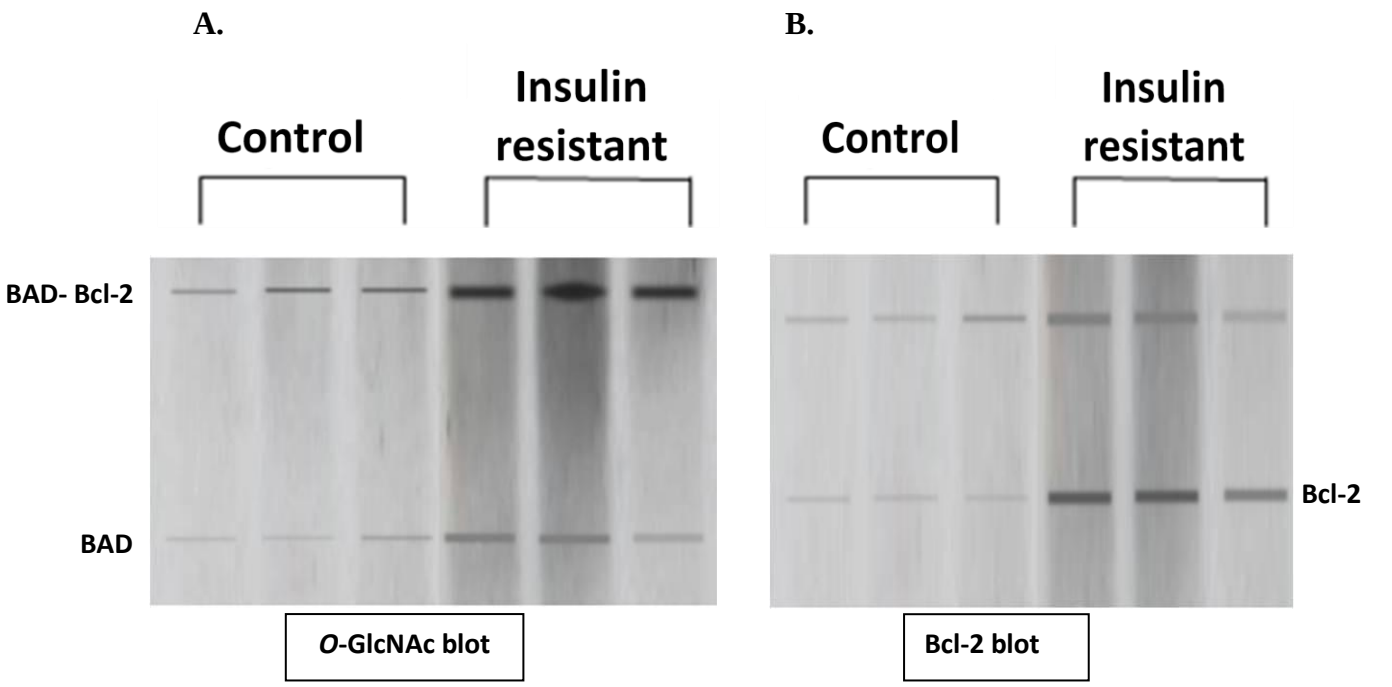

Figure 3.41: Reverse co-precipitation demonstrating greater BAD-Bcl-2 dimerization under *in vivo* hyperglycaemic conditions.

A) Immunoblot generated by BAD immunoprecipitation and thereafter probed for O-GlcNAc; 23 kDa band = BAD; ~50 kDa band = BAD-Bcl-2 dimer, B) The same immunoblot was stripped and thereafter probed for Bcl-2; 26 kDa band = Bcl-2. (n=6).

3.6.2 Measurement of BAD-Bcl-2 dimerization by fluorescence microscopy

We further confirmed our Western blotting data by employing fluorescence microscopy co-localization studies. We performed dual fluorescence in H9c2 myoblasts as explained in Section 2.7.2 of this thesis. In brief, we employed Texas Red and FITC-green to stain Bcl-2 and BAD, respectively. An overlay of the two dyes produces a yellow color which is a marker for BAD-Bcl-2 dimerization. In agreement with our blotting analysis, we found increased BAD-Bcl-2 co-localization under hyperglycaemic conditions compared to controls (Figure 3.42). Furthermore, PUGNAc increased BAD-Bcl-2 dimerization while antioxidant treatment significantly attenuated it.

A.

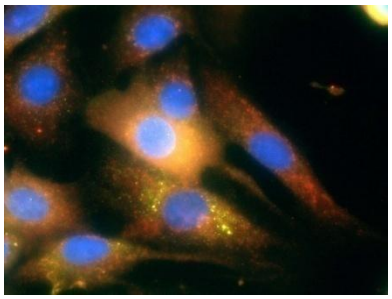

5.5 mM Glucose

B.

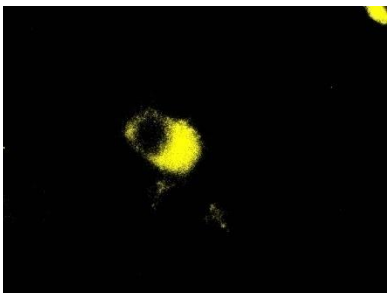

5.5 mM Glucose - co-localized

C.

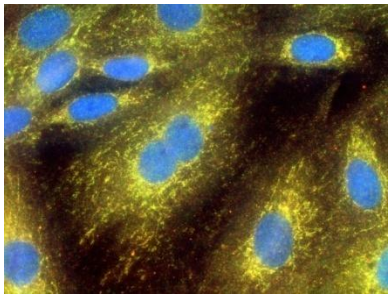

33 mM Glucose

D.

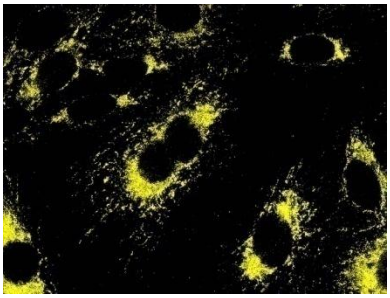

33 mM Glucose - co-localized

E.

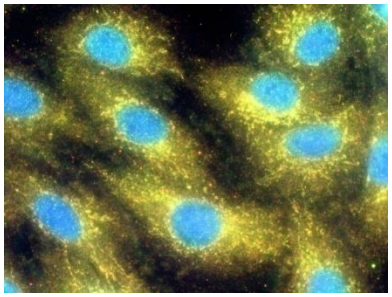

33 mM Glucose + PUGNAc

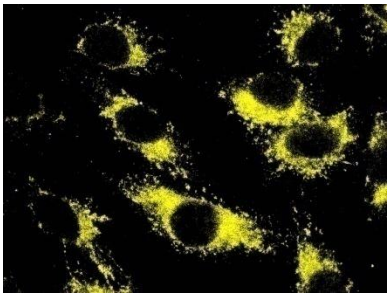

33 mM Glucose + PUGNAc - co-localized

G.

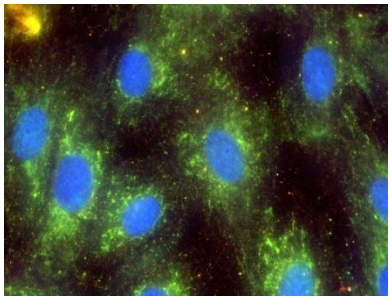

33 mM Glucose + PUGNAc + α-OHCA

H.

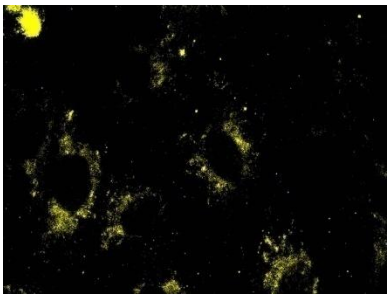

33 mM Glucose + PUGNAc + α-OHCA – co-localized

I.

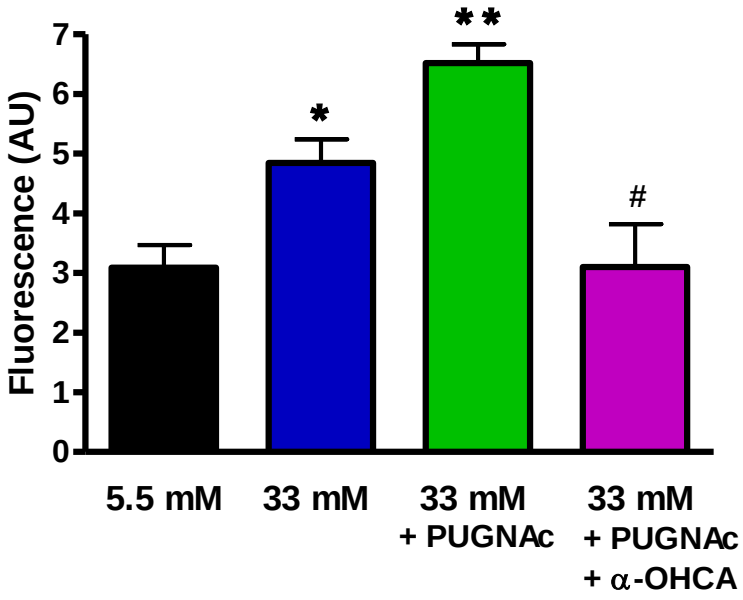

Figure 3.42: Fluorescence microscopy demonstrating BAD-Bcl-2 dimerization by co-localization analysis using two fluorescent dyes.

*A) 5.5 mM glucose (dual staining), B) 5.5 mM glucose (co-localized), C) 33 mM glucose (dual staining), D) 33 mM glucose (co-localized), E) 33 mM glucose + PUGNAc (dual staining), F) 33 mM glucose + PUGNAc (co-localized), G) 33 mM glucose + PUGNAc + α-OHCA (dual staining), H) 33 mM glucose + PUGNAc + α-OHCA (co-localized), and I) bar graph represents the fluorescence intensity of BAD-GlcNAcylation as described in the Materials and Methods section of this thesis (Section 2.7.2). AU: Arbitrary Units. Values are expressed as mean ± SEM (n=3). * p<0.05 vs. 5.5 mM glucose controls, ** p<0.05 vs. 33 mM glucose, # p<0.001 vs. 33 mM PUGNAc.*

In an attempt to find out the position of these proteins (Bad, Bcl-2), specifically to confirm if they are located near the mitochondria, we stained the mitochondria using Mitotracker Red (1:200) and compared it to the Bad-Bcl-2 stained cells. Interestingly, it was found that the pattern of mitochondrial distribution significantly matched the pattern of BAD-Bcl-2 distribution in the cells (Figure 3.43).

A.

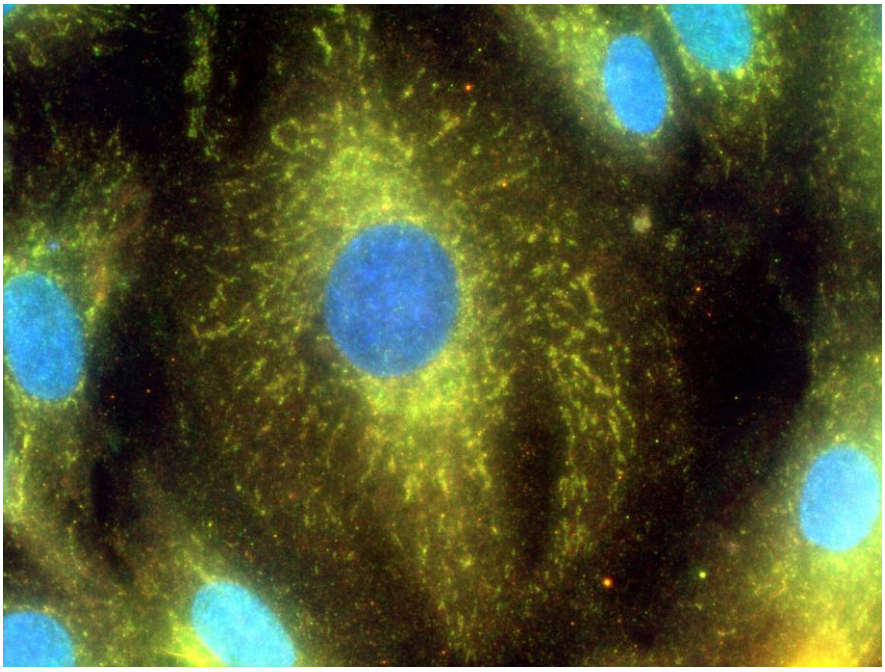

B.

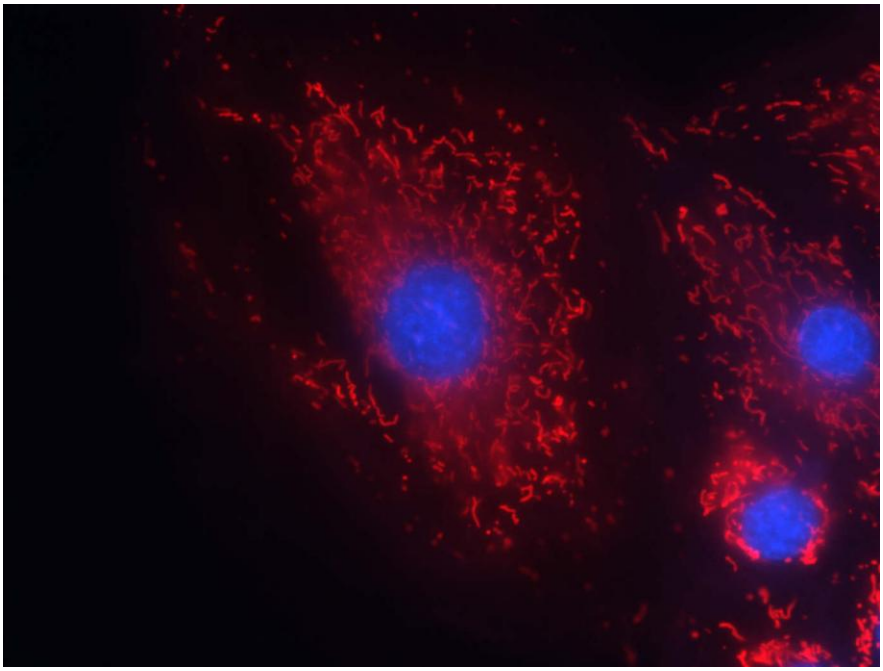

<u>Figure 3.43:</u> Fluorescence microscopy comparing BAD-Bcl-2 with Mitotracker Red.

A) BAD-Bcl-2 (dual staining), B) Mitotracker Red

3.7 GFAT OVEREXPRESSION INCREASES HBP END-PRODUCT AND HBP-MEDIATED BAD-Bcl-2 DIMERIZATION

We next transfected H9c2 myoblasts (cultured in low glucose media – 5.5 mM) with a GFAT construct with or without a dominant negative GFAT construct. GFAT over-expression significantly increased overall *O*-GlcNAc levels as revealed by Western blotting analysis while co-transfection with the dominant negative GFAT construct decreased it (Figure 3.44).

A.

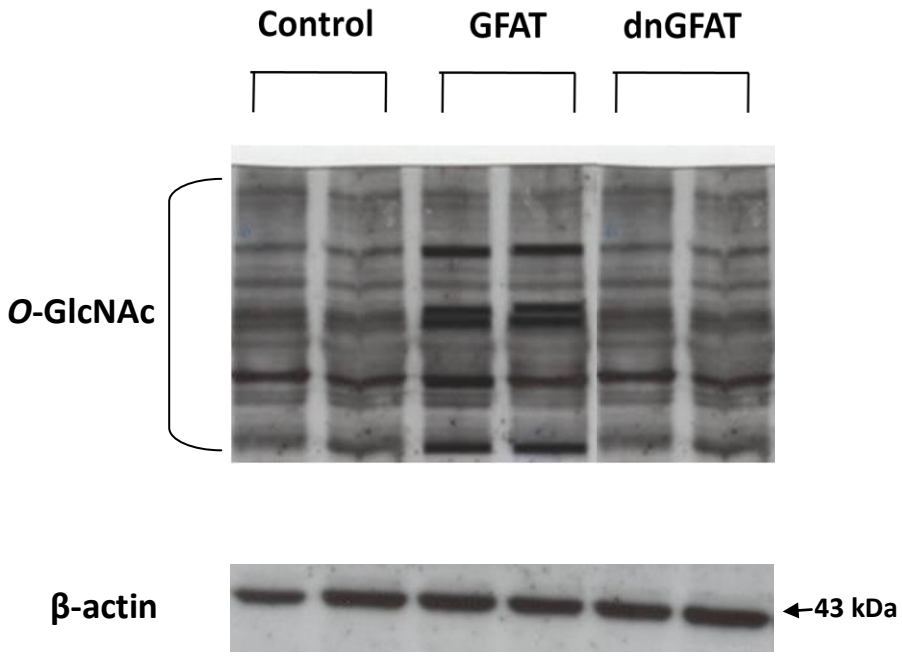

B.

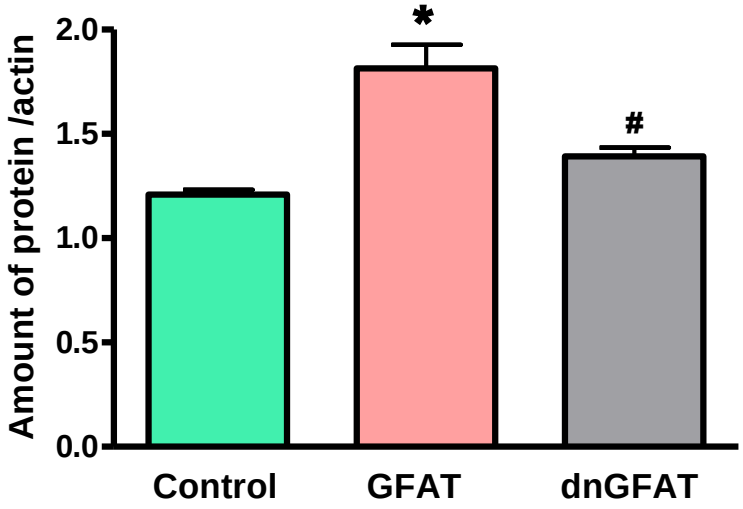

Figure 3.44: Western blot showing increased *O*-GlcNAcylation with GFAT transfection.

*A) Representative O-GlcNAc blot showing increased O-GlcNAc levels in GFAT transfection but decreased by dominant negative GFAT transfection; B) Bar graphs depict densitometric analysis of O-GlcNAc levels – data represent the average for 3 different protein bands normalized against β-actin. AU: Arbitrary Units. Values are expressed as mean ± SEM (n=4). * p<0.001 vs. control,*

*** p<0.01 vs. GFAT.*

As before, immunoprecipitation of *O*-GlcNAcylated proteins and subsequent probing for BAD revealed 2 bands, i.e. 50 kDa and 23 kDa corresponding to BAD-Bcl-2 dimers and BAD, respectively. When the membrane was stripped and re-probed with Bcl-2, the 50 kDa band was observed together with a 26 kDa band corresponding to Bcl-2 (Figure 3.45).

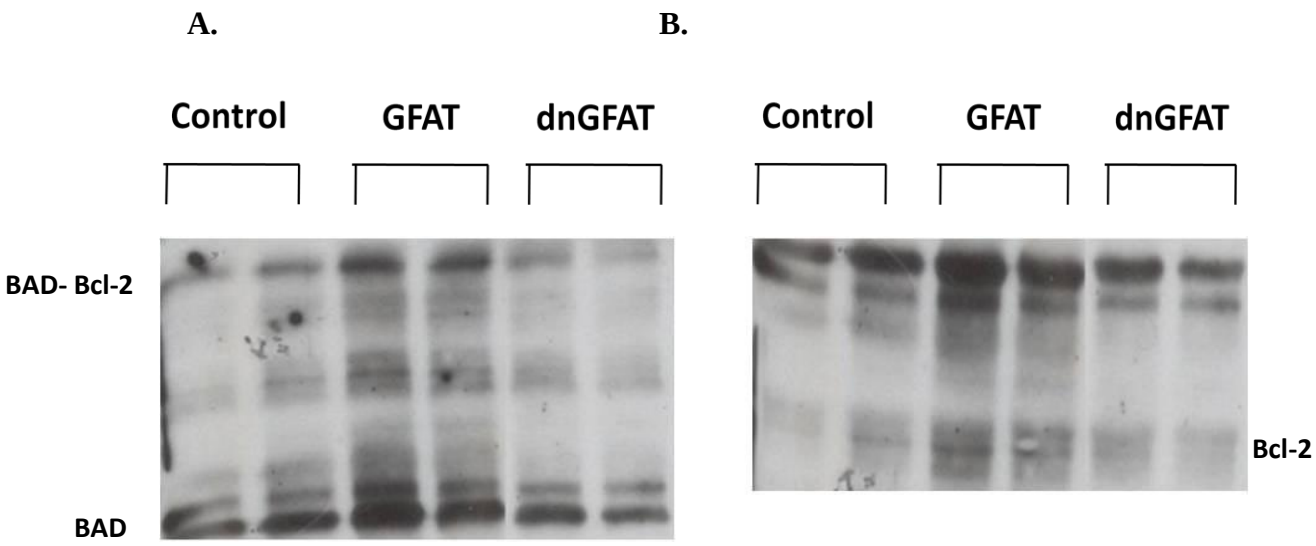

Figure 3.45: Immunoblot demonstrating greater BAD-Bcl-2 dimerization with GFAT transfection.

A) Immunoblot generated by O-GlcNAc immunoprecipitation and thereafter probed for BAD; 23 kDa band = BAD; ~50 kDa Band = BAD-Bcl-2 dimer; B) The same immunoblot was stripped and thereafter probed for Bcl-2; 26 kDa band = Bcl-2. (n=4).

We confirmed these results by performing the reverse experiment. For this BAD was immunoprecipitated using standard methods and thereafter probed for *O*-GlcNAc. As before, we observed similar banding patterns as before (Figure 3.46).

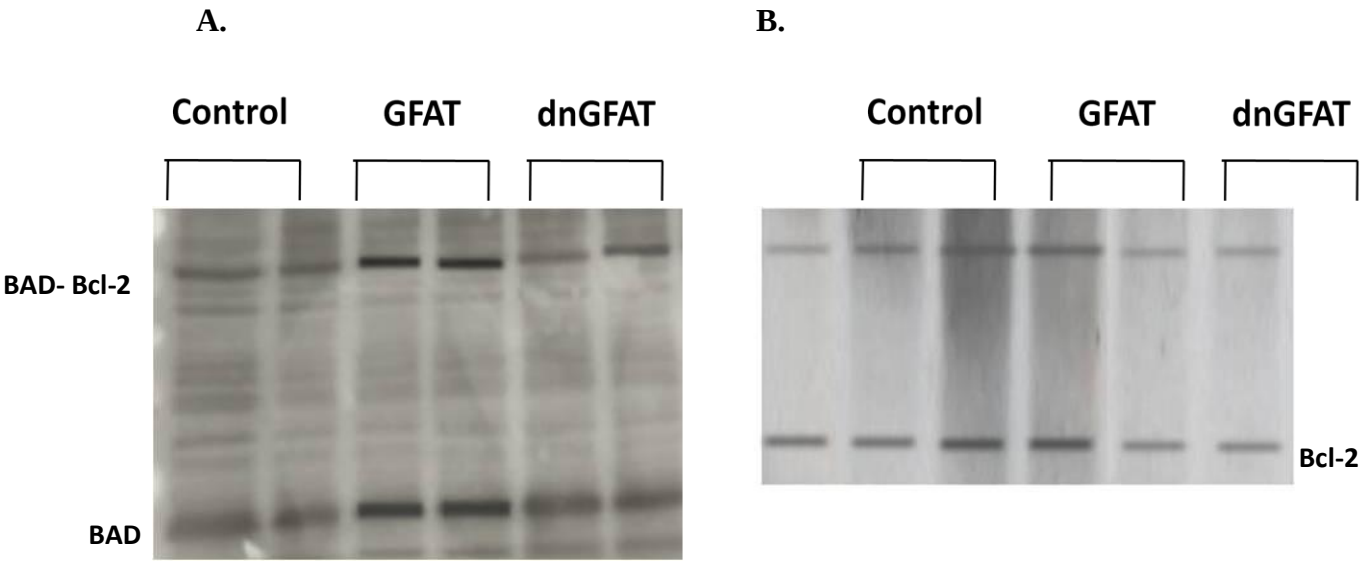

Figure 3.46: Immunoblot demonstrating greater BAD-Bcl-2 dimerization under *in vitro* hyperglycaemic conditions.

A) Immunoblot generated by BAD immunoprecipitation and thereafter probed for O-GlcNAc; 23 kDa band = BAD; ~50 kDa Band = BAD-Bcl-2 dimer; B) The same immunoblot was stripped and thereafter probed for Bcl-2; 26 kDa band = Bcl-2. (n=4).

3.8 A SECOND CELL-BASED MODEL OF APOPTOSIS

We tested whether the novel HBP-mediated death pathway identified in this study would also be activated in a second model of apoptosis. We employed a TNF-α-mediated cell model of apoptosis previously described (Section 2.8). Since there is no hyperglycaemia and oxidative stress associated with this model, we predicted that the HBP would not be triggered and that apoptosis would occur via non-HBP-mediated pathways. In response to 50 ng/ml TNF-α

treatment for 48 hours, it was found that both DON and PUGNAc treatment did not significantly increase or decrease the degree of apoptosis (Figure 3.47).

A.

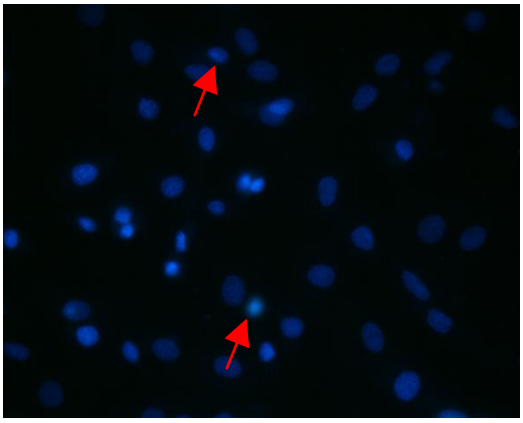

5.5 mM glucose

B.

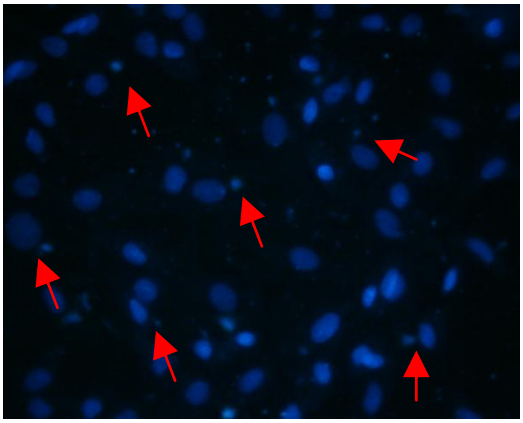

5.5 mM glucose + 50 ng/ml TNF-α

C.

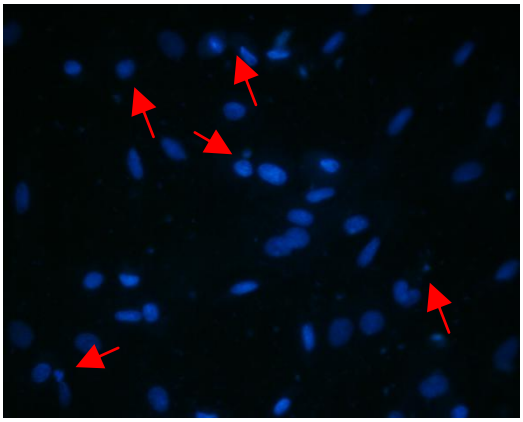

5.5 mM glucose + 50 ng/ml TNF-α + 40 µM DON

D.

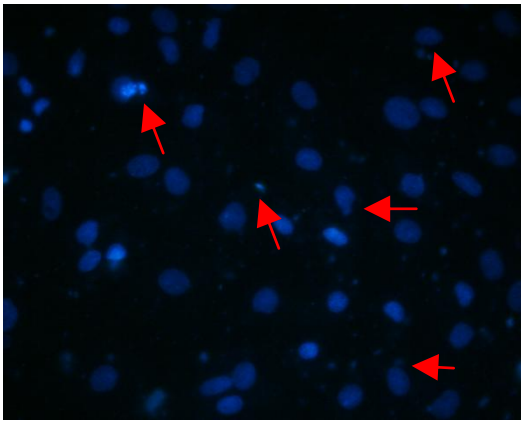

5.5 mM glucose + 50 ng/ml TNF-α + 50 µM PUGNAc

E.

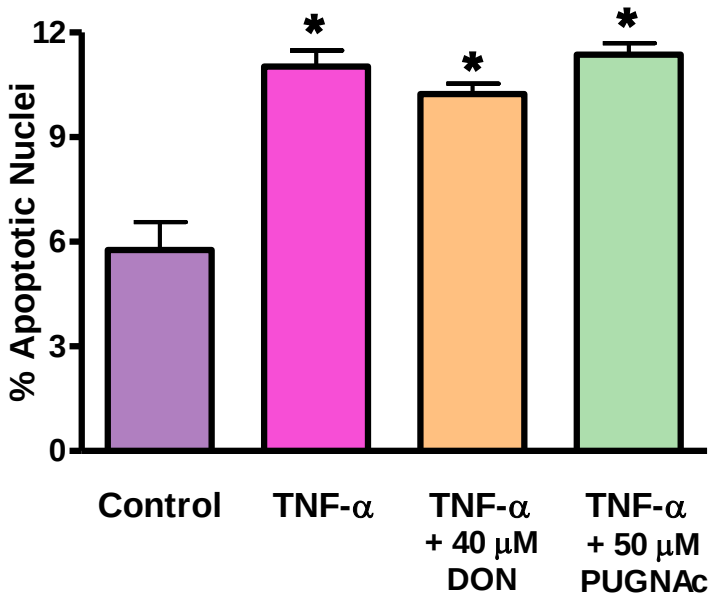

Figure 3.47: Hoechst nuclear staining positive control.

*A) 5.5 mM glucose, B) 5.5 mM glucose + TNF-α, C) 5.5 mM glucose + TNF-α + DON, D) 5.5 mM + TNF-α + PUGNAc (red arrows indicate apoptotic nuclei,) and E) bar graphs represent the number of apoptotic nuclei counted using criteria stipulated in the Materials and Methods section of this thesis (Section 2.3.1). Values are expressed as mean ± SEM (n=3). * p<0.001 vs. 5.5 mM control. N=4.*

REFERENCES FOR RESULTS

1. **Buse, M.G., *Hexosamines, insulin resistance, and the complications of diabetes: current status.* Am J Physiol Endocrinol Metab, 2006. 290(1): p. E1-E8.**

2. **Wang, Z., M. Gucek, and G.W. Hart, *Cross-talk between GlcNAcylation and phosphorylation: site-specific phosphorylation dynamics in response to globally elevated O-GlcNAc.* Proc Natl Acad Sci U S A, 2008. 105(37): p. 13793-8.**

4. DISCUSSION

Introduction

Type 2 diabetes and related metabolic perturbations are closely linked to cardiovascular complications [1-3]. In support, several studies demonstrate increased risk for CVD-related mortality under hyperglycaemic conditions [4-6]. Hyperglycaemia-mediated flux through glucose utilizing pathways, e.g. the HBP is robustly implicated in the development of insulin resistance, type 2 diabetes [7] and CVD [8]. However, the precise mechanisms mediating these processes are unclear. In light of this, we hypothesized that hyperglycaemia-mediated activation of the HBP increases *O*-GlcNAcylation of apoptotic proteins resulting in myocardial apoptosis, thereby contributing to contractile dysfunction and cardiovascular disease. The main findings of this study are: 1*) Hyperglycaemia-mediated activation of the HBP mediates myocardial apoptosis; 2) Oxidative stress plays a crucial role in hyperglycaemia/HBP-mediated apoptosis; and 3) Identification of a novel apoptotic pathway in the heart involving HBP-induced O-GlcNAcylation of BAD.*

4.1 HYPERGLYCAEMIA-MEDIATED ACTIVATION OF THE HBP MEDIATES MYOCARDIAL APOPTOSIS

Previous studies showed that hyperglycaemia could trigger apoptosis [9]. For instance, elevated glucose culturing conditions result in greater glucose oxidation, increased superoxide production [10] and DNA damage. PARP is subsequently activated [11] resulting in apoptosis [12]. Likewise, hyperglycaemia may result in cytochrome-c release thereby activating caspase-3 [9] and apoptosis. In agreement, high glucose treatments (15 mM) caused a significant degree of

apoptosis in human mononuclear cells [13]. Phaeochromocytoma cells from rat adrenal medulla displayed increased DNA fragmentation, a high Bax/Bcl-2 ratio causing more mitochondrial membrane disruption and increased caspase-8, caspase-9 and caspase-3 levels when exposed to hyperglycaemic conditions [14]. Furthermore, a significant increase in apoptosis was found in human umbilical vein endothelial cells exposed to 30 mM glucose for 72 hours [15]. Also, it has been shown that trypsin digests of retinal micro capillaries under hyperglycaemic conditions showed a 2.5 fold upregulation of apoptotic regulatory genes like BAD, Bax, etc. [16]. Conversely, microarray studies have shown a decrease in apoptotic gene expression in diabetic rats [17, 18]. We believe that differences in published data may be due to the stage of disease progression and experimental model employed. For example, the abovementioned microarray study was performed at a relatively early time point during the progression towards full-blown diabetes, while others done at later time points may yield different findings.

Despite progress in this field not many studies have investigated hyperglycaemia-mediated apoptosis in the heart. In light of this, we established an *in vitro* model of hyperglycaemia-mediated apoptosis by employing rat cardiac-derived H9c2 myoblasts. Here we initially administered 22 and 33 mM glucose, respectively, for five days versus 5.5 mM controls. This was in line with previous cell-based studies which employed similar glucose concentrations [9, 15, 19, 20]. Both concentrations caused a significant degree of apoptosis, i.e. as revealed by Hoechst and Annexin-V staining and increased caspase activity. Moreover, we found increased expression of caspase-3, BAD and cytochrome-c under hyperglycaemic conditions. To establish proof-of-concept, we subsequently focussed on the 33 mM concentration (more pronounced effects). We are confident that our *in vitro* data are robust since a) 33 mM mannitol showed no

significant apoptosis thus ruling out osmotic effects and proving that apoptosis observed in our model is due to hyperglycaemia *per se;* and b) *in vitro* findings were paralleled in hearts of a rat model of insulin resistance and hyperglycaemia.

Previous studies show that HBP activation results in apoptosis [21, 22]. For example, increased *O*-GlcNAcylation of p53 (a tumor suppressor protein), leads to greater synthesis of angiotensin-II, thereby causing apoptosis. Here enzymatic p53 glycosylation leads to angiotensin II formation which binds to AT1 receptors. This post-translational modification increases p53 stability, thereby prolonging activation of angiotensin II and causing apoptosis. Bax expression levels were also elevated leading to increased apoptosis and cytochrome-c release [23]. Glycosylation may also interfere with the proteolysis system of the cell, i.e. by *O*-GlcNAcylation of proteosomes. This could result in ineffective proteolysis of proteins including pro-apoptotic proteins such as BAD and thereby leading to greater apoptosis [24]. However, it is unclear whether hyperglycaemia-mediated HBP activation causes apoptosis in the heart. Our data show a significant increase in total *O*-GlcNAcylation of cardiac proteins as demonstrated by immunofluorescence microscopy, Western blotting analysis and GFAT overexpression. This elevation was closely linked to higher incidence of apoptosis. Together these data show increased HBP flux under hyperglycaemic conditions is associated with a higher degree of apoptosis. In agreement, elevated *O*-GlcNAcylation of proteins and apoptosis were observed in *in vivo* heart tissue of insulin resistant/hyperglycaemic rats.

To further investigate these interesting findings, we next attenuated HBP flux by inhibiting GFAT, the rate-limiting enzyme of this pathway. DON is an analogue of glutamine that inhibits glutamine-requiring enzymes e.g. (GFAT) and is widely used as a GFAT inhibitor [25]. As predicted, we found that DON administration resulted in decreased cardiac *O*-GlcNAcylation of proteins and attenuated apoptosis when compared to hyperglycaemic conditions. We also inhibited *O*-GlcNAcase thereby increasing the *O*-GlcNAcylation of target proteins. For this purpose, we employed PUGNAc, an inhibitor of N-acetylglucosaminidase, that is routinely used to inhibit *O*-GlcNAcase and thereby increase *O*-GlcNAcylation of proteins [26]. We found that PUGNAc treatment increased *O*-GlcNAcylation of proteins in cardiac myoblasts. In parallel, myoblast apoptosis was increased. Collectively the data therefore strongly supporting a role for the HBP in hyperglycaemia-induced apoptosis in cardiac myoblasts.

However, Chatham *et al*. proposed that HBP and *O*-GlcNAcylation trigger cardioprotective mechanisms thereby enhancing cell survival [27]. For example, they found that PUGNAc treatment resulted in improved survival of monkey kidney cells in response to thermal treatments [28]. GFAT inhibition also resulted in the opposite effect, i.e. decreased *O*-GlcNAcylation and increased cell death [29]. Also, activation of HBP in perfused hearts (glucosamine or glutamine treatment) before an ischaemic insult resulted in elevated *O*-GlcNAc levels, improved contractile function and decreased tissue injury after reperfusion [30, 31]. Likewise, others found that inhibition of *O*-GlcNAcase significantly augmented *O*-GlcNAc levels and reduced post-hypoxic cell death in isolated cardiac myocytes [8]. This study also found increased post-hypoxic cell death and reduced mitochondrial membrane potential recovery when *O*-GlcNAcase expression was elevated.

How could activation of the same pathway result in opposite effects? We propose that different proteins are likely to be *O*-GlcNAcylated in the experimental models employed. It is likely that glucosamine and glutamine treatment "tagged" (i.e. *O*-GlcNAcylated) anti-apoptotic proteins while high glucose treatments tagged pro-apoptotic proteins. This is an intriguing question that requires further investigation, i.e. *why* and *how* does the cell know which proteins to target for *O*-GlcNAcylation within a particular context, e.g ischaemic-reperfusion or hyperglycaemia. These questions are currently vigorously pursued in our laboratory.

4.2 OXIDATIVE STRESS PLAYS A CRUCIAL ROLE IN HYPERGLYCAEMIA/HBP-MEDIATED APOPTOSIS

The involvement of oxidative stress in cell damage under hyperglycaemic conditions is well documented. For instance, Brownlee's laboratory proposed that hyperglycaemia increases the inner mitochondrial membrane potential, resulting in greater mitochondrial superoxide production and DNA damage [10, 32, 33]. Subsequently, PARP is released as a DNA reparative mechanism. But PARP also inhibits GAPDH thereby resulting in the accumulation of upstream glycolytic metabolites like fructose-6-phosphate that may increase HBP flux [11].

We measured overall ROS production in our model of hyperglycaemia-induced apoptosis by employing fluorescence microscopy and flow cytometry. Our results show markedly elevated ROS levels in response to hyperglycaemia at both single cellular (microscopy) and cell population (flow cytometry) levels. Hyperglycaemia is generally known to induce superoxide

production [34] and we speculate the same for our model. In support, others found that hyperglycaemia-induced ROS production in renal cells mediates apoptosis and contributes to diabetic nephropathy [35]. Moreover, diabetic rats display increased expression of genes involved in oxidative stress and apoptosis [36], while H9c2 myoblasts exposed to high glucose levels exhibit decreased expression of heat shock protein 27, resulting in oxidative stress and apoptosis [37].

We strengthened our hypothesis by including the antioxidant 4-OHCA that acts by inhibiting pyruvate transport into mitochondria, thereby reducing mitochondrial ROS production. As expected, antioxidant treatment attenuated ROS levels observed under both hyperglycaemic conditions and with PUGNAc treatment. In parallel, antioxidant administration diminished HBP-mediated cardiac *O*-GlcNAc levels and apoptosis.

We also found that treatment with PUGNAc alone increased ROS levels. This raises the question: why would higher *O*-GlcNAcylation trigger increased ROS production? We speculate that there may be increased *O*-GlcNAcylation of anti-oxidant proteins like superoxide dismutase (SOD) thereby inactivating it and decreasing antioxidant capacity. It is also possible that antioxidant protein expression may be decreased due to *O*-GlcNAcylation and inactivation of transcription factors that usually induce expression of these genes. It may also be possible that *O*-GlcNAcylation of antioxidant proteins such as SOD could render them less stable and therefore more prone to proteosomal degradation. These interesting concepts need to be investigated.

Taken together our results strongly support the concept that increased ROS production and greater HBP flux orchestrate hyperglycaemia-mediated apoptosis in cardiac myoblasts [32].

4.3 IDENTIFICATION OF A NOVEL APOPTOTIC PATHWAY IN THE HEART INVOLVING HBP-INDUCED O-GLCNACYLATION OF BAD

Since we found increased apoptosis (↑ cytochrome-c release) in our hyperglycaemic cell model and insulin resistant heart tissues, we explored underlying mechanisms mediating this process. Cytochrome-c is released as a result of mitochondrial membrane disruption which is most commonly caused by apoptotic protein dimers such as Bax and Bak [38]. It has been documented that hyperglycaemia induces increased Bax expression and apoptosis [39]. Moreover, reduced apoptotic rates were observed in transgenic $Bax^{-/-}$ (Bax-deficient) mice exposed to hyperglycaemia [39] indicating that Bax does indeed play a major role in the apoptotic cascade.

But, how does Bax cause apoptosis? This occurs via a pathway involving BAD (Bcl-2 associated death promoter protein) and Bcl-2. BAD in its dephosphorylated form usually forms a heterodimer with Bcl-2 or Bcl-xL (Figure 4.1). Bcl-2/Bcl-xL are anti-apoptotic proteins present on the mitochondrial membrane to prevent apoptosis by heterodimerizing with Bax and Bak to prevent them from forming homodimers since Bax:Bax and Bak:Bak homodimers usually insert into the mitochondrial membrane causing cytochrome-c release [40].

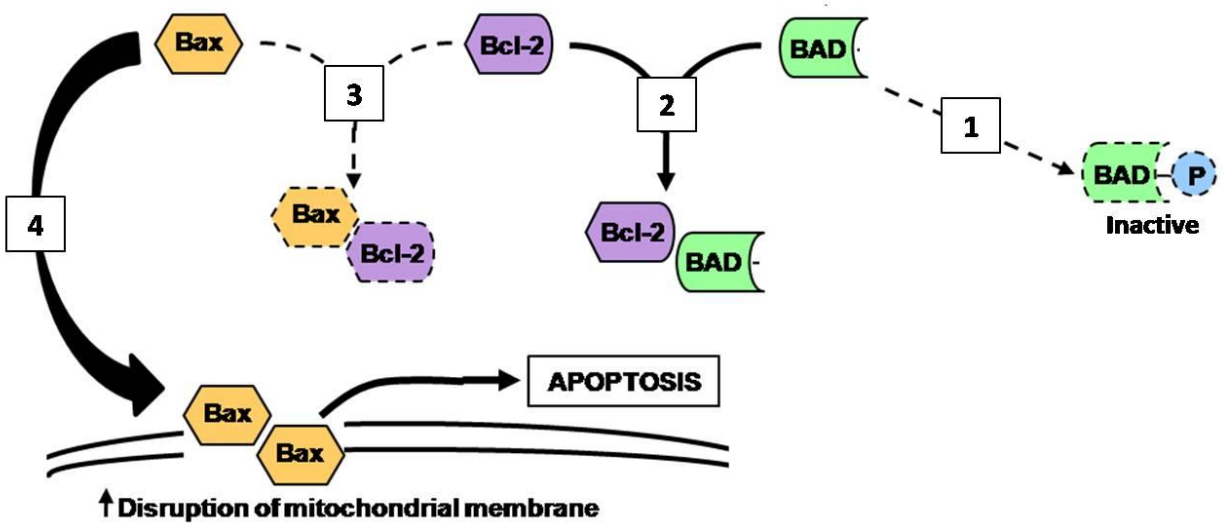

Figure 4.1: Representation showing Bad mediated apoptosis.

Step 1: Bad phosphorylation renders it inactive. Step 2: Unphosphorylated Bad dimerizes with Bcl-2 forming a heterodimer. Step 3: Reduced Bcl-2 dimerization with Bax. Step 4: Free Bax now forms homodimers leading to disruption of the mitochondrial membrane, thereby inducing apoptosis.

However, when BAD is dephosphorylated, it binds to Bcl-2 and prevents the Bcl-2 mediated sequence of events, thereby resulting in apoptosis. Conversely, when BAD is phosphorylated its binding affinity to Bcl-2 is decreased, meaning formation of Bax:Bcl-2 dimers and greater cell survival. Hence the phosphorylation status of BAD plays a crucial role in cell survival. Several upstream regulators are implicated in determining the phosphorylation status of BAD, including PIM2 kinase [41], C-Raf kinase [42], p38 MAP kinase [24], p90-Rsk-1 [43], PKA and PKB.

What happens when BAD is *O*-GlcNAcylated? Previous work have shown that a "yin-yang" relationship may prevail between phosphorylation and *O*-GlcNAcylation, i.e. competition between phosphorylation and *O*-GlcNAcylation for the same site or closely located sites on target proteins [44]. Under circumstances of increased HBP flux, there is greater *O*-GlcNAcylation of BAD thus likely decreasing its phosphorylation status. We propose that *O*-GlcNAcylation of BAD occurs in the near vicinity or at the same site(s) as BAD phosphorylation, resulting in reduced access to upstream kinases. As a result, BAD remains in a dephosphorylated state thereby triggering apoptosis. In support of this concept, glucosamine treatment of pancreatic β–cells resulted in increased *O*-GlcNAcylation of Akt and reduced phosphorylation at Ser473 [45], i.e. O-GlcNAcylation ''out-competing'' phosphorylation. Since the Akt signaling pathway results in phosphorylation of BAD [46] these findings suggest that defects in Akt activation may eventually enhance apoptosis. Alternatively, glycosylation may also interfere with the proteolysis system of the cell, i.e. by *O*-GlcNAcylation of proteasome. This could result in ineffective rate of proteolysis of proteins including pro-apoptotic proteins such as BAD and thereby leading to greater apoptosis [24]. Another possibility is that *O*-GlcNAcylation may directly alter BAD's activity and thereby trigger apoptosis. These interesting possibilities require further investigation.

We explored this mechanism in both our *in vitro* and *in vivo* models. We initially measured the degree of BAD *O*-GlcNAcylation, followed by the determination of BAD:Bcl-2 dimer formation. Dual fluorescence staining and co-localization studies revealed that there is augmented *O*-GlcNAcylation of BAD under hyperglycaemic conditions. In agreement, BAD *O*-GlcNAcylation was attenuated by HBP inhibition and increased by PUGNAc treatment. Moreover, BAD *O*-GlcNAcylation was attenuated when an antioxidant was co-administered thus

supporting our hypothesis that oxidative stress plays a vital role in this process. These *in vitro* results were well supported by data generated from our *in vivo* rat model of insulin resistance.

Our *in vitro* and *in vivo* immunoblotting and co-localization data reveal that BAD does indeed form a dimer with Bcl-2.Dimer formation increases under hyperglycaemic conditions and with PUGNAc treatment, suggesting that *O*-GlcNAcylation maintains BAD in its active form, i.e. dimerizing with Bcl-2 and resulting in increased apoptosis (Figure 4.1).

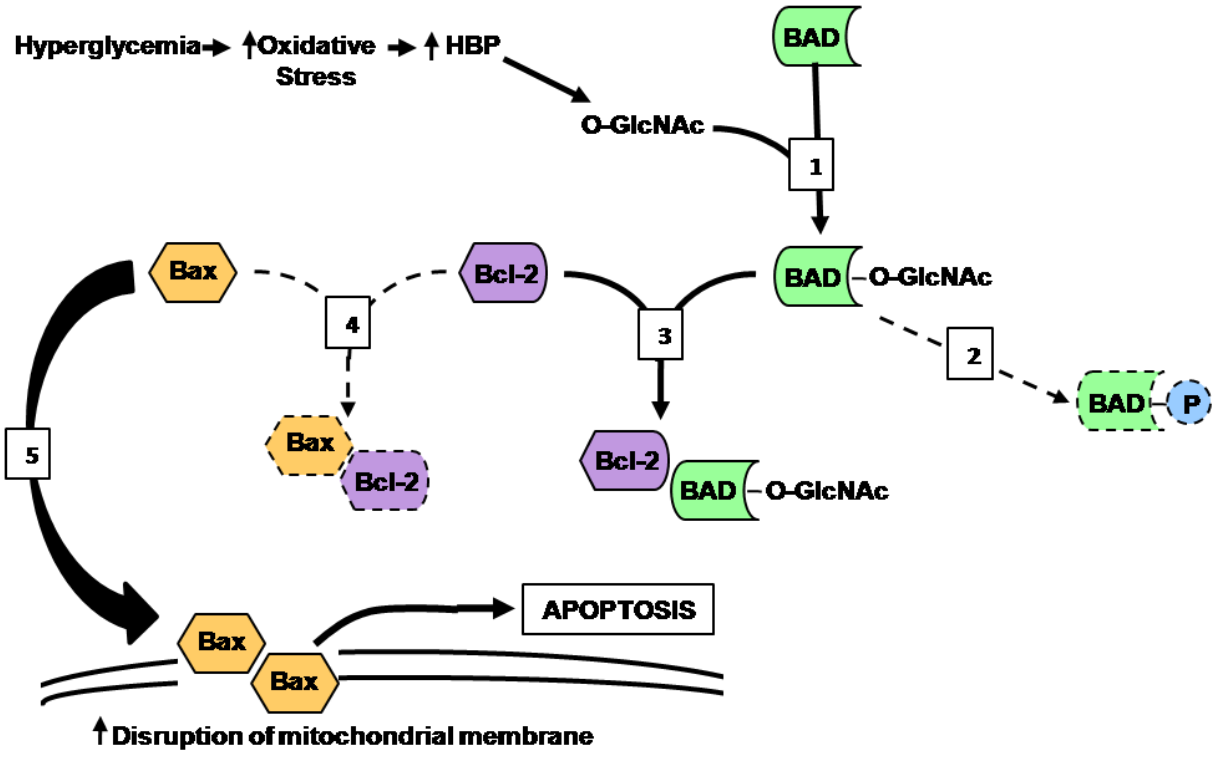

Figure 4.2: Representation showing how increased Bad *O*-GlcNAcylation triggers apoptosis.

Step 1: Hyperglycaemia-induced increased HBP flux results in increased O-GlcNAcylation of Bad. Step 2: Higher O-GlcNAcylation leads to reduced Bad phosphorylation. Step 3: Increased dimerization of O-GlcNAcylated Bad with Bcl-2. Step 4: Reduced Bcl-2 dimerization with Bax. Step 5: Free Bax now forms homodimers leading to disruption of the mitochondrial membrane, thereby inducing apoptosis.

Moreover, antioxidant treatment blunted these effects. Our data suggest that there is increased BAD *O*-GlcNAcylation and increased BAD:Bcl-2 dimerization under hyperglycaemic conditions. We propose that increased dimer formation plays a crucial role in hyperglycaemia-mediated apoptosis observed in both our experimental models. It is predicted that increased myocardial apoptosis will result in contractile dysfunction. Evaluation of heart functional measurements fell outside the scope of this study and thesis and is currently being pursued by others in our laboratory.

Limitations of the study

1) no controls for immunoprecipitation, e.g. IgG; 2) additional reverse immunoprecipitation of Bcl-2 and probing for BAD was not done; 3) HbA1c levels in the rat model were not available to confirm longstanding hyperglycaemia; and 4) BAD phosphorylation was not measured but is a crucial parameter to determine in order to observe the yin-yang relation between phosphorylation and *O*-GlcNAcylation. These are ongoing studies in our laboratory.

In summary, we identified a novel pathway (for the first time as far as we are aware) whereby hyperglycaemia results in greater oxidative stress, increased BAD *O*-GlcNAcylation and BAD-Bcl-2 dimer formation, thereby mediating HBP-induced myocardial apoptosis. It is likely that this maladaptive pathway may be triggered with repetitive hyperglycaemic spikes in pre-diabetic patients and/or in diabetic patients with chronically elevated glucose levels. We propose that these factors converge to contribute to contractile dysfunction within this context, i.e. the diabetic cardiomyopathy. Our work offers unique possibilities for novel therapeutic interventions that could play a significant role to help attenuate the growing global burden of diabetes and CVD.

FUTURE WORK

- Determine whether there are other proteins linked to the two dimerizing proteins i.e. Bad and Bcl-2
- Employ streptozotocin-induced diabetic rodents to test for similar effects in a type 1 model of diabetes
- Employ 2-deoxyglucose as a control and test for its effects
- Employ cardiac-specific transgenic GFAT knock-out mice to assess potential cardioprotective effects
- Evaluate whether similar findings obtained when using isolated adult cardiomyocytes as an experimental system.

REFERENCES FOR DISCUSSION

1. **Boudina, S. and E.D. Abel, *Diabetic cardiomyopathy revisited.* Circulation, 2007. 115(25): p. 3213-23.**

2. **Wei, M., et al., *Effects of diabetes and level of glycemia on all-cause and cardiovascular mortality. The San Antonio Heart Study.* Diabetes Care, 1998. 21(7): p. 1167-72.**

3. **Gu, K., C.C. Cowie, and M.I. Harris, *Diabetes and decline in heart disease mortality in US adults.* JAMA, 1999. 281(14): p. 1291-7.**

4. **Garcia, M.J., et al., *Morbidity and mortality in diabetics in the Framingham population. Sixteen year follow-up study.* Diabetes, 1974. 23(2): p. 105-11.**

5. **Saydah, S.H., et al., *Age and the burden of death attributable to diabetes in the United States.* Am J Epidemiol, 2002. 156(8): p. 714-9.**

6. **Morgan, C.L., C.J. Currie, and J.R. Peters, *Relationship between diabetes and mortality: a population study using record linkage.* Diabetes Care, 2000. 23(8): p. 1103-7.**

7. **Marshall, S., V. Bacote, and R.R. Traxinger, *Discovery of a metabolic pathway mediating glucose-induced desensitization of the glucose transport system. Role of hexosamine biosynthesis in the induction of insulin resistance.* J Biol Chem, 1991. 266(8): p. 4706-12.**

8. **Ngoh, G.A., et al., *Unique hexosaminidase reduces metabolic survival signal and sensitizes cardiac myocytes to hypoxia/reoxygenation injury.* Circ Res, 2009. 104(1): p. 41-9.**

9. **Cai, L., et al., *Hyperglycemia-induced apoptosis in mouse myocardium: mitochondrial cytochrome C-mediated caspase-3 activation pathway.* Diabetes, 2002. 51(6): p. 1938-48.**

10. **Nishikawa, T., et al., *Normalizing mitochondrial superoxide production blocks three pathways of hyperglycaemic damage.* Nature, 2000. 404(6779): p. 787-90.**

11. **Du, X., et al., *Inhibition of GAPDH activity by poly(ADP-ribose) polymerase activates three major pathways of hyperglycemic damage in endothelial cells.* J Clin Invest, 2003. 112(7): p. 1049-57.**

12. **Zhang, D.X., et al., *Production and metabolism of ceramide in normal and ischemic-reperfused myocardium of rats.* Basic Res Cardiol, 2001. 96(3): p. 267-74.**

13. **Hsieh, M.S. and W.H. Chan, *Impact of Methylglyoxal and High Glucose Co-treatment on Human Mononuclear Cells.* Int J Mol Sci, 2009. 10(4): p. 1445-64.**

14. **Sharifi, A.M., et al.,** ***Involvement of caspase-8, -9, and -3 in high glucose-induced apoptosis in PC12 cells.*** **Neurosci Lett, 2009. 459(2): p. 47-51.**

15. **Ido, Y., D. Carling, and N. Ruderman,** ***Hyperglycemia-induced apoptosis in human umbilical vein endothelial cells: inhibition by the AMP-activated protein kinase activation.*** **Diabetes, 2002. 51(1): p. 159-67.**

16. **Kowluru, R.A. and P.S. Chan,** ***Metabolic memory in diabetes - from in vitro oddity to in vivo problem: Role of Apoptosis.*** **Brain Res Bull, 2009.**

17. **Balwierz, A., et al.,** ***Angiogenesis in the New Zealand obese mouse model fed with high fat diet.*** **Lipids Health Dis, 2009. 8: p. 13.**

18. **Herrman, C.E., et al.,** ***Decreased apoptosis as a mechanism for hepatomegaly in streptozotocin-induced diabetic rats.*** **Toxicol Sci, 1999. 50(1): p. 146-51.**

19. **Yu, X.Y., et al.,** ***Glucose induces apoptosis of cardiomyocytes via microRNA-1 and IGF-1.*** **Biochem Biophys Res Commun, 2008. 376(3): p. 548-52.**

20. **Kim, M.H., et al.,** ***High-glucose induced protective effect against hypoxic injury is associated with maintenance of mitochondrial membrane potential.*** **Jpn J Physiol, 2003. 53(6): p. 451-9.**

21. **Fulop, N., R.B. Marchase, and J.C. Chatham,** ***Role of protein O-linked N-acetyl-glucosamine in mediating cell function and survival in the cardiovascular system.*** **Cardiovasc Res, 2007. 73(2): p. 288-97.**

22. **Favaro, E., et al.,** ***Hyperglycemia induces apoptosis of human pancreatic islet endothelial cells: effects of pravastatin on the Akt survival pathway.*** **Am J Pathol, 2008. 173(2): p. 442-50.**

23. **Fiordaliso, F., et al.,** ***Hyperglycemia activates p53 and p53-regulated genes leading to myocyte cell death.*** **Diabetes, 2001. 50(10): p. 2363-75.**

24. **Zhang, F., et al.,** ***O-GlcNAc modification is an endogenous inhibitor of the proteasome.*** **Cell, 2003. 115(6): p. 715-25.**

25. **Lagranha, C.J., et al.,** ***Glutamine enhances glucose-induced mesangial cell proliferation.*** **Amino Acids, 2008. 34(4): p. 683-5.**

26. **Clark, R.J., et al.,** ***Diabetes and the accompanying hyperglycemia impairs cardiomyocyte calcium cycling through increased nuclear O-GlcNAcylation.*** **J Biol Chem, 2003. 278(45): p. 44230-7.**

27. **Laczy, B., et al.,** ***Protein O-GlcNAcylation: a new signaling paradigm for the cardiovascular system.*** **Am J Physiol Heart Circ Physiol, 2009. 296(1): p. H13-28.**

28. **Zachara, N.E., et al.,** ***Dynamic O-GlcNAc modification of nucleocytoplasmic proteins in response to stress. A survival response of mammalian cells.*** **J Biol Chem, 2004. 279(29): p. 30133-42.**

29. Sohn, K.C., et al., *OGT functions as a catalytic chaperone under heat stress response: a unique defense role of OGT in hyperthermia.* Biochem Biophys Res Commun, 2004. 322(3): p. 1045-51.

30. Liu, J., R.B. Marchase, and J.C. Chatham, *Glutamine-induced protection of isolated rat heart from ischemia/reperfusion injury is mediated via the hexosamine biosynthesis pathway and increased protein O-GlcNAc levels.* J Mol Cell Cardiol, 2007. 42(1): p. 177-85.

31. Liu, J., et al., *Increased hexosamine biosynthesis and protein O-GlcNAc levels associated with myocardial protection against calcium paradox and ischemia.* J Mol Cell Cardiol, 2006. 40(2): p. 303-12.

32. Ricci, J.E., R.A. Gottlieb, and D.R. Green, *Caspase-mediated loss of mitochondrial function and generation of reactive oxygen species during apoptosis.* J Cell Biol, 2003. 160(1): p. 65-75.

33. Brownlee, M., *Biochemistry and molecular cell biology of diabetic complications.* Nature, 2001. 414(6865): p. 813-20.

34. Munusamy, S. and L.A. MacMillan-Crow, *Mitochondrial superoxide plays a crucial role in the development of mitochondrial dysfunction during high glucose exposure in rat renal proximal tubular cells.* Free Radic Biol Med, 2009. 46(8): p. 1149-57.

35. Wagener, F.A., et al., *The role of reactive oxygen species in apoptosis of the diabetic kidney.* Apoptosis, 2009.

36. Gerhardinger, C., et al., *The TGF-{beta} pathway is a common target of drugs that prevent experimental diabetic retinopathy.* Diabetes, 2009.

37. Gawlowski, T., et al., *Heat Shock Protein 27 Modification is Increased in the Human Diabetic Failing Heart.* Horm Metab Res, 2009.

38. Orrenius, S., *Mitochondrial regulation of apoptotic cell death.* Toxicol Lett, 2004. 149(1-3): p. 19-23.

39. Moley, K.H., *Hyperglycemia and apoptosis: mechanisms for congenital malformations and pregnancy loss in diabetic women.* Trends Endocrinol Metab, 2001. 12(2): p. 78-82.

40. Adams, J.M. and S. Cory, *The Bcl-2 protein family: arbiters of cell survival.* Science, 1998. 281(5381): p. 1322-6.

41. Yan, B., et al., *The PIM-2 kinase phosphorylates BAD on serine 112 and reverses BAD-induced cell death.* J Biol Chem, 2003. 278(46): p. 45358-67.

42. Rapp, U.R., et al., *BAD association with membranes is regulated by Raf kinases and association with 14-3-3 proteins.* Adv Enzyme Regul, 2007. 47: p. 281-5.

43. del Peso, L., et al., *Interleukin-3-induced phosphorylation of BAD through the protein kinase Akt.* Science, 1997. 278(5338): p. 687-9.

44. **Wang, Z., M. Gucek, and G.W. Hart,** ***Cross-talk between GlcNAcylation and phosphorylation: site-specific phosphorylation dynamics in response to globally elevated O-GlcNAc.*** **Proc Natl Acad Sci U S A, 2008. 105(37): p. 13793-8.**

45. **Park, J., et al.,** ***Proteomic analysis of O-GlcNAc modifications derived from streptozotocin and glucosamine induced beta-cell apoptosis.*** **J Biochem Mol Biol, 2007. 40(6): p. 1058-68.**

46. **Datta, S.R., et al.,** ***Akt phosphorylation of BAD couples survival signals to the cell-intrinsic death machinery.*** **Cell, 1997. 91(2): p. 231-41.**

Appendix

Appendix 1

1.1 Modified RIPA Buffer:

A 100 ml modified RIPA buffer contains:

- 50 mM Tris-HCl (790 mg of Tris in 75 ml distilled water and 900 mg of NaCl and pH made 7.4 using HCl)
- 10 ml of 10% NP-40 [final concentration 1%]
- 2.5 ml of 10% sodium deoxycholate [final concentration 0.25%]
- 1 ml of 100 mM EDTA pH 7.4 [final concentration 1 mM]
- Protease inhibitors
    - 500 µL of 200 mM phenylmethylsulfonyl fluoride (PMSF) [final concentration 1 mM]
    - 100 µL of Leupeptin (1 mg/ml water) [final concentration 1 µg/ml]
    - 80 µL of SBT1 (5 mg/ml water) [final concentration 4 µg/ml]
    - 100 µL of Benzamidine (1 M) [final concentration 1 mM]
- Protein phosphatase inhibitors
    - 500 µL of 200 mM activated sodium orthovanadate (Na_2VO_3) [final concentration 1 mM]
    - 500 µL of 200 mM NaF [final concentration 1mM]
- 1 ml Triton X-100

This buffer is then made up to a final volume of 100 ml with distilled water and stored at -20°C.

1.2 Denaturing Lysis Buffer for Immunoprecipitation:

The RIPA buffer for immunoprecipitation was made up separately containing:

- 50 mM Tris HCl
- 150 mM NaCl
- 1% NP-40
- 0.5% Na deoxycholate
- 0.1% SDS

The protease inhibitors (PMSF- 50 µg/ml, Aprotonin- 1µg/ml) are added just before use.

1.3 Non-denaturing Lysis Buffer for Immunoprecipitation:

The non-denaturing lysis buffer contained:

- 20 mM Tris HCl
- 137 mM NaCl
- 10% glycerol
- 1% Triton X-100
- 2 mM EDTA

The protease inhibitors (PMSF- 50 µg/ml, Aprotonin- 1µg/ml) are added just before use.

Appendix 2

Bradford protein quantification method:

Bradford reagent

- 500 mg of Coomassie Brilliant Blue G in 250 ml of 95% ethanol
- 500 ml of phosphoric acid

This is made up to 1 litre using distilled water, filtered and stored at 4°C.

Working solution:

The Bradford stock is diluted in 1:5 ratio using distilled water, filtered and used for protein quantification.

Bradford method:

- BSA (1 mg/ml) is diluted in a 1:4 ratio using distilled water.
- A protein standard with varying protein concentrations is prepared as follows

BSA (µL)	BSA concentration (µg)	Volume of distilled water (µL)
0	Blank	100
10	2	90
20	4	80
40	8	60
60	12	40
80	16	20
100	20	0
5	Unknown protein sample	95

- To all these protein and BSA standards, 900 µL of Bradford working solution is added and vortexed gently.

- Samples were allowed to stand for ~ 5 minutes.
- The absorbancies of each sample was read using a spectrophotometer at 595 nm. (If the protein absorbancies fall outside the protein standard, the proteins must be diluted with RIPA buffer and reading taken again).
- The absorbancies were then plotted to construct a linear plot for the standards. Thereafter the amounts of protein in unknown samples were quantified in relation to the linear standard plot.

Sample preparation:

- A stock solution of sample buffer containing 850 µL sample buffer and 150 µL mercaptoethanol is prepared.
- A volume of sample buffer equivalent to 1/3 final volume of the sample if added (under the fume hood).
- The appropriate amounts of proteins are added to each tube calculated previously.
- Tiny holes are punched on the lids of microfuge tubes (containing the prepared sample) and placed in boiling water for about 5 minutes.
- The tubes are then briefly spun in a table top centrifuge.
- Samples can now be used for Western blot analysis or alternatively be stored at -80°C for later use.
- If samples are stored at -80°C, they must be boiled for 5 minutes in boiling water and shortly centrifuged before being used for western blotting analysis.

Appendix 3

Electrotransfer of proteins:

Solutions for Electrotransfer:

Anode Buffer 1:

0.3 M Tris-base, pH 10.4

20% methanol

Anode Buffer 2:

25 mM Tris-base, pH 10.4

20% methanol

Cathode Buffer:

25 mM Tris-base

40 mM ε-aminohexanoic acid (pH 9.4)

20% methanol

Electrophoresed proteins were subsequently transferred onto a PVDF membrane (Immobilon-P, Millipore Corporation, MA, USA) by electrotransfer on a semidry transfer apparatus (Bio-RAD® Semi-Dry Transfer Cell, Bio-RAD Laboratories, California, USA)., Eight Whatmann 3MM papers and one PVDF membrane were cut to size of the gel. The membrane was first soaked in methanol for 15 seconds, washed with distilled water and then soaked in anode buffer 2.

Three Whatmann papers were well soaked in anode buffer one and placed onto the anode plate of the transfer apparatus. The papers were rolled dry to make sure that there were no bubbles. A

single Whatmann paper was soaked in anode buffer two and placed over the other papers in the apparatus. The PVDF membrane, soaked in anode buffer two, was then placed over the Whatmann papers. The electrophoresed gel soaked in anode buffer two was placed on top of this and rolled dry. Finally, the remaining four Whatmann papers were soaked in cathode buffer and placed over the gel and rolled dry. The cathode plate of the apparatus is then placed over the gel sandwich, closed and run at 15 volts (current of 0.5 A) for one hour. After the transfer, the protein in the membrane was fixed by placing it in methanol for a few seconds.

Appendix 4

Detection of proteins (Western blots):

Probing the membrane

Non-specific binding in the membrane is blocked overnight at 4°C with 5% milk solution (5 g fat free milk powder in 100 ml TBS Tween). After blocking, the membrane is washed in 1x TBS containing 0.1% Tween (TBS-Tween) and thereafter incubated overnight at 4°C with the primary antibody investigated. We employed a 1:1000 dilution of the primary antibody. The membrane was then thoroughly washed in TBS-Tween and incubated for one hour at room temperature with secondary anti-mouse HRP monoclonal antibody (1:4000). The membrane was then washed three to fourtimes in TBS-Tween and finally once in plain 1x TBS and developed.

Developing the membrane

The membrane was treated with 2.5 ml KPL LumiGLO..... (KPL Inc., Maryland, USA) for one minute and making sure that the reagent is evenly distributed over the membrane. It was then dried on tissue paper, placed between transparencies and was then developed in a dark room. A developing film (Hyperfilm, Amersham, Buckinghamshire, UK) was placed over the sandwiched membrane and exposed for 5-10 minutes. The film was then developed by placing it in developing solution for 5 minutes followed by 15 seconds in a fixative. This film was then used for densitometric analysis.

Appendix 5

O-GlcNAc Western blot detection:

Note: This procedure is described as per the manufacturer's instructions of the O-GlcNAc Western blot detection kit (Pierce, Catalogue number: 24565, Rockford, Illinois, USA) using the reagents supplied with the kit.

Buffers required for O-GlcNAc Western blot detection:

Wash Buffer:

One pack of BuPH™ Phosphate Buffer Saline (PBS) is reconstituted in 500 ml ultrapure water and 2.5 ml of 10% Tween®-20 to a final concentration of ~ 0.05 % is added.

Blocking Buffer:

The 10x dilution buffer provided in the kit is diluted to 1x using the previously prepared wash buffer.

Goat Anti-Mouse IgM- HRP Conjugate (Secondary antibody):

A 1 mg/ml stock of the secondary antibody is prepared by reconstituting the antibody in 75 µL ultrapure water. This is then divided into 6 µL aliquots followed by the addition of an equal volume of glycerol. The final concentration of each aliquot is 0.5 mg/ml and aliquots were stored at -20°C.

O-GlcNAc detection:

After electrotransfer of proteins onto the PVDF membrane, the non-specific sites were blocked overnight at 4°C using the supplied blocking buffer. The membrane was then treated with the primary O-GlcNAc antibody (1:5000 dilution in blocking buffer) and incubated overnight at 4°C. Thereafter, it was thoroughly washed in wash buffer and exposed to secondary antibody (1:5000 dilution in blocking buffer) for one hour at room temperature with gentle shaking. The membrane was thoroughly washed and developed.

Developing the membrane

The membrane was then treated for 5 minutes with detection reagent (5 ml of Stable Peroxide Solution and 5 ml of Luminol/Enhancer supplied with the kit) and placed between transparencies. This was then developed in a dark room. A developing film (Hyperfilm, Amersham, Buckinghamshire, UK) was placed over the sandwiched membrane and exposed for ~ 7 seconds. The film was placed in developing solution for ~ 30 seconds and then in a fixative for 15 seconds. Densitometric analysis was performed as described before.